Multi-Agent Market Equilibria: Mathematical Models and Empirical Analyses

a thesis presented for the degree of

Doctor of Philosophy of Imperial College London

by

Alessandro Micheli

Department of Mathematics

Imperial College London

180 Queen's Gate

London SW7 2BZ

December 2022

Degree: PhD

Thesis title: Multi-Agent Market Equilibria: Mathematical Models and Empirical Analyses

Candidate: Alessandro Micheli

First supervisor: Prof. Damiano Brigo

Second supervisor: Dr. Eyal Neuman

Department of Mathematics, Imperial College London, 180 Queen's Gate London SW7 2BZ

Statement of Originality

I certify that this thesis and the research to which it refers are the product of my own work, and that any ideas or quotations from the work of other people, published or otherwise, are fully acknowledged in accordance with the standard referencing practices of the discipline. Where work is derived from joint collaborations with the author, the author's original contribution will be clearly highlighted and the work of collaborators will be appropriately acknowledged.

Copyright

Abstract

This thesis examines the framework of multi-agent market equilibria through mathematical models and empirical analyses.

Chapter 2 considers a model for the interaction between a slow institutional investor and a high- frequency trader by means of a stochastic multi-period Stackelberg game. We determine the unique multi-period Stackelberg equilibrium of the game in terms of the resolvent of a Fredholm integral equation. Our results provide an explicit solution which shows that the high-frequency trader can adopt either predatory or cooperative strategies in each period, depending on the trade-off between the order-flow and the trading signal. We also show that the institutional investor's strategy is more profitable when the order-flow of the high-frequency trader is taken into account.

In Chapter 3 we study a model for a multi-player stochastic differential game, where agents interact through their joint price impact on an asset that they trade to exploit a common trading signal. We prove that a closed-loop Nash equilibrium exists if the price impact parameter is small enough. A comparison with the corresponding open-loop Nash equilibrium shows that both the agents' optimal trading rates and their performance move towards the central-planner solution, since excessive trading due to lack of coordination is reduced. Nevertheless, we find that the size of this effect is modest for plausible parameter values.

Chapter 4 develops a methodology which accurately replicates the FTSE Russell indexes reconstruction, including the quarterly rebalancings due to new initial public offerings (IPOs). We apply our index reconstruction protocol to compute the permanent and temporary price impact on the Russell 3000 annual additions and deletions, and on the quarterly additions of new IPOs. Our findings show that the index portfolios following the Russell 3000 index and rebalanced on an annual basis are overall more crowded than those following the index on a quarterly basis.

To my mother

Acknowledgements

I would like to thank my supervisors, Prof. Damiano Brigo and Dr. Eyal Neuman, for their help, support and guidance throughout my Ph.D. Their teachings and my memories of the time spent together will accompany me for the rest of my life. I wish to thank Prof. Johannes Muhle-Karbe from whom I was able to learn many insightful lessons during our collaboration. I thank Prof. Umut Cetin and Dr. Nikolas Kantas for taking the time to read my thesis and agreeing to be the examiners for my viva.

I would like to thank the EPSRC CDT in Mathematics of Random Systems for supporting me financially throughout this journey.

Many thanks go also to my family and friends for believing me in the good and bad times. Finally, my most heartfelt thanks go to Mélodie, with whom I had the pleasure to share this adventure and hope to share many more in the future.

Contents

1

Introduction

The advent of electronic markets has substantially changed the way market participants interact. The traditional open outcry exchanges where traders communicated by shouting and using hand signals gave way to the server rooms of electronic exchanges' data centers in which algorithms quietly execute trading strategies with laser-like precision. Fifty years after the opening of the first electronic stock exchange, the NASDAQ, the effects of this transformation have yet to be fully understood. The electronification of order submissions has reduced the core of modern financial markets to a collection of logical rules and completely removed the human-factor from the trading process. This has been a blessing, in that it has improved market transparency, but also a curse, as the removal of any physical barrier has incentivised fragmentation and complexity.

The uncharted territories of modern financial markets have been the subject of increasing attentions from regulators, practitioners and academics. The new rules of trading stimulated the development of market microstructural and mathematical models describing the strategic interaction of financial players. Among those, multi-agent market equilibria have found particular success in striking a balance between providing a parsimonious description of the rational behaviour of traders and a sufficient flexibility to span a broad range of securities and markets. This thesis aims to contribute to the growing literature of multi-agent market equilibria through novel mathematical models and empirical analyses.

1.1 Background

1.1.1 Trading, Fast and Slow

Despite investors of all kinds trade on markets with the same single purpose, making money, what goes behind the scene of trading is a more complex business.

Institutional investors make profits by tracking long-term investment goals and adjusting their portfolios accordingly. They trade infrequently, nevertheless, the sheer volumes of share they execute each time they trade is substantial. This poses the problem on how to liquidate such supersized orders since, given their volumes, they cannot be executed immediately due to insufficient market liquidity. Furthermore, they must face a multitude of costs which are conventionally bucketed into two macro categories:

- ◇ **Explicit costs:** which are known in advance and are mostly in the form of commission costs charged by exchanges and execution desks;
- ◇ **Implicit costs:** which are uncertain economic losses mainly arising from market impact.

While explicit costs can be mitigated by an adequate selection of venues and brokerage and eventually result in an irreducible fraction of the total execution costs, implicit costs are harder to constrain and substantially affect the execution quality of a trade.

The paramount importance of implicit costs has attracted substantial attention from regulators and has pushed them to enforce new duties for investment firms, often collectively named *"best execution"* practices. In Europe, the Markets in Financial Instruments Directive (MiFID) requires investment firms "to take all sufficient steps to obtain, when executing orders, the best possible result for their clients taking into account price, costs, speed, likelihood of execution and settlement, size" (see European Commission (2018)). In this context, several benchmark

prices have been used to quantify executions costs, a common one being the arrival price, that is the mid-price of the asset at the time the order is given to execute. The execution costs measured with respect to the arrival price are known as the *implementation shortfall* (see (Perold, 1988; Almgren and Chriss, 2000)) and they represent the extra costs one would need to pay for implementing a liquidation strategy which until then existed only on paper.

Starting from the seminal papers of (Almgren and Chriss, 2000; Obizhaeva and Wang, 2013), substantial academic efforts have been made on developing models to help institutional investors devise optimal liquidation strategies in increasingly realistic settings. The prototypical optimal liquidation strategy slices the large initial order into smaller orders while accounting for transitory and permanent effects each transaction will have on quoted prices due to market resilience.

Overall, institutional investors represent the traditional side of finance where, still to this date, trades are frequently based on the expertise and the discretionary decisions of traders and portfolio managers. For their strong human-based nature and their substantially analog trading systems, they have been dubbed as low-frequency traders (see O'Hara (2014)).

The advent of modern technology has had a substantial impact on the financial world. The increasing automation of market venues has established a fertile ground for a class of market participants adopting trading strategies whose decisions are made by algorithms running on computers. The practice of highly automatized trading, known as *algorithmic trading*, has pushed traditional finance beyond human biases and reaction times. In particular, large computational powers and fast network connectivity have sustained the growth of a class of technologically advanced market participants called *High-Frequency Traders* (HFTs). Typically, HFTs are characterized by high speeds and high turnover rates that leverage real-time high-frequency financial signals and electronic trading tools. HFTs trade for their own account and, in order to minimise their risk exposure, they do not consume significant amounts of capital, accumulate positions or hold their positions overnight.

Whether HFTs help improving market quality or not is an important open question and often debated among practitioners, academics and regulators. One of the main concerns is that HFTs could employ predatory algorithms to exploit market inefficiencies, for example, to benefit from predictable liquidation strategies employed by low-frequency traders. On the other hand, it has been observed that, under certain circumstances, the presence of HFTs has a positive effect on liquidity by narrowing spreads, reducing adverse selection and improving trade-related price discovery (see Hendershott et al. (2011)).

1.1.2 Skate to Where the Puck is Going

The problem of optimal portfolio selection is one of the pillars of modern mathematical finance. At its core it entails finding an optimal allocation of an investor's economical resources to multiple uncertain assets. In practice, determining such optimal allocation is a complex task as asset managers are faced with several layers of complexities. More precisely, the universe of candidate securities to include in their portfolios may present strong and persistent interdependencies, as assets returns are often correlated and future returns can be forecasted using an array of market signals. Furthermore, each trade must account for investors' risk preferences and, as discussed in Section 1.1.1, for explicit and implicit costs.

Therefore, investors are faced with the problem of weighing the expected benefit of trading against its risks and costs. Mathematically speaking, the following statistical properties are often considered as the leading factors of successful investment portfolios:

- ◇ **Expected returns**, as assets with higher returns often correlate with higher financial performance;
- ◇ **Variance of returns**, as higher variance presents higher uncertainty and risk, for example, in terms of large losses.

From these considerations, Markowitz (1952) proposed a framework for discrete-

time optimal portfolio selection accounting for the portfolios' expected returns and variances. Specifically, an ideal investor would rank her preferences for different portfolios according to a *mean-variance* utility function where she would weigh a putative portfolio's expected returns with its variance in order to account for her risk preferences.

Since Markowitz (1952), the mean-variance approach to portfolio selection has been extended to more general and realistic settings. Relevant to this thesis are the discrete and continuous time models of Gârleanu and Pedersen (2013) and Gârleanu and Pedersen (2016). Specifically, their results provide a solution to the problem of portfolio optimization in the presence of transaction costs and time-dependent signals. The optimal portfolios of Gârleanu and Pedersen (2013) and Gârleanu and Pedersen (2016) present several simple and intuitive properties which can be understood in terms of two principles: (1) aim in front of the target and (2) trade partially toward the current aim. For a fixed level of risk and in absence of transaction costs, a Markowitz portfolio analogous to the one derived in Markowitz (1952) is the optimal portfolio to keep. Nevertheless, when returns are time-dependent, the Markowitz portfolio behave as a stochastic moving target as the expected returns can change at any time, thus, making the current Markowitz portfolio ephemeral and the future ones uncertain. Therefore, in the presence of market frictions the benefit of tightly tracking the Markowitz portfolio should be weighed with the transaction costs arising from high turnover needed to track this moving target. The solution to this conundrum can be stated in the words of the NHL player Wayne Gretzky:

> *"A great hockey player skates to where the puck is going to be, not where it is."*

Indeed, the optimal strategies of Gârleanu and Pedersen (2013) and Gârleanu and Pedersen (2016) entail tracking an aim portfolio consisting of a weighted average of the current Markowitz portfolio and the expected Markowitz portfolios on all future dates, in order to account for the future trajectories of the uncertain price returns. Accounting for future expectations is a recurring feature of many moving

targets problems which has found practical success in areas beyond mathematical finance including missile systems, competitive shooting and, indeed, professional hockey.

1.1.3 Birds of a Feather Flock Together

The second week of August 2007 will be long remembered in the world of quantitative finance. The technological developments at the end of the last century allowed hedge funds managers to develop trading strategies which could go beyond human limitations. Specifically, a new class of strategies called *"long/short equity market-neutral"* allowed to bet on the mean reverting properties of stock returns. Typically, one such strategy would entail buying past losers and selling past winners in order to profit from the reversal of stock prices over a given time window. Therefore, a profitable long/short equity market-neutral portfolio is constructed by assigning weights to a basket of stocks with the property that their sum equals zero. Stocks with positive weights will have long positions which are offset, potentially in equal measure, by the short positions of those with negative weights. Practically speaking, strategies of this kind must be implemented over thousands of stocks in order to be successful, making their management beyond human capabilities and requiring the usage of modern computers. From a risk-management perspective, market-neutral strategies were seen as a relative robust and conservative as they are, by design, less exposed to market movements.

As reported in Figure 3 of Khandani and Lo (2008) this family of strategies had witnessed a steady decline in financial performance over the years 1995 to 2007. This is due to the increase in competition and the growth in assets devoted to these strategies. Such consistent decline in profitability had profound implications on the financial practices undertaken by hedge funds over those years. In order to guarantee their investors the same levels of expected returns in the face of lower profitability, hedge funds had to strongly rely on leverage, the practice of undertaking loans with the intent of transforming small profit opportunities into larger ones.

The early months of 2007 had witness an alarming increase of delinquencies on U.S. home mortgages, the effects of which rippled throughout the financial world. As reported by (Ip and Perry, 2007; Zuckermann et al., 2007), the Wall Street trading giant Bear Stearns Cos. had seen two of its own credit hedge funds collapse after they had made substantial bets on securities backed by subprime mortgage loans. The corresponding market turmoils fueled further uncertainty in market participants as well as, in a conservative move to avoid further credit risk, hesitation and reluctance to lend each other money.

Such uncertain and mutating circumstances had an enormous impact on those same hedge funds who were juicing up their returns with leverage. On one hand, as discussed in (Khandani and Lo, 2008, Section 7), hedge funds were forced to reduce their exposure to reduce their risk limits, either voluntarily or out of a request from their prime brokers and other creditors. On the other hand, those funds who weren't able anymore to get the short-term cash needed to fund their trades, for example, were forced to sell their holdings (see Ip and Perry (2007)). As noticed by Wigglesworth (2017), it is also plausible that some of the players hit by subprime mortgage losses were forced to sell their more liquid but highly leveraged equity portfolios in order to fulfill the investors' cash withdrawals.

The simultaneous occurrence of these factors created the perfect storm for tremendous losses among hedge funds, especially those specializing in market neutral strategies. As reported by Zuckermann et al. (2007), Renaissance Technologies, one of the most successful hedge funds in recent years, had lost 8.7% in August. Similarly, AQR Capital Management, another big american hedge fund, had seen losses in the first week of August in investments employing market-neutral strategies. Many other funds were equally affected. Overall, during the second week of August 2007, the Dow Jones Industrial Average and the S&P 500 experienced their second-worst losses of the year (see Ossinger (2007)).

The collective drawdown of market neutral strategies has often been dubbed as the *"quant quake"* or *"quant meltdown"*. What might have triggered the quant meltdown will never be known exactly, nevertheless, many agree that too many investors

adopting similar strategies might have been a substantial contributing factor (see (Khandani and Lo, 2008, Section 10) and Zuckermann et al. (2007)). Specifically, quantitative funds, including the aforementioned market-neutral funds, adopt similar data and similar computer models to guide their trading decisions. This has the undesired effect that they might end up making the same trade and holding the same positions without, however, accounting for the popularity of the models themselves. Such overlap in portfolios has been extensively studied in the quantitative finance literature under the name of *crowding* and has attracted the attention of practitioners willing to enhance their strategies as well as regulators trying to save financial markets. As noticed by Wigglesworth (2017) and (Khandani and Lo, 2008, Section 7), the losses of August 2007 are likely due to a large liquidation of market-neutral portfolio affecting participants with similar trades and triggering new rounds of liquidations. Indeed, as many funds try to escape the same trades at exactly the same moment, this generates a spiral which has a multiplier effect on the losses that everyone experiences.

1.2 Outline of the contributions

We now present a summary of the significant contributions made in this thesis towards advancing the study of multi-agent market equilibria. In the first project we consider a stochastic game between a slow institutional investor and a high-frequency trader who are trading a risky asset and their aggregated order-flow impacts the asset price. We model this system by means of two coupled stochastic control problems, in which the high-frequency trader exploits the available information on a price predicting signal more frequently, but is also subject to periodic "end of day" inventory constraints. We first derive the optimal strategy of the high-frequency trader given any admissible strategy of the institutional investor. Then, we solve the problem of the institutional investor given the optimal signal-adaptive strategy of the high-frequency trader, in terms of the resolvent of a Fredholm integral equation, thus establishing the unique multi-period Stackelberg equilibrium

of the game. Our results provide an explicit solution to the game, which shows that the high-frequency trader can adopt either predatory or cooperative strategies in each period, depending on the tradeoff between the order-flow and the trading signal. We also show that the institutional investor's strategy is considerably more profitable when the order-flow of the high-frequency trader is taken into account in her trading strategy.

In the second project we study a multi-agent stochastic differential game, where agents interact through their joint price impact on an asset that they trade to exploit a common trading signal. Our model is an extension of the single-agent model of Gârleanu and Pedersen (2016) to the multi-agent setting. We prove that a closed-loop Nash equilibrium for the game exists if the price impact parameter is small enough. Compared to the corresponding open-loop Nash equilibrium, both the agents' optimal trading rates and their performance move towards the central-planner solution, in that excessive trading due to lack of coordination is reduced.

In the third project we develop a methodology which replicates in great accuracy the FTSE Russell indexes reconstitutions, including the quarterly rebalancings due to new initial public offerings (IPOs). We demonstrate the accuracy of this methodology by comparing it to the original Russell US indexes for the time period between 1989 to 2019. As an application, we use our index reconstruction protocol to compute the permanent and temporary price impact on the Russell 3000 annual additions and deletions, and on the quarterly additions of new IPOs. We find that the index portfolios following the Russell 3000 index and rebalanced on an annual basis are overall more crowded than those following the index on a quarterly basis. This phenomenon implies that transaction costs of indexing strategies could be significantly reduced by buying new IPOs additions in proximity to quarterly rebalance dates.

1.3 Thesis Structure

This thesis is structured as follows. In Chapter 2 and 3 we study the interaction of market players by developing novel mathematical models for multi-agent market equilibria in the context of high-frequency trading and portfolio optimisation. The empirical analysis of Chapter 4 sheds light on the adoption of index strategies among market participants and provides new insights on crowding. Finally, in Chapter 5 we provide further research directions which could represent valuable extensions to the content presented in this thesis.

Chapter 2, 3 corresponds to papers Micheli and Neuman (2022), Micheli et al. (2021) and Micheli and Neuman (2019), respectively, and they can be read independently of the others. We remark that the notation across this thesis may vary as each chapter is designed to be self-contained. The majority of the mathematical proofs are provided at the end of each chapter while only minor mathematical results are postponed to the appendix.

2

Fast and Slow Optimal Trading with Exogenous Information

This chapter is based on the paper Micheli and Neuman (2022) which is a joint work with Dr. Eyal Neuman. The paper Micheli and Neuman (2022) has been submitted to *Finance & Stochastics* for publication.

2.1 Introduction

Modern financial markets involve a range of participants who place buy and sell orders across a wide spectrum of time scales: on one end, pension funds rebalance their portfolio on an annual basis and mutual fund managers rebalance typically on a monthly time scale while, on the other end of the spectrum, electronic market makers and high frequency trading firms submit several thousands of orders per second (see e.g. Cont (2011)), while having strict inventory constraints (see p.4 of U.S. Securities and Exchange Commission (2014)). Although this heterogeneity in time scales has been always present, the development of computerized trading in electronic markets has substantially widened the range of frequencies at which various market participants operate. The interaction between the flow of buy and sell orders from these different participants results in an aggregate order flow which is the superposition of components across a wide range of frequencies. The

consequences of this phenomenon for market volatility, price dynamics and market stability have yet to be systematically explored.

This heterogeneity in time frequencies stands in contrast with mathematical models of market microstructure and price dynamics which are often formulated in terms of homogeneous agents operating at a single time scale as in (Gârleanu and Pedersen, 2016; Evangelista and Thamsten, 2020; Voß, 2019; Neuman and Schied, 2022; Micheli et al., 2021; Drapeau et al., 2019; Casgrain and Jaimungal, 2020; Fu et al., 2021; Neuman and Voß, 2021; Garnier et al., 2015) among others. Yet, the repeated occurrence of 'flash crashes' (see Kirilenko et al. (2017)) demonstrates that components at different frequencies may strongly interact and possibly lead to market disruption, calling for a modeling framework which incorporates in some way the co-existence of agents operating at different time scales.

As a first step to investigate these phenomena, we propose a model for the dynamics of prices and order flow in a market where participants of two different frequencies submit buy and sell orders on a risky asset. Specifically, we consider a stochastic game between an institutional investor and a high-frequency trader who are exploiting an exogenous signal which interacts with the price process in the drift term. The institutional investor and high-frequency trader, which will be referred to as *major agent* and *minor agent*, respectively, interact through their aggregated order-flow, which is resulting by their own trades. The trades of both agents create temporary and permanent price impact which affect the asset price process. We model this system by means of two coupled multi-period stochastic control problems over a fixed time horizon T, where the high-frequency trader exploits the exogenous information continuously, but is also subject to periodic inventory constraints at the end of any sub-period $0 < t_1 < ... < t_n = T$, for some $n \geq 1$. On the other hand, the institutional investor has a limited access to the signal but she is only subject to inventory constraints at time T. Since in the setting that we wish to describe the minor agent has a clear advantage in terms of information exploitation, it is natural to look for a Stackelberg equilibrium in this game, where the minor agent takes advantage of the signal and the order-flow

which is created by the major agent's transactions.

Our first result derives the unique optimal strategy of the high-frequency trader given any admissible strategy of the major agent (see Theorem 2.3.2). The challenging part in establishing a Stackelberg equilibrium is to derive the strategy of the player who plays first, namely the major agent. We develop a novel approach for this class of Stackelberg games in order to derive the major agent's optimal strategy given the optimal signal-adaptive strategy of the minor agent using tools from the theory of integral equations. Specifically, in Theorem 2.3.5 we describe the unique optimal major agent's strategy in terms of the resolvent of a Fredholm integral equation, thus establishing the unique multi-period Stackelberg equilibrium of the game. In Section 2.4 we illustrate the solutions to the Stackelberg game and in Section 2.5 we derive the additional technical steps that are needed in order to obtain such explicit results directly from Theorems 2.3.2 and 2.3.5.

From our main theoretical results we derive explicit expressions for both agents equilibrium strategies which have fascinating economic interpretation regarding the trading behaviour of high-frequency traders and on the best practices for institutional investors who are executing large meta-orders. We summarise these insights in the following list and refer the reader for the comprehensive discussion in Section 2.4:

(i) Our results suggest that the high-frequency trader can adopt either predatory or cooperative strategy with respect to the major agent in each period, depending on the tradeoff between the order-flow of the major agent and the trading signal during the period. See Figure 2.1 for specific realisations of such strategies.

(ii) We compare the revenues of the major agent's optimal order execution with a benchmark optimal strategy in which the agent is not taking into account of the minor agent's trading activity. In Figure 2.5 we show that the major agent's optimal strategy on average considerably outperforms the benchmark strategy. This contrasts with the common belief that high-frequency traders

order-flow can be regarded as noise.

(iii) We show that the major agent's and minor agent's optimal trading strategies induce the well-known U-shaped pattern of intraday trading volume, where the traded volume peaks at the beginning and at the end of the day (see Figure 2.6).

Our model is related to a class of predatory trading models which was introduced by Carlin et al. (2007) for a single period and further developed by Schied and Schöneborn (2009) for two-periods. In Carlin et al. (2007) a single-period multi-agent game was introduced where traders are liquidating simultaneously where while creating both temporary and permanent price impact which affects the price process. In their model there are two types of agents: *sellers* which start with a positive amount of assets and *competitors* who have zero initial positions. All agents are seeking to maximise simultaneously similar revenue functionals, using strictly deterministic strategies. Their main results derive a Nash equilibrium for the game. In the single period case it is shown that, under some assumptions on the model parameters, if the seller is liquidating then the competitor is first selling and later buying her position back due to inventory constraints (see Figure 1 in Schied and Schöneborn (2009)). In the two period model the seller can liquidate only in the first period, while the competitor can execute her strategy over two periods. Depending on the price impact parameters, there are two possible scenarios: either the competitor is buying in the first period and then selling in the second period, i.e. introducing cooperative strategies in the game (see Figure 8 therein), or doing a round trip of selling first and then closing the position all in the first period.

Our model is different from the Schied and Schöneborn (2009) in a few critical points. First, we assume that minor agent (resp. competitor) is trading at a higher frequency than the major agent (resp. seller). This is reflected in the model as periodic inventory constraints in the minor agent's revenue functional. This term do not appear in the major agent's objective, who has a fuel constraint only at the end to the trading time horizon. The minor agent is also reacting continuously to exogenous information while the major agent has access to the information only at

the beginning of the trade. This means also that the minor agent's optimal strategy is stochastic, unlike the deterministic game which was studied in Schied and Schöneborn (2009). Another major difference between these models is in the type of equilibrium which is derived. In Schied and Schöneborn (2009) an open-loop Nash equilibrium was derived, which means that all traders optimise simultaneously. From market microstructure setting with various frequencies, it is essential to consider a Stackelberg equilibrium as the minor agent is indeed reacting to the major agent's selling strategy. As stated before, neither Carlin et al. (2007) nor Schied and Schöneborn (2009) take into account exogenous information, therefore, their optimal strategies are always found to be deterministic. One of the main conclusions of our analysis is that this aspect has a prominent effect on the behaviour of the major agent and the minor agent, which is not captured in Carlin et al. (2007) and Schied and Schöneborn (2009). Finally, despite the clear asymmetry in our model between the agents in the access to information, type of equilibrium and inventory constraints, which make the problem quite involved and required us to introduce new methods for Stackelberg games, we are able to derive explicit solutions for any number of time periods, in contrast to Schied and Schöneborn (2009), where only the two period model is tractable.

We briefly mention in this context that Roşu (2019) studied a discrete-time model where fast traders, whose decisions depend on a market signal, trade simultaneously with slow traders, who can only observe a lagged version of that same signal. However besides this difference in the access to information, the fast agents do not have different objective functionals nor inventory constraints which differ them from the slow agents, which are some of the main ingredients in our model.

The rest of the chapter is organised as follows. In Section 2.2 we define the two player model. Our main results regarding the explicit solution to the Stackelberg game are presented in Section 2.3. Section 2.4 contains the illustrations and the financial interpretation of the main results. In Section 2.5 we derive rigorously the numerical scheme that we have used in order to plot the solutions in Section 2.4. The proofs of the results of this chapter are given in Sections 2.6–2.10.

2.2 Model Setup

We define the Stackelberg game between a major agent liquidating an initial amount of shares in a risky assets and a proprietary high frequency trader (HFT) trading on the same asset and who, throughout this chapter, we will regard as a minor agent. Let $T > 0$ denote a finite deterministic time horizon and fix a filtered probability space $(\Omega, \mathcal{F}, (\mathcal{F}_t)_{t\in[0,T]}, \mathbb{P})$ satisfying the usual conditions of right continuity and completeness. The set $\mathcal{H}^2$ represents the class of all (special) semimartingales $P = (P_t)_{t\in[0,T]}$ whose canonical decomposition $P = M + A$ into a (local) martingale $M = (M_t)_{t\in[0,T]}$ and a predictable finite-variation process $A = (A_t)_{t\in[0,T]}$ satisfies

$$\mathbb{E}\left[\langle M\rangle_T\right] + \mathbb{E}\left[\left(\int_0^T |dA_s|\right)^2\right] < \infty. \tag{2.2.1}$$

We denote by $L^2([0,T])$ the space of square integrable functions $f : [0,T] \to \mathbb{R}$ and by $\langle\cdot,\cdot\rangle_{L^2}$ the inner product on $L^2([0,T])$, that is

$$\langle f, g\rangle_{L^2} = \int_0^T f(t)g(t)dt, \quad f, g \in L^2([0,T]),$$

and by $||\cdot||_{L^2}$ the associated norm.

Admissible strategies and price impact. The major agent has an initial holding of $q_0 \in \mathbb{R}$ shares in a risky asset. Her trading rate $\nu^0 = (\nu^0_t)_{t\in[0,T]}$ is chosen from the class of fuel-constrained *deterministic* admissible strategies $\mathcal{A}^{q_0}_M$, which is defined as

$$\mathcal{A}^{q_0}_M := \left\{\nu \in L^2([0,T]) \text{ s.t. } \int_0^T \nu_t dt = q_0\right\}. \tag{2.2.2}$$

Her trading rate ν^0 affects her inventory process Q^{0,ν^0} so that

$$Q^{0,\nu^0}_t = q_0 - \int_0^t \nu^0_s ds, \quad 0 \le t \le T. \tag{2.2.3}$$

The minor agent, being a proprietary high frequency trader, is assumed to have a zero initial position in the risky asset. Her trading rate $\nu^1 = (\nu^1_t)_{t\in[0,T]}$ is chosen

from a class of *adaptive* admissible strategies

$$\mathcal{A}_m := \left\{ \nu \text{ progressively measurable s.t. } \mathbb{E}\left[\int_0^T \nu_s^2 ds\right] < \infty \right\}. \tag{2.2.4}$$

Her trading rate ν^1 affects her inventory process Q^{1,ν^1} so that

$$Q_t^{1,\nu^1} = -\int_0^t \nu_s^1 ds, \quad 0 \le t \le T. \tag{2.2.5}$$

Throughout, we use the notation $\nu = (\nu^0, \nu^1)$ for the major agent's control ν^0 and the minor agent's control ν^1. Once ν is fixed, the visible asset mid-price P^ν satisfies

$$P_t^\nu = P_t - Y_t^\nu, \quad 0 \le t \le T, \tag{2.2.6}$$

where $P \in \mathcal{H}^2$ and where Y^ν is the permanent price impact price impact à la Almgren and Chriss (2000), which is generated by both agents and which is given by

$$Y_t^\nu = \int_0^t (\kappa_0 \nu_s^0 + \kappa_1 \nu_s^1) ds, \tag{2.2.7}$$

where κ_i, $i = 1, 2$, are positive constants.

Major agent's objective. The major agent's execution price is affected instantaneously in an adverse manner through the presence of linear temporary price impact. The major agent's execution price is taken to be

$$S_t^{0,\nu} = P_t^\nu - \lambda_0 \nu_t^0, \tag{2.2.8}$$

where λ_0 is a positive constant measuring the magnitude of her temporary price impact. As a result, the major agent's cash process satisfies

$$X_t^{0,\nu} = x_0 + \int_0^t S_s^{0,\nu} \nu_s^0 ds, \quad 0 \le t \le T. \tag{2.2.9}$$

The major agent's objective is to optimally unwind her initial position q_0 by the trading horizon T, so to minimise her execution costs. This is equivalent to max-

imising the expected revenues from her liquidation, therefore, we take the major agent's performance functional to be[1]

$$H^0\left(\nu^0;\nu^1\right) := \mathbb{E}\left[X_T^{0,\nu}\right]. \tag{2.2.10}$$

Minor agent's objective. As in the case of the major agent, the transactions of the minor agent create temporary price impact, such that the execution price of her orders is given by

$$S_t^{1,\nu} = P_t^{\nu} - \lambda_1 \nu_t^1. \tag{2.2.11}$$

where λ_1 is a positive constant. Note that the temporary price impact parameter is likely to be smaller for the minor agent as HFTs can take advantage of the order-book real-time information in order to reduce their price impact.

The minor agent's cash process is given by

$$X_t^{1,\nu} = x_1 + \int_0^t S_s^{1,\nu}\nu_s^1 ds, \quad 0 \le t \le T. \tag{2.2.12}$$

The minor agent wishes to maximise her cash, however as an HFT, she is inclined to avoid *overnight risk*, specifically, in the form of non-zero overnight inventory. As an example, consider T to be one business week, such that $[0,T]$ can be partitioned in five disjoint and contiguous intervals of equal duration τ, where each intervals represents the market hours of each business day from Monday to Friday. Without loss of generality, in the context of our example we assume that the minor agent's intraday risk preferences are independent of the business day considered and we ignore the possibility of after-hours trading. Since the minor agent wishes to close her position by the end of each day, then as often done for terminal inventory penalties in the context of single-day liquidations, we can introduce a penalisation for non-zero inventory at the end of each day. These dynamic inventory preferences can be accounted by modelling the running inventory costs of the minor agent via a

[1]It is straightforward to show that maximising (2.2.10) is equivalent to minimising the implementation shortfall of the major agent's liquidation, see for example (Cartea et al., 2015, Chapter 6.3).

periodic function of period τ which drastically increases towards the end of each day (see e.g. (2.4.6)), i.e. as t approaches $\tau, 2\tau, 3\tau, 4\tau, 5\tau$ from the left. Mathematically, in order to capture the minor agent's dynamic inventory preferences of our example and more general ones, we define the minor agent's running inventory costs in terms of a function $\phi^1 : [0,T] \to \mathbb{R}_+$. Henceforth, we work under the following assumption:

Assumption 2.2.1. *We assume ϕ^1 is a piecewise continuous and locally bounded function.*

The minor agent risk-revenue functional is therefore given by

$$H^1(\nu^1;\nu^0) := \mathbb{E}\left[X_T^{1,\nu} + Q_T^{1,\nu^1}\left(P_T^{\nu} - \alpha Q_T^{1,\nu^1}\right) - \int_0^T \phi_t^1 \left(Q_t^{1,\nu^1}\right)^2 dt\right]. \tag{2.2.13}$$

The first two terms in (2.2.13) represent the trader's terminal wealth; that is, her final cash position, accounting for the accrued trading costs which are induced by temporary price impact and the permanent price impact of both agents as prescribed in (2.2.11), as well as the mark-to-market value of her terminal risky asset position. The third and fourth terms in (2.2.13) implement a penalty $\phi_t^1 > 0$ and $\alpha > 0$ on her running and terminal inventory, respectively. Also observe that $H^1(\nu^1;\nu^0) < \infty$ for any pair of admissible strategies $\nu^0 \in \mathcal{A}_M^{q_0}$ and $\nu^1 \in \mathcal{A}_m$.

The Stackelberg game. We formulate the competition between the major agent and the minor agent as a stochastic Stackelberg game in which the minor agent is reacting to the major agent's trading. Mathematically, the game unfolds in two steps:

(i) *Minor Agent's Problem:* for a given major agent's liquidation strategy $\nu^0 \in \mathcal{A}_M^{q_0}$, the minor agent chooses her own strategy $\nu^{1,*}(\nu^0) \in \mathcal{A}_m$ in order to maximise her objective functional H^1;

(ii) *Major Agent's Problem:* given the optimal minor agent's strategy $\nu^{1,*}$ established in (i), the major agent determines the optimal liquidation strategy $\nu^{0,*} \in \mathcal{A}_M^{q_0}$ in order to maximise her objective functional H^0.

In the context of our model, we formalise the definition of Stackelberg equilibrium as follows.

Definition 2.2.2 (Stackelberg equilibrium)**.** *A pair* $\nu^* := (\nu^{0,*}, \nu^{1,*}(\nu^{0,*}))$ *where* $\nu^{0,*}$ *and* $\nu^{1,*}(\nu^{0,*})$ *solve the major and minor agent's problems, respectively, is called a Stackelberg equilibrium.*

2.3 Main Results

Our main results derive explicitly the unique Stackelberg equilibrium of the game. As stated at the end of Section 2.2, we start by solving the minor agent's problem.

2.3.1 Solution to the Minor Agent's Problem

We denote by $L^2([0,T]^2)$ the space of measurable kernels $\mathcal{T} : [0,T]^2 \to \mathbb{R}$ such that

$$\int_0^T \int_0^T \mathcal{T}(t,s)^2 dtds < \infty. \tag{2.3.1}$$

Henceforth, we make the following assumption (see also Remark 2.3.3).

Assumption 2.3.1. *We assume that the parameters* α *in* (2.2.13) *and* κ_1 *in* (2.2.7) *are chosen such that*

$$2\alpha \geq \kappa_1.$$

As proved in Section 2.6, the solution to the minor agent's problem can be stated in terms of the solution of a Riccati equation and the solution of a BSDE. So, let $r^1 = (r_t^1)_{t\in[0,T]}$ be the solution to the following Riccati equation with a time varying coefficient,

$$\begin{cases} \partial_t r_t^1 &= \frac{1}{\lambda_1}\phi_t^1 - (r_t^1)^2, \\ r_T^1 &= -\frac{2\alpha-\kappa_1}{2\lambda_1}. \end{cases} \tag{2.3.2}$$

Under Assumption 2.3.1, the solution r^1 of (2.3.2) exists and is unique over $[0,T]$

(see Proposition 2.6.7). We further define

$$\xi_t^{\pm} := e^{\pm \int_0^t r_z^1 dz}, \quad 0 \leq t \leq T, \tag{2.3.3}$$

as well as the kernel $\mathcal{K} : [0,T]^2 \to \mathbb{R}_+$ which is given by

$$\mathcal{K}(t,s) := \xi_t^- \xi_s^+, \quad 0 \leq t, s \leq T. \tag{2.3.4}$$

Note that the kernel $\mathcal{K}$ is in $L^2([0,T]^2)$ (see Lemma 2.6.6). Moreover, for any $\nu^0 \in \mathcal{A}_M^{q_0}$ we define the predictable process

$$r_t^0 := \frac{1}{2\lambda_1} \mathbb{E}_t \left[\int_t^T \mathcal{K}(t,s)(dA_s - \kappa_0 \nu_s^0 ds) \right], \quad 0 \leq t \leq T. \tag{2.3.5}$$

where A is the finite variation component of the price process P. As shown in Section 2.6, the process r_t^0 is the solution to the BSDE 2.6.28. The solution to the minor agent problem is given in the following theorem.

Theorem 2.3.2 (Solution to the minor agent's problem)**.** *Let $\nu^0 \in \mathcal{A}_M^{q_0}$. Under Assumption 2.3.1, there exists a unique optimal strategy $\nu^{1,*}(\nu^0) \in \mathcal{A}_m$ that maximizes (2.2.13). This strategy is given by*

$$\nu_t^{1,*} = -\left(r_t^0 + r_t^1 \int_0^t \mathcal{K}(s,t) r_s^0 ds \right), \quad 0 \leq t \leq T. \tag{2.3.6}$$

The proof of Theorem 2.3.2 is given in Section 2.6.

Remark 2.3.3. *In Lemma 2.6.2 we show that Assumption 2.3.1 is a sufficient condition to guarantee the strict concavity of the minor agent's functional (2.2.13), hence the uniqueness of the solution to the minor agent's problem.*

Remark 2.3.4. *Note that minor agent's optimal control in (2.3.6) can be written in feedback form as follows,*

$$\nu_t^{1,*} = -\left(r_t^0 + r_t^1 Q_t^{1,\nu^{1,*}} \right), \quad 0 \leq t \leq T.$$

In the special case where there is no permanent price impact, that is $\kappa_i = 0$, $i = 1, 2$

and the risk aversion function ϕ^1 is a positive constant, (2.3.6) coincides with the optimal strategy in (Belak et al., 2019, Theorem 3.1).

2.3.2 Solution to the Major Agent's Problem

Our next step is to derive the maximiser of the major agent's objective functional (2.2.10), given the minor agent's optimal strategy $\nu^{1,*}$ in (2.3.6). As it is often the case in Stackelberg games, solving the second phase of the game is technically challenging and rarely achievable. In order to do so we make the following simplifying assumption on the signal A in (2.2.1). We assume that the signal process A is given by

$$A_t = \int_0^t \mu_s ds, \quad 0 \leq t \leq T.$$

where $\mu = (\mu_t)_{t\in[0,T]}$ is an $(\mathcal{F}_t)_{t\in[0,T]}$-adapted stochastic process satisfying

$$\int_0^T \mathbb{E}[\mu_t^2] dt < \infty. \tag{2.3.7}$$

Note that this assumption is an adaptation of the assumptions made in (Cartea and Jaimungal, 2016; Lehalle and Neuman, 2019) on the signal for single agent optimal execution problems to the present context. We further denote

$$\bar{\mu}_t := \mathbb{E}[\mu_t], \quad 0 \leq t \leq T. \tag{2.3.8}$$

Next, we introduce some essential definitions related to linear operators in $L^2([0,T])$.

Definitions for linear operators in $L^2([0,T])$. For any linear operator T from $L^2([0,T])$ to $L^2([0,T])$ we define the operator norm

$$||\mathsf{T}|| := \sup\left\{||\mathsf{T}\psi||_{L^2} : \psi \in L^2([0,T]),\ ||\psi||_{L^2} \leq 1\right\}, \tag{2.3.9}$$

and we denote by $B(L^2([0,T]))$ the space of all bounded linear operator from $L^2([0,T])$ to $L^2([0,T])$ with respect to the operator norm (2.3.9).

For any kernel $\mathcal{T} \in L^2([0,T]^2)$ (see (2.3.1)) we say that T is the integral operator generated by the kernel $\mathcal{T}$ if for any $\psi \in L^2([0,T])$,

$$(\mathsf{T}\psi)(t) = \int_0^T \mathcal{T}(t,s)\psi(s)ds, \quad 0 \le t \le T.$$

Any integral operator generated by a kernel in $L^2([0,T]^2)$ is in $B(L^2([0,T]))$ by the Cauchy-Schwarz inequality.

If T_1 and T_2 are two operators in $B(L^2([0,T]))$, then we denote by $\mathsf{T}_2\mathsf{T}_1$ the operator obtained by composing T_2 with T_1, that is for any $\psi \in L^2([0,T])$,

$$(\mathsf{T}_2\mathsf{T}_1\psi)(t) := (\mathsf{T}_2(\mathsf{T}_1\psi))(t), \quad 0 \le t \le T.$$

Special operators for our setting. Recall that $\mathcal{K}$ was defined in (2.3.4). We introduce the kernel $\mathcal{G} : [0,T]^2 \to \mathbb{R}_+$ defined as

$$\mathcal{G}(t,s) := \int_0^{t\wedge s} \mathcal{K}(u,t)\mathcal{K}(u,s)du, \quad 0 \le t,s \le T. \tag{2.3.10}$$

Note that the kernel $\mathcal{G}$ is symmetric and in $L^2([0,T]^2)$ (see Proposition 2.8.1). We define the operators G and S acting on any $\psi \in L^2([0,T])$ as follows,

$$(\mathsf{G}\psi)(t) := \int_0^T \mathcal{G}(t,s)\psi(s)ds, \tag{2.3.11}$$

$$(\mathsf{S}\psi)(t) := \frac{1}{2\lambda_0}\int_0^T \mathbb{1}_{\{s\le t\}}\psi(s)ds + \frac{\kappa_1}{4\lambda_1\lambda_0}(\mathsf{G}\psi)(t). \tag{2.3.12}$$

Note that the both operators G and S are in $B(L^2([0,T]))$ (see Proposition 2.7.4 and Lemma 2.7.10). Moreover, the operator G admits a spectral decomposition in terms of a sequence of positive eigenvalues $(\zeta_n)_{n\ge1}$ and a corresponding sequence of eigenfunctions $(\psi_n)_{n\ge1}$ in $L^2([0,T])$ (see Lemma 2.8.3). We define the *resolvent*

kernel $\mathcal{R} : [0,T]^2 \to \mathbb{R}$ as

$$\mathcal{R}(t,s) = -\frac{\kappa_1\kappa_0}{2\lambda_0\lambda_1}\mathcal{G}(t,s) + \sum_{n\geq 1} \frac{1}{1+\frac{\kappa_1\kappa_0}{2\lambda_0\lambda_1}\zeta_n}\left(\frac{\kappa_1\kappa_0}{2\lambda_0\lambda_1}\zeta_n\right)^2 \psi_n(t)\psi_n(s), \tag{2.3.13}$$

for all $t,s \in [0,T]$ and where the sum converges uniformly and uniformly-absolutely over $[0,T]^2$, see Remark 2.3.10 for details. Moreover, we define the *resolvent* operator R, acting on any $\psi \in L^2([0,T])$ as follows,

$$(\mathsf{R}\psi)(t) := \psi(t) + \int_0^T \mathcal{R}(t,s)\psi(s)ds, \quad 0 \leq t \leq T. \tag{2.3.14}$$

The operator R is also in $B(L^2([0,T]))$, this is proved later in Proposition 2.7.9.

Notation. We denote by $\mathit{1}(t)$ the constant function which equals to 1 everywhere on $[0,T]$.

We are ready to state our main result regarding the solution to major's agent problem conditional on the minor agent adopting the strategy $\nu^{1,*}$ given in (2.3.6). Recall that $\bar{\mu}$ was defined in (2.3.8) and S was defined in (2.3.12).

Theorem 2.3.5 (Solution to the major agent's problem)**.** *Assume that $\nu^{1,*}$ is given by (2.3.6) and that Assumption 2.3.1 holds. Then, there exists a unique optimal strategy $\nu^{0,*} \in \mathcal{A}_M^{q_0}$ that maximizes the major agent's objective functional (2.2.10). It is given by*

$$\nu_t^{0,*} = \frac{\eta}{2\lambda_0}(\mathsf{R}\mathit{1})(t) + (\mathsf{R}\mathsf{S}\bar{\mu})(t), \quad 0 \leq t \leq T, \tag{2.3.15}$$

where

$$\eta = 2\lambda_0 \frac{q_0 - \langle \mathsf{R}\mathsf{S}\bar{\mu}, \mathit{1}\rangle_{L^2}}{\langle \mathsf{R}\mathit{1}, \mathit{1}\rangle_{L^2}}. \tag{2.3.16}$$

Moreover, $\nu_t^{0,*}$ is continuous on $[0,T]$.

The proof of Theorem 2.3.5 is given in Section 2.7. In the proof of Theorem 2.3.5 we also show that the constant η in (2.3.16) is well-defined, which is an ingredient in proving the admissibility of the optimal strategy (2.3.15).

The following corollary follows immediately from Theorem 2.3.2 and Theorem

2.3.5.

Corollary 2.3.6. *Let $\nu^{0,*}$ and $\nu^{1,*}(\nu^{0,*})$ as in Theorem 2.3.5 and Theorem 2.3.2, respectively. Then, under Assumption 2.3.1, the pair $(\nu^{0,*}, \nu^{1,*}(\nu^{0,*})) \in \mathcal{A}_M^{q_0} \times \mathcal{A}_m$ is the unique Stackelberg equilibrium in the sense of Definition 2.2.2.*

The following remarks discuss the result of Corollary 2.3.6.

Remark 2.3.7. *Note that $\nu^{0,*}$ in (2.3.15) is given in terms of the resolvent operator R. In Section 2.5 we derive a numerical scheme that approximates $\nu^{0,*}$ by using finite dimensional projections of G. The problem of computing R and hence $\nu^{0,*}$ is reduced to a finite-dimensional problem of matrix inversion. We refer to Proposition 2.5.4 and Theorem 2.5.6 for the details.*

Remark 2.3.8. *The most challenging step in obtaining a Stackelberg equilibrium is to derive the strategy of the player who acts first, namely the major agent. In our case we needed to develop a novel approach for deriving the optimal strategy in (2.3.15), using tools from the theory of integral equations. In Section 2.4 we illustrate the solutions to the Stackelberg game and in Section 2.5 we derive additional technical steps, which are needed in order to plot such explicit solutions directly from Theorems 2.3.2 and 2.3.5.*

Remark 2.3.9. *Our illustrations in Section 2.4 suggest that the minor agent can adopt either predatory or cooperative strategy with respect to the major agent, in each period, depending on the trade-off between the order-flow of the major agent and the trading signal during the period (see Figure 2.1). This qualitative behaviour can be compared with the deterministic model of Schied and Schöneborn (2009), who showed that in the single period case the competitor is also selling and then buying her position back due to inventory constraints (see Figure 1 therein). In their two period model the seller is selling only the first period and then depending on the price impact parameters there are two possible scenarios: either the competitor is buying in the first period and then selling in the second period, i.e. introducing cooperative strategies in the game (see Figure 8 therein), or doing a round trip of selling first and then closing the position, all in the first period.*

Remark 2.3.10. *We remark that the sum appearing in (2.3.13) satisfies the following convergence properties. Define*

$$\mathfrak{R}_N(t,s) = \sum_{n=1}^{N} \frac{1}{1+\frac{\kappa_1\kappa_0}{2\lambda_0\lambda_1}\zeta_n} \left(\frac{\kappa_1\kappa_0}{2\lambda_0\lambda_1}\zeta_n\right)^2 \psi_n(t)\psi_n(s), \quad t,s\in[0,T],$$
$$\mathfrak{R}^{abs}_N(t,s) = \sum_{n=1}^{N} \left|\frac{1}{1+\frac{\kappa_1\kappa_0}{2\lambda_0\lambda_1}\zeta_n} \left(\frac{\kappa_1\kappa_0}{2\lambda_0\lambda_1}\zeta_n\right)^2 \psi_n(t)\psi_n(s)\right|, \quad t,s\in[0,T].$$

Then, it follows from the proof of (Porter and Stirling, 1990, Theorem 4.27) that $\mathfrak{R}_N$ *converges uniformly to the sum in* $\mathcal{R}$ *on* $(t,s)\in[0,T]^2$ *, and that* $\mathfrak{R}^{abs}_N$ *is uniformly convergent. The uniform convergence of* $\mathfrak{R}^{abs}_N$ *guarantees that the uniform convergence of* $\mathfrak{R}_N$ *is preserved even when the order of summation is changed. Therefore, as it is natural to expect, the solution* $\nu^{0,*}$ *in (2.3.15) is independent of how one enumerates the eigenvalues and the corresponding eigenfunctions of* G*.*

2.4 Illustrations

In this section we illustrate the agents' optimal equilibrium strategies, which were derived in Theorems 2.3.5 and 2.3.2. Motivated by Section 4 of Lehalle and Neuman (2019), we consider the case where the signal μ in (2.3.7) follows an Ornstein-Uhlenbeck process,

$$d\mu_t = -\beta\mu_t dt + \sigma dW_t, \quad \mu_0 = m_0, \tag{2.4.1}$$

where $W = (W_t)_{t\geq 0}$ is a standard Brownian motion and β and σ are positive constants. Here, the process μ could model a trading signal such as moving averages of past price changes (Gârleanu and Pedersen, 2013), order-book imbalances (Cont and de Larrard, 2013; Cont, Kukanov, and Stoikov, 2014; Lipton, Pesavento, and Sotiropoulos, 2013; Cartea and Jaimungal, 2016; Lehalle and Neuman, 2019), or price-dividend ratios (Barberis, 2000). Furthermore, we assume that M in (2.2.1) is given by

$$M_t = M_0 + \sigma_M \widetilde{W}_t, \tag{2.4.2}$$

where $\widetilde{W}$ is a standard Brownian motion independent from W, and M_0, σ_0 are positive constants. We fix the values of the price impact parameters λ_i, κ_i, the initial inventory of the major agent q_0 and the terminal penalty parameter α in (2.2.13) to be

$$\kappa_0 = 2, \quad \kappa_1 = 2, \quad \lambda_0 = 1, \quad \lambda_1 = 1, \quad q_0 = 10, \quad \alpha = 10, \tag{2.4.3}$$

as well as the parameters of M in (2.4.2) and of μ in (2.4.1),

$$m_0 = -0.5, \quad \beta = 0.1, \quad \sigma = 4, \quad M_0 = 100, \quad \sigma_M = 1. \tag{2.4.4}$$

The plots in this section are generated by using the numerical scheme which will described in detail in Section 2.5. We choose as a complete orthonormal basis $(a_i)_{i=1}^{\infty}$ the functions

$$a_i(t) := \begin{cases} 1/\sqrt{T} & i = 1 \\ \sqrt{2/T}\cos\left(\frac{(i-1)\pi t}{T}\right) & i = 2, 3, \dots \end{cases} \tag{2.4.5}$$

and such that each of corresponding degenerate kernel $\mathcal{G}_n$ defined in (2.5.4) represent the n^{th}-degree Fourier series approximation of the kernel $\mathcal{G}$ in (2.3.10). In order to strike a balance between numerical accuracy and computational efficiency, our simulations are generated by approximating the kernel $\mathcal{G}$ with the degenerate kernel $\mathcal{G}_{300}$.

The time dependence in the minor agent's inventory costs ϕ_t^1 (see (2.2.13)) can accommodate the setting of a liquidation carried out over several days. We take $T = k\tau$ for some positive integer k and for $\tau > 0$. Moreover, we choose the function ϕ^1 to be given by the following parametric form

$$\phi_t^1 = c_0 \left(\frac{t}{\tau} - \left\lfloor \frac{t}{\tau} \right\rfloor \right)^{c_1}, \quad 0 \le t \le T, \tag{2.4.6}$$

for two positive constants c_0 and c_1, which in the context of our simulations, we take to be $c_0 = 500$ and $c_1 = 15$. The function (2.4.6) is periodic of period τ

and increases to its maximum value as t approaches $\tau,\ 2\tau,\ 3\tau, \ldots,\ k\tau$ from the left, forcing the minor agent to liquidate most of her position at the end of each period. We consider a liquidation carried over a business week, from Monday to Friday, such that $T = 5$ (days) and $\tau = 1$ (day). Figure 2.1 illustrates three examples of a multi-day liquidation. Specifically, the top panel shows the major agent's deterministic optimal inventory (green line), deduced from (2.3.15), as well as three different realisations of the minor agent's optimal inventories that one obtains from (2.3.6) (blue, purple and red lines). The bottom panel shows the corresponding signal μ observed by the minor agent's while adopting the strategies at the top panel.

From (2.2.6) it follows that the price impact generated by the major agent's optimal strategy $\nu^{0,*}$ is perceived as a deterministic signal. The sell-off of shares by the major agent has the effect of pushing the price downwards, therefore, it generates opportunities which can be exploited by the minor agent. These considerations justify the fact that, as shown in (2.3.6), the minor agent adopts a trading strategy which tracks the "impacted" signal $\mu_t - \kappa_0 \nu_t^{0,*}$ instead of the raw market signal μ_t. Hence, depending on her forecast on the impacted signal $\mu_t - \kappa_0 \nu_t^{0,*}$, during each period the minor agent can decide whether to trade in the same direction of the major agent or not. This has the effect that, over the interval $[0, T]$, the observed trading style of the minor agent can be *predatory*, i.e. front running the major agent (blue line), *cooperative* (red line) or a *hybrid* of both (purple line).

To further understand several novel features of our model in the context of the multi-day liquidation we have just analysed, it is instructive to momentarily pause our discussion and consider the simpler case of a liquidation carried out over a single day. In particular, we wish to benchmark the major agent's optimal strategy in (2.3.15) against the strategy $\nu^{0,\mathrm{BM}}$ the major agent would use if she were unaware of the minor agent's trading activity. The strategy $\nu^{0,\mathrm{BM}}$ can be found by solving the major agent's problem with $\kappa_1 = 0$ and it is given by

$$\nu_t^{0,\mathrm{BM}} = \frac{q_0}{T} + \frac{m_0}{2\lambda_0 \beta}\left(\frac{1 - \beta T e^{-\beta t} - e^{-\beta T}}{\beta T}\right), \quad 0 \leq t \leq T. \tag{2.4.7}$$

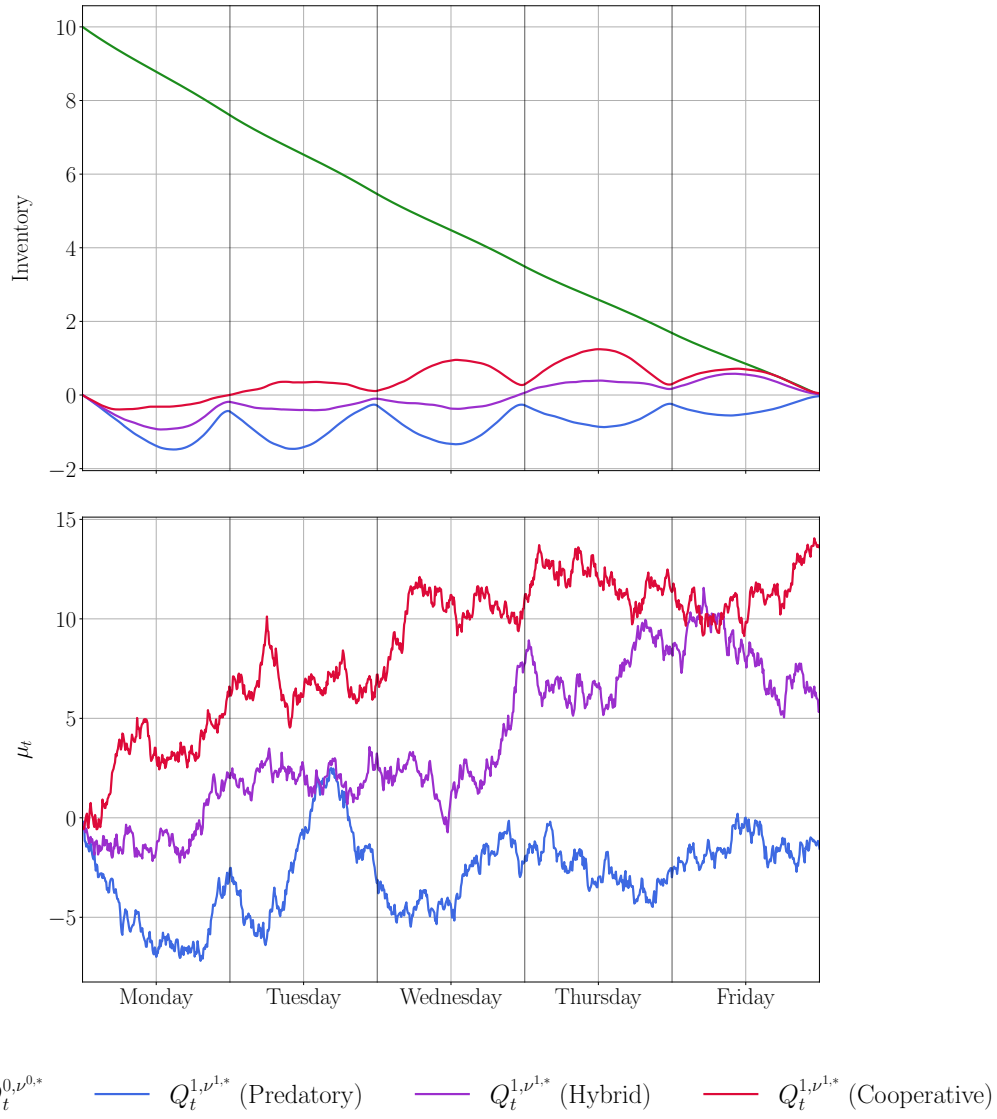

Figure 2.1: In the top panel, the green line represent the major agent's optimal inventory while the remaining solid lines represent the minor agent's optimal inventory when the minor agent is adopting a predatory trading style (blue line) and cooperative trading style (red line) or an hybrid of both (purple line). In the bottom panel, we show the signal μ_t corresponding to the realisations of the minor agent's inventories in the top panel.

Note that in the case of $m_0 = 0$ in (2.4.1), $\nu^{0,\mathrm{BM}}$ in (2.4.7) is a TWAP strategy.

We assume that the major agent wishes to liquidate his initial position over a time horizon of six hours, from 10 AM to 4 PM, hence we set $T = 6$ (hours).

In the present context, we slightly modify some of the parameters in (2.4.3) and (2.4.4): $\sigma = 1.5$, $\alpha = 50$ and $\phi_t^1 \equiv 1$. The top panel of Figure 2.2 shows the major agent's optimal trading rate $\nu^{0,*}$ (solid green line) and the benchmark trading rate $\nu^{0,\mathrm{BM}}$ (dashed green line). The bottom panel show 1000 realisations of minor agent's optimal trading rate $\nu^{1,*}$ (thin solid orange lines) and the cross-sectional average (thick solid brown line). We observe that the major agent's optimal strategy visibly deviate from the benchmark one in order to take into account the adverse effect of the minor agent's trading activity. We remark that since the major agent adopts a deterministic strategy, her decisions are based on the cross-sectional average of the minor agent's strategy, i.e. the solid brown line in the bottom panel of Figure 2.2. Initially, it is optimal to trade faster than the benchmark strategy in anticipation of the expected permanent price impact generated by the minor agent's reaction. Indeed, the early prices are more favourable to the major agent since they have not been affected yet by the extra price impact generated by presence of the minor agent. In the middle of the trading window the major agent's keeps trading but at a lower rate than the benchmark strategy. The explanation for this is that the major agent is aware that the minor agent could potentially trade in the same direction. Therefore, slowing down partially minimise the negative externality the minor agent's exerts on her via the aggregated permanent price impact. Finally, in the last section of the trading window two factors determine the behaviour of the major agent's optimal strategy. First, the major agent must increase her trading rate to meet the terminal inventory constraint $Q_T^{0,\nu^{0,*}} = 0$. Second, the major agent is aware that, on average, the minor agent will have to close her short position at the end of the time horizon, therefore, she will have to buy shares, generating market impact and pushing the price up again. Hence, the prices at the end of the trading window are more favourable for the major agent, therefore, a substantial portion of the liquidation is postponed to the last hour. Figure 2.3 presents the major

agent's and minor agent's inventories corresponding to the trading rates depicted in Figure 2.2.

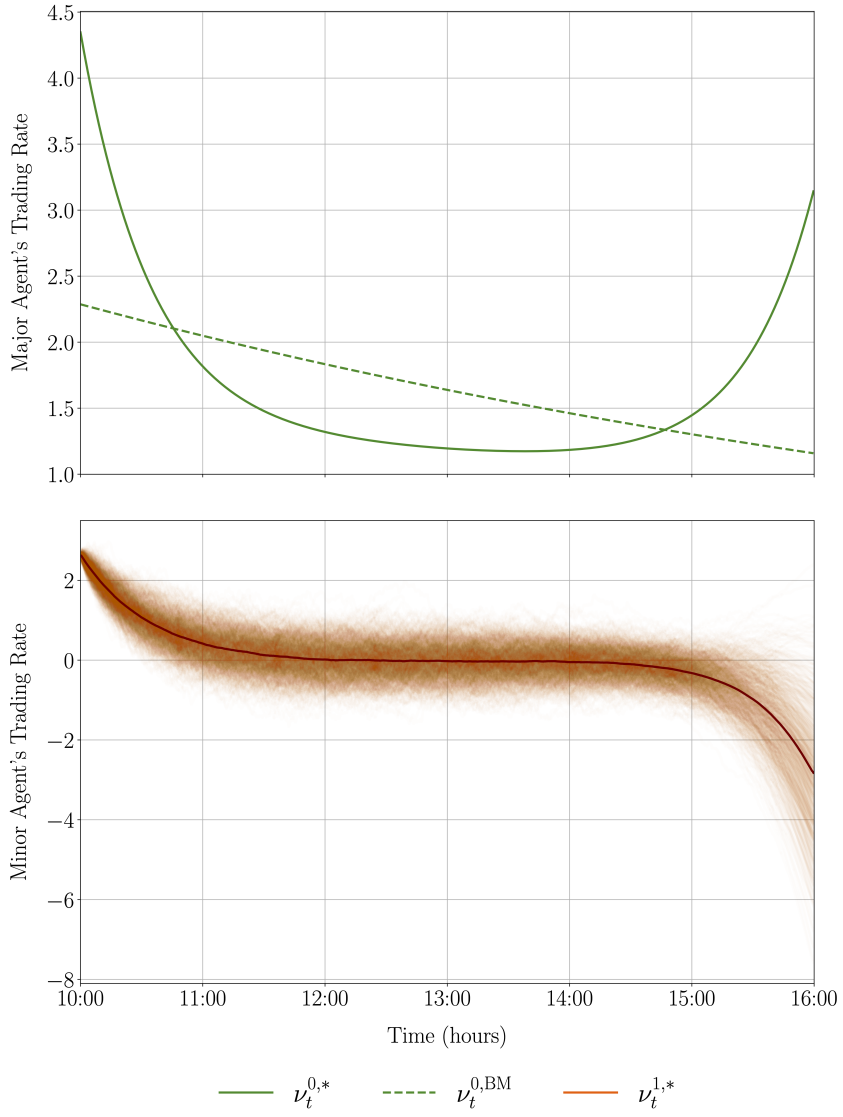

Figure 2.2: The major agent's and minor agent's optimal strategies in (2.3.15) and (2.3.6), respectively, for a single-day liquidation. In the top panel, the green solid line shows the major agent's optimal strategy while the dashed green line shows the benchmark strategy of (2.4.7). In the bottom panel, the thin orange solid lines depicts different realisations of the minor agent's optimal strategy. The brown solid line is the cross-sectional mean over the realisations.

Having established the major agent's and minor agent's trading patterns in the context of a single day liquidation, we turn again to the case of the multi-day liquidation presented in Figure 2.1. Analogously to Figure 2.2, the top panel of Figure 2.4 shows the major agent's optimal trading rate (solid green line) as well

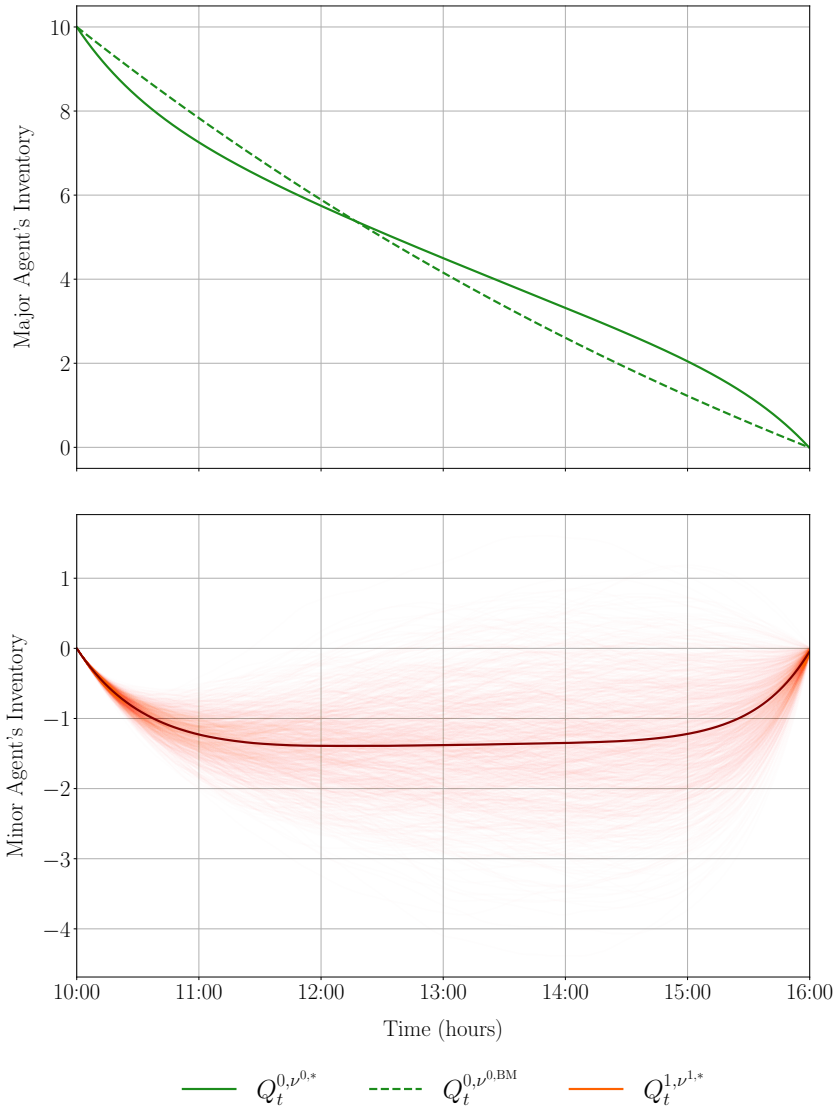

Figure 2.3: The major agent's and minor agent's optimal inventories corresponding to the strategies in (2.3.15) and (2.3.6), respectively, for a single-day liquidation. In the top panel, the solid green line shows the major agent's optimal inventory corresponding to the major agent's optimal strategy while the dashed green line shows the inventory corresponding to benchmark strategy in (2.4.7). In the bottom panel, the thin solid orange lines represent different realisations of the minor agent's optimal inventories corresponding to the strategy in (2.3.6) while the solid brown line is the cross-sectional mean over the realisations.

the trading rate of the benchmark strategy (dashed green line) in the context of the multiday-liquidation initially presented in Figure 2.1. Moreover, the bottom panel of Figure 2.4 presents 1000 realisations of the minor agent's trading rates (thin orange lines) as well as the cross-sectional average (solid brown line). We recover analogous trading patterns to the one observed in the single-day liquidation: the major agent's speed, when compared to the benchmark strategy, greatly increases at the beginning and at the end of each day. Moreover, on average, the minor agent acquires a short position at the beginning of each day, pushing the price down, and then, in order to meet her terminal inventory constraint at the end of each day, she pushes the price up again by buying shares. Note from Figure 2.1 that the predatory, cooperative and hybrid strategies share some common features. First, at the end of each day all the strategies have a very small inventory. This is because, by introducing the periodic running inventory costs of (2.4.6), the minor agent is strongly discouraged to hold a non-zero position at the end of each day, independently of her forecast for the impacted signal $\mu_t - \kappa_0 \nu_t^{0,*}$. Secondly, from Figure 2.1 we observe that that the major agent is not liquidating at constant speed. Indeed, over the first day she liquidates at a speed visibly larger than, for example, the one employed over the last day. Such an intense liquidation in the first day generates an equally large alpha-signal through the corresponding price impact term $\kappa_0 \nu_t^{0,*}$. In the first day, the market impact-generated signal $\kappa_0 \nu_t^{0,*}$ is large enough to outweigh any realistic realisation of the exogenous signal μ_t, therefore, pushing the minor agent to trade in the same direction of the major agent, independently of the trading style she will adopt later on in the remaining days.

It is of practical interest to compare the financial performance of the major agent's optimal strategy $\nu^{0,*}$ against those of the benchmark strategy $\nu^{0,\mathrm{BM}}$. In the interest of brevity, we limit ourselves to the case of the single-day liquidation presented in Figure 2.3. In Figure 2.5 we present a histogram of the empirical probability distribution of the performance of the major agent's optimal strategy in (2.3.15) relative to the benchmark strategy in (2.4.7) generated using 1,000 simulations. We compare the profit-and-loss (PnL) of the strategies in basis points

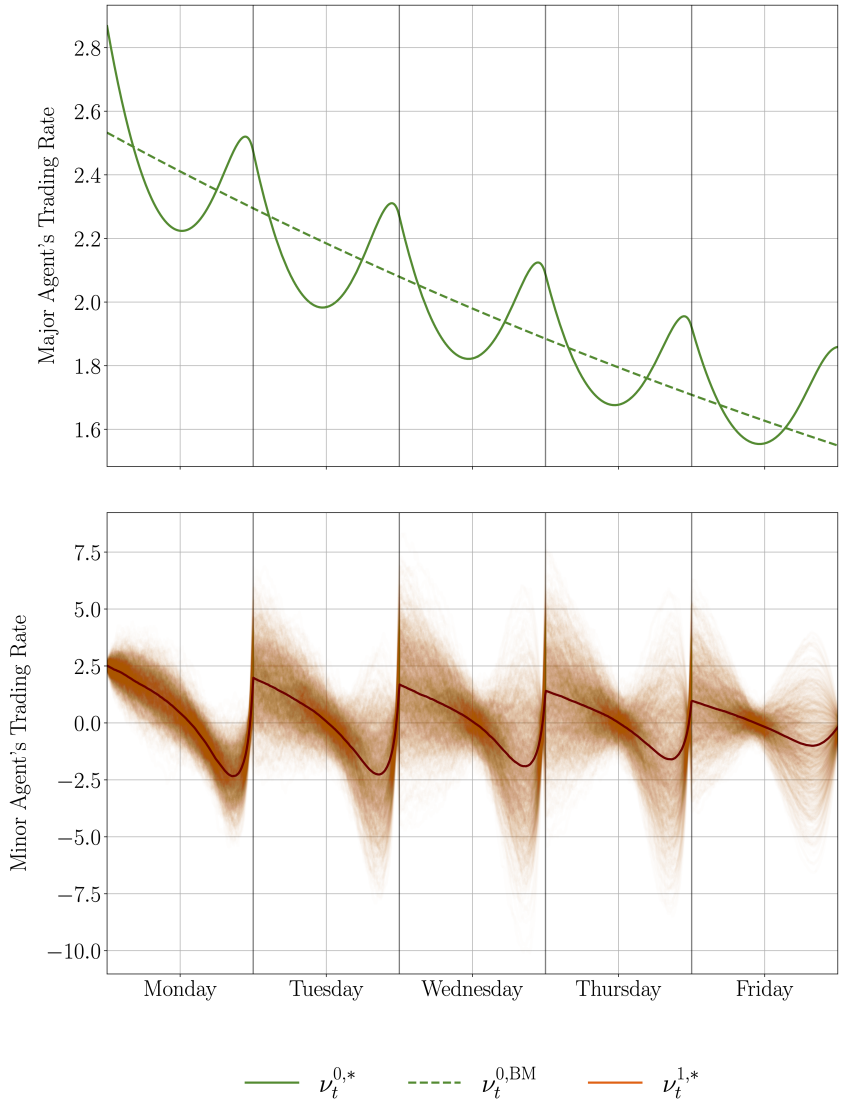

Figure 2.4: We present the major agent's and minor agent's optimal strategy in (2.3.15) and (2.3.6), respectively, for a multi-day liquidation. In the top panel, the green solid line shows the major agent's optimal strategy while the dashed green line shows the benchmark strategy of (2.4.7). In the bottom panel, the thin orange solid lines depicts different realisations of the minor agent's optimal strategy while the brown solid line represents the cross-sectional mean over the realisations.

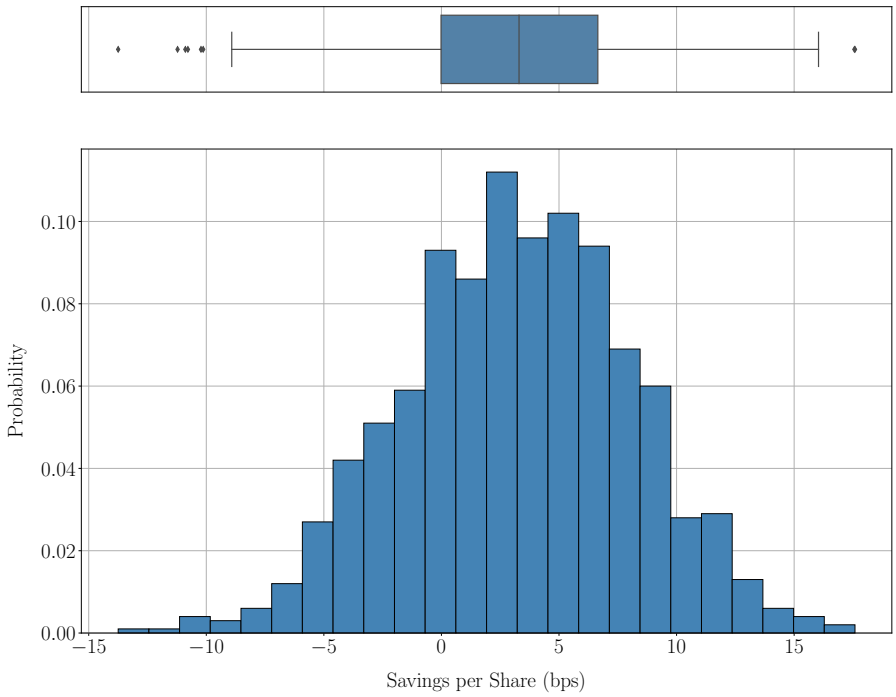

Figure 2.5: The savings per share, computed using (2.4.8), measured in basis points (bps) from following the major agent's optimal strategy relative to the benchmark strategy in (2.4.7). The top panel shows the box-plot corresponding to the distribution in the bottom panel.

(bps) through the following formula:

$$\frac{X_T^{0,\nu^{0,*}} - X_T^{0,\nu^{0,\mathrm{BM}}}}{X_T^{0,\nu^{0,\mathrm{BM}}}} \times 10^4, \tag{2.4.8}$$

where $X_T^{0,\nu^{0,\mathrm{BM}}}$ is the terminal cash obtained from employing the benchmark strategy $\nu^{0,\mathrm{BM}}$ and $X_T^{0,\nu^{0,*}}$ is the terminal cash obtained from employing the optimal strategy $\nu_t^{0,*}$. Notice that in the computation of $X_T^{0,\nu^{0,\mathrm{BM}}}$ we assume that the minor agent is still present in the market, she can still affect the major agent's execution price via her permanent price impact and that she adopts the optimal strategy $\nu^{1,*}(\nu^{0,\mathrm{BM}})$. The mean of the distribution in Figure 2.5 is strictly positive, hence the major agent's optimal strategy on average outperforms the benchmark strategy.

Finally, we show that the major agent's and minor agent's trading behaviour induces noteworthy patterns in the intraday volume. A well-known empirical pattern of intraday volume is that it follows a U-shaped curve, where the traded volume

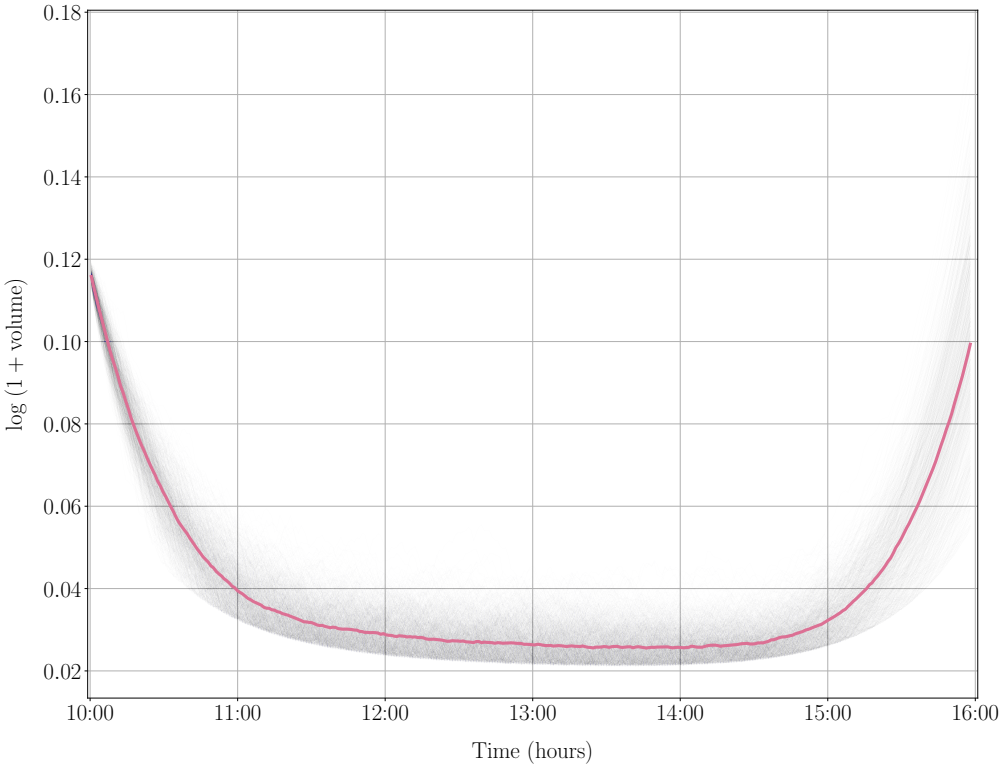

Figure 2.6: Intraday volume curve as a function of the time of day. Realisations of the volume curves are represented by blue lines, while the cross-sectional median is drawn in pink.

peaks at the beginning of the day and at the end of the day, see for example (Cartea et al., 2015, Chapter 4, Figure 4.2). In Figure 2.6 we present the intraday volume curve implied by the major agent's and minor agent's trading behaviour. Specifically, we simulate 1000 realisation of the minor agent's trading strategy and for each realisation we consider the absolute number of shares traded by the minor agent and the major agent over 1 minute bins from 10 AM to 4 PM. We call this quantity the "volume" traded in each minute bin. Then, we compute the natural logarithm of 1 + volume, where adding 1 allows to consider assets whose traded volume is a fraction of a share. Our procedure is completely analogous to the one described in Cartea et al. (2015). Each blue line in Figure 2.6 represents a realisation of the log-volume, while the magenta line is the median value of each 1-minute bin. The volume curves of Figure 2.6 visibly present a U-shaped pattern analogous, for example, to those empirically observed and reported in Cartea et al. (2015).

2.5 Numerical Scheme

Theorem 2.3.5 presents the unique major agent optimal strategy $\nu^{0,*}$ in closed-form. The optimal strategy $\nu^{0,*}$ is expressed in terms of the resolvent operator R, defined in (2.3.13), which in turn relies on the eigenvalues $(\zeta_n)_{n\geq 1}$ and eigenfunctions $(\psi_n)_{n\geq 1}$ of the operator G defined in (2.3.11). In several simple cases these eigenfunctions and eigenvalues can be computed explicitly.

For example, in the case of $\phi^1 \equiv 0$, $(\zeta_n)_{n\geq 1}$ and $(\psi_n)_{n\geq 1}$ can be explicitly determined in terms of the roots of a transcendental equation (see Appendix A.1). Nevertheless, a closed-form representation for the eigenvalues $(\zeta_n)_{n\geq 1}$ and the eigenfunctions $(\psi_n)_{n\geq 1}$ might be unattainable when ϕ^1 is a generic non-negative piecewise continuous function. Therefore, we dedicate this section to developing a numerical scheme to compute the major agent optimal strategy $\nu^{0,*}$ which fully bypass the need of determining these eigenvalues and eigenfunctions. As a by product, such numerical scheme will also determine the Stackelberg equilibrium of Corollary 2.3.6.

We denote by I the identity operator on $L^2([0,T])$, that is

$$(\mathsf{I}\psi)(t) = \psi(t) \quad \text{for all } 0 \leq t \leq T,\ \psi \in L^2([0,T]). \tag{2.5.1}$$

As usual, the resolvent operator in (2.3.14) can be written as

$$\mathsf{R} = \left(\mathsf{I} + \frac{\kappa_1\kappa_0}{2\lambda_0\lambda_1}\mathsf{G}\right)^{-1}.$$

This is proved rigorously in Proposition 2.7.9. It follows that the major agent optimal strategy $\nu^{0,*}$ in (2.3.15) satisfies to the following integral operator equation

$$\left(\mathsf{I} + \frac{\kappa_1\kappa_0}{2\lambda_0\lambda_1}\mathsf{G}\right)\nu^{0,*} = \mathsf{S}\bar{\mu} + \frac{\eta}{2\lambda_0}, \tag{2.5.2}$$

Here, the constant η is defined as in (2.3.16) and the operators G and S are defined as in (2.3.11) and (2.3.12), respectively. The idea is to replace (2.5.2) with a sequence of approximate equations (see (2.5.8)) whose solutions converge to the

desired optimal strategy $\nu^{0,*}$.

For the discussion that follows it is convenient to recall the definition of a finite-rank operator and that of a compact operator, which we will provide in Definition 2.7.2. In Proposition 2.7.4 we will show that the operator G is compact. Therefore, there exists a sequence of finite-rank operator $(\mathsf{G}_n)_{n\geq 1}$ in $B(L^2([0,T]))$ satisfying the approximation property

$$\lim_{n\to\infty} ||\mathsf{G}_n - \mathsf{G}|| = 0,$$

where $\|\cdot\|$ refers to the operator norm in (2.3.9).

In order to construct such sequence, we consider a complete orthonormal basis $(a_i)_{i=1}^{\infty}$ in $L^2([0,T])$. A possible choice of such complete orthonormal basis in $L^2([0,T])$ is given by (2.4.5).

Let the kernel $\mathcal{G}$ be defined as in (2.3.10) and let the functions $(b_i)_{i=1}^{\infty}$ be defined as

$$b_i(t) := \int_0^T \mathcal{G}(t,s)a_i(s)ds. \tag{2.5.3}$$

We recall the definition of a degenerate kernel (Porter and Stirling, 1990, Definition 3.1) which will be useful in the following.

Definition 2.5.1 (Degenerate Kernel)**.** *Let $n \geq 1$ and suppose there are finitely many functions $(a_i)_{i=1}^n$ and $(b_i)_{i=1}^n$ such that $a_i : [0,T] \to \mathbb{R}$ and $b_i : [0,T] \to \mathbb{R}$ for $i = 1,\dots,n$. Assume further that $\mathcal{T} : [0,T]^2 \to \mathbb{R}$ is a kernel such that*

$$\mathcal{T}(t,s) = \sum_{i=1}^{n} a_i(t)b_i(s), \quad t,s \in [0,T].$$

Then, the kernel $\mathcal{T}$ is said to be degenerate.

Define the sequence of degenerate kernels $(\mathcal{G}_n)_{n\geq 1}$ as the partial sums

$$\mathcal{G}_n(t,s) := \sum_{i=1}^{n} a_i(t)b_i(s), \quad n \geq 1. \tag{2.5.4}$$

Since $\mathcal{G}$ is a kernel in $L^2([0,T]^2)$ (see Proposition 2.8.1) then, as shown in the proof of (Porter and Stirling, 1990, Theorem 3.4), the sequence $(\mathcal{G}_n)_{n\geq 1}$ converges to $\mathcal{G}$ in the sense

$$\lim_{n\to\infty} \int_0^T \int_0^T (\mathcal{G}(t,s) - \mathcal{G}_n(t,s))^2 ds dt = 0. \tag{2.5.5}$$

Given the degenerate kernels $(\mathcal{G}_n)_{n\geq 1}$ we can define a corresponding sequence of so-called finite rank integral operators $(\mathsf{G}_n)_{n\geq 1}$ as

$$(\mathsf{G}_n\psi)(t) := \int_0^T \mathcal{G}_n(t,s)\psi(s)ds, \quad \psi \in L^2([0,T]). \tag{2.5.6}$$

The following proposition, which is proved in Section 2.10, gives the convergence result for the sequence $(\mathsf{G}_n)_{n\geq 1}$.

Proposition 2.5.2. *Under Assumption 2.3.1, let $(\mathsf{G}_n)_{n\geq 1}$ be defined as in (2.5.6) and let G be defined as in (2.3.11). Then the finite rank operators G_n are in $B(L^2([0,T]))$. Moreover, we have that*

$$\lim_{n\to\infty} ||\mathsf{G}_n - \mathsf{G}|| = 0. \tag{2.5.7}$$

Next, we consider the following sequence of approximate equations to (2.5.2),

$$\left(\mathsf{I} + \frac{\kappa_1\kappa_0}{2\lambda_0\lambda_1}\mathsf{G}_n\right)\nu^{0,(n)} = \mathsf{S}\bar{\mu} + \frac{\eta_n}{2\lambda_0}, \quad n \geq 1, \tag{2.5.8}$$

for a suitably defined sequence of constants $(\eta_n)_{n\geq 1}$.

Remark 2.5.3. *We remark that in (2.5.8) we continue to take the operator S to be defined in terms of G, as in (2.3.12), and not in terms of the sequence $(\mathsf{G}_n)_{n\geq 1}$. It is not necessary to approximate the operator S since it can be explicitly expressed in terms of the kernel $\mathcal{G}$ in (2.3.10), via the operator G, therefore, it can be computed explicitly via numerical integration (see also Remark 2.5.8).*

A solution to (2.5.8) exists if the inverse of the operator $\mathsf{I} + \frac{\kappa_1\kappa_0}{2\lambda_0\lambda_1}\mathsf{G}_n$ exists, with

the candidate solution $\nu^{0,(n)}$ being given by

$$\nu^{0,(n)} = \left(\mathsf{I} + \frac{\kappa_1\kappa_0}{2\lambda_0\lambda_1}\mathsf{G}_n\right)^{-1}\left(\mathsf{S}\bar{\mu} + \frac{\eta_n}{2\lambda_0}\right). \tag{2.5.9}$$

The next result shows that for sufficiently large n, the inverse of $\mathsf{I} + \frac{\kappa_1\kappa_0}{2\lambda_0\lambda_1}\mathsf{G}_n$ exists. Moreover, we show that the problem of finding such inverse is reduced to the finite dimensional problem of matrix inversion.

To state our results it is convenient to introduce the sequence of matrices $(\mathbb{G}_n)_{n\geq 1}$ where $\mathbb{G}_n \in \mathbb{R}^{n\times n}$ and whose entries are defined as

$$(\mathbb{G}_n)_{ij} := \langle a_i, b_j\rangle_{L^2} \tag{2.5.10}$$

for all $1 \leq i, j \leq n$ and with a_i and b_j defined as in (2.5.3). Moreover, we will denote by I_n the n-dimensional identity matrix, that is $I_n := \mathrm{diag}(1, \ldots, 1) \in \mathbb{R}^{n\times n}$.
We are now ready to state our next proposition, which is proved in Section 2.10.

Proposition 2.5.4. *Under Assumption 2.3.1, let $(\mathsf{G}_n)_{n\geq 1}$ be defined as in (2.5.6) and let $(\mathbb{G}_n)_{n\geq 1}$ be defined as in (2.5.10). Then, there exists $N \geq 1$ such that for all $n \geq N$ the operator $\mathsf{I} + \frac{\kappa_1\kappa_0}{2\lambda_0\lambda_1}\mathsf{G}_n$ and the matrix $I_n + \frac{\kappa_1\kappa_0}{2\lambda_0\lambda_1}\mathbb{G}_n$ are both invertible. In particular, for all $n \geq N$ it holds that*

$$\left(\mathsf{I} + \frac{\kappa_1\kappa_0}{2\lambda_0\lambda_1}\mathsf{G}_n\right)^{-1}\psi = \psi - \frac{\kappa_1\kappa_0}{2\lambda_0\lambda_1}\sum_{i,j=1}^{n}\left(I_n + \frac{\kappa_1\kappa_0}{2\lambda_0\lambda_1}\mathbb{G}_n\right)^{-1}_{i,j}\langle\psi, b_j\rangle_{L^2}\ a_i, \tag{2.5.11}$$

for any $\psi \in L^2([0,T])$.

Note that both operators $\mathsf{I}+\frac{\kappa_1\kappa_0}{2\lambda_0\lambda_1}\mathsf{G}$ and $\mathsf{I}+\frac{\kappa_1\kappa_0}{2\lambda_0\lambda_1}\mathsf{G}_n$ are invertible (see Proposition 2.7.17), nevertheless, only in the case of the latter the inverse operator can be computed via matrix inversion by exploiting the corresponding degenerate kernel decomposition, see also Remark 2.5.8 for additional discussion.

The next result shows that that the candidate solutions in (2.5.9) converge *in mean* to the optimal strategy $\nu^{0,*}$ of Theorem 2.3.5. Henceforth, we take the

sequence of constants $(\eta_n)_{n\geq 1}$ to be defined as

$$\eta_n := 2\lambda_0 \frac{q_0 - \left\langle \left(\mathsf{I} + \frac{\kappa_1\kappa_0}{2\lambda_0\lambda_1}\mathsf{G}_n\right)^{-1} \mathsf{S}\bar{\mu}, 1 \right\rangle_{L^2}}{\left\langle \left(\mathsf{I} + \frac{\kappa_1\kappa_0}{2\lambda_0\lambda_1}\mathsf{G}_n\right)^{-1} 1, 1 \right\rangle_{L^2}}, \quad n \geq 1. \tag{2.5.12}$$

Proposition 2.5.5. *Under Assumption 2.3.1, let $\nu^{0,*}$ and $\nu^{0,(n)}$ be defined as in (2.3.15) and (2.5.9), respectively. Then, there exists $N \geq 1$ such that for all $n \geq N$ the functions $\nu^{0,(n)}$ are well-defined and are in $L^2([0,T])$. Moreover,*

$$\lim_{n\to\infty} \left\| \nu^{0,*} - \nu^{0,(n)} \right\|_{L^2} = 0. \tag{2.5.13}$$

The proof of Proposition 2.5.5 is postponed to Section 2.10. Lemma 2.10.4 shows that for sufficiently large n, the constants η_n in (2.5.12) are well-defined.

In order to obtain an approximating sequence which converges *uniformly* to the optimal control $\nu^{0,*}$ we introduce the sequence of candidate functions $(\hat{\nu}^{0,(n)})_{n\geq 1}$ defined as

$$\hat{\nu}_t^{0,(n)} := -\frac{\kappa_1\kappa_0}{2\lambda_0\lambda_1} \left(\mathsf{G}\nu^{0,(n)}\right)(t) + (\mathsf{S}\bar{\mu})(t) + \frac{\eta_n}{2\lambda_0} \tag{2.5.14}$$

for all $t \in [0,T]$ and for all $n \geq 1$. Our main result for this section is the following convergence theorem.

Theorem 2.5.6. *Under Assumption 2.3.1, let $\nu^{0,*}$, $\hat{\nu}^{0,(n)}$ and $\nu^{1,*}$ be defined as in (2.3.15), (2.5.14) and (2.3.6), respectively. Then, there exists an $N \geq 1$ such that for all $n \geq N$ the functions $\hat{\nu}^{0,(n)}$ are in $L^2([0,T])$ and the controls $\nu^{1,*}(\hat{\nu}^{0,(n)})$ are in $\mathcal{A}_m$. Furthermore, we have that:*

(i)

$$\lim_{n\to\infty} \sup_{t\in[0,T]} \left| \nu_t^{0,*} - \hat{\nu}_t^{0,(n)} \right| = 0,$$

(ii)

$$\lim_{n\to\infty} \sup_{t\in[0,T]} \left| \nu_t^{1,*}\left(\nu^{0,*}\right) - \nu_t^{1,*}\left(\hat{\nu}^{0,(n)}\right) \right| = 0, \quad \mathbb{P}-\text{a.s.}$$

The proof of Theorem 2.5.6 is postponed to Section 2.10.

Proposition 2.5.4 and Theorem 2.5.6 show that the infinite-dimensional problem of determining the solution to (2.5.2), can be reduced to the finite-dimensional problem of matrix inversion.

Remark 2.5.7. *The proofs of the results of Proposition 2.5.5 and Theorem 2.5.6 do not rely on the existence of the orthonormal expansion in* (2.5.4) *and the corresponding convergence* (2.5.5)*. Indeed, our result can be extended to any generic sequence of operators* $(\mathsf{G}_n)_{n\geq 1}$ *in* $B(L^2([0,T]))$ *satisfying the approximation property of Proposition 2.5.2 and which do not necessarily enjoy a integral representation of the form in* (2.5.6)*.*

Remark 2.5.8. *The matrix entries in* (2.5.10) *must be computed numerically. The use of a numerical evaluation in* (2.5.10) *will lead to numerical errors in the entries of the matrix* $I_n + \frac{\kappa_1\kappa_0}{2\lambda_0\lambda_1}\mathbb{G}_n$*. As shown in (Atkinson, 1997, Chapter 2.3.4), for a sufficiently accurate estimation the numerical error arising from these computations is negligible. A similar discussion applies to, among others, the numerical evaluation of the inverse of the matrix* $I_n + \frac{\kappa_1\kappa_0}{2\lambda_0\lambda_1}\mathbb{G}_n$ *and of the integral* $\mathsf{S}\bar{\mu}$*. These are all elementary and well-understood convergence problems in numerical analysis and the corresponding convergence rate could be easily incorporated in the convergence results of this section. Hence, our discussion assumes that the aforementioned quantities are taken to be exact and that the corresponding numerical errors are negligible.*

Remark 2.5.9. *The numerical scheme we have presented has an advantage from an implementation standpoint too. Specifically, if one were to determine the major agent's optimal strategy by using the result of Theorem 2.3.5, she would need to mathematically determine the eigenvalues* $(\zeta_n)_{n\geq 1}$ *and eigenfunctions* $(\psi_n)_{n\geq 1}$ *each time she wishes to change the function* ϕ^1*, as shown, for example, in Appendix A.1. On the other hand, with the numerical scheme of Theorem 2.5.6, to achieve the same goal it is sufficient to change the expression of* ϕ^1 *in the numerical solver of the Riccati ODE* (2.3.2)*, which usually amounts to change solely few lines of code.*

2.6 Proof of Theorem 2.3.2

We show how the Stackelberg equilibrium can be found by *backward induction*, that is by first solving the minor agent's problem and then the major agent's problem. We determine the minor agent's optimal strategy via a calculus of variations argument, as similarly done in Neuman and Voß (2022). The following results also borrow ideas from Casgrain and Jaimungal (2019).

Henceforth, we assume that $\nu^0 \in \mathcal{A}_M^{q_0}$ is a fixed major agent liquidation strategy and with a slight abuse of notation we write $H^1(\nu)$ for $H^1(\nu;\nu^0)$. We start by determining an alternative representation for the minor agent's objective.

Lemma 2.6.1. *The minor agent's objective H^1 in (2.2.13) can be alternatively represented as*

$$\begin{aligned} H^1(\nu^1) = x_1 - \mathbb{E}\Bigg[\lambda_1 \int_0^T (\nu_t^1)^2 dt + \alpha \left(Q_T^{1,\nu^1}\right)^2 + \int_0^T \phi_t^1 \left(Q_t^{1,\nu^1}\right)^2 dt \\ + \int_0^T Q_t^{1,\nu^1}(\kappa_0 \nu_t^0 dt + \kappa_1 \nu_t^1 dt - dA_t)\Bigg], \end{aligned} \tag{2.6.1}$$

for any $\nu^1 \in \mathcal{A}_m$.

Proof. We use (2.2.12), (2.2.11) and the Itô's product rule on $Q_T^{1,\nu^1} P_T^\nu$ to get

$$\begin{aligned} &\mathbb{E}\left[X_T^{1,\nu^1} + Q_T^{1,\nu^1} P_T^\nu\right] \\ &= x_1 + \mathbb{E}\left[\int_0^T (P_t^\nu - \lambda_1 \nu_t^1)\nu_t^1 dt + \int_0^T Q_t^{1,\nu^1} dP_t^\nu + \int_0^T P_t^\nu dQ_t^{1,\nu^1}\right], \end{aligned} \tag{2.6.2}$$

where we also used $Q_0^{1,\nu^1} = 0$ by (2.2.5). Recall that $P = M + A$. We apply (2.2.5),

(2.2.6) and (2.2.7) to (2.6.2) in order to obtain

$$\begin{aligned}\mathbb{E}\left[X_T^{1,\nu^1}+Q_T^{1,\nu^1}P_T^{\nu}\right] &= x_1+\mathbb{E}\bigg[-\lambda_1\int_0^T(\nu_t^1)^2dt+\int_0^T Q_t^{1,\nu^1}dP_t^{\nu}\bigg]\\ &= x_1-\mathbb{E}\bigg[\lambda_1\int_0^T(\nu_t^1)^2dt-\int_0^T Q_t^{1,\nu^1}dM_t\\ &\qquad+\int_0^T Q_t^{1,\nu^1}(\kappa_0\nu_t^0dt+\kappa_1\nu_t^1dt-dA_t)\bigg].\end{aligned}\tag{2.6.3}$$

Since $\nu^1\in\mathcal{A}_m$ (see (2.2.4)), then we can drop the martingale term in (2.6.3) and obtain

$$\begin{aligned}\mathbb{E}\left[X_T^{1,\nu^1}+Q_T^{1,\nu^1}P_T^{\nu}\right] &= x_1-\mathbb{E}\bigg[\lambda_1\int_0^T(\nu_t^1)^2dt\\ &\qquad+\int_0^T Q_t^{1,\nu^1}(\kappa_0\nu_t^0dt+\kappa_1\nu_t^1dt-dA_t)\bigg].\end{aligned}\tag{2.6.4}$$

Substituting (2.6.4) in (2.2.13) returns (2.6.1). □

In the next result we use the representation of (2.6.1) to show that the minor agent's objective is strictly concave.

Lemma 2.6.2. *Under Assumption 2.3.1, the functional H^1 defined in (2.2.13) is strictly concave for $\nu^1\in\mathcal{A}_m$.*

Proof. In order to prove that the functional H^1 is strictly concave, we must show that for any $0<\rho<1$ and $\nu,\omega\in\mathcal{A}_m$, such that ν and ω are $d\mathbb{P}\otimes dt$ distinguishable, it holds that

$$\mathcal{I}^1(\rho,\nu,\omega):=H^1(\rho\nu+(1-\rho)\omega)-\rho H^1(\nu)-(1-\rho)H^1(\omega)>0.\tag{2.6.5}$$

It is convenient to introduce the constant $\theta:=\frac{2\alpha-\kappa_1}{2}$ as well as to define the function Γ^1 as follows

$$\Gamma_t^1=\begin{pmatrix}\lambda_1 & -\theta\\ -\theta & \phi_t^1\end{pmatrix},\quad 0\le t\le T.\tag{2.6.6}$$

Note that under Assumption 2.3.1 it holds that $\theta \geq 0$. From (2.2.5) and integration by parts we get

$$\left(Q_T^{1,\nu^1}\right)^2 = -2\int_0^T Q_t^{1,\nu^1}\nu_t^1 dt. \tag{2.6.7}$$

Using (2.6.7) we rewrite the minor agent's objective in (2.6.1) in terms of the function Γ^1 as

$$H^1(\nu^1) = x_1 - \mathbb{E}\left[\int_0^T \begin{pmatrix} \nu_t^1 \\ Q_t^{1,\nu^1} \end{pmatrix}^\intercal \Gamma_t^1 \begin{pmatrix} \nu_t^1 \\ Q_t^{1,\nu^1} \end{pmatrix} dt + \int_0^T Q_t^{1,\nu^1}(\kappa_0 \nu_t^0 dt - dA_t)\right]. \tag{2.6.8}$$

Note that, given the representation in (2.6.8), in the case of $\theta > 0$ and $\phi_t^1 > 0$ for all $t \in [0,T]$ the strict concavity of $H^1(\nu^1)$ follows from (2.2.5) and the fact that Γ_t^1 is a positive-definite matrix for all $t \in [0,T]$. In what follows we will use (2.6.8) to show that $H^1(\nu^1)$ is strictly concave also under the assumption that $\phi_t^1 \geq 0$ and $\theta \geq 0$.

We observe that $Q^{1,\nu}$ is linear with respect to ν, that is

$$Q_t^{1,\rho\nu+(1-\rho)\omega} = \rho Q_t^{1,\nu} + (1-\rho)Q_t^{1,\omega} \quad \text{for all } \rho \in [0,1],\ \nu, \omega \in \mathcal{A}_m.$$

We substitute (2.6.8) in (2.6.5) and we use the linearity of $Q^{1,\cdot}$ to cancel out the $Q_t^{1,\cdot}(\kappa_0\nu_t^0 dt - dA_t)$ terms. This yields

$$\begin{aligned}\mathcal{I}^1(\rho,\nu,\omega) = \mathbb{E}\Bigg[\int_0^T &\rho \begin{pmatrix} \nu_t \\ Q_t^{1,\nu} \end{pmatrix}^\intercal \Gamma_t^1 \begin{pmatrix} \nu_t \\ Q_t^{1,\nu} \end{pmatrix} dt + (1-\rho)\begin{pmatrix} \omega_t \\ Q_t^{1,\omega} \end{pmatrix}^\intercal \Gamma_t^1 \begin{pmatrix} \omega_t \\ Q_t^{1,\omega} \end{pmatrix} dt \\ &- \left(\rho\begin{pmatrix} \nu_t \\ Q_t^{1,\nu} \end{pmatrix} + (1-\rho)\begin{pmatrix} \omega_t \\ Q_t^{1,\omega} \end{pmatrix}\right)^\intercal \Gamma_t^1 \left(\rho\begin{pmatrix} \nu_t \\ Q_t^{1,\nu} \end{pmatrix} + (1-\rho)\begin{pmatrix} \omega_t \\ Q_t^{1,\omega} \end{pmatrix}\right) dt\Bigg],\end{aligned}$$

where after multiplying out all the terms we get

$$\begin{aligned}&\mathcal{I}^1(\rho,\nu,\omega) = \\ &\mathbb{E}\left[\int_0^T \rho(1-\rho)\left(\begin{pmatrix} \nu_t \\ Q_t^{1,\nu} \end{pmatrix} - \begin{pmatrix} \omega_t \\ Q_t^{1,\omega} \end{pmatrix}\right)^\intercal \Gamma_t^1 \left(\begin{pmatrix} \nu_t \\ Q_t^{1,\nu} \end{pmatrix} - \begin{pmatrix} \omega_t \\ Q_t^{1,\omega} \end{pmatrix}\right) dt\right].\end{aligned} \tag{2.6.9}$$

It is convenient to introduce the function $\delta_t := \nu_t - \omega_t$ for all $t \in [0,T]$. From (2.2.5) it follows that $Q_t^{1,\delta} = Q_t^{1,\nu} - Q_t^{1,\omega}$ for all $t \in [0,T]$. We can rewrite (2.6.9) in terms of δ and $Q^{1,\delta}$ as

$$\begin{aligned}\mathcal{I}^1(\rho,\nu,\omega) = \rho(1-\rho)\Big(\mathbb{E}\left[\int_0^T \lambda_1 \delta_t^2 dt\right] + \mathbb{E}\left[\int_0^T \phi_t^1 \left(Q_t^{1,\delta}\right)^2 dt\right] \\ - \mathbb{E}\left[\int_0^T 2\theta \delta_t Q_t^{1,\delta} dt\right]\Big),\end{aligned} \tag{2.6.10}$$

where we have used (2.6.6).

Since $\phi_t^1 \geq 0$ for all $t \in [0,T]$, we have

$$\mathbb{E}\left[\int_0^T \phi_t^1 \left(Q_t^{1,\delta}\right)^2 dt\right] \geq 0.$$

From (2.2.5) it holds that $Q_t^{1,\delta} = -\int_0^t \delta_t dt$, therefore by (2.6.7) we get

$$-\mathbb{E}\left[\int_0^T 2\delta_t Q_t^{1,\delta} dt\right] = \mathbb{E}\left[\left(Q_T^{1,\delta}\right)^2\right] \geq 0. \tag{2.6.11}$$

Finally, notice that since ν and ω are $d\mathbb{P} \otimes dt$ distinguishable then

$$\mathbb{E}\left[\int_0^T \delta_t^2 dt\right] > 0.$$

This shows that $\mathcal{I}^1(\rho,\nu,\omega) > 0$ for any $\theta \geq 0$, $0 < \rho < 1$ and any $\nu, \omega \in \mathcal{A}_m$, such that ν and ω are $d\mathbb{P} \otimes dt$ distinguishable. □

As similarly show in Neuman and Voß (2022), a probabilistic and convex analytic calculus of variations approach can be readily applied to derive a system of coupled linear FBSDEs which characterises the unique solution to the minor agent's problem.

Since under Assumption 2.3.1 the map $\nu^1 \to H^1(\nu^1)$ in (2.6.1) is strictly concave, then it admits a unique maximiser characterised by the critical point at which

the Gâteaux derivative

$$\langle \mathcal{D}H^1(\nu^1), \omega \rangle := \lim_{\epsilon \to 0} \frac{H^1(\nu^1 + \epsilon\omega) - H^1(\nu^1)}{\epsilon} \tag{2.6.12}$$

vanishes. In the following lemma we obtain an explicit expression for the Gâteaux derivative of H^1.

Lemma 2.6.3. *The Gâteaux derivative of H^1 in (2.6.1), in direction $\omega \in \mathcal{A}_m$ is given by*

$$\begin{aligned}\big\langle \mathcal{D}H^1(\nu^1), \omega \big\rangle = \mathbb{E}\Bigg[\int_0^T \omega_t \Big(&- 2\lambda_1 \nu_t^1 + 2\alpha Q_T^{1,\nu^1} - \kappa_1 Q_t^{1,\nu^1} + A_t \\ &+ \int_t^T \Big(2\phi_s^1 Q_s^{1,\nu^1} + \kappa_0 \nu_s^0 + \kappa_1 \nu_s^1 \Big)\, ds - A_T \Big) dt \Bigg],\end{aligned} \tag{2.6.13}$$

for any $\nu^1 \in \mathcal{A}_m$.

Proof. Let $\epsilon > 0$ and $\nu^1, \omega \in \mathcal{A}_m$. We note that from (2.2.5) it follows that

$$Q_t^{1,\nu^1+\epsilon\omega} = Q_t^{1,\nu^1} - \epsilon \int_0^t \omega_s ds, \quad \text{for all } 0 \le t \le T. \tag{2.6.14}$$

We use the alternative representation of H^1 in (2.6.1) and (2.6.14) to get

$$\begin{aligned}H^1(\nu^1 + \epsilon\omega) - H^1(\nu^1) = \epsilon\mathbb{E}\Bigg[&\int_0^T \omega_t(-2\lambda_1 \nu_t^1 + 2\alpha Q_T^{1,\nu^1} - \kappa_1 Q_t^{1,\nu^1}) dt \\ &+ \int_0^T \left(\int_0^t \omega_s ds \right) (2\phi_t^1 Q_t^{1,\nu^1} dt + \kappa_0 \nu_t^0 dt + \kappa_1 \nu_t^1 dt - dA_t) \Bigg] \\ &+ \epsilon^2 \mathbb{E}\Bigg[- \lambda_1 \int_0^T \omega_s^2 ds - \alpha \left(\int_0^T \omega_s ds \right)^2 \\ &- \int_0^T \phi_t^1 \left(\int_0^t \omega_s ds \right)^2 dt + \kappa_1 \int_0^T \omega_t \left(\int_0^t \omega_s ds \right) dt \Bigg].\end{aligned} \tag{2.6.15}$$

From (2.6.12) and (2.6.15) we get

$$\langle \mathcal{D}H^1(\nu^1), \omega \rangle = \mathbb{E}\Bigg[\int_0^T \omega_t(-2\lambda_1 \nu_t^1 + 2\alpha Q_T^{1,\nu^1} - \kappa_1 Q_t^{1,\nu^1})dt \\ + \int_0^T \left(\int_0^t \omega_s ds \right) (2\phi_t^1 Q_t^{1,\nu^1} dt + \kappa_0 \nu_t^0 dt + \kappa_1 \nu_t^1 dt - dA_t) \Bigg]. \tag{2.6.16}$$

Since $\nu^1, \omega \in \mathcal{A}_m$, $\nu^0 \in \mathcal{A}_M^{q_0}$ and $\mathbb{E}[(\int_0^T |dA_t|)^2] < \infty$, then use Fubini's theorem in (2.6.16) to get

$$\langle \mathcal{D}H^1(\nu^1), \omega \rangle = \mathbb{E}\Bigg[\int_0^T \omega_t \Big(-2\lambda_1 \nu_t^1 + 2\alpha Q_T^{1,\nu^1} - \kappa_1 Q_t^{1,\nu^1} + A_t \\ + \int_t^T \left(2\phi_s^1 Q_s^{1,\nu^1} + \kappa_0 \nu_s^0 + \kappa_1 \nu_s^1 \right) ds - A_T \Big) dt \Bigg],$$

which concludes the result. □

From the explicit expression of the Gâteaux derivative in (2.6.13) we can derive a first order optimality condition. It takes the form of a coupled system of linear forward backward stochastic differential equations (FBSDE), as described in following lemma.

Lemma 2.6.4. *Under Assumption 2.3.1, the control $\nu^{1,*} \in \mathcal{A}_m$ is the unique maximiser to the minor agent's objective functional H^1 in (2.6.1) if and only if the process $(Q^{1,\nu^{1,*}}, \nu^{1,*})$ satisfies the following coupled linear FBSDE system*

$$\begin{aligned} dQ_t^{1,\nu^{1,*}} &= -\nu_t^{1,*} dt, \quad Q_0^{1,\nu^{1,*}} = 0, \\ d\nu_t^{1,*} &= \frac{1}{2\lambda_1} d\mathcal{N}_t + \frac{1}{2\lambda_1} d\mathcal{M}_t - \frac{\phi_t^1}{\lambda_1} Q_t^{1,\nu^{1,*}} dt - \frac{\kappa_0}{2\lambda_1} \nu_t^0 dt + \frac{1}{2\lambda_1} dA_t, \\ \nu_T^{1,*} &= \frac{2\alpha - \kappa_1}{2\lambda_1} Q_T^{1,\nu^{1,*}} \end{aligned} \tag{2.6.17}$$

$d\mathbb{P} \otimes dt$-a.e. on $\Omega \times [0,T]$ where $\mathcal{M} = (\mathcal{M}_t)_{t\in[0,T]}$ and $\mathcal{N} = (\mathcal{N}_t)_{t\in[0,T]}$ are two suitable square integrable martingales.

Proof. In Lemma 2.6.2 we have shown that under Assumption 2.3.1, the functional

$H^1(\nu^1)$ is strictly concave of any $\nu^1 \in \mathcal{A}_m$. Therefore, we may apply Proposition 2.1 of (Ekeland and Témam, 1999, Chapter II) to obtain that

$$\langle \mathcal{D}H^1(\nu^{1,*}), \omega \rangle = 0 \quad \text{for all } \omega \in \mathcal{A}_m \iff \nu^{1,*} = \arg\sup_{\nu \in \mathcal{A}_m} H^1(\nu). \tag{2.6.18}$$

The strict concavity of H^1 guarantees that the optimiser $\nu^{1,*}$ is unique.

Necessity: We assume that

$$\nu^{1,*} = \arg\sup_{\nu \in \mathcal{A}_m} H^1(\nu).$$

Then, (2.6.18) and (2.6.13) imply that for all $\omega \in \mathcal{A}_m$ it holds

$$\begin{aligned}\langle \mathcal{D}H^1(\nu^{1,*}), \omega \rangle = \mathbb{E}\Bigg[\int_0^T \omega_t \Big(&- 2\lambda_1 \nu_t^{1,*} + 2\alpha Q_T^{1,\nu^{1,*}} - \kappa_1 Q_t^{1,\nu^{1,*}} + A_t \\ &+ \int_t^T \left(2\phi_s^1 Q_s^{1,\nu^{1,*}} + \kappa_0 \nu_s^0 + \kappa_1 \nu_s^{1,*} \right) ds - A_T \Big) dt \Bigg] = 0.\end{aligned}$$

By applying the optional projection theorem we get

$$\begin{aligned}\mathbb{E}\Bigg[\int_0^T \omega_t \Bigg(&- 2\lambda_1 \nu_t^{1,*} + \mathbb{E}_t \left[2\alpha Q_T^{1,\nu^{1,*}} - A_T \right] - \kappa_1 Q_t^{1,\nu^{1,*}} + A_t \\ &+ \mathbb{E}_t \left[\int_t^T \left(2\phi_s^1 Q_s^{1,\nu^{1,*}} + \kappa_0 \nu_s^0 + \kappa_1 \nu_s^{1,*} \right) ds \right] \Bigg) dt \Bigg] = 0, \end{aligned} \tag{2.6.19}$$

As (2.6.19) holds for all $\omega \in \mathcal{A}_m$ we deduce the following first order condition holds

$$\begin{aligned}&- 2\lambda_1 \nu_t^{1,*} + \mathbb{E}_t \left[2\alpha Q_T^{1,\nu^{1,*}} - A_T \right] - \kappa_1 Q_t^{1,\nu^{1,*}} + A_t \\ &\qquad + \mathbb{E}_t \left[\int_t^T \left(2\phi_s^1 Q_s^{1,\nu^{1,*}} + \kappa_0 \nu_s^0 + \kappa_1 \nu_s^{1,*} \right) ds \right] = 0, \end{aligned} \tag{2.6.20}$$

$d\mathbb{P} \otimes dt$-a.e. on $\Omega \times [0, T]$.

We define the following martingales

$$\begin{aligned}\mathcal{M}_t &:= \mathbb{E}_t\left[\int_0^T \left(2\phi_s^1 Q_s^{1,\nu^{1,*}} + \kappa_0\nu_s^0 + \kappa_1\nu_s^{1,*}\right) ds\right],\\ \mathcal{N}_t &:= \mathbb{E}_t\left[2\alpha Q_T^{1,\nu^{1,*}} - A_T\right].\end{aligned} \tag{2.6.21}$$

Note that $\mathcal{M}$ and $\mathcal{N}$ are square-integrable since $\mathbb{E}[(\int_0^T |dA_t|)^2] < \infty$, $\nu^{1,*}, \omega \in \mathcal{A}_m$ and $\nu^0 \in \mathcal{A}_M^{q_0}$.

We plug $\mathcal{M}$ and $\mathcal{N}$ in (2.6.20) to get

$$-2\lambda_1\nu_t^{1,*} + \mathcal{N}_t - \kappa_1 Q_t^{1,\nu^{1,*}} + A_t + \mathcal{M}_t - \int_0^t \left(2\phi_s^1 Q_s^{1,\nu^{1,*}} + \kappa_0\nu_s^0 + \kappa_1\nu_s^{1,*}\right) ds = 0, \tag{2.6.22}$$

From (2.2.5) and (2.6.22) it follows that $\nu^{1,*}$ solves the following BSDE

$$\begin{cases} d\nu_t^{1,*} &= \frac{1}{2\lambda_1} d\mathcal{N}_t + \frac{1}{2\lambda_1} d\mathcal{M}_t - \frac{1}{\lambda_1}\phi_t^1 Q_t^{1,\nu^{1,*}} dt - \frac{\kappa_0}{2\lambda_1}\nu_t^0 dt + \frac{1}{2\lambda_1} dA_t,\\ \nu_T^{1,*} &= \frac{2\alpha-\kappa_1}{2\lambda_1} Q_T^{1,\nu^{1,*}},\end{cases}$$

this gives (2.6.17).

Sufficiency: Assume that $(Q^{1,\nu^{1,*}}, \nu^{1,*})$ solves (2.6.17) $d\mathbb{P}\otimes dt$-a.e. and that $\nu^{1,*} \in \mathcal{A}_m$. We will show that $\langle \mathcal{D}H^1(\nu^{1,*}), \omega\rangle$ vanishes for all $\omega \in \mathcal{A}_m$ which, once combined with (2.6.18), implies that $\nu^{1,*}$ is the solution to the minor agent's problem. Since $(Q^{1,\nu^{1,*}}, \nu^{1,*})$ solves (2.6.17) we get that

$$\begin{aligned} 2\lambda_1\nu_t^{1,*} &= \mathbb{E}_t\left[(2\alpha-\kappa_1) Q_T^{1,\nu^{1,*}}\right] - \mathbb{E}_t\left[\int_t^T dA_s\right] + \mathbb{E}_t\left[\int_t^T \left(\kappa_0\nu_s^0 + 2\phi_t^1 Q_s^{1,\nu^{1,*}}\right) ds\right]\\ &= \mathbb{E}_t\left[2\alpha Q_T^{1,\nu^{1,*}} - A_T\right] - \kappa_1 Q_t^{1,\nu^{1,*}} + A_t\\ &\quad + \mathbb{E}_t\left[\int_t^T \left(\kappa_0\nu_s^0 + 2\phi_t^1 Q_s^{1,\nu^{1,*}} + \kappa_1\nu_s^{1,*}\right) ds\right], \quad d\mathbb{P}\otimes dt - \text{a.e.},\end{aligned} \tag{2.6.23}$$

where we used (2.2.5) in the second equality. Hence, $\nu_t^{1,*}$ satisfies (2.6.20), therefore the left-hand side of (2.6.18) hold. □

For the remainder of this section we focus on the derivation of the explicit

solution to (2.6.17). We first describe the heuristics of the proof.

Heuristics for the solution to (2.6.17). The solution to the FBSDE system (2.6.17) determines the solution to the minor agent's problem. The main obstacle in solving the system (2.6.17) is that it presents a general time dependent coefficient ϕ_t^1. In order to solve this equation, we formulate an ansatz for the minor agent's optimal strategy $\nu^{1,*}$. Then, we demonstrate that the ansatz solution for $\nu^{1,*}$ is the unique solution to (2.6.17) and therefore the solution to the minor agent's problem. Due to the linear structure of the system (2.6.17), we make the ansatz that there are two progressively measurable processes $r^0 = (r_t^0)_{t\in[0,T]}$ and $r^1 = (r_t^1)_{t\in[0,T]}$ such that $\nu^{1,*}$ can be expressed as

$$\nu_t^{1,*} = -\left(r_t^0 + r_t^1 Q_t^{1,\nu^{1,*}}\right), \quad 0 \leq t \leq T. \tag{2.6.24}$$

We differentiate (2.6.24) via Itô's lemma and by using $dQ_t^{1,\nu^{1,*}} = -\nu_t^{1,*}dt$ to get

$$d\nu_t^{1,*} = -dr_t^0 - dr_t^1 Q_t^{1,\nu^{1,*}} + \nu_t^{1,*} r_t^1 dt. \tag{2.6.25}$$

We plug (2.6.25) into (2.6.17) and we arrive at

$$\begin{aligned} 0 = &\left(2\lambda_1 dr_t^1 - 2\phi_t^1 dt + 2\lambda_1 (r_t^1)^2 dt\right) Q_t^{1,\nu^{1,*}} \\ &+ \left(2\lambda_1 dr_t^0 + 2\lambda_1 r_t^1 r_t^0 dt - \kappa_0 \nu_t^0 dt + dA_t + d\mathcal{M}_t + d\mathcal{N}_t\right). \end{aligned} \tag{2.6.26}$$

Equation (2.6.26) must hold $d\mathbb{P} \otimes dt$ almost everywhere for all values $Q_t^{1,\nu^{1,*}}$. We conjecture that the terms within each of the brackets must vanish independently. The terms from (2.6.26) yield to two coupled differential equations for r^0 and r^1 independent of the process $Q^{1,\nu^{1,*}}$, where we determine the terminal conditions from (2.6.17). Specifically, the process r^1 must satisfy dt-a.e. the following non-autonomous Riccati ODE

$$\partial_t r_t^1 = \frac{1}{\lambda_1}\phi_t^1 - (r_t^1)^2, \quad r_T^1 = -\frac{2\alpha - \kappa_1}{2\lambda_1}, \tag{2.6.27}$$

while r^0 must satisfy the following BSDE

$$-dr_t^0 = r_t^1 r_t^0 dt - \frac{\kappa_0}{2\lambda_1}\nu_t^0 dt + \frac{1}{2\lambda_1}dA_t + \frac{1}{2\lambda_1}d\mathcal{M}_t + \frac{1}{2\lambda_1}d\mathcal{N}_t, \quad r_T^0 = 0. \tag{2.6.28}$$

An explicit formula for the solution of (2.6.27) does not exist when ϕ_t^1 is a general piecewise continuous function as in the case at hand. Nevertheless, we will prove that the solution to (2.6.27) exists and it is unique. Once a solution to (2.6.27) is found, then we can plug it to (2.6.28) and derive r^0.

Our next result proves the existence and uniqueness of the solution to (2.6.27).

Lemma 2.6.5. *Under Assumption 2.3.1, the Riccati equation (2.6.27) has a unique continuous solution.*

Proof. Let $\hat{r}^1$ be the solution to the following equation

$$\begin{cases} \partial_t \hat{r}_t^1 &= -\frac{1}{\lambda_1}\phi_t^1 + (\hat{r}_t^1)^2, \quad 0 \le t \le T, \\ \hat{r}_T^1 &= \frac{2\alpha - \kappa_1}{2\lambda_1}. \end{cases} \tag{2.6.29}$$

Since, $\hat{r}_T^1 \ge 0$ and ϕ^1 is a piecewise continuous, locally bounded non-negative function over $[0,T]$, then by Theorem 2.1 of Wonham (1968) there exists a unique solution $\hat{r}^1$, which is absolutely continuous on $[0,T]$ (see also Theorem 3.5 in Freiling (2002) for a more recent reference). As stated by Wonham (1968), the function $\hat{r}^1$ satisfies (2.6.29) only dt almost everywhere. Note that by taking $r_t^1 = -\hat{r}_t^1$, it follows that r^1 is an absolutely continuous solution to (2.6.27). Uniqueness of the solution to (2.6.27) then follows by the uniqueness for (2.6.29). □

In order to prove the existence of a solution to the BSDE (2.6.28) we need the following techinical result.

Lemma 2.6.6. *Let r^1 be the unique solution of (2.6.27). Then, the kernel $\mathcal{K}$ is jointly continuous over $[0,T]^2$. In particular, $\mathcal{K}$ is bounded over $[0,T]^2$ and is in $L^2([0,T]^2)$.*

Proof. Lemma 2.6.5 proves that r^1 is continuous on $[0,T]$. Then, from (2.3.3) it follows that the functions $\xi_t^{\pm}$ are continuous. Therefore, from (2.3.4) we get that $\mathcal{K}$ is jointly continuous on $[0,T]^2$ hence it $\mathcal{K}$ is bounded on $[0,T]^2$ and

$$\int_0^T \int_0^T |\mathcal{K}(t,s)|^2 \, dsdt < \infty,$$

that is $\mathcal{K}$ is in $L^2([0,T]^2)$. □

In the following proposition we derive the existence and uniqueness of the solutions to (2.6.27) and (2.6.28).

Proposition 2.6.7. *Under Assumption 2.3.1, there exists a unique continuous function r^1 that satisfies the non-autonomous Riccati ODE (2.6.27) dt-a.e. on $[0,T]$. Furthermore, the BSDE (2.6.28) admits a closed form solution r^0 given by (2.3.5). Moreover,*

$$\mathbb{E}\left[\int_0^T (r_t^0)^2 dt\right] < \infty. \tag{2.6.30}$$

Proof. In Lemma 2.6.5 we have established that (2.6.27) has a unique continuous solution r^1. We prove the rest of the claims in the following two steps.

Step 1. We show that r_t^0 given by (2.3.5) solves the BSDE (2.6.28); Note that since r^1 is continuous, the function ξ^+ in (2.3.3) is the unique solution of the ODE

$$\frac{d\xi_t^+}{dt} = r_t^1 \xi_t^+, \quad \xi_0^+ = 1. \tag{2.6.31}$$

Since r_t^1 is continuous on $[0,T]$, it holds that

$$\int_0^T (\xi_t^+)^2 dt < \infty. \tag{2.6.32}$$

Since ξ_t^+ satisfies (2.6.32), then the process

$$\xi_t^+ r_t^0 := \frac{1}{2\lambda_1} \mathbb{E}_t \left[\int_t^T \xi_s^+ (dA_s - \kappa_0 \nu_s^0 ds)\right], \quad 0 \le t \le T, \tag{2.6.33}$$

is the unique strong solution to the following linear BSDE

$$\begin{cases} d(\xi_t^+ r_t^0) & = \frac{\xi_t^+}{2\lambda_1}(\kappa_0 \nu_t^0 dt - dA_t) - \frac{1}{2\lambda_1}\xi_t^+ d\mathcal{M}_t - \frac{1}{2\lambda_1}\xi_t^+ d\mathcal{N}_t, \\ \xi_T^+ r_T^0 & = 0. \end{cases} \tag{2.6.34}$$

We multiply both sides in (2.6.33) by ξ_t^- from (2.3.3) and use the identity $\xi_t^- \xi_t^+ = 1$. By doing so, we can obtain an expression for r_t^0, that is

$$r_t^0 = \frac{1}{2\lambda_1}\mathbb{E}_t\left[\int_t^T \xi_t^- \xi_s^+ (dA_s - \kappa_0 \nu_s^0 ds)\right]. \tag{2.6.35}$$

We now show that r^0 from (2.6.35) is the solution to (2.6.28). From (2.6.34) and Itô's product rule we get

$$d\xi_t^+ r_t^0 + \xi_t^+ dr_t^0 = \frac{\xi_t^+}{2\lambda_1}(\kappa_0 \nu_t^0 dt - dA_t) - \frac{1}{2\lambda_1}\xi_t^+ d\mathcal{M}_t - \frac{1}{2\lambda_1}\xi_t^+ d\mathcal{N}_t. \tag{2.6.36}$$

Next, we use (2.6.31) and (2.6.36) to get

$$\xi_t^+ \left(r_t^1 r_t^0 dt + dr_t^0 - \frac{1}{2\lambda_1}(\kappa_0 \nu_t^0 dt - dA_t) + \frac{1}{2\lambda_1} d\mathcal{M}_t + \frac{1}{2\lambda_1} d\mathcal{N}_t \right) = 0. \tag{2.6.37}$$

Since $\xi_t^+ > 0$ for all $t \in [0, T]$, we have

$$r_t^1 r_t^0 dt + dr_t^0 - \frac{1}{2\lambda_1}(\kappa_0 \nu_t^0 dt - dA_t) + \frac{1}{2\lambda_1} d\mathcal{M}_t + \frac{1}{2\lambda_1} d\mathcal{N}_t = 0.$$

with terminal condition $r_T^0 = 0$ which follows from (2.6.35). By comparing this with (2.6.28), it follows that r_t^0 is the solution to the BSDE (2.6.28). Recall the definition of $\mathcal{K}$ in (2.3.4). We substitute the expression for $\mathcal{K}(t, s)$ from (2.3.4) into (2.6.35) from which it follows that r_t^0 given by (2.3.5) solves (2.6.28).

Step 2. We show (2.6.30). From (2.3.4) it follows that $\mathcal{K}(t, s) > 0$ for all $t, s \in [0, T]^2$. Moreover by Lemma 2.6.6, $\mathcal{K}$ is bounded on $[0, T]^2$. Since A is of bounded variation and $\mathcal{K}$ is bounded, then by using the conditional Jensen's

inequality and the tower property we get

$$\sup_{t\in[0,T]} \mathbb{E}\left[\left(\mathbb{E}_t\left[\int_t^T \mathcal{K}(t,s)dA_s\right]\right)^2\right] \leq C\mathbb{E}\left[\left(\int_0^T |dA_s|\right)^2\right] < \infty, \tag{2.6.38}$$

where we used (2.2.1) in the last inequality. Similarly, we can obtain that

$$\sup_{t\in[0,T]} \mathbb{E}\left[\left(\mathbb{E}_t\left[\int_t^T \mathcal{K}(t,s)\nu_s^0 ds\right]\right)^2\right] \leq C\mathbb{E}\left[\int_0^T (\nu_s^0)^2 ds\right] < \infty, \tag{2.6.39}$$

where we used the fact that $\nu^0 \in \mathcal{A}_M^{q_0}$ and (2.2.2). From (2.3.5), (2.6.38) and (2.6.39) we get

$$\sup_{t\in[0,T]} \mathbb{E}[(r_t^0)^2] < \infty,$$

and (2.6.30) follows. □

Remark 2.6.8. *As stated in Proposition 2.6.7, the function r^1 satisfies the Riccati ODE (2.6.27) only dt almost everywhere. This is to be expected since ϕ^1 is assumed to be piecewise continuous and the derivatives of r^1 may not exists at the points of discontinuity. Nevertheless, as we will show in the proof of Theorem 2.3.2, this is sufficient for our needs as we wish to solve the FBSDE system (2.6.17) only $d\mathbb{P}\otimes dt$ almost everywhere.*

We are now ready to prove Theorem 2.3.2. In order to simplify the notation, we will often denote the process $\nu^{1,*}(\nu^0)$ by $\nu^{1,*}$.

Proof of Theorem 2.3.2. Let $\nu^{1,*}$ as in (2.3.6) with r^1 as in (2.6.27) and r^0 as in (2.3.5).

Step 1: We determine an explicit expression for $Q^{1,\nu^{1,*}}$. We argue that

$$Q_t^{1,\nu^{1,*}} = \int_0^t \mathcal{K}(s,t) r_s^0 ds. \tag{2.6.40}$$

This could verified by using (2.3.4) so we can write (2.6.40) as

$$Q_t^{1,\nu^{1,*}} = \xi_t^+ \int_0^t \xi_s^- r_s^0 ds. \tag{2.6.41}$$

From (2.3.3) we note that ξ^+ satisfies the following ODE,

$$\frac{d\xi_t^+}{dt} = r_t^1 \xi_t^+ \quad 0 \le t \le T. \tag{2.6.42}$$

Taking the derivative in (2.6.41) and using (2.3.3), (2.3.4) and (2.6.42) we arrive at

$$\begin{aligned} dQ_t^{1,\nu^{1,*}} &= r_t^1 \left(\xi_t^+ \int_0^t \xi_s^- r_s^0 ds \right) dt + r_t^0 dt \\ &= \left(r_t^0 + r_t^1 \int_0^t \mathcal{K}(s,t) r_s^0 ds \right) dt. \end{aligned} \tag{2.6.43}$$

From (2.6.43) and (2.2.5) we get (2.6.40).

Step 2: We show that $\nu^{1,*}$ solves (2.6.17). Note that from (2.2.5) and (2.3.6) we can rewrite $\nu^{1,*}$ as

$$\nu_t^{1,*} = -\left(r_t^0 + r_t^1 Q_t^{1,\nu^{1,*}} \right), \quad 0 \le t \le T. \tag{2.6.44}$$

By plugging in (2.6.44) into (2.6.17) we conclude that it is enough to prove that (2.6.26) holds. Since r_t^0 satisfies (2.6.28) and r_t^1 satisfies (2.6.27) dt-a.e. on $[0,T]$, then (2.6.26) holds $d\mathbb{P} \otimes dt$ almost everywhere. Next, using the terminal conditions of r^0 and r^1 from (2.6.28) and (2.6.27) we deduce from (2.6.44) that the terminal condition in (2.6.17) is satisfied. Recall that the forward component in (2.6.17) is satisfied by (2.2.5). Therefore, $(Q^{1,\nu^{1,*}}, \nu^{1,*})$ solve the system (2.6.17), $d\mathbb{P} \otimes dt$ almost everywhere.

Step 3: We show that $\nu^{1,*} \in \mathcal{A}_m$. From (2.2.4) it follows that we need to verify that

$$\mathbb{E}\left[\int_0^T (\nu_t^{1,*})^2 dt \right] < \infty. \tag{2.6.45}$$

Form (2.6.40), Proposition 2.6.7, Lemma 2.6.6 and Cauchy-Schwartz inequality we

get

$$\mathbb{E}\left[\int_0^T \left(Q_t^{1,\nu^{1,*}}\right)^2 dt\right] \leq \mathbb{E}\left[\int_0^T \left(\int_0^t \mathcal{K}(s,t)^2 ds\right)\left(\int_0^t (r_s^0)^2 ds\right) dt\right] \\ < \infty. \tag{2.6.46}$$

From Proposition 2.6.7 it follows that r^1 is continuous hence bounded on $[0,T]$ and that r^0 is square-integrable. Using this, (2.6.44) and Cauchy-Schwartz inequality gives

$$\mathbb{E}\left[\int_0^T (\nu_t^{1,*})^2 dt\right] \leq 2\mathbb{E}\left[\int_0^T (r_t^0)^2 dt\right] + 2\mathbb{E}\left[\int_0^T (r_t^1)^2 \left(Q_t^{1,\nu^{1,*}}\right)^2 dt\right] \\ < \infty. \tag{2.6.47}$$

Therefore, $\nu^{1,*}$ is admissible and it solves (2.6.17), hence by Lemma (2.6.4) it is the unique maximiser to the minor agent's objective functional H^1 in (2.6.1). □

2.7 Proof of Theorem 2.3.5

In this section we derive the major agent's optimal strategy via a calculus of variation argument. We start be defining operators which are essential to our proofs. Then we derive an equivalent representation the major agent's objective H^0 which is more convenient to our method of proof. Throughout this section we assume that Assumption 2.3.1 holds and that the minor agent is adopting the strategy $\nu^{1,*}$ from Theorem 2.3.2. Henceforth, with a slight abuse of notation we write $H^0(\nu^0)$ for $H^0(\nu^0, \nu^{1,*}(\nu^0))$.

Essential definitions of $L^2([0,T])$ operators. We denote by $\mathcal{T}^*$ the adjoint kernel of $\mathcal{T}$ for $\langle\cdot,\cdot\rangle_{L^2}$, that is

$$\mathcal{T}^*(t,s) := \mathcal{T}(s,t), \quad s,t \in [0,T], \tag{2.7.1}$$

and by T^* the corresponding adjoint integral operator.

We define the kernel $\mathcal{K}_1 : [0,T]^2 \to \mathbb{R}_+$ as

$$\mathcal{K}_1(t,s) := \mathcal{K}(s,t)\mathbb{1}_{\{s\leq t\}}, \quad s,t \in [0,T], \tag{2.7.2}$$

where $\mathcal{K}$ is given in (2.3.4). We let K_1 to be the integral operator generated by the kernel $\mathcal{K}_1$, that is

$$(\mathsf{K}_1\psi)(t) := \int_0^T \mathcal{K}_1(t,s)\psi(s)ds, \quad t \in [0,T],\ \psi \in L^2([0,T]), \tag{2.7.3}$$

The following lemma, which is proved in Section 2.8, outlines some useful properties of K_1. Recall that the class of operators $B(L^2([0,T]))$ was defined after (2.3.9).

Lemma 2.7.1. *The operator K_1 is in $B(L^2([0,T]))$. Moreover, $\mathsf{K}_1^* \in B(L^2([0,T]))$ is given by*

$$(\mathsf{K}_1^*\psi)(t) = \int_0^T \mathcal{K}(t,s)\psi(s)\mathbb{1}_{\{t\leq s\}}ds, \quad t \in [0,T],\ \psi \in L^2([0,T]). \tag{2.7.4}$$

We recall the definition of a compact operator from Porter and Stirling (1990), (see Definition 3.2 therein).

Definition 2.7.2. *An operator $\mathsf{T} : L^2([0,T]) \to L^2([0,T])$ is said to have finite rank if its image $\{\mathsf{T}\psi : \psi \in L^2([0,T])\}$ has finite dimension. An operator $\mathsf{L} \in B(L^2([0,T]))$ is said to be compact if there is a sequence $(\mathsf{L}_n)_{n\geq 1}$ of finite-rank operators in $B(L^2([0,T]))$ such that $||\mathsf{L}_n - \mathsf{L}|| \to 0$ as $n \to \infty$.*

A particularly important result that we will use states that any operator generated by a kernel in $L^2([0,T]^2)$ is compact (see Theorem 3.4 in Porter and Stirling (1990)). We remark that not all operators in $B(L^2([0,T]))$ are compact operators as pointed out in example 3.6 in Porter and Stirling (1990).

Next we define non-negative and positive operators in $B(L^2([0,T]))$ as in (Porter and Stirling, 1990, Definition 6.1).

Definition 2.7.3. *Let $\mathsf{T} \in B(L^2([0,T]))$ be a self-adjoint operator. T is said to be non-negative if and only if $\langle \mathsf{T}\psi, \psi\rangle_{L^2} \geq 0$ for all $\psi \in L^2([0,T])$. It is said to be*

positive if and only if $\langle \mathsf{T}\psi, \psi\rangle_{L^2} > 0$ *for all* $\psi \neq 0$ *in* $L^2([0,T])$. *If there a positive constant* m *for which* $\langle \mathsf{T}\psi, \psi\rangle_{L^2} \geq m||\psi||^2_{L^2}$ *for all* $\psi \in L^2([0,T])$, *then* T *is said to be positive and bounded below.*

Our next result outlines several important properties of the operator G in (2.3.11). Recall that K_1 was defined in (2.7.3).

Proposition 2.7.4. *Let* G *be defined as in* (2.3.11). *Then* $\mathsf{G} \in B(L^2([0,T]))$ *is a positive, compact and self-adjoint operator. Moreover, it satisfies*

$$(\mathsf{G}\psi)(t) = (\mathsf{K}_1\mathsf{K}_1^*\psi)(t), \quad \text{for all } t \in [0,T],\ \psi \in L^2([0,T]). \tag{2.7.5}$$

The proof of Proposition 2.7.4 is given in Section 2.8.

In the following lemma we determine an alternative representation for the major agent's objective functional.

Lemma 2.7.5. *Let* H^0 *be the major agent's objective functional in* (2.2.10). *Then, for any* $\nu^0 \in \mathcal{A}_M^{q_0}$ *it holds that*

$$\begin{aligned} H^0(\nu^0) = x_0 + M_0 q_0 - \kappa_0 \frac{q_0^2}{2} - \frac{\kappa_1\kappa_0}{2\lambda_1}\int_0^T \nu_t^0(\mathsf{G}\nu^0)(t)dt \\ + \int_0^T \left(\frac{\kappa_1}{2\lambda_1}\nu_t^0(\mathsf{G}\bar{\mu})(t) + Q_t^{0,\nu^0}\bar{\mu}_t\right)dt - \lambda_0\int_0^T (\nu_t^0)^2 dt. \end{aligned} \tag{2.7.6}$$

The proof of Lemma 2.7.5 is postponed to Section 2.9.

The following proposition establishes the uniqueness of the maximiser of H^0.

Proposition 2.7.6. *There exists at most one admissible maximiser to the major agent's objective functional* H^0 *in* (2.2.10)

Proof. To show the desired result, it is sufficient to show that the objective functional H^0 is strictly concave over $\mathcal{A}_M^{q_0}$.

Notice that since $\nu^{1,*} \in \mathcal{A}_m$, $\nu^0 \in \mathcal{A}_M^{q_0}$ and μ satisfies (2.3.7), then H^0 is finite. Therefore, in order to show that the objective H^0 is strictly concave over $\mathcal{A}_M^{q_0}$ we

must verify that

$$\mathcal{I}^0(\rho,\nu,\omega) := H^0(\rho\nu+(1-\rho)\omega) - \rho H^0(\nu) - (1-\rho)H^0(\omega) > 0 \tag{2.7.7}$$

for any $\rho \in (0,1)$ and for any dt-distinguishable $\nu, \omega \in \mathcal{A}_M^{q_0}$.

We now fix such ρ and ν, ω. From (2.2.3) and (2.3.11) it follows that $Q^{0,\nu}$ and $\mathsf{G}\nu$ are linear in ν. Then from (2.7.6) and (2.7.7) we get

$$\begin{aligned}\mathcal{I}^0(\rho,\nu,\omega) = \rho(1-\rho)\lambda_0 \int_0^T (\nu_t-\omega_t)^2 dt \\ + \rho(1-\rho)\frac{\kappa_1\kappa_0}{2\lambda_1}\int_0^T (\nu_t-\omega_t)(\mathsf{G}(\nu-\omega))(t)dt.\end{aligned} \tag{2.7.8}$$

Note that the left to show that the right-hand side of (2.7.8) is strictly positive since G is a positive operator by Proposition 2.7.4 and ν and ω are dt-distinguishable. □

As similarly done in Section 2.6, we can apply a convex analytic calculus of variation approach to derive a first order optimality conditions which characterizes the unique solution to the major agent's problem.

Since the map $\nu^0 \to H^0(\nu^0)$ in (2.2.10) is strictly concave, then H^0 admits a unique maximiser characterised by the critical point at which the Gâteaux derivative $\langle \mathcal{D}H^0(\nu^0), \omega\rangle$, as defined in (2.6.12), vanishes. We remind the reader that the minor agent optimal strategy $\nu^{1,*}$ was fixed to be the one in (2.3.6), therefore, making the major agent's objective functional H^0 only a function of the major agent control ν^0. In the next lemma we explicitly compute the first-order Gâteaux derivative of H^0. Recall that $\mathcal{A}_M^{q_0}$ was defined in (2.2.2).

Lemma 2.7.7. *The Gâteaux derivative of H^0 in (2.7.6), in a direction $\omega \in \mathcal{A}_M^0$ is given by*

$$\begin{aligned}\langle \mathcal{D}H^0(\nu^0), \omega\rangle = \\ \int_0^T \omega_t \left(-2\lambda_0\nu_t^0 - \frac{\kappa_1\kappa_0}{\lambda_1}(\mathsf{G}\nu^0)(t) + \frac{\kappa_1}{2\lambda_1}(\mathsf{G}\bar{\mu})(t) - \int_t^T \bar{\mu}_s ds \right) dt,\end{aligned} \tag{2.7.9}$$

for any $\nu^0 \in \mathcal{A}_M^{q_0}$.

Proof. Let $\epsilon > 0$, $\nu^0 \in \mathcal{A}_M^{q_0}$ and $\omega \in \mathcal{A}_M^0$. From (2.7.6) we get

$$\begin{aligned} &H^0(\nu^0 + \epsilon\omega) - H^0(\nu^0) \\ &= \epsilon\Bigg(\int_0^T \omega_t \left(-2\lambda_0 \nu_t^0 + \frac{\kappa_1}{2\lambda_1}(\mathsf{G}\bar{\mu})(t) \right) dt - \frac{\kappa_1\kappa_0}{2\lambda_1} \int_0^T \omega_t (\mathsf{G}\nu^0)(t) dt \\ &\quad - \frac{\kappa_1\kappa_0}{2\lambda_1} \int_0^T \nu_t^0 (\mathsf{G}\omega)(t) dt - \int_0^T \bar{\mu}_t \left(\int_0^t \omega_s ds \right) dt \Bigg) \\ &\quad + \epsilon^2 \Bigg(- \lambda_0 \int_0^T \omega_s^2 ds - \frac{\kappa_1\kappa_0}{2\lambda_1} \int_0^T \omega_t (\mathsf{G}\omega)(t) dt \Bigg). \end{aligned} \tag{2.7.10}$$

Notice that all the terms in (2.7.10) are finite as a consequence of $\omega \in \mathcal{A}_M^0$, $\nu^0 \in \mathcal{A}_M^{q_0}$, μ satisfying (2.3.7) and $\mathsf{G} \in B(L^2([0,T]))$ as shown in Proposition 2.7.4. It follows that

$$\begin{aligned} \langle \mathcal{D}H^0(\nu^0), \omega \rangle = \int_0^T \omega_t \Big(&- 2\lambda_0 \nu_t^0 - \frac{\kappa_1\kappa_0}{2\lambda_1} (\mathsf{G}\nu^0)(t) + \frac{\kappa_1}{2\lambda_1} (\mathsf{G}\bar{\mu})(t) \Big) dt \\ &- \frac{\kappa_1\kappa_0}{2\lambda_1} \int_0^T \nu_t^0 (\mathsf{G}\omega)(t) dt - \int_0^T (\bar{\mu}_t) \left(\int_0^t \omega_s ds \right) dt. \end{aligned} \tag{2.7.11}$$

Proposition 2.7.4 shows that $\mathsf{G} \in B(L^2([0,T]))$. Since μ satisfies (2.3.7), then $\bar{\mu}$ is in $L^2([0,T])$ by Jensen's inequality. Since $\omega \in \mathcal{A}_M^0$ and $\bar{\mu} \in L^2([0,T])$, then we can apply Fubini's theorem to obtain

$$\int_0^T (\bar{\mu}_t) \left(\int_0^t \omega_s ds \right) dt = \int_0^T \omega_s \int_s^T \bar{\mu}_t dt ds. \tag{2.7.12}$$

As claimed in Proposition 2.7.4, G is self-adjoint, therefore, it holds that

$$\begin{aligned} \int_0^T \nu_t^0 (\mathsf{G}\omega)(t) dt &= \langle \nu^0, (\mathsf{G}\omega) \rangle_{L^2} \\ &= \langle \omega, (\mathsf{G}\nu^0) \rangle_{L^2} \\ &= \int_0^T \omega_t (\mathsf{G}\nu^0)(t) dt. \end{aligned} \tag{2.7.13}$$

Finally, we use (2.7.12) and (2.7.13) in (2.7.11) to get (2.7.9).

□

Recall the definition of the operator S in (2.3.12). In the following lemma we derive an optimality condition that takes the form of an integral equation.

Proposition 2.7.8. *A strategy $\nu^{0,*} \in \mathcal{A}_M^{q_0}$ maximises the major agent's performance functional (2.2.10) if there exists a constant $\eta \in \mathbb{R}$ such that,*

$$\nu_t^{0,*} + \frac{\kappa_1 \kappa_0}{2\lambda_0 \lambda_1}(\mathsf{G}\nu^{0,*})(t) = (\mathsf{S}\bar{\mu})(t) + \frac{\eta}{2\lambda_0}, \quad \textit{for all } 0 \leq t \leq T. \tag{2.7.14}$$

Proof. In the proof of Proposition 2.7.6 we have shown that the objective functional H^0 is strictly concave over $\mathcal{A}_M^{q_0}$. Therefore, by Proposition 2.1 in Chapter 2 in Ekeland and Témam (1999) if an admissible strategy $\nu^{0,*}$ satisfies

$$\langle \mathcal{D}H^0(\nu^{0,*}), \omega \rangle = 0, \quad \text{for all } \omega \in \mathcal{A}_M^0, \tag{2.7.15}$$

then it is the maximiser of H^0.

Recalling the result of Lemma 2.7.7, we plug (2.7.14) into (2.7.9) to get

$$\begin{aligned} \langle \mathcal{D}H^0(\nu^{0,*}), \omega \rangle &= -\int_0^T \omega_t \left(2\lambda_0 (\mathsf{S}\bar{\mu})(t) + \eta - \frac{\kappa_1}{2\lambda_1}(\mathsf{G}\bar{\mu})(t) + \int_t^T \bar{\mu}_s ds \right) dt \\ &= -\left(\int_0^T \bar{\mu}_s ds + \eta \right) \int_0^T \omega_t dt \end{aligned} \tag{2.7.16}$$

where we used (2.3.12) in the second equality. Recall that $\omega \in \mathcal{A}_M^0$, then from (2.2.2) we get (2.7.15). □

The following proposition, which is proved in Section 2.8, derives some properties of the operator R in (2.3.14) that are crucial to the proof of Theorem 2.3.5.

Proposition 2.7.9. *Let R be defined as in (2.3.14) and G be defined as in (2.3.11). Then the following holds:*

(i) *The inverse operator of* $\mathsf{I} + \frac{\kappa_1\kappa_0}{2\lambda_0\lambda_1}\mathsf{G}$ *exists and it satisfies*

$$\mathsf{R} = \left(\mathsf{I} + \frac{\kappa_1\kappa_0}{2\lambda_0\lambda_1}\mathsf{G}\right)^{-1}. \tag{2.7.17}$$

(ii) R *is positive, bounded from below and is in* $B(L^2([0,T]))$.

(iii) *If* $f \in C([0,T])$, *then* $(\mathsf{R}f) \in C([0,T])$.

The following lemma derive some essential properties of the operator S in (2.3.12).

Lemma 2.7.10. *Let* S *be as in* (2.3.12). *Then* S *is in* $B(L^2([0,T]))$ *and for any* $\psi \in L^2([0,T])$,$(\mathsf{S}\psi)(t)$ *is continuous on* $0 \le t \le T$.

Proof. Proposition 2.7.4 proves that G is in $B(L^2([0,T]))$, hence it follows from (2.3.12) that also S is in $B(L^2([0,T]))$.

Next, let $\psi \in L^2([0,T])$. From Proposition 2.9.4 it follows that $\mathsf{G}\psi$ is continuously differentiable on $[0,T]$, hence by (2.3.12) the continuity of $(\mathsf{S}\psi)(\cdot)$ follows. □

We are now ready to prove Theorem 2.3.5.

Proof of Theorem 2.3.5. Recall that $\nu^{0,*}$ and η were defined in (2.3.15) and (2.3.16), respectively. We split the proof into the following steps.

Step 1. We show that $(\nu^{0,*}, \eta)$ is the unique solution to (2.7.14). Recall that R was defined in (2.3.14). From (2.3.7) and Lemma 2.7.10 it follows that $\mathsf{S}\bar{\mu}(\cdot)$ is in $L^2([0,T])$. Then, from Proposition 2.7.9 we get that the unique solution to (2.7.14) is given by

$$\begin{aligned} \nu_t^{0,*} &= \left(\left(\mathsf{I} + \frac{\kappa_1\kappa_0}{2\lambda_0\lambda_1}\mathsf{G}\right)^{-1}\left(\frac{\eta}{2\lambda_0} + \mathsf{S}\bar{\mu}\right)\right)(t) \\ &= \frac{\eta}{2\lambda_0}(\mathsf{R}1)(t) + (\mathsf{R}\mathsf{S}\bar{\mu})(t), \quad 0 \le t \le T. \end{aligned} \tag{2.7.18}$$

Step 2. We verify that $\nu^{0,*}$ satisfies the fuel constraint in (2.2.2). Note that

we need to show that $\langle \nu^{0,*}, 1 \rangle_{L^2} = q_0$. From (2.3.15) and (2.3.16) we get

$$\begin{aligned} \langle \nu^{0,*}, 1 \rangle_{L^2} &= \frac{\eta}{2\lambda_0} \langle \mathsf{R}1, 1 \rangle_{L^2} + \langle \mathsf{RS}\bar{\mu}, 1 \rangle_{L^2} \\ &= \left(\frac{q_0 - \langle \mathsf{RS}\bar{\mu}, 1 \rangle_{L^2}}{\langle \mathsf{R}1, 1 \rangle_{L^2}} \right) \langle \mathsf{R}1, 1 \rangle_{L^2} + \langle \mathsf{RS}\bar{\mu}, 1 \rangle_{L^2} \\ &= q_0. \end{aligned} \tag{2.7.19}$$

Note that by Proposition 2.7.9(ii) the operator R is positive and bounded from below. Therefore the denominator in (2.3.16) is strictly positive and the constant η is well-defined.

Step 3. We verify that $\nu^{0,*}$ is in $L^2([0,T])$. From Lemma 2.7.10 it follows that $(\mathsf{S}\bar{\mu})(t)$ is continuous on $[0,T]$. Proposition 2.7.9(iii) and (2.7.18) then imply that $\nu_t^{0,*}$ is continuous and therefore bounded on $[0,T]$. This concludes the proof. □

2.8 Proofs of Lemma 2.7.1 and Propositions 2.7.4 and 2.7.9

Proof of Lemma 2.7.1. Recall that kernels $\mathcal{K}$ and $\mathcal{K}_1$ were defined in (2.3.4) and (2.7.2) respectively. Let ψ be in $L^2([0,T])$. From (2.7.1) we get

$$\mathcal{K}_1^*(t,s) = \mathcal{K}(t,s)\mathbb{1}_{\{t \le s\}}, \quad \text{for all } 0 \le t, s \le T, \tag{2.8.1}$$

which verifies (2.7.4). From Lemma 2.6.6 we get that $\mathcal{K}$ is in $L^2([0,T]^2)$. Then by (2.7.2) and (2.8.1) also $\mathcal{K}_1^*$ and $\mathcal{K}_1$ are in $L^2([0,T]^2)$, therefore, K_1 and K_1^* are in $B(L^2([0,T]))$. □

The following lemma describes several properties of the kernel $\mathcal{G}$ in (2.3.10) which are essential to the proof of Proposition 2.7.9.

Lemma 2.8.1. *Let $\mathcal{G}$ as in (2.3.10). Then, $\mathcal{G}$ is symmetric and jointly continuous on $[0,T]^2$. Moreover, $\mathcal{G}$ is in $L^2([0,T]^2)$.*

Proof. From (2.3.10) it follows that $\mathcal{G}$ is symmetric. Recall that ξ^+ and ξ^- were defined as in (2.3.3). Note that ξ^+ and ξ^- are continuous on $[0,T]$ and that ξ^- belongs to $L^2([0,T])$. It follows that $t \mapsto \int_0^t (\xi_u^-)^2 du$ is continuous on $[0,T]$. From (2.3.4) and (2.3.10) it follows that the kernel $\mathcal{G}$ can be rewritten as follows,

$$\mathcal{G}(t,s) = \xi_t^+ \xi_s^+ \int_0^{t\wedge s} (\xi_u^-)^2 du, \quad \text{for all } 0 \le t,s \le T.$$

Therefore, $\mathcal{G}(t,s)$ is jointly continuous on $[0,T]^2$, hence it is in $L^2([0,T]^2)$. □

The following lemma is needed for the proof of Proposition 2.7.4.

Lemma 2.8.2. *Let* K_1 *be defined as in* (2.7.3) *and let* $\psi \in L^2([0,T])$. *If* $(\mathsf{K}_1\psi)(t) = 0$ *for all* $0 \le t \le T$, *then* $\psi(t) = 0$ *a.e. on* $[0,T]$.

Proof. Let $\psi \in L^2([0,T])$ and assume that $(\mathsf{K}_1\psi)(t) = 0$ for all $0 \le t \le T$. From (2.3.4), (2.7.2) and (2.7.3) we get

$$(\mathsf{K}_1\psi)(t) = \xi_t^+ \left(\int_0^t \xi_s^- \psi(s) ds \right) = 0, \quad \text{for all } 0 \le t \le T. \tag{2.8.2}$$

From (2.3.3) it follows that $\xi_t^\pm > 0$ for all $0 \le t \le T$, therefore

$$\int_0^t \xi_s^- \psi(s) ds = 0, \quad \text{for all } 0 \le t \le T. \tag{2.8.3}$$

Since $\xi_t^\pm$ are also continuous for all $t \in [0,T]$ and $\psi \in L^2([0,T])$, then $\xi^-\psi$ is integrable. Then from Lebesgue differentiation theorem and (2.8.3) we conclude that

$$\xi_t^- \psi(t) = 0, \quad dt\text{-a.e. on } [0,T].$$

But again since $\xi_t^- > 0$ on $[0,T]$ we get that

$$\psi(t) = 0, \quad dt\text{-a.e. on } [0,T],$$

which proves the result. □

Proof of Proposition 2.7.4. Let $\psi \in L^2([0,T])$. From (2.3.10) we get

$$\begin{aligned}(\mathsf{G}\psi)(t) &= \int_0^T \mathcal{G}(t,u)\psi(u)du \\ &= \int_0^T \psi(u)\int_0^{t\wedge u} \mathcal{K}(s,t)\mathcal{K}(s,u)dsdu \\ &= \int_0^T\int_0^T \mathcal{K}(s,t)\mathcal{K}(s,u)\psi(u)\mathbb{1}_{\{s\le t\}}\mathbb{1}_{\{s\le u\}}duds.\end{aligned}$$

Together with (2.7.2) and (2.8.1) it follows that

$$\begin{aligned}(\mathsf{G}\psi)(t) &= \int_0^T \mathcal{K}_1(t,s)\int_0^T \mathcal{K}_1^*(s,u)\psi(u)duds \\ &= (\mathsf{K}_1\mathsf{K}_1^*\psi)(t), \quad \text{for all } 0\le t\le T,\end{aligned} \tag{2.8.4}$$

which proves (2.7.5). Since by Lemma 2.7.1, $\mathsf{K}_1, \mathsf{K}_1^* \in B(L^2([0,T]))$, a straightforward application of the Cauchy-Schwartz inequality and (2.8.4) shows that $\mathsf{G} \in B(L^2([0,T]))$. Note that (2.8.4) also implies that G is self-adjoint, that is

$$\begin{aligned}\mathsf{G}^* &= (\mathsf{K}_1\mathsf{K}_1^*)^* \\ &= (\mathsf{K}_1^*)^*\mathsf{K}_1^* \\ &= \mathsf{G}.\end{aligned} \tag{2.8.5}$$

Next, using (2.3.11) we prove that G is compact (see Definition 2.7.2). From Lemma 2.8.1 it follows that $\mathcal{G}$ is in $L^2([0,T]^2)$. Then the result follows from Theorem 3.4 in Porter and Stirling (1990), which shows that any integral operator generated by a kernel in $L^2([0,T]^2)$ is compact.

Finally, we prove that G is a positive operator in the sense of Definition 2.7.3. We have shown that $\mathsf{G} = \mathsf{K}_1\mathsf{K}_1^*$. Since for any $\psi \in L^2([0,T])$ we have

$$\langle \mathsf{G}\psi, \psi\rangle = \langle \mathsf{K}_1\mathsf{K}_1^*\psi, \psi\rangle = ||\mathsf{K}_1\psi||^2 \ge 0,$$

it follows that G is non-negative. By Lemma 2.8.2 we have $(\mathsf{K}_1\psi)(t) = 0$ for all $t \in [0,T]$ only for $\psi = 0$ a.e. on $[0,T]$. Therefore, G is positive. □

In the following we present a sequence of results which are essential to the proof of Proposition 2.7.9. Using the results of Proposition 2.7.4 we are in a position to fully characterise the spectral properties of the integral operator G.

Lemma 2.8.3 (Spectral Decomposition of G)**.** *Let G be defined as in (2.3.11). Then G has a sequence of positive eigenvalues $(\zeta_n)_{n\geq 1}$ and a corresponding orthonormal sequence $(\psi_n)_{n\geq 1}$ of eigenfunctions in $L^2([0,T])$, such that for each $\varphi \in L^2([0,T])$, we have that*

$$\mathsf{G}\varphi = \sum_{n\geq 1} \zeta_n \langle \varphi, \psi_n \rangle_{L^2} \psi_n.$$

Moreover, for all $N \geq 1$, define $\mathsf{G}_N, \mathsf{G}_N^{abs} \in B(L^2([0,T]))$ by

$$\begin{aligned} \mathsf{G}_N\varphi &= \sum_{n=1}^{N} \zeta_n \langle \varphi, \psi_n \rangle_{L^2} \psi_n, \\ \mathsf{G}_N^{abs}\varphi &= \sum_{n=1}^{N} \left| \zeta_n \langle \varphi, \psi_n \rangle_{L^2} \psi_n \right|. \end{aligned} \tag{2.8.6}$$

Then, $\mathsf{G}_N\varphi$ converges uniformly to $\mathsf{G}\varphi$,

$$\lim_{N\to\infty} \sup_{t\in[0,T]} |(\mathsf{G}_N\varphi)(t) - (\mathsf{G}\varphi)(t)| = 0, \tag{2.8.7}$$

and $\mathsf{G}_N^{abs}\varphi$ is uniformly convergent, that is, there exists a function $\Phi \in L^2([0,T])$ such that

$$\lim_{N\to\infty} \sup_{t\in[0,T]} \left| (\mathsf{G}_N^{abs}\varphi)(t) - \Phi(t) \right| = 0. \tag{2.8.8}$$

Proof. From Proposition 2.7.4 it follows that G is a self-adjoint compact operator in $B(L^2([0,T]))$. Therefore, from Theorem 4.15 of Porter and Stirling (1990) there is a sequence $(\zeta_n)_{n\geq 1}$ of non-zero eigenvalues of G and a corresponding orthonormal sequence $(\psi_n)_{n\geq 1}$ of eigenfunctions in $L^2([0,T])$ such that $\mathsf{G}\psi = \sum_{n\geq 1} \zeta_n \langle \psi, \psi_n \rangle_{L^2} \psi_n$. Moreover, the operator G_N converges to G in mean, i.e. $||\mathsf{G} - \mathsf{G}_N|| \to 0$ as $N \to \infty$. From Proposition 2.7.4 it follows that G is positive and self-adjoint, hence from Lemma 6.1 in Porter and Stirling (1990) we get that all of its eigenvalues $(\zeta_n)_{n\geq 1}$ are positive. Since by Proposition 2.8.1 $\mathcal{G}$ is continuous and symmetric, then from Theorem 4.22 of Porter and Stirling (1990) it follows that $\mathsf{G}_N\psi$ and $\mathsf{G}_N^{\text{abs}}$ satisfy the

convergence in (2.8.7) and (2.8.8). □

Remark 2.8.4. *In Appendix A.1 we provide an example for the spectral decomposition of* G *in Lemma 2.8.3.*

Lemma 2.8.5. *Let* G *be defined as in (2.3.11). Then, the operator* $\mathsf{I} + \frac{\kappa_1\kappa_0}{2\lambda_0\lambda_1}\mathsf{G}$ *is positive and bounded from below in the sense of Definition 2.7.3.*

Proof. Let $\psi \in L^2([0,T])$. Since G is positive by Proposition 2.7.4 and $\kappa_0, \kappa_1, \lambda_0, \lambda_1 > 0$, we get that

$$\left\langle \left(\mathsf{I} + \frac{\kappa_1\kappa_0}{2\lambda_0\lambda_1}\mathsf{G} \right) \psi, \psi \right\rangle_{L^2} \geq ||\psi||^2_{L^2}. \tag{2.8.9}$$

Therefore, $\mathsf{I} + \frac{\kappa_1\kappa_0}{2\lambda_0\lambda_1}\mathsf{G}$ is positive and bounded from below. □

Recall that we assume that constants $\lambda_0, \lambda_1, \kappa_1$ and κ_0 are strictly positive and that we proved in Lemma 2.8.3 that the eigenvalues of G are all positive. The following lemma is therefore an easy corollary.

Lemma 2.8.6. *Let* $\zeta^* = -\frac{2\lambda_0\lambda_1}{\kappa_1\kappa_0}$ *and let* G *be defined as in (2.3.11). Then,* ζ^* *is not an eigenvalue of the integral operator* G.

We recall Theorem 4.27 of Porter and Stirling (1990) which will be useful in the proof of Proposition 2.7.9.

Proposition 2.8.7 ((Porter and Stirling, 1990, Theorem 4.27))**.** *Let* $f \in L^2([0,T])$. *Suppose that* $\mathcal{T} : [0,T]^2 \to \mathbb{R}$ *is a continuous symmetric kernel and that* T *is the integral operator generated by* $\mathcal{T}$. *Let* $(\mu_n)_{n\geq 1}$ *and* $(\varphi_n)_{n\geq 1}$ *be the sequence of eigenvalues and eigenfunctions of the operator* T. *Moreover, suppose that* $\frac{1}{\lambda}$ *is not an eigenvalue of* T. *Then the unique solution to the integral equation*

$$\psi(t) - \lambda \int_0^T \mathcal{T}(t,s)\psi(s)dt = f(t), \quad t \in [0,T], \tag{2.8.10}$$

is given by

$$\psi(t) = f(t) + \int_0^T \widetilde{\mathcal{R}}(t,s)f(s)ds, \quad t \in [0,T],$$

where

$$\widetilde{\mathcal{R}}(t,s) = \lambda\mathcal{T}(t,s) + \sum_{n\geq 1} \frac{\lambda\mu_n}{1-\lambda\mu_n}\varphi_n(t)\varphi_n(s),$$

is jointly continuous on $[0,T]^2$.

We are now ready to prove Proposition 2.7.9.

Proof of Proposition 2.7.9. (i) Note that the operator G and the corresponding kernel $\mathcal{G}$ satisfy the assumptions of Proposition 2.8.7. Specifically, from Lemma 2.8.6 it follows that $-\frac{2\lambda_0\lambda_1}{\kappa_1\kappa_0}$ is not an eigenvalue of G. Moreover, in Proposition 2.8.1 we have shown that $\mathcal{G}$ is continuous and symmetric on $[0,T]^2$. Therefore, we can apply the result of Proposition 2.8.7 to the following integral equation,

$$\psi(t) + \frac{\kappa_1\kappa_0}{2\lambda_0\lambda_1}\int_0^T \mathcal{G}(t,s)\psi(s)ds = f(t), \quad t\in[0,T], \tag{2.8.11}$$

and determine that the unique solution to (2.8.11) is given by

$$\psi(t) = f(t) + \int_0^T \mathcal{R}(t,s)f(s)ds, \tag{2.8.12}$$

with $\mathcal{R}$ as in (2.3.13). Moreover, it follows from Proposition 2.8.7 that the kernel $\mathcal{R}$ is jointly continuous on $[0,T]^2$.

Next, we show that the inverse of $\mathsf{I} + \frac{\kappa_1\kappa_0}{2\lambda_0\lambda_1}\mathsf{G}$ is given by R. Since by Lemma 2.8.6, $-\frac{2\lambda_0\lambda_1}{\kappa_1\kappa_0}$ is not an eigenvalue of G, the operator $\left(\mathsf{I} + \frac{\kappa_1\kappa_0}{2\lambda_0\lambda_1}\mathsf{G}\right)^{-1}$ exists. Let ψ be the solution of (2.8.11). Since $\mathsf{I} + \frac{\kappa_1\kappa_0}{2\lambda_0\lambda_1}\mathsf{G}$ is invertible it follows from (2.8.11) that ψ can be written as follows,

$$\psi = \left(\mathsf{I} + \frac{\kappa_1\kappa_0}{2\lambda_0\lambda_1}\mathsf{G}\right)^{-1} f. \tag{2.8.13}$$

On the other hand, from (2.3.14) and (2.8.12) we have that

$$\psi = \mathsf{R}f. \tag{2.8.14}$$

Therefore, by comparing (2.8.13) and (2.8.14) we find that

$$\left(\mathsf{I}+\frac{\kappa_1\kappa_0}{2\lambda_0\lambda_1}\mathsf{G}\right)^{-1} f = \mathsf{R}f. \tag{2.8.15}$$

Since (2.8.15) holds for any $f \in L^2([0,T])$, (i) follows.

(ii) From Proposition 2.7.4 it follows that G is a compact operator. Since G is a compact and the inverse of $\mathsf{I}+\frac{\kappa_1\kappa_0}{2\lambda_0\lambda_1}\mathsf{G}$ exists by (i), we get from the remark below the proof of Theorem 3.3 of Porter and Stirling (1990), that the inverse of $\mathsf{I}+\frac{\kappa_1\kappa_0}{2\lambda_0\lambda_1}\mathsf{G}$ is in $B(L^2([0,T]))$. From (2.7.17) it follows that R is also in $B(L^2([0,T]))$. Recall that Lemma 2.8.5 shows that $\mathsf{I}+\frac{\kappa_1\kappa_0}{2\lambda_0\lambda_1}\mathsf{G}$ is positive and bounded from below, hence from Lemma 6.2 of Porter and Stirling (1990) it follows that its inverse is positive and bounded from below. From (2.7.17) we conclude that R is positive and bounded from below in the sense of Definition 2.7.3.

(iii) Assume that $f \in C([0,T])$ then (iii) follows from (2.8.14) and since $\mathcal{R}$ is jointly continuous on $[0,T]^2$ by (i). □

2.9 Proof of Lemma 2.7.5

Throughout this section we assume Assumption 2.3.1 such that minor agent's optimal control $\nu^{1,*}$ is well-defined. Before proving Lemma 2.7.5 we prove several intermediate results.

Lemma 2.9.1. *Let r^0 be defined as in (2.3.5) and K_1 be defined as in (2.7.3). Then the following holds for any $\nu^0 \in \mathcal{A}_M^{q_0}$,*

$$\mathbb{E}[r_t^0(\nu^0)] = \frac{1}{2\lambda_1}(\mathsf{K}_1^*\bar{\mu})(t) - \frac{\kappa_0}{2\lambda_1}(\mathsf{K}_1^*\nu^0)(t), \quad \text{for all } 0 \le t \le T, \tag{2.9.1}$$

Moreover $(\mathbb{E}[r_t^0(\nu^0)])_{t\in[0,T]}$ is in $L^2([0,T])$.

Proof. Let $\nu^0 \in \mathcal{A}_M^{q_0}$ and recall that $\mathcal{K}$ was defined in (2.3.4). From Lemma 2.6.6, (2.3.7) and (2.3.8) it follows that the conditions of Fubini's theorem are satisfied

and we get that

$$\mathbb{E}\left[\int_t^T \mathcal{K}(t,s)\mu_s ds\right] = \int_t^T \mathcal{K}(t,s)\bar{\mu}_s ds, \quad \text{for all } 0 \le t \le T. \tag{2.9.2}$$

Using (2.3.5), (2.9.2) and the tower property we get

$$\begin{aligned}\mathbb{E}[r_t^0(\nu^0)] &= \frac{1}{2\lambda_1}\mathbb{E}\left[\mathbb{E}_t\left[\int_t^T \mathcal{K}(t,s)(\mu_s - \kappa_0\nu_s^0)ds\right]\right] \\ &= \frac{1}{2\lambda_1}\int_0^T \mathcal{K}(t,s)(\bar{\mu}_s - \kappa_0\nu_s^0)\mathbb{1}_{\{t\le s\}}ds.\end{aligned} \tag{2.9.3}$$

Using the expression for K_1^* from (2.7.4) in (2.9.3) we arrive at (2.9.1).

From Lemma 2.7.1 it follows that the operators K_1 and K_1^* are in $B(L^2([0,T]))$. By assumption $\nu^0, \bar{\mu} \in L^2([0,T])$, then from (2.9.1) it follows that $(\mathbb{E}[r_t^0(\nu^0)])_{t\in[0,T]}$ is in $L^2([0,T])$. □

Lemma 2.9.2. *Let $\nu^{1,*}$ be defined as in (2.3.6). Then or any $\nu^0 \in \mathcal{A}_M^{q_0}$ the following holds*

$$\mathbb{E}[\nu_t^{1,*}(\nu^0)] = \frac{\kappa_0}{2\lambda_1}[(\mathsf{K}_1^*\nu^0)(t) + r_t^1(\mathsf{G}\nu^0)(t)] - \frac{1}{2\lambda_1}[(\mathsf{K}_1^*\bar{\mu})(t) + r_t^1(\mathsf{G}\bar{\mu})(t)],$$

for all $0 \le t \le T$.

Proof. Lemmas 2.9.1 and 2.6.6 prove that $\mathbb{E}[r^0(\nu^0)] \in L^2([0,T])$ and $\mathcal{K} \in L^2([0,T]^2)$, respectively. Then from (2.3.6) and Fubini's theorem it follows that

$$\mathbb{E}[\nu_t^{1,*}(\nu^0)] = -\mathbb{E}\left[r_t^0(\nu^0)\right] - r_t^1\int_0^t \mathcal{K}(s,t)\mathbb{E}\left[r_s^0(\nu^0)\right]ds.$$

Together with (2.9.1) we get

$$\begin{aligned}\mathbb{E}[\nu_t^{1,*}(\nu^0)] = &-\frac{1}{2\lambda_1}(\mathsf{K}_1^*\bar{\mu})(t) + \frac{\kappa_0}{2\lambda_1}(\mathsf{K}_1^*\nu^0)(t) \\ &- r_t^1\int_0^t \mathcal{K}(s,t)\left(\frac{1}{2\lambda_1}(\mathsf{K}_1^*\bar{\mu})(s) - \frac{\kappa_0}{2\lambda_1}(\mathsf{K}_1^*\nu^0)(s)\right)ds.\end{aligned} \tag{2.9.4}$$

By using (2.7.2), (2.7.3) and (2.7.5) in (2.9.4) we get the result. □

The following lemma simply follows from (2.2.2) and integration by parts hence we omit the proof.

Lemma 2.9.3. *Let M be a martingale as in (2.2.1). Then for any $\nu^0 \in \mathcal{A}_M^{q_0}$, we have*

$$\mathbb{E}\left[\int_0^T M_t \nu_t^0 dt\right] = M_0 q_0.$$

In the following proposition we derive an operator differential equation which is satisfied by the operator G in (2.3.11).

Proposition 2.9.4. *For any $\psi \in L^2([0,T])$ the operator G satisfies the following differential equation,*

$$\frac{d}{dt}(\mathsf{G}\psi)(t) = r_t^1(\mathsf{G}\psi)(t) + (\mathsf{K}_1^*\psi)(t), \quad (\mathsf{G}\psi)(0) = 0, \quad 0 \le t \le T. \tag{2.9.5}$$

Moreover, $(\mathsf{G}\psi)(t)$ is continuously differentiable on $[0,T]$.

Proof. Let $\psi \in L^2([0,T])$. From Proposition 2.8.1 it follows that $\mathcal{G}$ is jointly continuous on $[0,T]^2$ hence by (2.3.11) we get that $(\mathsf{G}\psi)(t)$ is continuous on $[0,T]$.

Note that by (2.3.3) we have

$$\frac{d\xi^{\pm}}{dt} = \pm r_t^1 \xi_t^{\pm}, \quad \text{for all } 0 \le t \le T. \tag{2.9.6}$$

Since by Proposition 2.6.7 r^1 is continuous over $[0,T]$, it follows from (2.9.6) that $\xi^{\pm}$ are continuously differentiable on $[0,T]$. From (2.8.2), (2.8.4) and (2.9.6) we get that

$$\begin{aligned}
\frac{d}{dt}(\mathsf{G}\psi)(t) &= \frac{d}{dt}\left(\xi_t^+ \int_0^t \xi_s^-(\mathsf{K}_1^*\psi)(s)ds\right) \\
&= r_t^1\left(\xi_t^+ \int_0^t \xi_s^-(\mathsf{K}_1^*\psi)(s)ds\right) + (\mathsf{K}_1^*\psi)(t) \\
&= r_t^1(\mathsf{G}\psi)(t) + (\mathsf{K}_1^*\psi)(t).
\end{aligned}$$

Since by (2.7.5) that the operator G can be represented in terms of K_1 and K_1^* and Lemma 2.6.6 shows that $\mathcal{K}$ is jointly continuous on $[0,T]^2$, it follows from (2.7.3) and (2.7.4) that $(\mathsf{G}\psi)(t)$ and $(\mathsf{K}_1^*\psi)(t)$ are continuous on $[0,T]$. Since we have show

that r_t^1 is also continuous, it follows that $\frac{d}{dt}(\mathsf{G}\psi)$ is continuous over $[0,T]$. Finally, note that

$$(\mathsf{K}_1\psi)(0) = \int_0^T \mathcal{K}(s,0)\mathbb{1}_{\{s\leq 0\}}\psi(s)ds = 0.$$

From (2.7.5) we have $(\mathsf{G}\psi)(t) = (\mathsf{K}_1\mathsf{K}_1^*\psi)(t)$. This proves that $(\mathsf{G}\psi)(0) = 0$ and completes the proof. □

Now we are ready to prove Lemma 2.7.5.

Proof of Lemma 2.7.5. Let $\nu^0 \in \mathcal{A}_M^{q_0}$. Recall that minor agent's strategy is assumed to be $\nu^{1,*}$ in (2.3.6). We define

$$Z_t^\nu = Y_t^\nu - \int_0^t \mu_s ds, \quad 0 \leq t \leq T. \tag{2.9.7}$$

Note that from (2.2.7) it follows that $Z_0^\nu = 0$.

Using (2.2.9) and (2.2.8) we get

$$\mathbb{E}\left[X_T^{0,\nu^0}\right] = x_0 + \mathbb{E}\left[\int_0^T (P_t^\nu - \lambda_0\nu_t^0)\nu_t^0 dt\right].$$

Together with (2.2.6), (2.2.3) and (2.9.7) we arrive at

$$\mathbb{E}\left[X_T^{0,\nu^0}\right] = x_0 + \mathbb{E}\left[\int_0^T M_t\nu_t^0 dt\right] + \mathbb{E}\left[\int_0^T Z_t^\nu dQ_t^{0,\nu^0}\right] - \int_0^T \lambda_0(\nu_t^0)^2 dt. \tag{2.9.8}$$

Recall that $Z_0^\nu = 0$ and $Q_T^{0,\nu^0} = 0$. Using integration by parts, (2.2.7), (2.9.7) and Fubini's theorem we obtain

$$\begin{aligned}\mathbb{E}\left[\int_0^T Z_t^\nu dQ_t^{0,\nu^0}\right] &= -\mathbb{E}\left[\int_0^T Q_t^{0,\nu^0} dZ_t^\nu\right] \\ &= -\int_0^T Q_t^{0,\nu}\left(\kappa_0\nu_t^0 + \kappa_1\mathbb{E}\left[\nu_t^{1,*}(\nu^0)\right] - \bar{\mu}_t\right) dt.\end{aligned} \tag{2.9.9}$$

Moreover, it follows from (2.2.3) that

$$\int_0^T Q_t^{0,\nu^0}\nu_t^0 dt = \frac{q_0^2}{2}. \tag{2.9.10}$$

By substituting (2.9.3), (2.9.9) and (2.9.10) into (2.9.8) we get

$$\mathbb{E}\left[X_T^{0,\nu^0}\right] = x_0 + M_0 q_0 - \kappa_0 \frac{q_0^2}{2} - \int_0^T Q_t^{0,\nu^0}(\kappa_1 \mathbb{E}[\nu_t^{1,*}(\nu^0)] - \bar{\mu}_t)dt - \int_0^T \lambda_0 (\nu_t^0)^2 dt. \tag{2.9.11}$$

Notice that from Proposition 2.9.4 and Lemma 2.9.2 we have

$$\mathbb{E}[\nu_t^{1,*}(\nu^0)] = \frac{\kappa_0}{2\lambda_1}\frac{d}{dt}(\mathsf{G}\nu^0)(t) - \frac{1}{2\lambda_1}\frac{d}{dt}(\mathsf{G}\bar{\mu})(t), \quad \text{for all } 0 \le t \le T. \tag{2.9.12}$$

Plugging in (2.9.12) into (2.9.11) gives

$$\begin{aligned}\mathbb{E}\left[X_T^{0,\nu^0}\right] = x_0 + M_0 q_0 - \kappa_0 \frac{q_0^2}{2} - \frac{\kappa_1\kappa_0}{2\lambda_1}\int_0^T Q_t^{0,\nu^0}\frac{d}{dt}(\mathsf{G}\nu^0)(t)dt \\ + \int_0^T Q_t^{0,\nu^0}\left(\frac{\kappa_1}{2\lambda_1}\frac{d}{dt}(\mathsf{G}\bar{\mu})(t) + \bar{\mu}_t\right)dt - \lambda_0\int_0^T (\nu_t^0)^2 dt.\end{aligned} \tag{2.9.13}$$

Since by (2.3.7) and (2.3.8), $\bar{\mu} \in L^2([0,T])$ and by (2.2.2) also $\nu^0 \in L^2([0,T])$, we get that from Proposition 2.9.4 that $(\mathsf{G}\bar{\mu})(0) = (\mathsf{G}\nu^0)(0) = 0$. Then by additional integration by parts and recalling that $Q_T^{0,\nu^0} = 0$ we get

$$\int_0^T Q_t^{0,\nu^0}\frac{d}{dt}(\mathsf{G}\nu^0)(t)dt = \int_0^T \nu_t^0(\mathsf{G}\nu^0)(t)dt, \tag{2.9.14}$$

as well as

$$\int_0^T Q_t^{0,\nu^0}\frac{d}{dt}(\mathsf{G}\bar{\mu})(t)dt = \int_0^T \nu_t^0(\mathsf{G}\bar{\mu})(t)dt. \tag{2.9.15}$$

Hence, by plugging in (2.9.14) and (2.9.15) into (2.9.13) we obtain

$$\begin{aligned}\mathbb{E}\left[X_T^{0,\nu^0}\right] = x_0 + M_0 q_0 - \kappa_0 \frac{q_0^2}{2} - \frac{\kappa_1\kappa_0}{2\lambda_1}\int_0^T \nu_t^0(\mathsf{G}\nu^0)(t)dt \\ + \int_0^T \left(\frac{\kappa_1}{2\lambda_1}\nu_t^0(\mathsf{G}\bar{\mu})(t) + Q_t^{0,\nu^0}\bar{\mu}_t\right)dt - \lambda_0\int_0^T (\nu_t^0)^2 dt,\end{aligned} \tag{2.9.16}$$

which together (2.2.10), proves the result. □

2.10 Proofs of the Numerical Results in Section 2.5

Throughout this section we assume that Assumption 2.3.1 holds. Our first goal is to prove Proposition 2.5.2, but before getting to the proof we introduce an auxiliary lemma.

Lemma 2.10.1. *Let $(\mathcal{G}_n)_{n\geq 1}$ be defined as in (2.5.4). Then, $\mathcal{G}_n$ is in $L^2([0,T]^2)$ for any $n \geq 1$.*

Proof. Recall that G was defined in (2.3.11). From Proposition 2.7.4 it follows that G is an operator in $B(L^2([0,T]))$. Recall $(a_i)_{i\geq 1}$ is a complete orthonormal basis in $L^2([0,T])$, hence from (2.5.3) we get that $(b_i)_{i\geq 1}$ are in $L^2([0,T])$. We therefore get from (2.5.4) that

$$\begin{aligned}\int_0^T \int_0^T \mathcal{G}_n(t,s)^2 dsdt &\leq n \sum_{i=1}^{n} \left(\int_0^T a_i^2(t)dt\right)\left(\int_0^T b_i^2(s)ds\right) \\ &< \infty,\end{aligned} \tag{2.10.1}$$

and the result follows. □

Proof of Proposition 2.5.2. The result follows directly from Lemma 2.10.1 and (2.5.5). □

Before we prove Proposition 2.5.4 we introduce the following theorem from Atkinson (1997).

Theorem 2.10.2 ((Atkinson, 1997, Theorem 2.1.1))**.** *Let G be in $B(L^2([0,T]))$ and let $\lambda \in \mathbb{R}$. Assume that $\mathsf{I} - \lambda\mathsf{G}$ is invertible on $L^2([0,T])$. Furthermore, assume that $(\mathsf{G}_n)_{n\geq 1}$ is a sequence of operators in $B(L^2([0,T]))$ with*

$$\lim_{n\to\infty} ||\mathsf{G} - \mathsf{G}_n|| = 0.$$

Then the following holds:

(i) *there exists an* $N \geq 1$ *such that for all* $n \geq N$ *the operators* $(\mathsf{I} - \lambda \mathsf{G}_n)^{-1}$ *exists and are in* $B(L^2([0,T]))$*;*

(iii) $(\mathsf{I} - \lambda \mathsf{G}_n)^{-1}$ *converges to* $(\mathsf{I} - \lambda \mathsf{G})^{-1}$ *in* $B(L^2([0,T]))$*, that is*

$$\lim_{n \to \infty} \left|\left|(\mathsf{I} - \lambda \mathsf{G}_n)^{-1} - (\mathsf{I} - \lambda \mathsf{G})^{-1}\right|\right| = 0;$$

(iii) $\left|\left|(\mathsf{I} - \lambda \mathsf{G}_n)^{-1}\right|\right|$ *converges to* $\left|\left|(\mathsf{I} - \lambda \mathsf{G})^{-1}\right|\right|$*, that is*

$$\lim_{n \to \infty} \left|\left|(\mathsf{I} - \lambda \mathsf{G}_n)^{-1}\right|\right| = \left|\left|(\mathsf{I} - \lambda \mathsf{G})^{-1}\right|\right|.$$

We define

$$\mathsf{R}_n := \left(\mathsf{I} + \frac{\kappa_1 \kappa_0}{2\lambda_0 \lambda_1} \mathsf{G}_n\right)^{-1}, \quad n \geq 1. \tag{2.10.2}$$

Proof of Proposition 2.5.4. Recall that $(\mathsf{G}_n)_{n \geq 1}$ was defined in (2.5.6) and that G was defined as in (2.3.11). From Propositions 2.5.2, 2.7.4 and 2.7.9 it follows that the assumptions of Theorem 2.10.2 hold, hence there exists an $N \geq 1$ such that for all $n \geq N$ the operators $\mathsf{I} + \frac{\kappa_1 \kappa_0}{2\lambda_0 \lambda_1} \mathsf{G}_n$ are invertible. Since for any $n \geq N$ the corresponding kernels $\mathcal{G}_n$ in (2.5.4) are degenerate, hence it follows from Theorem 2.1.2 of Atkinson (1997) that the matrices $I_n + \frac{\kappa_1 \kappa_0}{2\lambda_0 \lambda_1} \mathbb{G}_n$ are invertible (recall (2.5.10) for the definition of $\mathbb{G}_n$).

Let $g, \psi \in L^2([0,T])$ and define

$$\gamma_i = -\frac{\kappa_1 \kappa_0}{2\lambda_0 \lambda_1} \sum_{j=1}^{n} \left(I_n + \frac{\kappa_1 \kappa_0}{2\lambda_0 \lambda_1} \mathbb{G}_n\right)^{-1}_{ij} \langle \psi, b_j \rangle_{L^2}, \quad i = 1, \ldots, n,$$

for any $n \geq N$. As shown in Chapter 3 of Porter and Stirling (1990) (see equations (3.5) – (3.7) therein) the unique solution to

$$\left(\mathsf{I} + \frac{\kappa_1 \kappa_0}{2\lambda_0 \lambda_1} \mathsf{G}_n\right) g = \psi,$$

is given by

$$g(t) = \psi(t) + \sum_{i=1}^{n} \gamma_i a_{i,n}(t), \quad \text{for all } 0 \le t \le T, \quad n \ge N,$$

and (2.5.11) follows. □

Before proving Proposition 2.5.5, we need to present two intermediate lemmas.

Lemma 2.10.3. *Let* R *be defined as in* (2.3.14) *and let* $(\mathsf{R}_n)_{n\ge1}$ *be defined as in* (2.10.2). *Then the following holds:*

(i)

$$\liminf_n \langle \mathsf{R}_n 1\,,\, 1\rangle_{L^2} > 0,$$

(ii)

$$\lim_{n\to\infty} \frac{1}{\langle \mathsf{R}_n 1\,,\, 1\rangle_{L^2}} = \frac{1}{\langle \mathsf{R} 1\,,\, 1\rangle_{L^2}}.$$

Proof. (i) We have shown in the proof of Proposition 2.5.4 that the assumptions of Theorem 2.10.2 hold, hence there exists an $N \ge 1$ such that for all $n \ge N$ the operators R_n exist. From the Cauchy-Schwarz inequality and since $\|1\|_{L^2} = T$ we get

$$\begin{aligned} |\langle \mathsf{R}_n 1\,,\, 1\rangle_{L^2} - \langle \mathsf{R} 1\,,\, 1\rangle_{L^2}| &\le \|\mathsf{R}_n - \mathsf{R}\| \|1\|_{L^2}^2 \\ &\le \|\mathsf{R}_n - \mathsf{R}\| T^2. \end{aligned} \tag{2.10.3}$$

From Proposition 2.7.9(ii) it follows that the operator R is bounded from below, therefore, by Definition 2.7.3, there exists $\varepsilon > 0$ such that

$$\langle \mathsf{R} 1\,,\, 1\rangle_{L^2} > \varepsilon. \tag{2.10.4}$$

From Theorem 2.10.2(iii) we get that there exists an $N_1 \ge N$ such that for all $n \ge N_1$ we have that

$$||\mathsf{R}_n - \mathsf{R}|| < \varepsilon T^{-2}/2. \tag{2.10.5}$$

From (2.10.3)–(2.10.5) we get (i).

(ii) follows directly from (2.10.3), (2.10.4) and (i). □

Next, we prove the convergence of the sequence of constants $(\eta_n)_{n\geq 1}$ from (2.5.12).

Lemma 2.10.4. *Let η and η_n be defined as in (2.3.16) and (2.5.12), respectively. Then, there exists $N \geq 1$ such that for all $n \geq N$ the constants η_n are well-defined. Moreover,*

$$\lim_{n\to\infty} \eta_n = \eta. \tag{2.10.6}$$

Proof of Lemma 2.10.4. From Lemma 2.10.3(i), (2.3.16) and (2.10.2) if follows that for all n sufficiently large η_n is well defined. The same claim holds for η by (2.5.12), (2.10.4) and Proposition 2.7.9(i). From Cauchy-Schwarz inequality we get

$$|\langle \mathsf{R}_n \mathsf{S}\bar{\mu}, 1\rangle_{L^2} - \langle \mathsf{R}\mathsf{S}\bar{\mu}, 1\rangle_{L^2}| \leq \|\mathsf{R} - \mathsf{R}_n\| \|\mathsf{S}\bar{\mu}\|_{L^2} \|1\|_{L^2},$$

and together with Theorem 2.10.2(iii) and Lemma 2.7.10 it follows that

$$\lim_{n\to\infty} |\langle \mathsf{R}_n \mathsf{S}\bar{\mu}, 1\rangle_{L^2} - \langle \mathsf{R}\mathsf{S}\bar{\mu}, 1\rangle_{L^2}| = 0. \tag{2.10.7}$$

From (2.3.16) and (2.5.12) we have

$$|\eta_n - \eta| = \left| \frac{\langle \mathsf{R}_n \mathsf{S}\bar{\mu}, 1\rangle_{L^2}}{\langle \mathsf{R}_n 1, 1\rangle_{L^2}} - \frac{\langle \mathsf{R}\mathsf{S}\bar{\mu}, 1\rangle_{L^2}}{\langle \mathsf{R}1, 1\rangle_{L^2}} \right|, \tag{2.10.8}$$

hence (2.10.6) follows from Lemma 2.10.3 and (2.10.7). □

We are now ready to prove Proposition 2.5.5.

Proof of Proposition 2.5.5. From (2.3.15), (2.5.9) and (2.10.2) we have

$$\nu^{0,*} - \nu^{0,(n)} = (\mathsf{R} - \mathsf{R}_n)(\mathsf{S}\bar{\mu}) + \frac{1}{2\lambda_0}(\eta \mathsf{R}1 - \eta_n \mathsf{R}_n 1).$$

It follows that

$$\begin{aligned} ||\nu^{0,*} - \nu^{0,(n)}||_{L^2} \leq ||(\mathsf{R} - \mathsf{R}_n)(\mathsf{S}\bar{\mu})||_{L^2} + \frac{\eta}{2\lambda_0} ||(\mathsf{R} - \mathsf{R}_n)\, 1||_{L^2} \\ + \frac{1}{2\lambda_0} |\eta_n - \eta| \|\mathsf{R}_n 1\|_{L^2}. \end{aligned}$$

Hence by Lemma 2.10.4, Theorem 2.10.2(iii) and following similar lines as in the proof of (2.10.7) we get

$$\lim_{n\to\infty} \left|\left|\nu^{0,*} - \nu^{0,(n)}\right|\right|_{L^2} = 0.$$

□

Finally, we we prove Theorem 2.5.6.

Proof of Theorem 2.5.6. Throughout the proof we consider n's large enough such that the results of Lemma 2.10.4 and Proposition 2.5.5 hold, even if it is not stated explicitly.

(i) From (2.5.14) and (2.7.14) we get

$$\begin{aligned}\nu_t^{0,*} - \hat{\nu}_t^{0,(n)} &= -\frac{\kappa_1\kappa_0}{2\lambda_0\lambda_1}\left(\mathsf{G}\left(\nu^{0,*} - \nu^{0,(n)}\right)\right)(t) + \frac{\eta - \eta_n}{2\lambda_0} \\ &= -\frac{\kappa_1\kappa_0}{2\lambda_0\lambda_1}\int_0^T \mathcal{G}(t,s)\left(\nu_s^{0,*} - \nu_s^{0,(n)}\right) ds + \frac{\eta - \eta_n}{2\lambda_0},\end{aligned}$$

where we used (2.3.11) in the second equality.

From Cauchy-Schwarz inequality we get for all $0 \le t \le T$ and n sufficiently large,

$$\left|\nu_t^{0,*} - \hat{\nu}_t^{0,(n)}\right| \le \frac{\kappa_1\kappa_0}{2\lambda_0\lambda_1}\left(\int_0^T |\mathcal{G}(t,s)|^2 ds\right)^{1/2} \left|\left|\nu^{0,*} - \nu^{0,(n)}\right|\right|_{L^2} + \frac{|\eta - \eta_n|}{2\lambda_0}.$$

Hence, from Proposition 2.8.1, Lemma 2.10.4 and Proposition 2.5.5, we get (i).

(ii) From Proposition 2.6.7 it follows that r^1 is bounded over $[0,T]$ and from Lemma 2.6.6 we get that the kernel $\mathcal{K}$ is bounded over $[0,T]^2$. Together with (2.3.6) we get that there exists a constant $C > 0$ such that for all $0 \le t \le T$ and n sufficiently large we have

$$\begin{aligned}\left|\nu_t^{1,*}\left(\nu^{0,*}\right) - \nu_t^{1,*}\left(\hat{\nu}^{0,(n)}\right)\right| \le{}& \left|r_t^0\left(\hat{\nu}^{0,(n)}\right) - r_t^0\left(\nu^{0,*}\right)\right| \\ &+ C\left|\int_0^t \left(r_s^0\left(\hat{\nu}^{0,(n)}\right) - r_s^0\left(\nu^{0,*}\right)\right) ds\right|.\end{aligned} \tag{2.10.9}$$

By plugging in (2.3.5) into (2.10.9) and observing that the stochastic part in the right hand side of (2.3.5) cancels, we conclude that

$$\begin{aligned}\left|\nu_t^{1,*}\left(\nu^{0,*}\right)-\nu_t^{1,*}\left(\hat{\nu}^{0,(n)}\right)\right| \leq C_1 \int_t^T \left|\hat{\nu}_s^{0,(n)}-\nu_s^{0,*}\right| ds \\ + C_2 \int_0^t \left(\int_s^T \left|\hat{\nu}_r^{0,(n)}-\nu_r^{0,*}\right| dr\right) ds,\end{aligned} \tag{2.10.10}$$

for some constants $C_1, C_2 > 0$ independent from n and t. Then (ii) follows from (2.10.10) and (i). □

3

Closed-Loop Nash Competition for Liquidity

The results presented in this chapter are based on the paper Micheli et al. (2021) and are joint work with Prof. Johannes Muhle-Karbe and Dr. Eyal Neuman. The paper Micheli et al. (2021) has been revised and submitted to *Mathematical Finance* for publication.

3.1 Introduction

Most quantitative trading strategies are based on some form of "signals" about future price changes. A major obstacle to make such strategies profitable in practice is the adverse price impact caused by the rapid execution of large orders. In particular for large portfolios, this requires to strike a delicate balance between exploiting trading opportunities, but only doing so if the respective signals are strong and persistent enough to outweigh the associated trading costs.

Accordingly, a large and rapidly growing literature studies how to optimally exploit trading signals with various dynamics in the presence of superlinear trading costs as in the models pioneered by Almgren and Chriss (2000), cf., e.g., Gârleanu and Pedersen (2013, 2016); Cartea and Jaimungal (2016); Moreau, Muhle-Karbe,

and Soner (2017); Lehalle and Neuman (2019); Collin-Dufresne, Daniel, and Saglam (2020) and the references therein[1]. In this context, many investors use variants of the same trading signals, such as moving averages of past price changes (Gârleanu and Pedersen, 2013), order-book imbalances (Cont and de Larrard, 2013; Cont, Kukanov, and Stoikov, 2014; Lipton, Pesavento, and Sotiropoulos, 2013; Cartea and Jaimungal, 2016; Lehalle and Neuman, 2019), or price-dividend ratios (Barberis, 2000). Such "crowded" signals naturally lead to stochastic games, where the agents interact through the rates at which they draw on the same pool of liquidity.

"Market-impact games" of this kind have been analyzed in depth for the optimal execution of a single exogenously given order, exploiting that the corresponding optimal trading patterns are deterministic in many cases as, cf. Brunnermeier and Pedersen (2005); Carlin, Lobo, and Viswanathan (2007); Schied and Schöneborn (2009) as well as many more recent studies.[2] More recently, a number of papers also analyze the competition for liquidity between agents that trade to exploit a common trading signal (Voß, 2019; Drapeau, Luo, Schied, and Xiong, 2019; Evangelista and Thamsten, 2020; Neuman and Voß, 2021). To obtain tractable results, these papers focus on *open-loop* Nash equilibria. This means that each player considers the others' actions to be fixed, when deciding whether to unilaterally deviate from the putative equilibrium. Each player's optimality condition can in turn be derived in analogy to the single-agent version of the model, with the other agents' actions acting as additional exogenous inputs. A Nash equilibrium can in turn be derived in a second step by imposing the consistency condition that all single-agent optimality conditions must hold simultaneously. For optimal trading problems with mean-reverting signals and linear price impact, this leads to multidimensional but linear systems of forward-backward stochastic differential equations, which admit closed-form solutions.

Even more tractable results obtain in the mean-field limit of many small agents, which often reduces the analysis to single-agent stochastic control problems with

[1] Linear costs corresponding to bid-ask spreads, which are the dominant frictions for somewhat smaller portfolios, are studied in De Lataillade et al. (2012); Martin (2014), for example.

[2] In particular, Chen, Choi, Larsen, and Seppi (2021b) show how to endogenize price dynamics, interest rates, and permanent price impact in a setting with deterministic trading schedules.

the average of all agents actions acting as an additional exogenous input. In the present context, such models have been studied by Cardaliaguet and Lehalle (2018); Casgrain and Jaimungal (2019, 2020); Fu, Graewe, Horst, and Popier (2021); Neuman and Voß (2021), for example.

In contrast, much less is known about *closed-loop* Nash equilibria, where other agents react to unilateral deviations from a putative equilibrium. More specifically, each agent then assumes that the feedback form of the others' controls are fixed but takes into account unilateral deviations through their impact on the state variables of the model. The controls of the other agents in turn can no longer be treated as an exogenous input for the single-agent optimization, leading to a much more involved coupling between the agents' individual optimality conditions.

In this chapter, we study a stylized model for such closed-loop Nash equilibria, and analyze how this more sophisticated form of competition changes optimal trading patterns and welfare relative to the open-loop and to a central-planner solution. In order to obtain tractable results, we focus on a symmetric infinite-horizon model,[3] where a finite number of identical agents trade a risky asset, whose returns are partially predictable through a trading signal with Ornstein-Uhlenbeck dynamics. All agents' trading problems are intertwined through their common linear (instantaneous) price impact on the asset's execution price.

We show that the corresponding individual optimality and consistency conditions can be expressed in terms of a system of nonlinear algebraic equations. Unlike in more complex settings with endogenous price dynamics (Sannikov and Skrzypacz, 2016; Obizhaeva and Wang, 2019), we then prove that this system has a unique solution when the price impact parameter λ is small enough. With this solution in hand, we can in turn verify that the proposed candidate indeed is a closed-loop Nash equilibrium, which is unique in the linear class that contains the (globally unique) open-loop and central-planner solutions. This analysis is compli-

[3] Finite-horizon models lead to analytically intractable systems of coupled differential equations already for stochastic factor processes, compare Carmona and Yang (2008). In a different price impact model (where agents' holdings affect future expected returns), existence results for a finite horizon model have been obtained by Chen, Choi, Larsen, and Seppi (2021a).

cated by the fact that even in the limit $\lambda = 0$, the system does not admit a tractable solution as in single-agent models (Gârleanu and Pedersen, 2016). Therefore, in order to show that our candidate value function is well defined and establish a verification theorem, we need to establish and exploit various implicit properties of the solution.

At the leading order for small price impact, the equilibrium trading rates admit asymptotic expansions, which disentangle the effects of trading costs, inventory costs and Nash competition between the agents. In our model, limited liquidity creates a negative externality, where agents only internalize the adverse effects that their price impact has on their own execution rates but not others'. Accordingly, Nash competition leads to excessive trading relative to the central-planner benchmark. Closed-loop equilibria, where agents react to out-of-equilibrium deviations, move part of the way from the open-loop solution to its central-planner counterpart. By somewhat reducing excessive trading, they in turn also reduce the "price of anarchy" by which the agents' optimal performance is reduced due to the lack of perfect coordination[4] due to the changes in the investment opportunity set.

However, both asymptotically and by the numerical computation of the exact equilibrium for realistic model parameters from Collin-Dufresne et al. (2020), we find that the closed-loop equilibrium quantitatively lies much closer to its open-loop counterpart than to the central-planner solution. At least for the symmetric model that we consider here, this suggests that open-loop models can indeed serve as an accurate but much more tractable proxy for closed-loop Nash equilibria.

To the best of our knowledge, the present chapter is the first existing example in the literature where open-loop and closed-loop equilibria are compared qualitatively and quantitatively in a finite-player game with interaction through the controls. Such comparisons were derived by Carmona et al. (2013) for systemic risk games, for example, which involve interactions through the state processes, but not through the controls. Lacker and Zariphopoulou (2019); Lacker and Soret (2020); Chen et al.

[4]Unlike in Chen et al. (2021b), where the difference between Nash equilibria and central planner solutions disappears over time, this difference is persistent in our model

(2021b) computed explicit closed-loop Nash equilibria for games with interactions through the controls, but the controls happen to be deterministic so that the open-loop and closed-loop equilibria coincide.

Some related work has appeared recently on convergence of the finite-player Nash equilibrium to the corresponding mean-field equilibrium in various settings. Laurière and Tangpi (2020) proved such convergence results for open-loop equilibria of games with idiosyncratic noise for each of the players. Neuman and Voß (2021) studied the corresponding problem for execution games with common noise. Lacker and Le Flem (2021) and Djete (2021) proved the convergence of closed-loop solutions (under the a-priori assumption that they exist) to the mean-field solution in the case where each player is influenced by idiosyncratic and common noise. In both these papers the idiosyncratic noise is crucial to establish the convergence. Even though the game in the present chapter only has common noise, numerical evidence suggests that open- and closed-loop nevertheless converge to the same mean-field limits. A rigorous proof of this result is a challenging open problem for future research.

The remainder of this chapter is organized as follows. In Section 3.2 we present the multiplayer game. Section 3.3 contains our main results on the corresponding closed-loop Nash equilibrium. A comparison between the closed-loop, open-loop and central-planner solution is subsequently presented in Section 3.4. Section 3.5 outlines the heuristic derivation of the closed-loop equilibrium. The rigorous proofs of these results are in turn developed in Section 3.6; the most onerous calculations are delegated to Appendix B for better readability.

3.2 Model Setup

3.2.1 Financial Market

Throughout this chapter, we fix a filtered probability space $(\Omega, \mathcal{F}, (\mathcal{F}_t)_{t\geq 0}, \mathbb{P})$ supporting two standard Brownian motions $(W_t^P)_{t\geq 0}$ and $(W_t)_{t\geq 0}$. We consider a

financial market with two assets. The first one is safe, with price normalised to one. The other asset is risky; its exogenous unaffected price process $(P_t)_{t\geq 0}$ has dynamics

$$dP_t = \mu_t dt + \sigma_P dW_t^P, \quad P_0 = p_0, \tag{3.2.1}$$

for a positive constant p_0. Here, the volatility is a positive constant σ_P; the expected returns have mean-reverting Ornstein-Uhlenbeck dynamics

$$d\mu_t = -\beta\mu_t dt + \sigma dW_t, \quad \mu_0 = m, \tag{3.2.2}$$

for positive constants β, σ and for $m \in \mathbb{R}$. (We set the mean-reversion level to zero to simplify the already involved algebra below.) The current expected return μ_t can be interpreted as a signal about future price changes, such as dividend yields (Barberis, 2000), moving averages of past returns (Gârleanu and Pedersen, 2013; Martin, 2014), or order-book imbalances (Cont et al., 2014; Lipton et al., 2013; Cartea and Jaimungal, 2016; Lehalle and Neuman, 2019), for example.

3.2.2 Agents

The assets are traded by $N \geq 2$ identical agents indexed by $n = 1, \ldots, N$. Starting from an initial position $x \in \mathbb{R}$, they adjust their risky holdings $\varphi^n = (\varphi_t^n)_{t\geq 0}$ at absolutely continuous trading rates $\dot{\varphi}_t^n = d\varphi_t^n/dt$, because their *aggregate* trading activity $\dot{\varphi} = (\dot{\varphi}^1, \ldots, \dot{\varphi}^N)$ has an adverse linear temporary impact on the execution price:

$$P_t^{\dot{\varphi}} = P_t + \lambda \sum_{i=1}^{N} \dot{\varphi}_t^i, \qquad t \geq 0, \tag{3.2.3}$$

for a positive constant λ. For each agent n, the others' trading rates are denoted by

$$\dot{\varphi}^{-n} = (\dot{\varphi}^1, \ldots, \dot{\varphi}^{n-1}, \dot{\varphi}^{n+1}, \ldots, \dot{\varphi}^N).$$

As in Gârleanu and Pedersen (2016), the agents choose their trading rates $\dot{\varphi}^n$ to maximize expected discounted returns over an infinite horizon, penalized for risk

and transaction costs (relative to the unaffected execution prices):

$$J^n(\dot{\varphi}^n; \dot{\varphi}^{-n}) = \mathbb{E}\left[\int_0^\infty e^{-\rho t}\left(\mu_t \varphi_t^n - \frac{\gamma}{2}(\varphi_t^n)^2 - \lambda \dot{\varphi}_t^n \left(\sum_{i=1}^N \dot{\varphi}_t^i\right)\right) dt\right]. \tag{3.2.4}$$

Here, $\rho > 0$ is the time-discount rate and $\gamma > 0$ penalizes risk through a running cost on the agents' squared inventories.[5] To ensure that all terms in these goal functionals are well defined, we focus on *admissible* trading rates for which $\dot{\varphi} = (\dot{\varphi}^1, \dots, \dot{\varphi}^N) \in \mathcal{A}_\rho^N$ and $\varphi = (\varphi^1, \dots, \varphi^N) \in \mathcal{A}_\rho^N$, where $\mathcal{A}_\rho$ denotes the progressively measurable processes $(X_t)_{t\geq 0}$ that satisfy $\mathbb{E}\left[\int_0^\infty e^{-\rho t} X_t^2 dt\right] < \infty$ and $\mathcal{A}_\rho^N$ is the space of N-dimensional vectors of such processes.

3.2.3 Nash Equilibrium

Due to their joint impact on the execution price (3.2.3) of the risky asset, the agents' optimization problems (3.2.4) are intertwined. Their interaction accordingly has to be studied in a game-theoretic fashion:

Definition 3.2.1. *Admissible trading rates $\dot{\varphi} = (\dot{\varphi}^1, \dots, \dot{\varphi}^N)$ form a* Nash equilibrium *if, given the trading rates $\dot{\varphi}^{-n}$ of the other agents, no agent $n = 1, \dots, N$ has an incentive to deviate from the equilibrium because $\dot{\varphi}^n$ already maximizes the corresponding goal functional* (3.2.4).

In dynamic models, different notions of Nash equilibria arise depending on whether agents anticipate that others may react if they deviate from the equilibrium. In the present context, a number of recent papers (Voß, 2019; Casgrain and Jaimungal, 2020; Neuman and Voß, 2021) study *open-loop* Nash equilibria, where each agent treats the others' trading rates as fixed stochastic processes. This means that agents do not consider at all how the others may react if they were to deviate from the equilibrium.

[5] As in many related studies, this is a reduced-form proxy for an exponential utility function with constant absolute risk aversion. Formally carrying out the analysis below for such a goal functional is still feasible by adapting single-agent results (Champonnois and Sefton, 2021). However, in the present game-theoretic context this would lead to a very high-dimensional system of nonlinear equations for which existence is unclear as in Obizhaeva and Wang (2019).

In this chapter, we extend this analysis by solving for a *closed-loop* Nash equilibrium in feedback form (Carmona, 2016, Chapter 5.1.2). To wit, each agent considers the others' feedback controls to be fixed, but takes into account how their own deviations from the equilibrium impact others' trading through their effect on the model's state variables.[6] In the present context, single-agent optimal trading rates (Gârleanu and Pedersen, 2016) and open-loop Nash equilibria (Voß, 2019) are functions of the (exogenous) trading signal μ_t and the (endogenous) risky positions $\varphi_t = (\varphi_t^1, \ldots, \varphi_t^N)$ of the agents. We therefore naturally search for a closed-loop equilibrium in the same class of strategies. If agents unilaterally deviate from the equilibrium, this changes their positions and then in turn feeds back into the trades of the other agents.

Formally, this leads to the following notion of Nash equilibrium.

Definition 3.2.2 ((Admissible) Feedback Controls)**.** *A* feedback trading rate *is a function* $\dot{\varphi} : \mathbb{R}^{1+N} \to \mathbb{R}^N$ *that maps the current value of the signal* μ_t *and the agents' risky positions* $\varphi_t = (\varphi_t^1, \ldots, \varphi_t^N)$ *to the rates at which the agents' risky positions are adjusted. A trading rate is* admissible *if the* $\mathbb{R}^N$*-valued system of controlled positions*

$$d\varphi_t = \dot{\varphi}(\mu_t, \varphi_t)dt$$

has a unique solution for which $\dot{\varphi} = (\dot{\varphi}(\mu_t, \varphi_t))_{t\geq 0}$ *and* φ *belongs to* $\mathcal{A}_\rho^N$*.*

Definition 3.2.3 (Closed-Loop Nash Equilibrium)**.** *An admissible feedback control is a* closed-loop Nash equilibrium*, if no agent* $n = 1, \ldots, N$ *has an incentive to deviate from the equilibrium in that*

$$J^n(\dot{\varphi}^n; \dot{\varphi}^{-n}) \geq J^n(\dot{\psi}^n; \dot{\varphi}^{-n}),$$

for all admissible feedback trading rates $\dot{\psi} = (\dot{\varphi}^1, \ldots, \dot{\varphi}^{n-1}, \dot{\psi}^n, \dot{\varphi}^{n+1}, \ldots, \dot{\varphi}^N)$ *where the other agents' feedback controls remain fixed.*

[6] The even more sophisticated notion of "subgame perfect Nash equilibria" is studied by Chen, Choi, Larsen, and Seppi (2021a) in a model where agents' holdings affect the expected returns of the risky asset. This means that even the feedback controls of the other agents are not fixed out of equilibrium, but have to solve an appropriate optimization problem, too. For the present model with instantaneous trading costs, this form of interaction does not appear to be tractable.

In order to further elucidate the notion of closed-loop Nash equilibrium we compare it with the following definition of open-loop Nash equilibrium.

Definition 3.2.4 (Open-Loop Nash Equilibrium)**.** *Admissible trading rates* $\dot{\varphi} = (\dot{\varphi}^1, \dots, \dot{\varphi}^N)$ *form an* open-loop Nash equilibrium *if no agent* $n = 1, \dots, N$ *has an incentive to deviate from the equilibrium, in that*

$$J^n(\dot{\varphi}^n, \dot{\varphi}^{-n}) \geq J^n(\dot{\psi}^n, \dot{\varphi}^{-n}),$$

for all admissible trading rates $\dot{\psi}^n \in \mathcal{A}_\rho$ *of agent* n*.*

Remark 3.2.5. *Let us emphasize the difference between this notion and the closed-loop Nash competition studied in the present chapter. In Definition 3.2.4, each agent treats the others' trading strategies as fixed stochastic processes when considering whether to deviate unilaterally from the equilibrium. In contrast, in closed-loop equilibria as in Definition 3.2.3, such deviations change the agent's own inventory and in turn feed back into the other agents' trading decisions through their feedback controls.*

3.3 Main Results

We are now ready to state our main result. It shows that, for sufficiently small price impact λ, there exists a symmetric closed-loop Nash equilibrium. The corresponding equilibrium trading rate is linear with respect to the signal μ_t and the agents inventories $\varphi_t = (\varphi_t^1, \dots, \varphi_t^N)$. More specifically, it tracks an "aim portfolio" (a constant multiple M_{aim} of the frictionless optimal holdings μ_t/γ) with a constant (relative) trading rate M_{rate}. This parallels results for single-agent models (Gârleanu and Pedersen, 2016), a central planner (Section 3.4.1), or open-loop equilibria (Voß (2019); Casgrain and Jaimungal (2020) or Section 3.4.2). However the coefficients as well as the corresponding optimal value all depend on the form of the agents' strategic interaction. We discuss this in more detail in Section 3.4.3 below.

Theorem 3.3.1 (Closed-Loop Nash Equilibrium)**.** *For sufficiently small λ, there exists a symmetric closed-loop equilibrium, where*

$$\dot{\varphi}_t^n = M_{rate}\left(M_{aim}\frac{\mu_t}{\gamma} - \varphi_t^n\right), \quad n = 1, \dots, N, \tag{3.3.1}$$

for some positive constants M_{rate}, M_{aim}. For zero initial positions ($\varphi_0^1 = \dots = \varphi_0^N = 0$) and a zero initial signal ($\mu_0 = 0$), the corresponding equilibrium value of the agents' goal functionals (3.2.4) is

$$\begin{aligned} J^n(\dot{\varphi}^n; \dot{\varphi}^{-n}) = &\left(1 + 2\lambda N M_{rate}^2 \frac{M_{aim}}{\gamma}\right) \frac{M_{rate} M_{aim}}{\gamma} \frac{\sigma^2}{\rho(2\beta + \rho)(\beta + \rho + M_{rate})} \\ &- \frac{1}{\rho(2\beta + \rho)} \left(\frac{\sigma M_{rate} M_{aim}}{\gamma}\right)^2 \left(\lambda N + \frac{\gamma + 2\lambda N M_{rate}^2}{(\rho + 2M_{rate})(\beta + \rho + M_{rate})}\right). \end{aligned} \tag{3.3.2}$$

For better readability, the lengthy proof of Theorem 3.3.1 is deferred to Section 3.6.

Remark 3.3.2. *The coefficients M_{rate} and M_{aim} in Theorem 3.3.1 are given by (3.6.8) and (3.6.18) in terms of the solution to the system of equations (3.5.5)–(3.5.11), (3.5.12)–(3.5.14), which can be determined via the scalar equation (3.5.19). See Section 3.5 for more details.*

The constants in Theorem 3.3.1 are determined by the root of the scalar equation (3.5.19), which can readily be solved numerically. However, in order to disentangle the effects of holding costs γ, trading costs λ, and competition between N agents, it is also instructive to expand the solution for small λ. The proof of this result is again deferred to Section B.1.

Proposition 3.3.3. *For small price impact $\lambda \to 0$,*

$$M_{rate} = \sqrt{\frac{\gamma}{\lambda}}\Delta(N) + \mathcal{O}(1), \quad M_{aim} = 1 + \mathcal{O}(\sqrt{\lambda}), \tag{3.3.3}$$

for a nonnegative function $\Delta(N)$ that only depends on the number of agents N, cf. (3.5.22). For zero initial positions ($\varphi_0^1 = \dots = \varphi_0^N = 0$) and a zero initial signal

$(\mu_0 = 0)$, *the corresponding equilibrium value of the agents' goal functional satisfies*

$$J^n(\dot{\varphi}^n; \dot{\varphi}^{-n}) = \frac{\sigma^2}{2\rho\gamma(2\beta+\rho)} - \frac{\sqrt{\lambda}\sigma^2(1+2\Delta(N)^2 N)}{4\gamma^{3/2}\rho\Delta(N)} + \mathcal{O}(\lambda)\,. \tag{3.3.4}$$

Here, the function $\Delta(N)$ is determined by the unique root of the limiting version (3.5.20) of the scalar equation (3.5.19), which only depends on N but not the other model parameters.

3.4 Other Forms of Interactions

We now discuss some of the quantitative and qualitative implications of Theorem 3.3.1 and Proposition 3.3.3. More specifically, we consider how the equilibrium trading rates and their performances depend on the number of agents and the nature of their strategic interaction.

3.4.1 Central Planner

To better understand the closed-loop Nash equilibrium, one natural reference point is the case where the agents cooperate perfectly, in that a "central planner" chooses all of their controls $\dot{\varphi} = (\dot{\varphi}^1, \ldots, \dot{\varphi}^N)$ simultaneously in order to maximize the agents' average welfare:

$$\bar{J}(\dot{\varphi}) = \frac{1}{N}\sum_{n=1}^{N} J^n(\dot{\varphi}^n; \dot{\varphi}^{-n}). \tag{3.4.1}$$

By symmetry, maximizing the average welfare of the agents is equivalent to a single agent problem with price impact parameter $N\lambda$.[7]

[7] Put differently, in the "mean-field scaling" where each agent has mass $1/N$ so that the total mass of agents does not depend on N, the central-planner problem is exactly the same as each single agent's.

Optimum The optimal trading rates chosen by the central planner are

$$\dot{\varphi}_t^n = M_{rate}^{\mathrm{CP}} \left(M_{aim}^{\mathrm{CP}} \frac{\mu_t}{\gamma} - \varphi_t^n \right), \quad n = 1, ..., N,$$

where

$$M_{rate}^{\mathrm{CP}} = \sqrt{\frac{\gamma}{2N\lambda} + \frac{\rho^2}{4}} - \frac{\rho}{2} \in (0, \infty), \quad M_{aim}^{\mathrm{CP}} = \frac{\sqrt{\frac{\gamma}{2N\lambda} + \frac{\rho^2}{4}} + \frac{\rho}{2}}{\sqrt{\frac{\gamma}{2N\lambda} + \frac{\rho^2}{4}} + \frac{\rho}{2} + \beta} \in (0, 1).$$

For zero initial positions and a zero initial signal, the corresponding optimal performance is

$$\bar{J}(\dot{\varphi}) = \frac{\sigma^2}{2\rho} \frac{1}{2N\lambda(\rho + 2\beta)} \left(\frac{\rho}{2} + \beta + \sqrt{\frac{\gamma}{2N\lambda} + \frac{\rho^2}{4}} \right)^{-2}.$$

Asymptotics For small price impact $\lambda \to 0$, Taylor-expansion of these explicit formulas shows

$$M_{rate}^{\mathrm{CP}} = \sqrt{\frac{\gamma}{2N\lambda}} + \mathcal{O}(1), \quad M_{aim}^{\mathrm{CP}} = 1 + \mathcal{O}(\lambda), \tag{3.4.2}$$

and

$$\bar{J}(\dot{\varphi}) = \frac{1}{2\gamma} \frac{\sigma^2}{\rho(2\beta + \rho)} - \frac{\sigma^2}{2\rho} \frac{\sqrt{2N}}{\gamma^{3/2}} \sqrt{\lambda} + \mathcal{O}(\lambda).$$

3.4.2 Open-Loop Nash Equilibrium

Another important benchmark is the case of *open-loop* Nash competition studied by Voß (2019); Drapeau et al. (2019); Casgrain and Jaimungal (2020); Neuman and Voß (2021) and introduced in Definition 3.2.4.

Equilibrium For an open-loop equilibrium, each agent's optimality condition can be derived in analogy to the single agent case by treating the other agents' trading rates as fixed. This model is analogous to the single-agent infinite time horizon model studied by (Bouchard et al., 2018) and to the two agents finite

time horizon model developed in (Voß, 2019). In the transaction cost term, the corresponding first-order condition then leads to an integral of $\lambda(2\dot{\varphi}_t^1 + \sum_{n=2}^N \dot{\varphi}_t^n)$ rather than $\lambda 2\dot{\varphi}_t^1$ in the single-agent model.

In the symmetric case where all agents are identical and their trading strategies must therefore be the same, it follows that the open-loop equilibrium is again of the same form as the single-agent model, up to replacing the constant 2 with $N+1$ rather than with $2N$ as in the central-planner model throughout.

More specifically, in the unique open-loop Nash equilibrium each agent's optimal trading speed is given by

$$\dot{\varphi}_t^n = M_{rate}^{\mathrm{OL}} \left(M_{aim}^{\mathrm{OL}} \frac{\mu_t}{\gamma} - \varphi_t^n \right), \quad n = 1, ..., N,$$

for

$$M_{rate}^{\mathrm{OL}} = \sqrt{\frac{\gamma}{(N+1)\lambda} + \frac{\rho^2}{4}} - \frac{\rho}{2} \in (0, \infty), \qquad M_{aim}^{\mathrm{OL}} = \frac{\sqrt{\frac{\gamma}{(N+1)\lambda} + \frac{\rho^2}{4}} + \frac{\rho}{2}}{\sqrt{\frac{\gamma}{(N+1)\lambda} + \frac{\rho^2}{4}} + \frac{\rho}{2}} + \beta \in (0, 1).$$

For zero initial positions and a zero initial signal, the agents' corresponding common optimal value is

$$\begin{aligned} J_{\mathrm{OL}}^n(\dot{\varphi}^n; \dot{\varphi}^{-n}) = & \left(1 + 2\lambda N (M_{rate}^{\mathrm{OL}})^2 \frac{M_{aim}^{\mathrm{OL}}}{\gamma} \right) \frac{M_{rate}^{\mathrm{OL}} M_{aim}^{\mathrm{OL}}}{\gamma} \frac{\sigma^2}{\rho(2\beta + \rho)(\beta + \rho + M_{rate}^{\mathrm{OL}})} \\ & - \frac{1}{\rho(2\beta + \rho)} \left(\frac{\sigma M_{rate}^{\mathrm{OL}} M_{aim}^{\mathrm{OL}}}{\gamma} \right)^2 \left(\lambda N + \frac{\gamma + 2\lambda N \left(M_{rate}^{\mathrm{OL}} \right)^2}{(\rho + 2M_{rate}^{\mathrm{OL}})(\beta + \rho + M_{rate}^{\mathrm{OL}})} \right). \end{aligned}$$

Asymptotics For small price impact $\lambda \to 0$, Taylor expansion of these explicit formulas shows that

$$M_{rate}^{\mathrm{OL}} = \sqrt{\frac{\gamma}{(N+1)\lambda}} + \mathcal{O}(1), \quad M_{aim}^{\mathrm{OL}} = 1 + \mathcal{O}(\lambda), \tag{3.4.3}$$

and

$$J_{\mathrm{OL}}^n(\dot{\varphi}^n; \dot{\varphi}^{-n}) = \frac{1}{2\gamma} \frac{\sigma^2}{\rho(2\beta + \rho)} - \frac{\sigma^2(1 + 3N)}{4\rho\gamma^{3/2}\sqrt{1+N}} \sqrt{\lambda} + \mathcal{O}(\lambda).$$

3.4.3 Comparison

We now compare the equilibrium trading strategies and their performance in the closed-loop equilibrium, the open-loop equilibrium, and the central-planner solution. To focus on the impact of the agents' Nash competition rather than changes in overall risk-bearing capacity, we consider throughout the "mean-field scaling" where each agent has mass $1/N$, so that the total mass of agents in the economy does not change with N. The price impact parameter λ is then replaced by λ/N in the formulas above.

Trading Rates Comparison of the asymptotic trading rates (3.3.3), (3.4.2), and (3.4.3) shows that, in each case, the equilibrium trading rates for small price impact track the frictionless optimal holdings μ_t/γ, in parallel to general results for single-agent models (Moreau et al., 2017).

The relative trading speed M_{rate} with which this target strategy is tracked also depends in the same way on the ratio γ/λ of inventory and trading costs, but scales differently with the number N of agents in each model. To wit, the trading rate chosen by the social planner is multiplied by the constant $1/\sqrt{2}$ – by symmetry, the social optimum that can be achieved with perfect cooperation evidently does not depend on the number of agents. The respective factor in the corresponding open-loop Nash equilibrium $\sqrt{N/(1+N)}$ is larger. This is an example of the "tragedy of the commons" – without perfect cooperation, the agents overuse the common pool of liquidity available to all of them, because they only internalize the negative impact their trading has on their own execution prices but not on others'.

In the closed-loop equilibrium, the relative trading speed scales with $\Delta(N)\sqrt{N}$. As depicted in Figure 3.1, this multiplier lies between its counterparts for the open-loop equilibrium and the social planner solution for all values of N. The intuition is that, with closed-loop controls, agents at least partially slow down their trading when others are trading in the same direction. This reduces the negative externality somewhat and moves the agents closer to the social optimum.

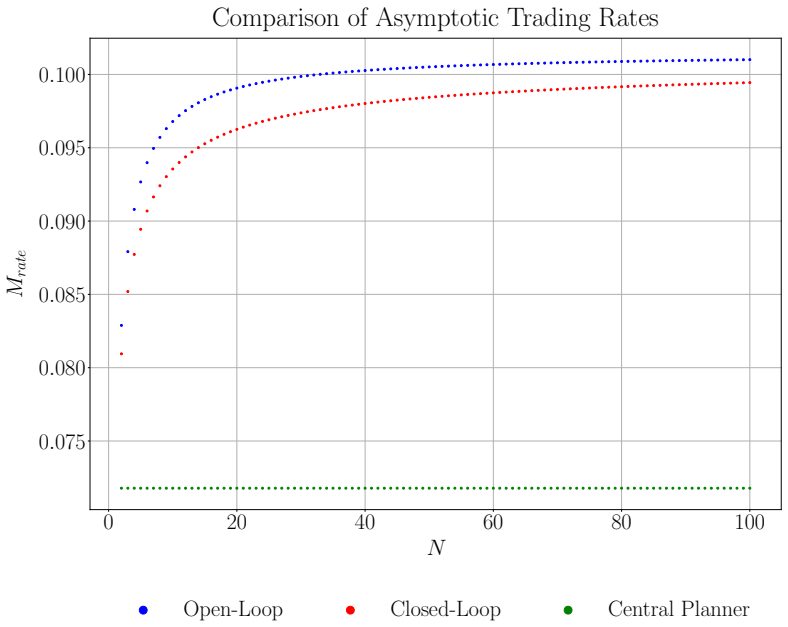

Figure 3.1: Leading-order asymptotics of the relative trading speeds in the central planner model (green, lowest curve), in the closed-loop equilibrium (red, middle curve) and in the open-loop equilibrium (blue, top curve) plotted against the number N of agents for the parameters from Table 3.1.

However, for all values of N and irrespective of the other model parameters, these asymptotic formulas suggest that the closed-loop equilibrium is a lot closer to its open-loop counterpart than to the social planner model. At least for the symmetric setting with identical agents studied here, this provides compelling evidence for using open-loop models as more tractable approximations of the generally very involved closed-loop analysis.

So far, we have focused on the crisp asymptotic formulas that one obtains in the limit for small price impact $\lambda \downarrow 0$. In this regime, the differences between the central-planner solution, open-loop and closed-loop Nash equilibria only depend on the number of agents, whereas the effect of all other model parameters scales out. We now assess the accuracy of the asymptotic approximations by comparing them to the numerical solution of the equations describing the exact closed-loop Nash equilibrium. Unlike for the asymptotic formulas, this requires realistic parameter values, both for the predictive signal and the trading and inventory cost parameters.

To this end, we follow Collin-Dufresne, Daniel, and Saglam (2020). For a

discrete-time version of the present model, they estimate the quadratic transaction cost parameter λ from a proprietary dataset of real transactions executed by a large investment bank. Whereas trading costs and volatilities are constant in our model, these are modulated by a four-state Markov chain in their paper, which also acts as a trading signal by affecting expected returns. In order to translate this to our model, we average volatilities and trading costs against the stationary distribution of the Markov chain, and estimate the parameters of our Ornstein-Uhlenbeck return (3.2.2) from a long simulated time series of the (centered) Markov chain.[8] For the inventory cost γ, we use the medium value from (Collin-Dufresne et al., 2020, Section 5.6). These parameter values are summarized in Table 3.1.

Parameter	**Value**
Price volatility σ_P	0.0088
Discount rate ρ	0.00004
Signal volatility σ	0.00015
Signal mean reversion β	0.070
Trading Cost λ	1.88×10^{-10}
Inventory Cost γ	$2.5 \times 10^{-8} \times \sigma_P^2$

Table 3.1: (Daily) Model Parameters

Figure 3.2 compares the asymptotic approximation of M_{rate} to its exact counterpart, computed numerically by solving the system of algebraic equations (3.5.5)–(3.5.11). Even though the size of the portfolios under consideration here is quite large (the frictionless portfolio μ_t/γ has a stationary standard deviation of about two hundred million shares), the asymptotic approximation of the relative trading speed turns out to be almost perfect for all values of N.

Aim Portfolios As illustrated by Figure 3.3, this is not the case for the aim portfolio. Indeed, for the large portfolio sizes considered here, the multiplier M_{aim} of the frictionless optimal portfolio is not close to its asymptotic value 1, but

[8] As already mentioned above, we do not incorporate a nonzero mean-reversion level of the signal process here in order not to make the lengthy calculations for the closed-loop model even more involved.

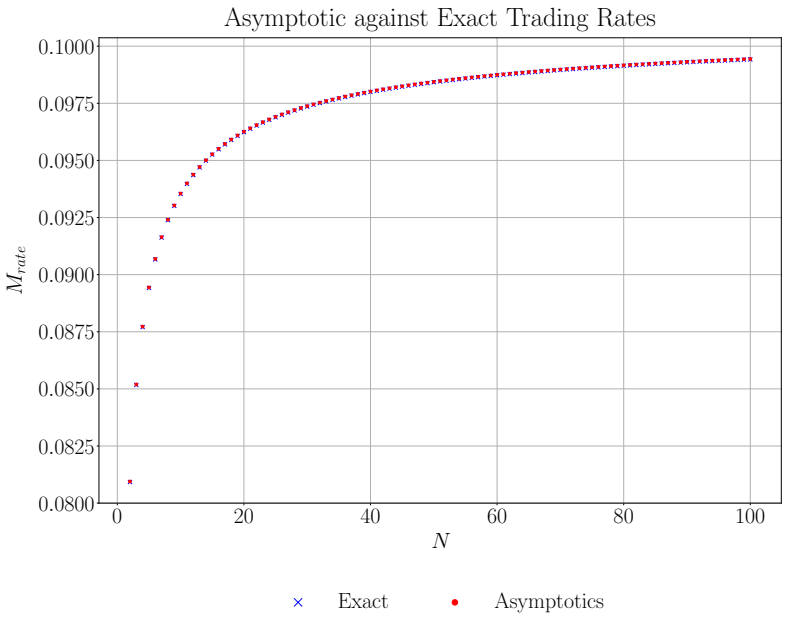

Figure 3.2: Relative trading speeds in the closed-loop equilibrium (blue crosses) and its asymptotic approximation (red dots), plotted against the number of agents N for the parameters from Table 3.1.

consistently below 70%.[9] As for the relative trading speeds, the aim portfolio for the closed-loop model lies between its counterparts for the central-planner and open-loop models. The interpretation again is that trading activity is scaled back somewhat towards the social optimum, but still remains much closer to the closed-loop equilibrium for all values of N.

Performance Since the aim portfolio changes considerably relative to its frictionless counterpart, the optimal values in the different models also need to be compared using the exact formulas in the respective models rather than relying on asymptotics alone. This is illustrated in Figure 3.4, where we plot the optimal performances with trading costs against the number N of agents in each model. To make these numbers easier to interpret, we report them as fractions of the optimal frictionless value. Recall that the closed-loop trading rates and aim portfolios move partially from the open-loop solution towards the central planner solution.

[9] In addition to the size of the portfolios, this is due to the relatively fast mean reversion of the trading signal considered in Collin-Dufresne et al. (2020). The dividend yield used as a predictor in Barberis (2000) is much more persistent, for example, so that the leading-order asymptotics are considerably more accurate in this case.

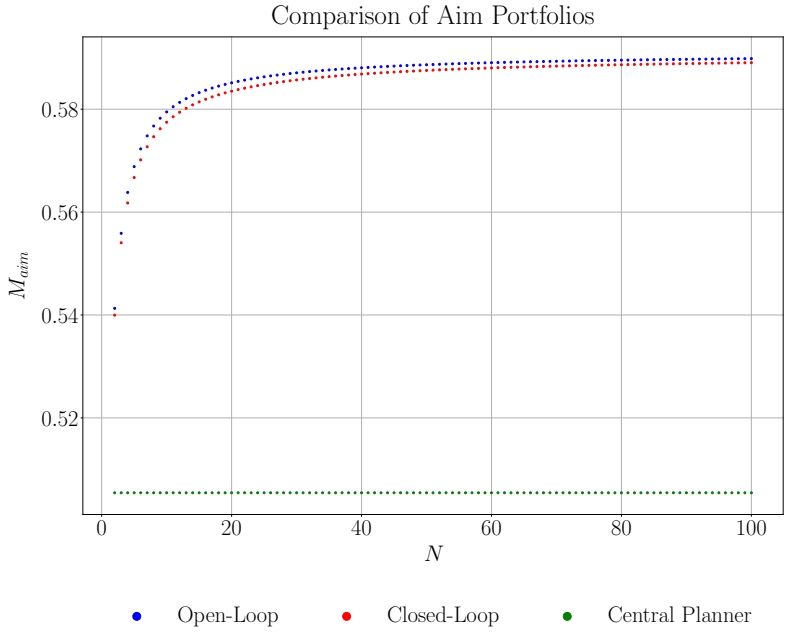

Figure 3.3: Multipliers M_{aim} for the aim portfolio $M_{aim} \times \mu_t/\gamma$ in the closed-loop equilibrium (red, middle curve), in the central-planner model M_{aim}^{CP} (green, lowest curve) and in the open-loop equilibrium, M_{aim}^{OL} (blue, top curve), plotted against the number of agents N for the parameters from Table 3.1.

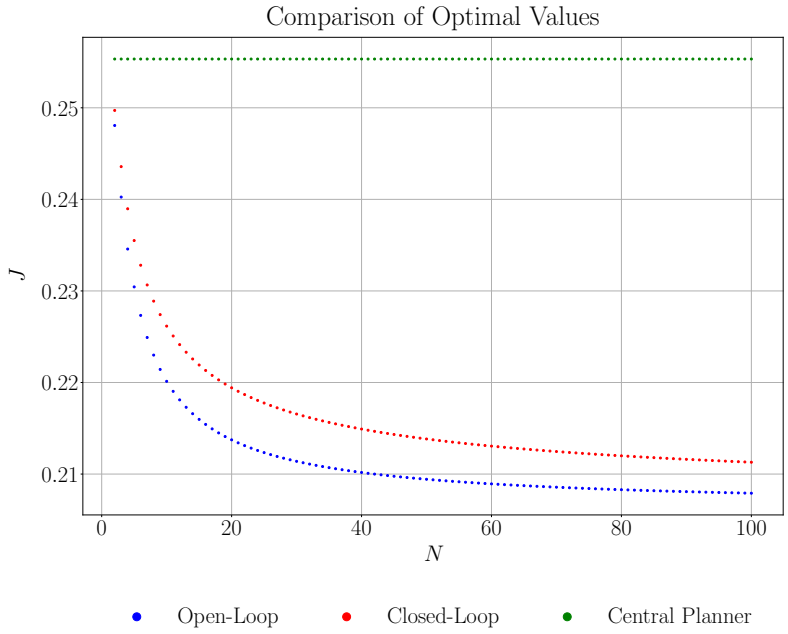

Figure 3.4: Optimal values in the central-planner model (green, top curve of dots), in the closed-loop equilibrium (red, middle curve), and in the open-loop equilibrium (blue, bottom curve) as fractions of the frictionless optimal value, plotted against the number of agents N for the parameters from Table 3.1.

Accordingly, the optimal values of the closed-loop equilibrium also fall between the open-loop model and the central-planner solution. The shortfall compared to the frictionless version of the model increases as the lack of cooperation becomes more and more severe for large N. This is called the "price of anarchy" in the game-theory literature.

Mean-Field Limit? The numerical results reported above suggest that the open-loop and closed-loop models lead to rather similar results for realistic parameter values. An intriguing theoretical question is whether the difference vanishes completely in the "mean-field limit" of many small agents.

Rigorous convergence results of this kind have recently been obtained for models with interaction through the controlled state processes (Lacker, 2020; Lacker and Le Flem, 2021) and for "extended" mean-field games with interaction through the agents' controls (Djete, 2021). However in their setup, each agent is also affected by an idiosyncratic noise, which is crucial to the proof of convergence. It is an important question for future research to study similar limiting results to generic "extended" mean-field games, where the only source of randomness is a common noise, as in the present chapter. To prove this convergence result in our setting, one would have to study the large-N asymptotics of the system of equations (3.5.5)–(3.5.11), (3.5.12)–(3.5.14) characterizing our closed-loop equilibrium for the rescaled trading cost λ/N. We do not pursue this here but report some positive numerical evidence. Specifically, in Figure 3.5 we plot the ratio of the optimal values in the closed-loop and open-loop models for numbers of agents up to $N = 1000$ which suggests the existence of *some* limiting model to which the closed-loop and open-loop equilibria converge.

3.5 Heuristics for the Closed-Loop Equilibrium

In single-agent models (Gârleanu and Pedersen, 2016), the optimal trading rate for Ornstein-Uhlenbeck returns (3.2.2) is linear both in the current trading signal and

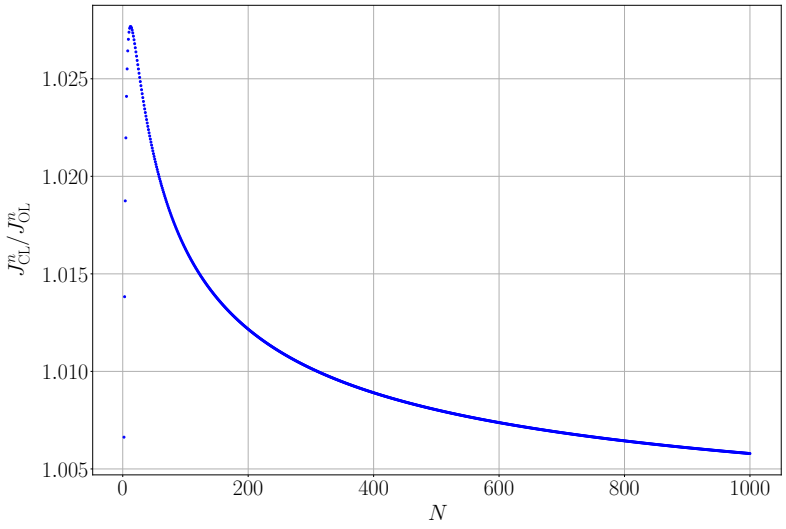

Figure 3.5: Ratio of the optimal values in the closed-loop and in the open-loop equilibriums, plotted against the number of agents N for the parameters from Table 3.1.

in the agent's current position. In open-loop equilibria, the agents' optimal trading rates also depend on these two state variables as well as the other agents' positions in a linear fashion (Voß, 2019; Casgrain and Jaimungal, 2020). Accordingly, we search for closed-loop equilibria in the same linear class.

To this end it suffices, by symmetry, to focus on the optimization problem of agent $n = 1$, when the feedback trading rates of the other agents are fixed:

$$\dot{\varphi}^n_t = \bar{a}\mu_t + \bar{b}\sum_{m\neq n}\varphi^m_t - \bar{c}\varphi^n_t, \quad n = 2,\dots,N. \tag{3.5.1}$$

Here, $\bar{a}, \bar{b}, \bar{c} > 0$, so that the above ansatz implies that agents try to reduce their own positions, but trade less to reduce price impact costs if others have the same objective. When the trading rates of agents $n = 2,\dots,N$ are all equal and fixed to be as in 3.5.1, agent $n = 1$ faces a standard stochastic control problem of choosing their own trading rate $\dot{\varphi}^1$ to maximize

$$\mathbb{E}\left[\int_0^\infty e^{-\rho t}\left(\mu_t\varphi^1_t - \frac{\gamma}{2}(\varphi^1_t)^2 - \lambda\dot{\varphi}^1_t\left(\dot{\varphi}^1_t + (N-1)(\bar{a}\mu_t + \bar{b}((N-2)\bar{\varphi}_t + \varphi^1_t) - \bar{c}\bar{\varphi}_t)\right)\right)dt\right].$$

Here, φ^1_t and the (symmetric) positions $\bar{\varphi}_t = \varphi^2_t = \ldots = \varphi^N_t$ of the other agents

have the coupled controlled dynamics

$$\begin{aligned} d\varphi_t^1 &= \dot{\varphi}_t^1 dt, \\ d\bar{\varphi}_t &= \left(\bar{a}\mu_t + \bar{b}((N-2)\bar{\varphi}_t + \varphi_t^1) - \bar{c}\bar{\varphi}_t\right) dt. \end{aligned}$$

By linearity of these dynamics and those of the exogenous state process μ_t, we make the ansatz that the value function of agent 1 is purely quadratic in the initial signal $\mu_0 = m$, agent 1's own initial position $\varphi_0^1 = x$ and (with a slight abuse of notation) the other agents' initial positions $\bar{\varphi}_0 = y$ (which are all the same given that they apply the same trading rates (3.5.1)):

$$V(x, y, m) = -\frac{a}{2}x^2 + \frac{b}{2}y^2 + \frac{c}{2}m^2 - dxy + exm + fym + g, \tag{3.5.2}$$

for constants a, b, c, d, e, f, g to be determined.

Remark 3.5.1. *If the Ornstein-Uhlenbeck state process (3.2.2) has a nonzero mean-reversion level, then this purely quadratic ansatz needs to be extended to include three further linear terms. The analysis below then generalizes, but involves three further equations. We therefore do not pursue this extension of the model in order not to complicate the already cumbersome calculations below.*

The corresponding standard infinite-horizon HJB equation is

$$\begin{aligned} \rho V =& mx - \frac{\gamma}{2}x^2 - \beta m\partial_m V + \frac{1}{2}\sigma^2\partial_m^2 V + \left[\bar{a}m + \bar{b}((N-2)y + x) - \bar{c}y\right]\partial_y V \\ &+ \sup_{\dot{\varphi}^1 \in \mathbb{R}} \Big\{ -\lambda\dot{\varphi}^1[\dot{\varphi}^1 + (N-1)\bar{a}m + (N-1)((N-2)\bar{b} - \bar{c})y \\ &\qquad + (N-1)\bar{b}x] + \dot{\varphi}^1\partial_x V \Big\}. \end{aligned} \tag{3.5.3}$$

After plugging in the quadratic ansatz (3.5.2), the pointwise maximizer can be computed as

$$\dot{\varphi}^1 = \frac{(e - \lambda(N-1)\bar{a})m - (a + \lambda(N-1)\bar{b})x - (d + \lambda(N-1)((N-2)\bar{b} - \bar{c}))y}{2\lambda}. \tag{3.5.4}$$

After inserting this back into the HJB equation, comparison of coefficients for the

terms proportional to x^2, y^2, m^2, xy, xm, ym and constant terms in turn yields the following seven equations that pin down the coefficients a, b, c, d, e, f, g of agent 1's value function for fixed trading rates (3.5.1) of the other agents:

$$0 = \frac{\rho a}{2} - \frac{\gamma}{2} - d\bar{b} + \frac{(a + \lambda(N-1)\bar{b})^2}{4\lambda}, \tag{3.5.5}$$

$$0 = -\frac{\rho b}{2} + b((N-2)\bar{b} - \bar{c}) + \frac{(d + \lambda(N-1)((N-2)\bar{b} - \bar{c}))^2}{4\lambda}, \tag{3.5.6}$$

$$0 = \rho d + b\bar{b} - d((N-2)\bar{b} - \bar{c}) + \frac{(a + \lambda(N-1)\bar{b})(d + \lambda(N-1)((N-2)\bar{b} - \bar{c}))}{2\lambda}, \tag{3.5.7}$$

$$0 = -g + \frac{\sigma^2}{2\rho}c, \tag{3.5.8}$$

$$0 = -\left(\frac{\rho + 2\beta}{2}\right)c + f\bar{a} + \frac{(e - \lambda(N-1)\bar{a})^2}{4\lambda}, \tag{3.5.9}$$

$$0 = -(\rho + \beta)e + 1 - d\bar{a} + \bar{b}f - \frac{(e - \lambda(N-1)\bar{a})(a + \lambda(N-1)\bar{b})}{2\lambda}, \tag{3.5.10}$$

$$b\bar{a} + f((N-2)\bar{b} - \bar{c}) = (\rho + \beta)f + \frac{(e - \lambda(N-1)\bar{a})(d + \lambda(N-1)((N-2)\bar{b} - \bar{c}))}{2\lambda}. \tag{3.5.11}$$

A symmetric Nash equilibrium is then identified by requiring that agent 1 has no incentive to deviate from the other agents' common controls, in that the same weights are placed on trading signals, own and others' inventories in each case. Comparison between (3.5.1) and (3.5.4) in turn leads to the following three additional equations:

$$\begin{aligned} \bar{a} &= \frac{(e - \lambda(N-1)\bar{a})}{2\lambda}, \\ (N-1)\bar{b} &= -\frac{d + \lambda(N-1)((N-2)\bar{b} - \bar{c})}{2\lambda}, \\ \bar{c} &= \frac{(a + \lambda(N-1)\bar{b})}{2\lambda}. \end{aligned}$$

By algebraic manipulations, this system of ten nonlinear equations for ten unknowns can be reduced to a single scalar equation. To wit, first observe that

$$\bar{a} = \frac{e}{(N+1)\lambda}. \tag{3.5.12}$$

Then, notice that the linear equations for $\bar{b}$ and $\bar{c}$ can be solved in terms of a and d:

$$\bar{b} = \frac{-aN + a + 2d}{\lambda - \lambda N^2}, \tag{3.5.13}$$

$$\bar{c} = -\frac{d - aN}{\lambda + \lambda N}. \tag{3.5.14}$$

After plugging in the expression for $\bar{b}$, (3.5.5) can in turn be solved for a in terms of d [10]

$$a(d) = \frac{d(6N+2) - \lambda(N+1)^2\left(-\sqrt{-\frac{4d^2(3N+1)}{\lambda^2(N-1)(N+1)^2} + \rho^2 + \frac{8\gamma N^2 - 4d\rho(3N+1)}{\lambda(N+1)^2}} + \rho\right)}{4N^2}. \tag{3.5.15}$$

We now use (3.5.6) to determine an expression for b only in terms of $a(d)$ and d. Specifically, $\bar{b}$ and $\bar{c}$ in (3.5.13) and (3.5.14) depend only on $a(d)$ and d. Furthermore, (3.5.6) depends only on $\bar{b}$, $\bar{c}$, d and b. Therefore, we first plug $\bar{b}$ and $\bar{c}$ in (3.5.6) to obtain a linear equation in b that only depends on $a(d)$ and d. We can now solve such linear equation for b and determine that

$$b(d) = \frac{2(N-1)(-a(d)N + a(d) + 2d)^2}{(N+1)\left(4a(d)(N-1) + 2d(N-3) + \rho\lambda\left(N^2-1\right)\right)}. \tag{3.5.16}$$

The remaining parameters c, e, f, g can in turn be sequentially expressed in terms of d only as well by proceeding as follows. First, plug in the expressions for $a(d)$, $b(d)$, and the formulas for $\bar{a}$ (a linear function of e) and for $\bar{b}$ and $\bar{c}$ (in terms of d only) into (3.5.10) and (3.5.11). This leads to two linear equations for $e(d)$ and $f(d)$, that can be solved explicitly in terms of d, see (B.2.1) for the lengthy explicit expressions. Then, after inserting these representations and the formula for $\bar{a}$ in terms of d,[11] (3.5.9) leads to an explicit formula for $c(d)$ in terms of d (see (B.2.1)). Finally, the coefficient $g(d)$ can be determined in terms of d by using the formula for $c(d)$ and (3.5.8), $g(d) = \frac{\sigma^2}{2\rho}c(d)$.

Finally, we use (3.5.7) to determine an algebraic equation for the parameter d.

[10] Note that $a(d)$ chosen in (3.5.15) is the only root of (3.5.5) that gives positive $\bar{a}, \bar{b}$ and $\bar{c}$.

[11] Note that $\bar{a}$ is determined in terms of d by (3.5.12) and our solution for e as $\bar{a}(d) = \frac{e(d)}{(1+N)\lambda}$.

Note that since $a(d)$ in (3.5.15) depends only on d, then, $b(d)$ in (3.5.16) depends only on d. Moreover, notice that $\bar{b}(d)$ and $\bar{c}(d)$ as stated in (3.5.13) and (3.5.14) only depend on d since they only depend on d and $a(d)$. Hence, we can plug the expressions for $a(d)$, $b(d)$, $\bar{b}(d)$ and $\bar{c}(d)$ from (3.5.15), (3.5.16), (3.5.13) and (3.5.14) into (3.5.7) to obtain a complex but explicit scalar equation for d:

$$\begin{aligned} 0 = \frac{-2a(d)^2N(N-1)^2}{\lambda(N-1)(N+1)^2} + \frac{a(d)(N-1)(b(d)N+b(d)+8dN)}{\lambda(N-1)(N+1)^2} \\ + \frac{d\left(-2b(d)(N+1)+d(N-6)N+d+\lambda(N-1)(N+1)^2\rho\right)}{\lambda(N-1)(N+1)^2}. \end{aligned} \tag{3.5.17}$$

We stress that although $a(d)$ and $b(d)$ appear in (3.5.17), via the identities in (3.5.15) and (3.5.16), (3.5.17) is a scalar equation depending *exclusively* on the parameter d. In order to identify a solution $d = d(\lambda)$ of (3.5.17) for fixed $N \geq 2$ and sufficiently small λ, we postulate the following factorization,

$$d(\lambda) = \sqrt{\gamma\lambda}\delta_N(\lambda), \tag{3.5.18}$$

for some function $\delta_N(\cdot)$ to be determined. The rescaling with $\sqrt{\lambda}$ is essential in order to obtain a nontrivial limit as $\lambda \downarrow 0$ in (3.5.17). The rescaling with $\sqrt{\gamma}$ leads to a limiting equation for $\lambda = 0$ which does not depend on γ but only on the number N of agents. This change of variables therefore asymptotically decouples the effects of trading costs (λ), inventory costs (γ) and competition (N), see Lemma 3.6.9(i).

With the change of variable in (3.5.18), the function $\delta_N(\lambda)$ is characterized as a root of a scalar equation obtained from (3.5.17):

$$\Phi_N(\lambda, \delta_N(\lambda)) = 0. \tag{3.5.19}$$

(See (3.6.22)–(3.6.23) for the explicit form of Φ_N.) In the limit $\lambda \downarrow 0$, we show in Lemma 3.6.9 that $\delta_N(0) =: \delta_N^* > 0$ is the unique root of this equation:

$$\Phi_N(0, \delta_N^*) = 0. \tag{3.5.20}$$

In fact, any root of this equation is the root of a cubic polynomial. Cardano's method therefore leads to three explicit candidates for the roots of $\Phi_N(0,\cdot)$. Using symbolic calculations detailed in the Mathematica companion of Micheli et al. (2021), we then verify that only one of these polynomial roots also is a root of $\Phi_N(0,\cdot)$.

Next, we also show that $\partial_y \Phi_N(\lambda, y)|_{(\lambda,y)=(0,\delta_N^*)} > 0$. The implicit function theorem in turn allows us to pin down $\delta_N(\lambda)$ as the unique continuous function defined on a neighbourhood of 0 such that (3.5.19) holds. For sufficiently small λ, this yields a solution $d(\lambda)$ of (3.5.17) and in turn our system of ten equations derived from the agents' optimality and consistency conditions.

The implicit function theorem also allows us to obtain the leading-order asymptotics of the agents' optimal policies and their performance. To wit,

$$\delta_N(\lambda) = \delta_N^* + \mathcal{O}(\lambda).$$

Together with (3.5.18) , it follows that

$$d = \sqrt{\lambda\gamma}\delta_N^* + \mathcal{O}(\lambda^{3/2}). \tag{3.5.21}$$

This allows us to obtain asymptotic expansions of all the coefficients in (3.5.5)–(3.5.12) since these can all be expressed as functions of d. For example, using the expansion (3.5.21) for d, (3.5.1), the assumption of symmetric equilibrium and Taylor expansion lead to the expansion of the relative trading speed M_{rate} from (3.3.3),

$$M_{rate} = \bar{c} - (N-1)\bar{b} = \sqrt{\frac{\gamma}{\lambda}}\Delta(N) + \mathcal{O}(1),$$

where

$$\Delta(N) = \frac{1}{2N^2}\sqrt{\frac{2N^3 - 2N^2 - 3N(\delta_N^*)^2 - (\delta_N^*)^2}{(N-1)}} + \frac{(2N+1)\delta_N^*}{2N^2}. \tag{3.5.22}$$

More details on the asymptotic expansions are provided in Section 3.6.2.

Remark 3.5.2. *The asymptotic analysis is complicated by the fact that δ_N^* is a root of a third order polynomial (see (3.6.30)), which does not admit a simple expression unlike in single-agent models (Gârleanu and Pedersen, 2016; Moreau et al., 2017). Explicit expressions for δ_N^* in terms of N can be derived using Cardano's method, and these allow to verify that only one of the polynomial roots also is a root of the equation for δ_N^*. However, the explicit expression (involving imaginary numbers) is too complex for deriving the analytical properties necessary to (i) show that our candidate value function is well defined and (ii) establish a verification theorem.*

As a way out, we therefore instead use implicit properties of δ_N^* to show that the other coefficients a, b, c, e, f, g are well defined (in terms of d, and therefore by (3.5.21) in terms of δ_N^*) and have the right signs to carry out the verification argument.

For example, in Lemma 3.6.10 we prove that for sufficiently small λ, $e(\lambda)$ is well defined and strictly positive. As follows from (3.5.12), this is needed in order to verify that $\bar{a} > 0$ in (3.6.1). Another example appears in Lemma B.1.3 where we prove that $M_{aim} = 1+\mathcal{O}(\sqrt{\lambda})$ for sufficiently small λ. This is essential to derive the asymptotics of the goal functionals $J^n(\dot{\varphi}^n; \dot{\varphi}^{-n})$ in Proposition 3.3.3. As pointed out in (B.1.13), the expansion of M_{aim} follows from a highly nontrivial connection between N, δ_N^*, and $\Delta(N)$ which is proved in Lemma B.1.2, and arrises directly from properties of the polynomial root δ_N^*.

3.6 Proofs

3.6.1 Proof of Theorem 3.3.1

This section is dedicated to the proof of Theorem 3.3.1. The most onerous part of the proof is to show that the optimality and consistency conditions derived in the previous section indeed have a solution with the right signs for sufficiently small λ. The lengthy proof of this result is postponed to Section 3.6.2 for better readability.

Lemma 3.6.1. *For sufficiently small $\lambda > 0$, there is a solution $(a, b, c, d, e, f, g, \bar{a}, \bar{b}, \bar{c})$ of the system (3.5.5)–(3.5.11), (3.5.12)–(3.5.14) which is well defined. Moreover, such solution satisfies*

$$\bar{a} > 0 \quad \text{and } \bar{c} - (N-1)\bar{b} > 0. \tag{3.6.1}$$

To prove our main result, Theorem 3.3.1, we focus without loss of generality on the optimization problem of agent 1, where the feedback controls of agents $2, \dots, N$ are fixed according to (3.5.1). Then, regardless of the policy chosen by agent 1, the trading rates and holdings of the other agents $n = 2, \dots, N$ will be the same, so it is convenient to simplify the notation by using that

$$\dot{\varphi}_t^2 = \frac{1}{N-1}\sum_{k=2}^{N} \dot{\varphi}_t^k, \quad \text{and} \quad \varphi_t^2 = \frac{1}{N-1}\sum_{k=2}^{N} \varphi_t^k, \quad t \geq 0.$$

Note that $d\varphi_t^2 = \dot{\varphi}_t^2 dt$ and, by (3.5.1),

$$\dot{\varphi}_t^2 = \frac{1}{N-1}\sum_{k=2}^{N} (\bar{a}\mu_t - \bar{c}\varphi_t^k + \bar{b}\sum_{m\neq k} \varphi_t^m) = \bar{a}\mu_t + \bar{b}\varphi_t^1 - (\bar{c} - (N-2)\bar{b})\varphi_t^2. \tag{3.6.2}$$

Using these observations, we can rewrite agent 1's goal functional (3.2.4) as follows:

$$\begin{aligned} &J^1(\dot{\varphi}^1; \dot{\varphi}^2)(x, y, m) \\ &= \mathbb{E}_{x,y,m}\Bigg[\int_0^\infty e^{-\rho t}\Bigg(\mu_t\varphi_t^1 - \frac{\gamma}{2}\left(\varphi_t^1\right)^2 \\ &\qquad - \lambda\dot{\varphi}_t^1\left(\dot{\varphi}_t^1 + (N-1)(\bar{a}\mu_t + \bar{b}\varphi_t^1 - (\bar{c} - (N-2)\bar{b})\varphi_t^2)\right)\Bigg)dt\Bigg]. \end{aligned} \tag{3.6.3}$$

Here the expectation $\mathbb{E}_{x,y,m}[\cdot]$ is taken conditional on the initial values $\varphi_0^1 = x$, $\varphi_0^2 = y$, and $\mu_0 = m$; to ease notation, we often suppress this dependence. The corresponding value function is denoted by (here, the supremum is taken over

admissible feedback controls in the sense of Definition 3.2.2):

$$V^1(x,y,m) = \sup_{\dot\varphi^1} J^1(\dot\varphi^1;\dot\varphi^2)(x,y,m). \tag{3.6.4}$$

Remark 3.6.2. *In fact, the subsequent analysis shows that deviations from the Nash equilibrium are also suboptimal among non-Markovian controls, as long as the resulting system of state equations has a sufficiently integrable solution.*

We will prove Theorem 3.3.1 using a verification argument that identifies agent 1's value function and optimal trading rate, and thereby shows that this (representative) agent has no incentive to deviate from the common feedback trading rate adopted by the other agents $n = 2,\dots,N$. As a preparation for this result, we first establish that our candidates for the equilibrium trading rates are indeed admissible.

Lemma 3.6.3. *For the coefficients $\bar a, \bar b, \bar c$ from Lemma 3.6.1, consider the feedback trading rates*

$$\dot\varphi^n_t = \bar a\mu_t - \bar c\varphi^n_t + \bar b\sum_{m\neq n}\varphi^m_t, \quad n = 1,\dots,N, \quad t \geq 0. \tag{3.6.5}$$

Then, the following linear forward SDE system

$$d\varphi^n_t = \dot\varphi^n_t dt, \quad \varphi^n_0 = x, \quad n = 1,\dots,N, \tag{3.6.6}$$

for $(\varphi^1,\dots,\varphi^N,\dot\varphi^1,\dots,\dot\varphi^N)$ has a unique solution, which satisfies $\dot\varphi^n,\varphi^n \in \mathcal{A}_\rho$ for all $n = 1,\dots,N$.

Proof. As all agents apply the same trading rates in the context of this lemma, the corresponding trading rates (3.6.5) simplify to

$$\dot\varphi^n_t = \bar a\mu_t + ((N-1)\bar b - \bar c)\varphi^n_t, \quad n = 1,\dots,N. \tag{3.6.7}$$

Put differently, the corresponding positions φ^n_t are the unique solution of a (ran-

dom) linear ODE. By the variation of constants formula, it is given by

$$\varphi_t^n = e^{-M_{rate}t}x + \int_0^t e^{-M_{rate}(t-s)}\bar{a}\mu_s ds, \quad \text{where } M_{rate} = \bar{c} - (N-1)\bar{b}. \tag{3.6.8}$$

Together with (3.6.7), it follows that

$$\dot{\varphi}_t^n = \bar{a}\mu_t - M_{rate}\int_0^t e^{-M_{rate}(t-s)}\bar{a}\mu_s ds - M_{rate}e^{-M_{rate}t}x. \tag{3.6.9}$$

As $M_{rate} > 0$ by (3.6.1), (3.6.8), Hölder inequality, Fubini's theorem and the second moment of the Ornstein-Uhlenbeck process (3.2.2) in turn yield the required integrability of the trading rate:

$$\begin{aligned}
\mathbb{E}\Big[\int_0^\infty e^{-\rho t}(\varphi_t^n)^2 dt\Big] &\leq \frac{x^2}{\rho + 2M_{rate}} + \bar{a}^2\mathbb{E}\Big[\int_0^\infty e^{-\rho t}\left(\int_0^t e^{-2M_{rate}(t-s)}ds\right)\left(\int_0^t \mu_s^2 ds\right)dt\Big] \\
&\leq \frac{x^2}{\rho + 2M_{rate}} + \frac{\bar{a}^2}{2M_{rate}}\int_0^\infty e^{-\rho t}\left(\int_0^t \mathbb{E}[\mu_s^2]ds\right)dt \\
&\leq \frac{x^2}{\rho + 2M_{rate}} + \frac{\bar{a}^2}{2M_{rate}}\left(\frac{\sigma^2}{2\beta}\right)\frac{1}{\rho},
\end{aligned}$$

and therefore $\varphi^n \in \mathcal{A}_\rho$. The corresponding integrability of the associated trading rate $\dot{\varphi}^n$ follows from the representation (3.6.9) along the same lines. □

The exogenous signal process μ evidently has the same integrability (this can be checked, e.g., using the formula for its second moment):

Lemma 3.6.4. *For $\rho > 0$ and μ from (3.2.2), we have $\mu \in \mathcal{A}_\rho$.*

The next ingredient for our verification theorem is to show that the local martingale that appears when Itô's formula is applied to the candidate value function is in fact a true martingale.

Lemma 3.6.5. *Suppose agents $n = 2, \ldots, N$ use the same admissible trading rates $\dot{\varphi}^2 = \ldots = \dot{\varphi}^N$ from (3.6.5) and define the function V as in (3.5.2). Then, for any admissible trading rate $\dot{\varphi}_1 \in \mathcal{A}_\rho$ of agent 1, the process*

$$M_t^1 = \int_0^t e^{-\rho t}\partial_m V(\varphi_t^1, \varphi_t^2, \mu_t)dW_t, \quad t \geq 0,$$

is a square-integrable true martingale.

Proof. From (3.5.2) we have $\partial_m V(x,y,m) = ex + fy + cm$. Accordingly, there exists a constant $C > 0$ such that

$$\mathbb{E}\left[\langle M^1\rangle_t\right] \leq C\mathbb{E}\left[\int_0^t \exp\{-2\rho t\}\Big((\varphi_s^1)^2 + (\varphi_s^2)^2 + (\mu_s)^2\Big)ds\right] < \infty, \quad \text{for all } t \geq 0.$$

Here, we used Lemma 3.6.4 and the admissibility of the trading rates in the last step. Hence, the local martingale M^1 is indeed a square-integrable martingale. □

Next, we show that the agents' *infinite-horizon* goal functionals are indeed well defined for admissible trading rates.

Lemma 3.6.6. *For any admissible trading rates $\dot{\varphi} = (\dot{\varphi}_1, ..., \dot{\varphi}_N)$, the following limit is finite:*

$$\begin{aligned}&\lim_{T\to\infty} \mathbb{E}\left[\int_0^T e^{-\rho t}\left(\mu_t\varphi_t^n - \frac{\gamma}{2}(\varphi_t^n)^2 - \lambda\dot{\varphi}_t^n\Big(\sum_{k=1}^N \dot{\varphi}_t^k\Big)\right)dt\right]\\ &= \mathbb{E}\left[\int_0^\infty e^{-\rho t}\left(\mu_t\varphi_t^n - \frac{\gamma}{2}(\varphi_t^n)^2 - \lambda\dot{\varphi}_t^n\Big(\sum_{k=1}^N \dot{\varphi}_t^k\Big)\right)dt\right].\end{aligned} \tag{3.6.10}$$

Proof. The triangle inequality and Hölder's inequality yield

$$\begin{aligned}F_T &= \left|\int_0^T e^{-\rho t}\left(\mu_t\varphi_t^n - \frac{\gamma}{2}(\varphi_t^n)^2 - \lambda\dot{\varphi}_t^n\Big(\sum_{k=1}^N \dot{\varphi}_t^k\Big)\right)dt\right|\\ &\leq \Big(\int_0^T e^{-\rho t}|\mu_t|^2dt\Big)^{1/2}\Big(\int_0^T e^{-\rho t}(\varphi_t^n)^2dt\Big)^{1/2} + \frac{\gamma}{2}\int_0^T e^{-\rho t}(\varphi_t^n)^2dt\\ &\quad + \lambda\Big(\int_0^T e^{-\rho t}|\dot{\varphi}_t^n|^2dt\Big)^{1/2}\Big(\int_0^T e^{-\rho t}\Big(\sum_{k=1}^N |\dot{\varphi}_t^k|\Big)^2dt\Big)^2.\end{aligned}$$

As a result, (3.6.10) follows from Lemmas 3.6.3 and 3.6.4 and dominated convergence. □

Finally, as the last ingredient for our verification argument, we show that the candidate value function satisfies a transversality condition.

Lemma 3.6.7. *Suppose agents $n = 2, \dots, N$ use the same admissible trading rates $\dot{\varphi}^2 = \dots = \dot{\varphi}^N$ from (3.6.5) and define the function V as in (3.5.2). Then, for any admissible trading rate $\dot{\varphi}^1$ of agent 1, we have*

$$\liminf_{T\to\infty} \mathbb{E}\left[e^{-\rho T} V(\varphi_T^1, \varphi_T^2, \mu_T)\right] = 0. \tag{3.6.11}$$

Proof. By Lemma 3.6.4 and admissibility of the trading rates, μ, φ^1 and φ^2 all belong to $\mathcal{A}_\rho$. In particular,

$$\liminf_{t\to\infty} \mathbb{E}\left[e^{-\rho t}(\varphi_t^1)^2\right] = 0, \quad \liminf_{t\to\infty} \mathbb{E}\left[e^{-\rho t}(\varphi_t^2)^2\right] = 0, \quad \liminf_{t\to\infty} \mathbb{E}\left[e^{-\rho t}(\mu_t)^2\right] = 0. \tag{3.6.12}$$

The transversality condition (3.6.11) in turn follows from the definition of V in (3.5.2), (3.6.12) and Hölder's inequality. □

Now, we are ready to prove a verification theorem which shows that the function V from (3.5.2) indeed is the value function V^1 of agent 1's optimization problem (3.6.4) for fixed feedback controls of the other agents. As a byproduct, we obtain the optimal feedback trading rate of agent 1, which indeed coincides with the fixed feedback trading rates of the other agents $n = 2, \dots, N$ as required for a Nash equilibrium.

Proposition 3.6.8. *Suppose λ is sufficiently small for the coefficients $(a, b, c, d, e, f, g, \bar{a}, \bar{b}, \bar{c})$ to satisfy the statement of Lemma 3.6.1. Define the trading rates $\dot{\varphi}^2, ..., \dot{\varphi}^N$ of agents $n = 2, \dots, N$ as in (3.6.5) and suppose agents $n = 2, \dots, N$ use the same admissible trading rates $\dot{\varphi}^2 = \dots = \dot{\varphi}^N$. Moreover, define the function V as in (3.5.2). Then, we have*

$$V \geq J^1(\dot{\varphi}^1; \dot{\varphi}^2), \tag{3.6.13}$$

for all admissible feedback trading rates $\dot{\varphi}^1$ of agent 1, with equality if $\dot{\varphi}^1$ is also given by (3.6.5).

Proof. Let $\dot{\varphi}^1(x, y, m)$ be any admissible feedback control for agent 1 and define

the operator

$$\mathcal{L} = \dot{\varphi}^1(x,y,m)\partial_x + (\bar{a}\mu + \bar{b}x - (\bar{c} - (N-2)\bar{b})y)\partial_y - \beta m \partial_m + \frac{\sigma^2}{2}\partial_m^2.$$

With this notation, Itô's formula yields

$$\begin{aligned} d\Big(e^{-\rho t}V(\varphi_t^1, \varphi_t^2, \mu_t)\Big) &= -\rho e^{-\rho t}V(\varphi_t^1, \varphi_t^2, \mu_t)dt + e^{-\rho t}\mathcal{L}V(\varphi_t^1, \varphi_t^2, \mu_t)dt \\ &\quad + \sigma e^{-\rho t}\partial_m V(\varphi_t^1, \varphi_t^2, \mu_t)dW_t. \end{aligned} \tag{3.6.14}$$

The stochastic integral in (3.6.14) is a true martingale by Lemma 3.6.5. Integrating and taking expectation on both sides of (3.6.14) in turn leads to

$$\begin{aligned} &V(x,y,m) - \mathbb{E}\left[e^{-\rho T}V(\varphi_T^1, \varphi_T^2, \mu_T)\right] \\ &\quad = \mathbb{E}\left[\int_0^T e^{-\rho t}\Big(\rho V(\varphi_t^1, \varphi_t^2, \mu_t) - \mathcal{L}V(\varphi_t^1, \varphi_t^2, \mu_t)\Big)dt\right]. \end{aligned} \tag{3.6.15}$$

As the coefficients $(a, b, c, d, e, f, g, \bar{a}, \bar{b}, \bar{c})$ satisfy (3.5.5)–(3.5.14) by Lemma 3.6.1 for λ small enough, the function V solves the HJB equation (3.5.3) (compare the derivation of (3.5.5)–(3.5.14) in Section 3.5). As a consequence, we have

$$\rho V - \mathcal{L}V \geq x\mu - \lambda\dot{\varphi}^1(\dot{\varphi}^1 + (N-1)(\bar{a}m + \bar{b}x - (\bar{c} - (N-2)\bar{b})y)) - \frac{\gamma}{2}x^2. \tag{3.6.16}$$

Together, (3.6.15) and (3.6.16) show

$$\begin{aligned} &V(x,y,m) - \mathbb{E}\left[e^{-\rho T}V(\varphi_T^1, \varphi_T^2, \mu_T)\right] \\ &\quad \geq \mathbb{E}\Bigg[\int_0^T e^{-\rho t}\Big(\mu_t\varphi_t^1 - \frac{\gamma}{2}(\varphi_t^1)^2 \\ &\qquad - \lambda\dot{\varphi}_t^1(\dot{\varphi}_t^1 + (N-1)(\bar{a}\mu_t + \bar{b}\varphi_t^1 - (\bar{c} - (N-2)\bar{b})\varphi_t^2))\Big)dt\Bigg]. \end{aligned} \tag{3.6.17}$$

In view of Lemma 3.6.6 and the transversality condition from Lemma 3.6.7, we can now take the limit $T \to \infty$ on both sides of (3.6.17) and obtain the asserted upper bound (3.6.13) for any admissible feedback control.

The admissibility of our candidate $\dot{\varphi}^1$ has already been established in Lemma 3.6.3. Moreover, note that when $\dot{\varphi}^1$ is given by (3.6.5) like the other agents' controls,

then it follows by construction that the inequality (3.6.16) holds with equality (because this choice corresponds to the pointwise maximizer in the HJB equation). Repeating the arguments leading to (3.6.17) then shows that (3.6.13) holds with equality.

As a result, V indeed is the value function of agent 1 given the feedback trading rates (3.6.5) of agents $n = 2, \ldots, N$. Moreover, the same feedback trading rate is indeed optimal for agent 1 as required for a Nash equilibrium. □

We finally complete the proof of the last missing items from Theorem 3.3.1.

Proof of Theorem 3.3.1. To finish the proof of Theorem 3.3.1, we first show that the feedback trading rate $\dot{\varphi}^1$ from (3.6.9) can be rewritten in the form (3.3.1). This follows by defining

$$M_{aim} = \frac{\bar{a}\gamma}{M_{rate}}, \tag{3.6.18}$$

and observing that (3.6.8) and (3.6.9) satisfy (3.3.1). In view of the results already established in Proposition 3.6.8, it now only remains to derive the representation (3.3.2) for the optimal equilibrium value. Henceforth, we assume a zero initial signal ($\mu_0 = 0$) and zero initial positions ($\varphi_0^1 = \ldots = \varphi_0^N = 0$). For the symmetric trading rates $\dot{\varphi}_t^1 = \ldots = \dot{\varphi}_t^N = \dot{\varphi}_t$ from (3.6.5), we can (with a slight abuse of notation) rewrite the goal functionals (3.2.4) as follows:

$$J(\dot{\varphi}) = \mathbb{E}\left[\int_0^\infty e^{-\rho t}\Big(\mu_t\varphi_t - \frac{\gamma}{2}(\varphi_t)^2 - \lambda N(\dot{\varphi}_t)^2\Big)dt\right]. \tag{3.6.19}$$

The representation (3.3.1) gives

$$(\dot{\varphi}_t)^2 = \left(\frac{M_{rate}M_{aim}}{\gamma}\right)^2 \mu_t^2 - 2M_{rate}^2\frac{M_{aim}}{\gamma}\mu_t\varphi_t + M_{rate}^2\,(\varphi_t)^2\,, \tag{3.6.20}$$

from which we obtain

$$J(\dot{\varphi}) = \mathbb{E}\Bigg[\int_0^\infty e^{-\rho t}\Bigg(\left(1 + 2\lambda N M_{rate}^2 \frac{M_{aim}}{\gamma}\right)\mu_t\varphi_t \\ - \left(\frac{\gamma}{2} + \lambda N M_{rate}^2\right)(\varphi_t)^2 - \lambda N\left(\frac{M_{rate}M_{aim}}{\gamma}\right)^2 \mu_t^2\Bigg)dt\Bigg]. \tag{3.6.21}$$

In order to derive the explicit expression for J it now remains to compute the integrals

$$\mathcal{I}_1 = \mathbb{E}\left[\int_0^\infty e^{-\rho t}\mu_t\varphi_t dt\right], \quad \mathcal{I}_2 = \mathbb{E}\left[\int_0^\infty e^{-\rho t}(\varphi_t)^2 dt\right], \quad \mathcal{I}_3 = \mathbb{E}\left[\int_0^\infty e^{-\rho t}\mu_t^2 dt\right].$$

A straightforward calculation shows that

$$\begin{aligned}
\mathcal{I}_1 &= \frac{M_{rate}M_{aim}}{\gamma}\frac{\sigma^2}{2\beta}\int_0^\infty e^{-\rho t}\int_0^t e^{-M_{rate}(t-s)}\left(e^{-\beta|t-s|} - e^{-\beta(t+s)}\right)dsdt,\\
\mathcal{I}_2 &= \left(\frac{M_{rate}M_{aim}}{\gamma}\right)^2\frac{\sigma^2}{2\beta}\\
&\quad\times\int_0^\infty e^{-\rho t}\int_0^t e^{-M_{rate}(t-u)}\int_0^t e^{-M_{rate}(t-s)}\left(e^{-\beta|u-s|} - e^{-\beta(u+s)}\right)dsdudt,\\
\mathcal{I}_3 &= \frac{\sigma^2}{2\beta}\int_0^\infty e^{-\rho t}(1 - e^{-2\beta t})dt.
\end{aligned}$$

Here, have used that

$$\mathbb{E}\left[\mu_t\mu_s\right] = \mathrm{cov}(\mu_t\mu_s) + \mathbb{E}\left[\mu_t\right]\mathbb{E}\left[\mu_s\right] = \frac{\sigma^2}{2\beta}\left(e^{-\beta|t-s|} - e^{-\beta(t+s)}\right).$$

Evaluation of the above integrals gives

$$\begin{aligned}
\mathcal{I}_1 &= \frac{M_{rate}M_{aim}}{\gamma}\frac{\sigma^2}{\rho(2\beta+\rho)(\beta+\rho+M_{rate})},\\
\mathcal{I}_2 &= \left(\frac{M_{rate}M_{aim}}{\gamma}\right)^2\frac{2\sigma^2}{\rho(2\beta+\rho)(\rho+2M_{rate})(\beta+\rho+M_{rate})},\\
\mathcal{I}_3 &= \frac{\sigma^2}{2\beta\rho+\rho^2}.
\end{aligned}$$

Plugging these expressions for $\mathcal{I}_1, \mathcal{I}_2$ and $\mathcal{I}_3$ into (3.6.21) in turn yields the asserted representation (3.3.2) from Theorem 3.3.1. □

3.6.2 Proof of Lemma 3.6.1

This section contains the lengthy proof of Lemma 3.6.1, which states that the system of the agents' optimality and consistency conditions has a solution with the properties required for our verification result, Proposition 3.6.8.

As derived heuristically in Section 3.5, the solution of the ten algebraic equations can be reduced to finding the root of a single complicated but explicit function $\Phi_N(\lambda, \cdot)$:

$$\begin{aligned}&\Phi_N(\lambda, y)\\ &= \frac{1}{\lambda(N-1)(N+1)^2}\Big(y\left((N+1)\sqrt{\gamma\lambda}\left(\rho\lambda\left(N^2-1\right)-2\Psi_N\right)+\gamma\lambda((N-6)N+1)y\right)\\ &\quad -2\Theta_N^2(N-1)^2N+\Theta_N(N-1)\left(N\Psi_N+8Ny\sqrt{\gamma\lambda}+\Psi_N\right)\Big),\end{aligned} \tag{3.6.22}$$

where

$$\Psi_N(\lambda, y) = \frac{2(N-1)\left(\Theta_N-\Theta_N N+2y\sqrt{\gamma\lambda}\right)^2}{(N+1)\left(\rho\lambda\left(N^2-1\right)+4\Theta_N(N-1)+2(N-3)y\sqrt{\gamma\lambda}\right)}$$

and

$$\begin{aligned}&\Theta_N(\lambda, y)\\ &= \frac{1}{4N^2}\Bigg[\lambda(N+1)^2\left(\sqrt{\rho^2+\frac{8\gamma N^2-4\rho(3N+1)y\sqrt{\gamma\lambda}}{\lambda(N+1)^2}-\frac{4\gamma(3N+1)y^2}{\lambda(N-1)(N+1)^2}}-\rho\right)\\ &\qquad +(6N+2)y\sqrt{\gamma\lambda}\Bigg].\end{aligned} \tag{3.6.23}$$

Notice that the functions $\Theta_N(\lambda, y)$ and $\Psi_N(\lambda, y)$ correspond to the functions $a(d)$ and $b(d)$, introduced in (3.5.15) and (3.5.16), after substituting the change of variable $d = \sqrt{\lambda\gamma}y$.

We now show that $\Phi_N(\lambda, \cdot)$ has a root $\delta(\lambda)$ for sufficiently small λ. Here, the limiting function $\Phi_N(0, \cdot)$ only depends on the number N of agents, but not the model parameters. Its roots are also roots of a polynomial of order three,

which leads to three candidates for the roots of $\Phi_N(0,\cdot)$. However, using symbolic calculations, we can show that only one of these is a root of $\Phi_N(0,\cdot)$. By verifying that the relevant derivative in this limiting point does not vanish, we can then extend the existence result to sufficiently small λ by means of the implicit function theorem.

Lemma 3.6.9. *Define $\Phi_N(\lambda, y)$ as in (3.6.22). Then, there exists an open set $\Lambda_N \subset \mathbb{R}$ containing $\lambda = 0$ such that:*

(i) *there exists a unique point δ_N^* such that $\Phi_N(0, \delta_N^*) = 0$; it satisfies*

$$\delta_N^* \in \left(0, \sqrt{2}N\sqrt{\tfrac{N-1}{3N+1}}\right]; \tag{3.6.24}$$

(ii) *there exists a unique continuously differentiable function $\delta_N : \Lambda_N \to \mathbb{R}$ such that*

$$\Phi_N(\lambda, \delta_N(\lambda)) = 0, \quad \text{for all } \lambda \in \Lambda_N, \quad \text{where } \delta_N(0) = \delta_N^*.$$

Proof. (i) Our goal is to show that there is a solution of

$$\Phi_N(\lambda, y) = 0 \tag{3.6.25}$$

for sufficiently small $\lambda \downarrow 0$. In this asymptotic regime, to first order (3.6.25) becomes

$$\gamma^{3/2}\frac{\Gamma(N,y)}{\Xi(N,y)} + \mathcal{O}(\lambda^{1/2}) = 0, \tag{3.6.26}$$

where,

$$\begin{aligned}\Gamma(N,y) =& -3N^7\sqrt{\tfrac{2N^3-2N^2-3Ny^2-y^2}{(N-1)(N+1)^2}} + 4N^6y^3 + 8N^6y^2\sqrt{\tfrac{2N^3-2N^2-3Ny^2-y^2}{(N-1)(N+1)^2}} \\ &+ 5N^6\sqrt{\tfrac{2N^3-2N^2-3Ny^2-y^2}{(N-1)(N+1)^2}} + 4N^5y^2\sqrt{\tfrac{2N^3-2N^2-3Ny^2-y^2}{(N-1)(N+1)^2}} \\ &+ 2N^5\sqrt{\tfrac{2N^3-2N^2-3Ny^2-y^2}{(N-1)(N+1)^2}} - 24N^4y^3 - 20N^4y^2\sqrt{\tfrac{2N^3-2N^2-3Ny^2-y^2}{(N-1)(N+1)^2}} \\ &- 6N^4\sqrt{\tfrac{2N^3-2N^2-3Ny^2-y^2}{(N-1)(N+1)^2}} - 8N^3y^3 - 14N^3y^2\sqrt{\tfrac{2N^3-2N^2-3Ny^2-y^2}{(N-1)(N+1)^2}} \\ &+ N^3\sqrt{\tfrac{2N^3-2N^2-3Ny^2-y^2}{(N-1)(N+1)^2}} + 18N^2y^3 + 10N^2y^2\sqrt{\tfrac{2N^3-2N^2-3Ny^2-y^2}{(N-1)(N+1)^2}} \\ &+ N^2\sqrt{\tfrac{2N^3-2N^2-3Ny^2-y^2}{(N-1)(N+1)^2}} + 10Ny^2\sqrt{\tfrac{2N^3-2N^2-3Ny^2-y^2}{(N-1)(N+1)^2}} \\ &+ 2y^2\sqrt{\tfrac{2N^3-2N^2-3Ny^2-y^2}{(N-1)(N+1)^2}} - 4N^7y + 17N^6y - 10N^5y - 12N^4y + 6N^3y \\ &+ 3N^2y + 12Ny^3 + 2y^3,\end{aligned} \tag{3.6.27}$$

and

$$\begin{aligned}\Xi(N,y) = 4(N-1)N^4\Bigg(& N^2\sqrt{\tfrac{\gamma\left(2N^3-2N^2-3Ny^2-y^2\right)}{(N-1)(N+1)^2}} \\ &- \sqrt{\tfrac{\gamma\left(2N^3-2N^2-3Ny^2-y^2\right)}{(N-1)(N+1)^2}} + \sqrt{\gamma}N^2y - \sqrt{\gamma}Ny - \sqrt{\gamma}y\Bigg).\end{aligned} \tag{3.6.28}$$

From (3.6.26) it follows that we can set $\Gamma(N,y) = 0$ to find the roots of (3.6.25) when $\lambda = 0$. We move all the terms with the square root to one side of the equality, and the rest of them to the other side of the equality. Then, squaring both sides and reorganizing gives

$$2N^6P_N(y) = 0, \tag{3.6.29}$$

for a polynomial of order three in y^2, whose coefficients depend on the number N of agents but not the other model parameters:

$$\begin{aligned}P_N(y^2) =& 8N^6(y^2)^3 + \left(-16N^7 + 4N^6 + 48N^5 - 52N^4 + 8N^3 + 20N^2 - 8N - 4\right)(y^2)^2 \\ &+ \left(8N^8 - 20N^7 + 46N^6 - 112N^5 + 114N^4 - 4N^3 - 46N^2 + 8N + 6\right)y^2 \\ &- 9N^8 + 48N^7 - 100N^6 + 96N^5 - 30N^4 - 16N^3 + 12N^2 - 1.\end{aligned} \tag{3.6.30}$$

The polynomial $P_N(y^2)$ has a root in the interval $(0, 2N^2\frac{N-1}{3N+1})$. This follows from

the intermediate value theorem, since $N \geq 2$ and in turn

$$\begin{aligned} P_N(0) &= -(N-1)^6(3N+1)^2 < 0, \\ P_N\left(2N^2\tfrac{N-1}{3N+1}\right) &= \tfrac{(N-1)^3(N(N(N(N(4N(2N-3)-13)+6)+12)+6)+1)^2}{(3N+1)^3} > 0. \end{aligned} \tag{3.6.31}$$

The equalities in (3.6.31) can be verified by expanding the products on the right-hand sides of (3.6.31) and comparing the corresponding result with $P_N(0)$ and $P_N\left(2N^2\frac{N-1}{3N+1}\right)$ obtained by using (3.6.30). In fact, the cubic polynomial P_N has three real roots, but not all of these are roots of $\Gamma(\cdot, N)$. Using symbolic calculations detailed in the Mathematica companion of Micheli et al. (2021), it can be verified that only one root δ_N^* of P_N satisfies $\Phi_N(0, \delta_N^*) = 0$. This completes the proof of (i).

(ii) Again using symbolic computations, it can be verified that $\partial_y \Phi_N(0, \delta_N^*) \neq 0$. (More details can be found in the Mathematica companion of Micheli et al. (2021).) Then, by the Implicit Function theorem there exists $b_N > 0$ and a function $\delta_N : [0, b_N) \to \mathbb{R}$, such that $\Phi_N(\lambda, \delta_N(\lambda)) = 0$ for $\lambda \in [0, b_N)$ as desired. □

In order to prove the main result of this section we first need to establish the following auxiliary lemma.

Lemma 3.6.10. *For all sufficiently small λ, $e = e(\lambda)$ is well defined and strictly positive.*

The proof of Lemma 3.6.10 is postponed to Appendix B.1 for better readability. We are now ready to prove the main result for this section.

Proof of Lemma 3.6.1. Let $N \geq 2$. The proof is split in two parts:

(i) We show that there exists a solution of the system (3.5.5)–(3.5.11), (3.5.12)–(3.5.14);

(ii) We show that the solution of Part (i) is well-defined and satisfies the constraint of (3.6.1);

We remark that to prove our result we will use certain identities for e, f and c (see (B.2.1) and (B.2.2)) which we have postponed to Appendix B.2 for better readability.

Part (i). By reverting the steps in Section 3.5 we recover the parameters $(a, b, c, d, e, f, g, \bar{a}, \bar{b}, \bar{c})$ in terms of d. We then find a solution $d = d(\lambda, N)$ to (3.5.17) for $N \geq 2$ and sufficiently small λ as described in (3.5.18)–(3.5.21) using Lemma 3.6.9. Moreover, it follows that there exists a neighbourhood Λ_N of 0 such that

$$\Phi_N(\lambda, \delta_N(\lambda)) = 0, \quad \text{for all } \lambda \in \Lambda_N, \tag{3.6.32}$$

which implies the existence of a solution $d = d(\lambda, N)$ to (3.5.17) for sufficiently small λ.

Part (ii). Recall that by Lemma 3.6.9(i), $\delta_N^* \in (0, \sqrt{2}N\sqrt{\frac{N-1}{3N+1}}]$. The Implicit Function theorem as applied in the proof of Lemma 3.6.9 yields

$$\delta_N(\lambda) = \delta_N^* + \mathcal{O}(\lambda). \tag{3.6.33}$$

Using (3.5.18) and (3.6.33) we find that

$$d = \sqrt{\lambda\gamma}\delta_N = \sqrt{\lambda\gamma}\delta_N^* + \mathcal{O}(\lambda^{3/2}). \tag{3.6.34}$$

Thus since $\delta_N^* > 0$, (3.6.34) shows that $d > 0$ for sufficiently small λ. Recall that in (3.5.15) a was defined in terms of d. Plugging (3.5.18) in (3.5.15) for the parameter

d, and expanding around $\lambda > 0$ gives

$$
\begin{aligned}
&a \\
&= \frac{1}{4N^2}\Bigg((6N+2)\sqrt{\gamma\lambda}\delta_N \\
&\quad + \lambda(N+1)^2\Bigg(\sqrt{\frac{8\gamma N^2}{\lambda(N+1)^2} - \frac{4(3N+1)\rho\sqrt{\gamma\lambda}\delta_N}{\lambda(N+1)^2} - \frac{4\gamma(3N+1)\delta_N^2}{\lambda(N-1)(N+1)^2} + \rho^2} - \rho\Bigg)\Bigg) \\
&= \sqrt{\gamma\lambda}\Bigg(\frac{1}{2}\sqrt{\frac{2N^3 - 2N^2 - 3N(\delta_N^*)^2 - (\delta_N^*)^2}{(N-1)(N+1)^2}} \\
&\qquad + \frac{1}{N}\sqrt{\frac{2N^3 - 2N^2 - 3N(\delta_N^*)^2 - (\delta_N^*)^2}{(N-1)(N+1)^2}} \\
&\qquad + \frac{1}{2N^2}\sqrt{\frac{2N^3 - 2N^2 - 3N(\delta_N^*)^2 - (\delta_N^*)^2}{(N-1)(N+1)^2}} + \frac{3N+1}{2N^2}\delta_N^*\Bigg) + \mathcal{O}(\lambda) \\
&= \sqrt{\gamma\lambda}\Bigg(\overline{D}\frac{(N+1)^2}{2N^2} + \frac{3N+1}{2N^2}\delta_N^*\Bigg) + \mathcal{O}(\lambda),
\end{aligned}
\tag{3.6.35}
$$

where

$$
\overline{D} = \sqrt{\frac{2N^3 - 2N^2 - 3N(\delta_N^*)^2 - (\delta_N^*)^2}{(N-1)(N+1)^2}}. \tag{3.6.36}
$$

Then, for sufficiently small λ, the arguments of all the square roots above are positive so that a is indeed well defined and positive. Next, note that for $\delta_N^* \in (0, \sqrt{2}N\sqrt{\frac{N-1}{3N+1}}]$ we have

$$
2N^3 - 2N^2 - 3N(\delta_N^*)^2 - (\delta_N^*)^2 \geq 0. \tag{3.6.37}
$$

Using (3.5.13), (3.5.14) , (3.5.15) and (3.5.18) we get that

$$
\bar{c} - (N-1)\bar{b} = -\frac{(N-1)\left(-aN + a + 2\sqrt{\gamma\lambda}\delta_N\right)}{\lambda - \lambda N^2} - \frac{\sqrt{\gamma\lambda}\delta_N - aN}{\lambda + \lambda N}. \tag{3.6.38}
$$

Together with a given in terms of δ_N by (3.6.35), we obtain a power series expansion for the left-hand side of (3.6.38) around $\lambda = 0$:

$$
\bar{c} - (N-1)\bar{b} = \sqrt{\frac{\gamma}{\lambda}}\Delta(N) + \mathcal{O}(1), \tag{3.6.39}
$$

where $\Delta(N) > 0$ was defined in (3.5.22). Therefore, for sufficiently small λ it holds that

$$\bar{c} - (N-1)\bar{b} > 0. \tag{3.6.40}$$

In order to verify (3.6.1), it now remains to prove that $\bar{a} > 0$. In view of (3.5.12), we have

$$\bar{a} = \frac{e}{(1+N)\lambda}.$$

so it suffices to establish $e > 0$. Lemma 3.6.10 shows, that for sufficiently small λ, the constant e is strictly positive and well defined. Therefore, the constant $\bar{a}$ is also strictly positive and well defined.

It remains to prove that (b, c, f, g) are well defined. Since $a, d > 0$ for sufficiently small λ, b in (3.5.16) is well defined. From the expression for f in (B.2.1) it follows that in order to verify that f is well defined we need to show that all the denominators appearing in (B.2.1) are different from zero when λ is small, namely

$$h_3(\lambda) - \beta - \rho \neq 0, \tag{3.6.41}$$

$$h_4(\lambda)\lambda(N+1)^2\left(4a(N-1) + 2d(N-3) + \lambda\left(N^2-1\right)\rho\right) \neq 0. \tag{3.6.42}$$

In view of Lemma 3.6.10 and since $e = 1/h_4$ by (B.2.1), we have $h_4(\lambda) > 0$, $a > 0$, $d > 0$ for sufficiently small λ and in turn (3.6.42). (The case $N = 2$ needs to be handled separately – in this case, it follows from (3.5.15) that for λ small enough we have $a \geq d/2$, which together with $h_4(\lambda) > 0$ gives (3.6.42).)

Using the expression for h_3 in (B.2.2) together with (3.6.34) and (3.6.35) we find that for sufficiently small λ we have

$$h_3 = \sqrt{\frac{\gamma}{\lambda}}\left(\frac{\left(-N^2+N+1\right)\delta_N^* - \left(N^2-1\right)\sqrt{\frac{\left(2N^3-2N^2-3N(\delta_N^*)^2-(\delta_N^*)^2\right)}{(N-1)(N+1)^2}}}{(N-1)N^2}\right) + \mathcal{O}(1) < 0,$$

where we also used (3.6.37) in the last step. This proves (3.6.41), so that f is well defined. Next note that g is well defined if c is well defined, hence in order to

complete the proof we need to prove that c is well defined. From (3.5.9) we have

$$c = \left(\frac{\rho + 2\beta}{2}\right)^{-1} \left(f\bar{a} + \frac{(e - \lambda(N-1)\bar{a})^2}{4\lambda}\right), \tag{3.6.43}$$

since we already showed that $(e, f, \bar{a})$ are well defined, the result follows. □

Remark 3.6.11. *We remark that there exists a unique solution to the system* (3.5.5)–(3.5.11), (3.5.12)–(3.5.14) *for which* (3.6.1) *and* (3.6.24) *are satisfied. Specifically, such unique solution can be characterised as the unique root of the polynomial* (3.6.30) *satisfying* (3.6.24) *while being also the root of* (3.6.26)*. Such solution identifies a unique closed-loop Nash equilibrium in the class of linear strategies. We remark the polynomial* (3.6.30) *has other roots (other than the one corresponding to the closed-loop Nash equilibrium), however, they either do not satisfy* (3.6.24) *or are not a root of* (3.6.26)*. We remind the reader that, as stated in the footnote of page 19, we had already initially excluded all the solutions corresponding to the other root of* (3.5.5) *as the corresponding solution did not present the correct sign in at least one of the parameters among* $\bar{a}, \bar{b}$ *and* $\bar{c}$*.*

4

Evidence of Crowding on Russell 3000 Reconstitution Events

This chapter, based on the paper Micheli and Neuman (2019), is a joint work with Dr. Eyal Neuman and it has been accepted for publication in *Market Microstructure and Liquidity*.

4.1 Introduction

FTSE Russell is, quoting the company web-page (cf. FTSE Russell (2020b)), a "*global provider of benchmarks, analytics, and data solutions with multi-asset capabilities*". The company maintains a wide range of indexes varying for geographic regions, weighting procedures and asset classes.

In US markets, FTSE Russell most prominent products are the *Russell US indexes*: the Russell 1000, 2000, 3000 and 3000E indexes track rosters of US companies across different market capitalizations. Part of the strength of Russell US indexes resides in their modularity. As shown in Table 4.1, each index is composed according to different investment styles, therefore offering an extended and meticulous coverage for the US equity market. As an example, the Russell 3000 measures the performance of the 3,000 largest public companies in the US by total market

capitalization and represents approximately 98 percent of the American public equity market. On the other hand, the Russell 1000 Defensive Index is much more specialized as it includes those Russell 1000 Index companies that are more stable and are less sensitive to economic cycles, credit cycles and market volatility.

Such indexes are often used by portfolio managers as benchmarks for US equity market performances across different market segments. It does not come as a surprise then, that Russell US indexes are the go-to equity universe for a wide body of academic literature, including portfolio management research (Cremers et al., 2020; Biktimirov et al., 2004; Boone and White, 2015; Chang et al., 2014; Chen et al., 2005) as well as market microstructure e.g. (Bucci et al., 2019; Volpati et al., 2020; Capponi and Cont, 2019; Zarinelli et al., 2015; Bucci et al., 2020a; Bormetti et al., 2015; Bucci et al., 2020b; Calcagnile et al., 2018).

The rosters of securities in the Russell U.S. indexes have also received attention for the presence of the so called *"index effects"*. It has been empirically observed that the securities added to equity indexes receive positive returns concurrently with their index additions and shortly thereafter. The main indexes on which such effects are observed are the S&P500 and the Russell U.S. indexes, with many studies, such as Madhavan (2003); Cai and Houge (2008); Chen (2006); Chang et al. (2014); Petajisto (2011), providing evidences in support of the existence of the aforementioned abnormal returns.

As for the Russell U.S. indexes, Madhavan Madhavan (2003) first analyzed the presence of statistically significant abnormal returns attributable to the annual reconstitution of Russell 2000 and Russell 3000 indexes. Moreover, Madhavan explained the abnormal returns due to microstructure effects such as price pressure and changes in liquidity. The mechanisms generating these abnormal returns phenomenon were further investigated and tested by Chen (2006). Cai and Houge (2008) compared the performance of a buy-and-hold strategy of the Russell 2000 index to the returns of a portfolio following the annually rebalanced Russell 2000 index. The latter was shown to be significantly more profitable in a time scale of 5 years. More recently, Onayev and Zdorovtsov (2008) have found evidence of strate-

gic predatory trading behaviour around the annual reconstitution, whereby closing prices of companies are manipulated in order to influence their index membership.

Russell U.S. Indexes		
Broad market	**Large cap**	**Small cap**
Russell 3000E Index	Russell 1000 Index	Russell 2000 Index
Russell 3000E Value Index	Russell 1000 Value Index	Russell 2000 Value Index
Russell 3000E Growth Index	Russell 1000 Growth Index	Russell 2000 Growth Index
Russell 3000 Index	Russell 1000 Defensive Index	Russell 2000 Defensive Index
Russell 3000 Value Index	Russell 1000 Dynamic Index	Russell 2000 Dynamic Index
Russell 3000 Growth Index	Russell 1000 Growth-Defensive Index	Russell 2000 Growth-Defensive Index
Russell 3000 Defensive Index	Russell 1000 Growth-Dynamic Index	Russell 2000 Growth-Dynamic Index
Russell 3000 Dynamic Index	Russell 1000 Value-Defensive Index	Russell 2000 Value-Defensive Index
Russell 3000 Growth-Defensive Index	Russell 1000 Value-Dynamic Index	Russell 2000 Value-Dynamic Index
Russell 3000 Growth-Dynamic Index		
Russell 3000 Value-Defensive Index		
Russell 3000 Value-Dynamic Index		

Table 4.1: Russell US indexes by investment style and market sector. Table originally published in Section "Construction and Methodology" of FTSE Russell (2020c).

One of the main features distinguishing the Russell U.S. indexes across all others US stocks equity indexes is their rebalance procedure. In general, rebalance procedure of equity indexes are not necessarily publicly disclosed and sometimes presents some degree of arbitrariness. For example, as discussed in Cai and Houge (2008); Petajisto (2011), Standard & Poor's maintains a proprietary selection process used to discern which stocks will belong to the new issue of the index and make adjustments whenever it considers it to be necessary. Nonetheless, even though such procedures remain undisclosed, the S&P500 historical constituents securities are available to researchers via the WRDS database maintained by the Wharton

School of the University of Pennsylvania.

On the other hand, we have the FTSE company that implements a publicly available fully deterministic rebalance algorithm for its Russell indexes, but which prefers not to publicly disclose their historical index compositions. Bloomberg L.P. terminals offer the list of the companies in the indexes but neither the constituents securities nor the index weights are available.

The FTSE index compositions are available to buy for financial institutions and funds. On the academic side, the WRDS database has recently started providing a Russell index historical dataset for 21 indexes, with a substantial annual fee. However, at the time of writing, this dataset provides only information on index weights and companies contributions to returns. It falls short of more refined information such as quarterly and annual ranking and rebalance days, and on historical lists of securities for companies which are traded across different classes of shares. We invite the reader to consult Section 4.2 for a detailed description of these features and their importance to index reconstitution. Since these features play a crucial role on indexes reconstitution, tracking them in a consistent framework is important for academic research (see e.g. the analysis in Section 4.5). There seems to be a gap in Russell data for research purposes, in the sense that there is no recognised source from which academic researchers and financial institutions' internal researchers can borrow detailed Russell US indexes data from. Therefore, it is very likely that the notion and composition which is used to approximate the Russell US indexes, e.g. the Russell 3000 or Russell 2000 indexes, could be diversified across different academic papers.

Agreeing upon a common *"definition"* of what are Russell indexes could benefit the financial research community as a whole and is one of the main goals of this work. On some very elementary scientific grounding, sharing the notion of initial data, common to all financial data analyses, allows for a higher degree of reproducibility of the results. In the first part of this chapter (Sections 4.2–4.4) we develop a methodology which is based only on data available in the CRSP database of the Wharton Research Data Services (see Section 4.3 for more details on the

database). This methodology allows us to replicate in great accuracy the Russell 1000, 2000 and 3000 indexes weights and returns, and to track new additions and deletions. We demonstrate the accuracy of this methodology by comparing our suggested reconstitution procedure versus the original Russell US indexes for the time period June 1989 to June 2019 (see Section 4.4). A python package named *pyndex* that generates the indexes according to our methodology is also provided in Micheli (2020).

The impact of sharing such initial data might vary across different studies, ranging from marginal to impactful, nonetheless we still remark that it could only be beneficial and would bring the research community a step closer to the conclusion of disputes on results based on the quality of the data being analysed. Similarly to the natural sciences, we remark that the validity of quantitative claims is settled only by referring to the observations of the phenomenon, which, by nature, strongly depend on the data analysed.

As a first application for our index reconstruction methodology, we study crowding on indexing strategies around Russell 3000 reconstitution events, which starting from 2004 occurs every quarter. Before we describe our analysis on this topic, we survey some existing literature on crowding in financial markets.

Over the last 20 years, the phenomenon of *crowding* in financial markets has increasingly gained attention both from academics as well as from financial institutions. It is a subject of many research works studying both theoretical and empirical aspects including (Cont and Bouchaud, 2000; Volpati et al., 2020; Bucci et al., 2020b; Barroso et al., 2017; Caccioli et al., 2015, 2014; Khandani and Lo, 2008).

Crowding is often considered to be an explanation for sub-par performances of investments as well the development of systemic risk in financial markets. The presence of largely overlapping portfolios comes at the expense of portfolio managers, also in terms of transaction costs, as affine positions usually lead to similar trades.

Cont and Bouchaud (2000) proposed a simple mathematical model in which the communication structure between agents gives rise to heavy tailed distribution for stock returns. This established a theoretical connection between crowding and stock markets shortfall. The aforementioned portfolios overlap was shown to be a considerable factor in the August 2007 Quant Meltdown. Using simulated returns of overlapping equity portfolios, Khandani and Lo (2008) showed that combined effects of portfolio deleveraging following by a temporary withdrawal of market-making risk capital was one of the main drivers of the 2007 Quant Meltdown. Caccioli et al. (2015, 2014) developed a mathematical model for a network of different banks holding overlapping portfolios. They investigated the circumstances under which systemic instabilities may occur as a result of various parameters, such as market crowding and market impact. Recently, Volpati et al. (2020) measured significant levels of crowding in U.S. equity markets for Momentum signals as well as for Fama-French factors signals, even though with smaller significance.

As already mentioned, we apply our index reconstruction methodology in order to measure crowding effect on Russell indexes around reconstitutions events. It was reported by Madhavan (2003) and others, that around annual index reconstitution events, there are significant abnormal returns on stocks which are new additions or deletions from the index. These returns are caused by portfolio trading strategies which anticipate the change in the stock price for new additions or deletions. The returns of these stocks are typically decomposed into two parts. The first is called temporary price impact, and it describes the returns that revert back within one month from index rebalance day. The permanent price impact captures sustainable stock returns, which accumulates within two months from the index reconstitution announcement (see more details in Section 4.5). It follows that the reconstitution events of the Russell 3000 index serve as prominent examples for studying crowding effects of trading strategies.

Starting from 2004, the Russell indexes received quarterly *additions* to take into account the changes brought in the market by newly listed securities, that is IPOs, which took place between annual rebalancings (see additional details in Section

4.2). The practice of quarterly updates to the indexes was continued ever since and is currently still in use. To our knowledge, none of the papers that studied the Russell index reconstitution effect has dealt with these quarterly additions. The reconstruction methodology, which is developed in this chapter, can assist us to preform a more refined analysis of crowding phenomenon on Russell 3000 index around reconstitution dates. This is the second objective of this chapter.

In Section 4.5 we compute the permanent and temporary price impact on the Russell 3000 stock additions and deletions, using the annual index portfolios generated with our protocol. We also track the quarterly additions to the Russell 3000 index. We find that the price impacts of the aforementioned quarterly additions are overall compatible with the hypothesis that the majority of market participants track the Russell 3000 index on an annual basis rather than on a quarterly basis. Such findings are consistent with the belief that the portfolio strategies following the Russell 3000 index rebalance on an annual basis are more crowded than those following the Russell 3000 index rebalance on a quarterly basis.

This chapter is structured as follows. In Section 4.2 we describe the precise methodology of the FTSE Russell indexes reconstitution which includes the quarterly rebalancings due to new initial public offerings (IPOs). In Section 4.3 we describe the data that we are using in order to reconstruct the indexes in this chapter. Section 4.4 is dedicated to our methodology which approximates the Russell US indexes to our results which replicate the indexes. In Section 4.5 we determine the temporary and permanent price impact generated by the annual index additions as well as examine the existence of crowded trades around the annual Russell 3000 reconstitution. In Section 4.6 we present the conclusions of this chapter.

4.2 The FTSE Russell indexes reconstitution Methodology

In this section we describe the main features in the original FTSE Russell indexes reconstitution methodology.

The FTSE Russell US 1000, 2000 and 3000 are equity capitalisation-weighted indexes that currently follow an annual rebalance procedure, which was first adopted in June 1989. As further discussed in Cai and Houge (2008), the indexes followed a quarterly rebalance schedule from 1979 to 1986 and a semi-annual one from 1987 to 1989. In the 2004 rebalance calendar, the Russell indexes received quarterly *additions* to take into account the changes brought in the market by newly listed securities, that is IPOs which took place between annual rebalancings. The practice of quarterly updates to the indexes was continued ever since and is currently still in use.

We remark that the newly issued securities added at each quarter do not replace any other company already in the indexes, in fact quoting the 2004 press release BusinessWire Press Release (2004) of Russell Investments[1]:

> *"As IPOs are added to Russell indexes each quarter, Russell will not delete existing index members to make room for them, but will continue to reconstitute the indexes fully each year at the end of the second quarter."*

Inclusion in the Russell indexes is established systematically via a set of rules which we will briefly summarise, without intending to be fully exhaustive. For the full list of the current selection rules we invite the reader to consider the official documentation available at FTSE Russell (2020c).

Each year on the *rank day*, which takes place in May, all U.S.-domiciled com-

[1]Russell Investments controlled the Russell US indexes until its index division was bought by LSE Group in 2015 and subsequently renamed FTSE Russell.

panies with stock prices greater than $1.00 are ranked according to their market capitalisation. The total market capitalisation of a company is computed by determining the shares of common stock, non-restricted exchangeable shares and partnership units/membership interests while excluding any other form of shares, such as convertible preferred stocks, foreign securities as well as American Depositary Receipts (ADR). Explicitly, as discussed in FTSE Russell (2020c), exchangeable shares are shares which may be exchanged, on a one-for-one basis, at the owner's option at any time, while membership interests or partnership units embody an economic interest in a limited liability company or limited partnership.

For a company which is traded across different classes of shares, e.g. Berkshire Hathaway, FTSE Russell first determines its so called *pricing vehicle*: the share class with the highest two-year trading volume as of the corresponding rank day in May. Hence, the total market capitalisation is computed by multiplying the cumulative sum of shares across all classes by the close price of the pricing vehicle on the rank day. Only companies with a total market capitalisation higher than 30 million U.S. dollars are included in the ranking of the Russell US indexes.

Once the ranking has been established, the 3000 companies with the highest market capitalisation fall in the Russell 3000 index. The top 1000 companies in the Russell 3000 index in turn, constitute the Russell 1000 index, while the bottom 2000 determine the Russell 2000 index. The top 4000 companies in the ranking with total market capitalisation higher than 30 million U.S. dollars, or all the available securities in case they are less than 4000, constitute the Russell 3000E.

The weight corresponding to each security admitted to the index is computed as follows. The outstanding shares of a security are adjusted to only include the number of available shares which can be traded by the public, the so called *"free float"*. In fact, it is possible that some of the shares, as those held by government or other third party, might not be available for trading. The adjustment is done based on information contained in governmental filings, such as those submitted to the Securities and Exchange Commission (SEC). Further information about the float-adjustment procedure for the rebalance year 2020 can be found in Section

"Methodology Enhancements" of FTSE Russell (2020a). A market capitalization computed via the free float shares is called float adjusted. Stocks in the Russell US indexes are weighted by their float-adjusted market capitalization times the closing price of the corresponding pricing vehicle.

The *rebalance day* is scheduled to be one month later than the ranking day, coinciding therefore with the end of June or beginning of July. On this day the new issues of the indexes officially replaces the previous ones in the stock market. Minor adjustments to the indexes are made in the period between the ranking day and the rebalance day, for example, in the case of mergers and spin-off of companies. Since the FTSE Russell acquisition of the Russell U.S. indexes, which took place in 2015, the exact reconstitution calendar have been published on the FTSE Russell webpage. In order to reliably retrieve the reconstitution calendar prior to FTSE Russell acquisition one has to consider the research literature. Specifically, in Table 4.2 we gather the rank days and rebalance days as described in Section "Index Construction and Sample Selection" of Cai and Houge (2008), Section 2 of Chen (2006) and Section 3.2 of Madhavan (2003). It is documented by the FTSE Russell webpage FTSE Russell (2017) that, starting from 2017, the Russell U.S. indexes rank day has seen a shift towards the first half of May, in agreement to what is also observed for the year 2020 in Table 4.2. The academic sources, that are dated before 2017, unanimously agree on the rank day coinciding with the 31st of March.

Academic Sources and Annual Reconstitution Calendars		
Source	**Rank Day**	**Rebalance Day**
FTSE Russell (2020a)	May 8	June 26
Cai and Houge (2008)	May 31	June 30
Madhavan (2003)	May 31	July 1
Chen (2006)	May 31	June 30

Table 4.2: A comparison of the Russell indexes reconstitution calendar across different sources.

In a similar fashion to the annual rebalance schedule, the ranking for inclusions

of IPOs takes place at the end of Q3, Q4 and Q1. Approximately one month after each quarterly ranking date the index gets extended with the new eligible IPOs, as it can be seen from the 2019 quarterly rebalance calendar in Table 4.3. As discussed in Section "Defining Membership by size" FTSE Russell (2020c), the quarterly rebalance days are taken to be the third Fridays of September, December and March and the corresponding rank days are set to be 5 weeks before each quarterly rebalance day.

Russell U.S. Quarterly Rebalance Calendar 2019			
Quarterly additions	2019-Q3 Additions	2019-Q4 Additions	2020-Q1 Additions
Initial offering period	IPOs which initially price/trade between May 13 and Aug 16.	IPOs which initially price/trade between Aug 17 and Nov 15.	IPOs which initially price/trade between Nov 16 and Feb 14.
Rank date	16 Aug 2019	15 Nov 2019	14 Feb 2020
Rebalance date	20 Sep 2019	20 Dec 2019	20 Mar 2020

Table 4.3: Quarterly IPO calendar for the 2019 Russell rebalance schedule.

The eligibility of the IPOs is established in two ways:

1. If the new issue released in the IPO belongs to a company which is already an index constituent, the following criterion is considered. FTSE Russell determines the value associated to the IPO by multiplying the number of shares released in the IPO by the price of the pricing vehicle of the company releasing the issue. If the IPO's value is larger than the market capitalisation of the company sitting at the bottom of the Russell 3000E index, the security released in the IPO is added to the index. The market capitalisation of the company at the bottom of the Russell 3000E index, before being used in the comparison with the IPO's values, is suitably adjusted to take into account the price variations of the stocks which have taken place since the annual rebalance day. Note that the index membership assigned to the new issue will be the same of the pricing vehicle. However, the new issue is added to the index as a separate entity, therefore, it does not contribute to the total

market capitalization of its company.

2. If the new issue belongs to a company which is *not* in the index at the time of the IPO, then the market capitalisation of the IPO is established by multiplying the number of shares released, by their price on the quarter IPO ranking day. If such market capitalisation falls within any of the capitalisation breakpoints established at the annual ranking day[2] then the company is added to the one or more of the indexes accordingly.

At every ranking day, either annual or quarterly, the index weights are recalculated based on the current capitalisation of the index constituents. The current annual cycle of the indexes is summarised by Fig. 4.1. Note that once a company is

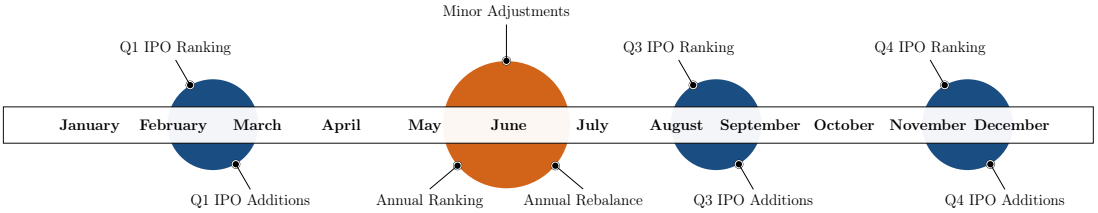

Figure 4.1: Russell US indexes annual reconstitution timeline starting from June 2004. The timeline for the years 1989-2004 is identical apart from the quarterly IPOs additions, i.e. the blue circles.

delisted from the market, the corresponding securities are not traded anymore. This implies that if any such company is part of any Russell US index, then the number of actively traded securities in the index might reduce during the course of the year. Nonetheless, FTSE decides not to alter the current composition of the index and therefore any stock in the index which is delisted is not replaced.

Finally, as discussed in Section "Long-Run Impact of Additions and Deletions" of Cai and Houge (2008), the index returns can be found by a weighted average of the daily stock returns belonging to the index under the assumption of dividends reinvestment.

[2]The capitalisation breakpoints are determined by the market capitalisation on the annual ranking day of the lowest ranking company in the Russell 1000 and 3000 index. For the Russell 2000 index they are similarly determined by the highest and lowest market capitalisation.

4.3 The Data

For the index reconstitution we will adopt the data available in the Wharton Research Data Services (WRDS) database, a research platform available to "*50,000 corporate, academic, government and nonprofit users at 400+ institutions in 30+ countries*" provided by the the Wharton School of the University of Pennsylvania. Specifically, we will limit ourselves to the financial data collected in the Center for Research in Security Prices (CRSP) U.S. Stock database, which offers highly accurate information for the U.S. stock market. As further discussed in Section "General Description: Coverage" of Wharton Research Data Services (2020), such database contains end-of-day and month-end prices for,

- *NYSE*, starting from December 31, 1925,
- *NYSE MKT*, starting from July 2, 1962,
- *NASDAQ*, starting from December 14, 1972,
- *Arca Exchanges*, starting from March 8, 2006.

Moreover, the securities listed in this database are only equity securities for U.S. companies or international companies which are traded in any of the stock market aforementioned. The CRSP database contains the necessary information about the financial securities to be used in our analysis, such as prices, quote data, shares outstanding as well as the information about corporate actions, including IPOs. We refer the reader to Appendix C.1 for further technical details regarding CRSP databases and their content.

4.4 Generating the Russell US indexes

We turn to discuss the main features of our analysis for reconstructing Russell 1000, 2000 and 3000 using CRSP datasets to a very high degree of accuracy. Our analysis

will not be free from approximations to the original Russell US index reconstitution, which currently counts more than 40 pages of methodology. Due to the restricted breadth of data we consider, which as mentioned in Section 4.3 is confined to the CRSP U.S. stock financial data, our reconstitution methodology departs in multiple ways from the one of Section 4.2. We will consider the time window starting from July 1989, the first year in which the annual rebalance schedule has been applied, and terminating in June 2019.

As already discussed in Section 4.2, the exact annual reconstitution calendar of the Russell U.S. indexes is not available to the public for the entire time period we consider here. Therefore, we will take the annual rank day to take place on the 31st of May while the annual rebalance day to be the last Friday of June, as similarly supported by the academic sources cited in Table 4.2. Following Table 4.3 and the methodology in FTSE Russell (2020c) we take the Q3, Q4 and Q1 rebalance days to fall on the third Friday of September, December and March respectively and the corresponding rank days to be 5 weeks theretofore. If any rank day, be it annual or quarterly, falls on a U.S. non-trading day then we move it to the preceding trading day. Instead, for a rebalance day, be it annual or quarterly, which falls on a U.S. non-trading day we shift it to the following trading day. We do so in order to avoid any look-ahead bias [3]. Such choice of schedule may deviate from the real one, but given that the rank and rebalance days often take place at the end of May and at the beginning of July respectively, we expect the deviation to be marginal and not to present any measurable effect on our final result.

Originally, as explained at length in Section 4.2, the pricing vehicle for each company is identified and then used to determine the market value of such company on the ranking day. Such procedure presents extra work required for companies with more than one share class: we would need to identify the pricing vehicle using the two-year trading volume of each share class. Figure 2 of Cai and Houge (2008) shows that it is possible to replicate, for the time period 1979-2004, to very high statistical accuracy the cumulative returns of the Russell 2000 index. This is done

[3] A look-ahead bias is any bias that can appear in the data which is caused by using information that would not have been known or available during the period being analyzed.

by computing the market capitalization of every company without determining its pricing vehicle, that is by multiplying the total shares outstanding of each security times the corresponding share price. This motivates us to deviate from the original methodology and to approximate the market capitalization of each company as in Cai and Houge (2008), for all the Russell U.S. indexes and for the entire time period 1989-2019. Moreover, we remark that such market capitalization would differ from the original one only for companies which are traded across two or more share classes and not for all the index constituents.

CRSP does not contain any information regarding cross-ownership or privately held shares. Such a piece of information is necessary in order to adjust for the free float, i.e. the fraction of shares which can be traded by the public. Hence, instead of computing the weights of the stock admitted to the index using the float-adjusted market capitalization, as in the original methodology, we use the the same market capitalization which was used to establish the index ranking.

Starting from the reconstitution calendar of May 2004, we introduce quarterly ranking days and rebalance days in order to update our index with the IPOs taking place between rank days. Note that this is one of the main differences from previous index reconstruction papers such as Cai and Houge (2008). As already discussed in Section 4.2, the way in which the original methodology considers adding newly issued securities to the index is two-fold, depending whether they belong to a company listed in the index or not. Our methodology deviates from the original as follows. We will add any newly issued securities belonging to companies not listed in the index. We require each security to satisfy the standard eligibility requirements for the admission to the index and whose IPO took place in the 3 months preceding the quarterly rank day. Once a new issues satisfies the eligibility requirements, then it can be added to one or more Russell U.S. indexes, only if its total market capitalization falls within the market capitalization breakpoints established during the most recent annual ranking day.

Finally, in accordance with the original FTSE Russell methodology any company in the index which is deleted between rebalance days is never replaced.

Now we are ready to present our main results regarding indexes replication. We first concentrate on the results of indexes replication between 1989-2004, where Russell indexes were rebalanced annually, without any quarterly IPOs additions. Then we focus on more recent results of indexes replication between 2004-2019, where quarterly rebalancings including companies IPOs were introduced.

Cai and Houge (2008) retrieved the roster of companies in the Russell 1000 and 2000 indexes for the time period 1979 to 2004 directly from Frank Russell Company. Figure 1 in Cai and Houge (2008) displays the total number of Russell 2000 membership changes for each annual rank date alongside the number of new issues, i.e. IPOs and spin-offs, picked up by the index each year. In Figure 4.2 we also compute the annual number of constituent changes to Russell 2000 index for each annual reconstitution. Specifically, the *"Total Index Additions"* bar at year t counts the number of companies added to the Russell index during the year t annual rebalance but which weren't in the index in the previous release of the index. The *"New Issues"* bar at year t quantifies the companies added to the Russell 2000 index during the year t annual rebalance whose IPO took place between May of year $t-1$ and May of year t. CRSP does not offer enough information regarding corporate actions in order to include spin-offs, as it was done in Figure 1 of Cai and Houge (2008). Over the years 1989 to 2004, where our methodology intersects with Cai and Houge (2008), we see that there is a very good agreement in terms of the number of new issues added to the index and the total number of index additions. Therefore, this guarantees that, for the time period 1989-2004, our methodology does not significantly differ from the original methodology which generated the rosters of companies studied by Cai and Houge and which were originally retrieved from Frank Russell Company. Figure 4.2 extends the results of Cai and Houge to the time period in which IPOs were included in the original methodology, that is from the year 2004 until the most recent data.

We visually compare the index returns generated with our methodology versus the original index returns. We retrieve the original daily returns for the Russell 1000, 2000 and 3000 from the Bloomberg L.P. terminal. As already discussed, the

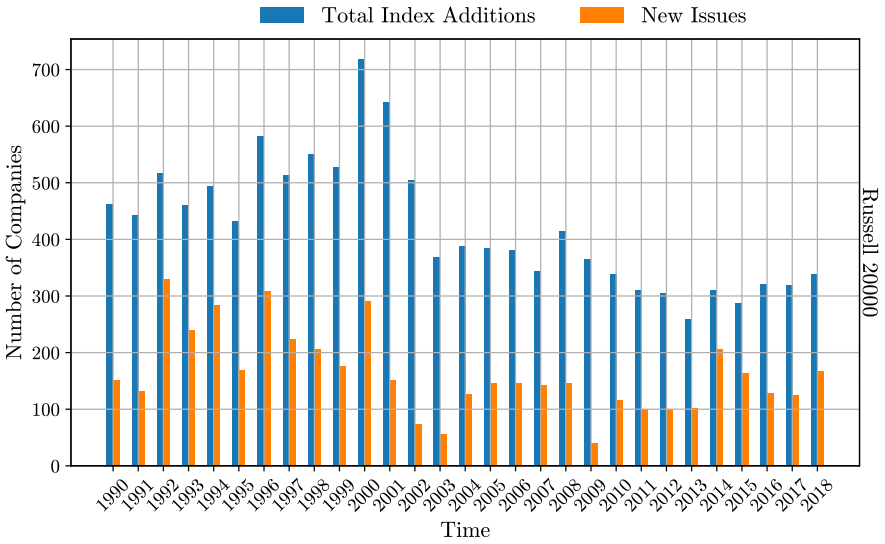

Figure 4.2: The annual index changes between 1989-2019, as well the total number of new IPOs taking place in 12 months before year the rebalance of each year and satisfying the requirements for index additions. Russell US indexes started receiving index additions due to IPOs from September 2004.

index daily returns can be computed by a weighted average of the stock returns using the index weights. Therefore, a correct combination of the stocks selection and their corresponding index weights should be capable to reproduce the original daily index returns. We remark that it would be very hard, if not impossible, to back-engineer the constituents and the corresponding weights given the original daily index returns for the entire time period considered. The daily index returns are too noisy to be used for any meaningful visual comparison, therefore we plot the *trailing three-months* (T3M) index gross returns. Let $0 \leq t_1 < t_2$ and let r_t be the daily net return from day $t-1$ to time t. The compounded gross returns on $[t_1, t_2]$ are given by,

$$\prod_{t \in [t_1, t_2]} (1 + r_t).$$

Hence, the trailing three-months gross returns at time t_2 are computed by taking $[t_1, t_2]$ to be a 3 months time window.

Figure 4.3 compares the T3M index gross returns based on the daily returns of our replicated indexes and the original Russell 1000, 2000 and 3000 indexes for the time window between July 1989 to June 2019. The Russell U.S. indexes

generated following our methodology are consistently capable of mimicking the original Russell indexes for the entire duration of the time window considered.

The visual agreement of Figure 4.3 is further assessed statistically via cross-correlations of daily returns of our replicated indexes against the original Russell U.S. indexes.
As discussed in Section "What is the problem with cross-correlating simultaneous autocorrelated time series?" of Dean and Dunsmuir (2016), the confidence bands of the cross-correlation between two time series has to be altered from the conventional cross-correlation limit, if the time series considered individually present significant autocorrelations. If such autocorrelations are not taken into account they may lead to the phenomenon of *"spurious correlations"*, in which, as also shown in Figure 1 of Dean and Dunsmuir (2016), where even two independent time series can present a significant correlation.

For the time window 1989-2004 and 2004-2019, we checked that none of the daily returns of the indexes, generated or original, present significant autocorrelation at any non-zero lag. The Pearson's correlations of generated and original indexes at zero lag are reported in Table 4.4, along with the 95% confidence bands which are given by $\pm 1.96/\sqrt{n}$, where n is the sample size. As a benchmark, in parentheses we report the cross-correlation at zero lag between a portfolio in which the components of the reconstructed Russell indexes are equally weighted and the original Russell indexes. All the Pearson's cross-correlations are strongly significant.

To further test the agreement among the series in terms of non linear measures of dependence, we also determine the Kendall's τ correlations between the reconstructed Russell indexes and the original ones. We report the values report in Table 4.5 along with 95% confidence bands which are given, for large samples, by $\pm 1.96\sqrt{\frac{2(2n+5)}{9n(n-1)}}$ where n is the sample size. Similarly to the case of Pearson's cross-correlations, we also report in parentheses the correlations between the equally weighted portfolio and the original Russell indexes. All the Kendall's τ correlations are strongly significant and outperform the benchmark of the equally weighted portfolio.

Cross-Correlations (Pearson's)				
Years	**Russell 3000**	**Russell 2000**	**Russell 1000**	**95% Confidence Bands**
1989-2004	0.98 (0.88)	0.97 (0.96)	0.98 (0.94)	± 0.03
2004-2019	0.99 (0.95)	0.99 (0.99)	0.99 (0.97)	± 0.03

Table 4.4: Pearson's cross-correlation at lag 0 days between daily net returns for Russell 1000, 2000 and 3000 generated with our reconstitution procedure versus the original Russell indexes. The values in parenthesis are the cross-correlations between a portfolio in which the components of the reconstructed Russell indexes are equally weighted and the original Russell indexes.

Cross-Correlations (Kendall's τ)				
Years	**Russell 3000**	**Russell 2000**	**Russell 1000**	**95% Confidence Bands**
1989-2004	0.92 (0.67)	0.88 (0.86)	0.92 (0.77)	± 0.02
2004-2019	0.96 (0.77)	0.94 (0.89)	0.95 (0.83)	± 0.02

Table 4.5: Kendall's τ cross-correlation at lag 0 days between daily net returns for Russell 1000, 2000 and 3000 generated with our reconstitution procedure versus the original Russell indexes. The values in parenthesis are the cross-correlations between a portfolio in which the components of the reconstructed Russell indexes are equally weighted and the original Russell indexes.

Similarly, as shown in Figure 4.4, the normalised distribution of the daily returns overlap to a very good degree between June 1989 to June 2004. The agreement is also confirmed by the corresponding Q-Q plot.

Next, we turn to the time window ranging from June 2004 to June 2019. As already discussed at the beginning of this section, we consider adding to our index only securities issued by companies which are not listed in the index at the time of their IPO. This approximation allows us to exclude the extra work of considering different criteria for the securities belonging to companies already in the index. The full discussion of such criteria was given in Section 4.2. Figure 4.5 displays a justification for such approximation. We compare, for each year from 2004 to 2019, the number of new issues from companies which are not in the index, namely *"New Issues not in Index"*, to the number of new issues from companies which belong to the Russell 1000 or 2000 indexes, that is the *"New Issues from Russell 1000"* and *"New Issues from Russell 2000"* bars. Specifically, the *"New Issues from Russell 1000"* bar at year t quantifies the eligible securities issued by a company

in the Russell 1000 index in the time window from year t to year $t+1$. Similarly, mutatis mutandis, for the *"New Issues from Russell 2000"* and the *"New Issues not in Index"* bars. We remark that given the hierarchical structure of the Russell 1000, 2000 and 3000 indexes the sum of the new issues from companies which belong to the Russell 1000 and 2000 indexes is simply the total number of new issues from companies in the Russell 3000 index.
For the entire duration of our analysis the *"New Issues not in Index"* IPOs are about two orders of magnitude larger than the *"New Issues from Russell 1000 and Russell 2000"* IPOs combined. In many years there are no new issues belonging companies belonging to the indexes, for example as in 2007 or 2016.

Similarly to the time period 1989-2004, we compare the T3M index gross returns of the reproduced Russell index against those of the original ones. Again, Figure 4.3 compares the T3M cumulative returns arising from the Russell 1000, 2000 and 3000 index generated with our methodology versus the original indexes between June 2004 to June 2019. Similarly to the pre-2004 returns, our generated index can fully imitate the original Russell indexes returns.

Moreover, for the time window 2004-2019, the daily returns do not show any autocorrelation both for the original and generated time series. As contained in Table 4.4, the cross-correlation between the generated and original returns is extremely significant for both the Russell 1000, 2000 and 3000 indexes.

When comparing the normalised distributions of the daily returns as in Figure 4.6 we observe a very good agreement between our and the original indexes, which is supported by the respective daily returns histogram (left panel) and Q-Q plot (right panel) for the Russell 3000.

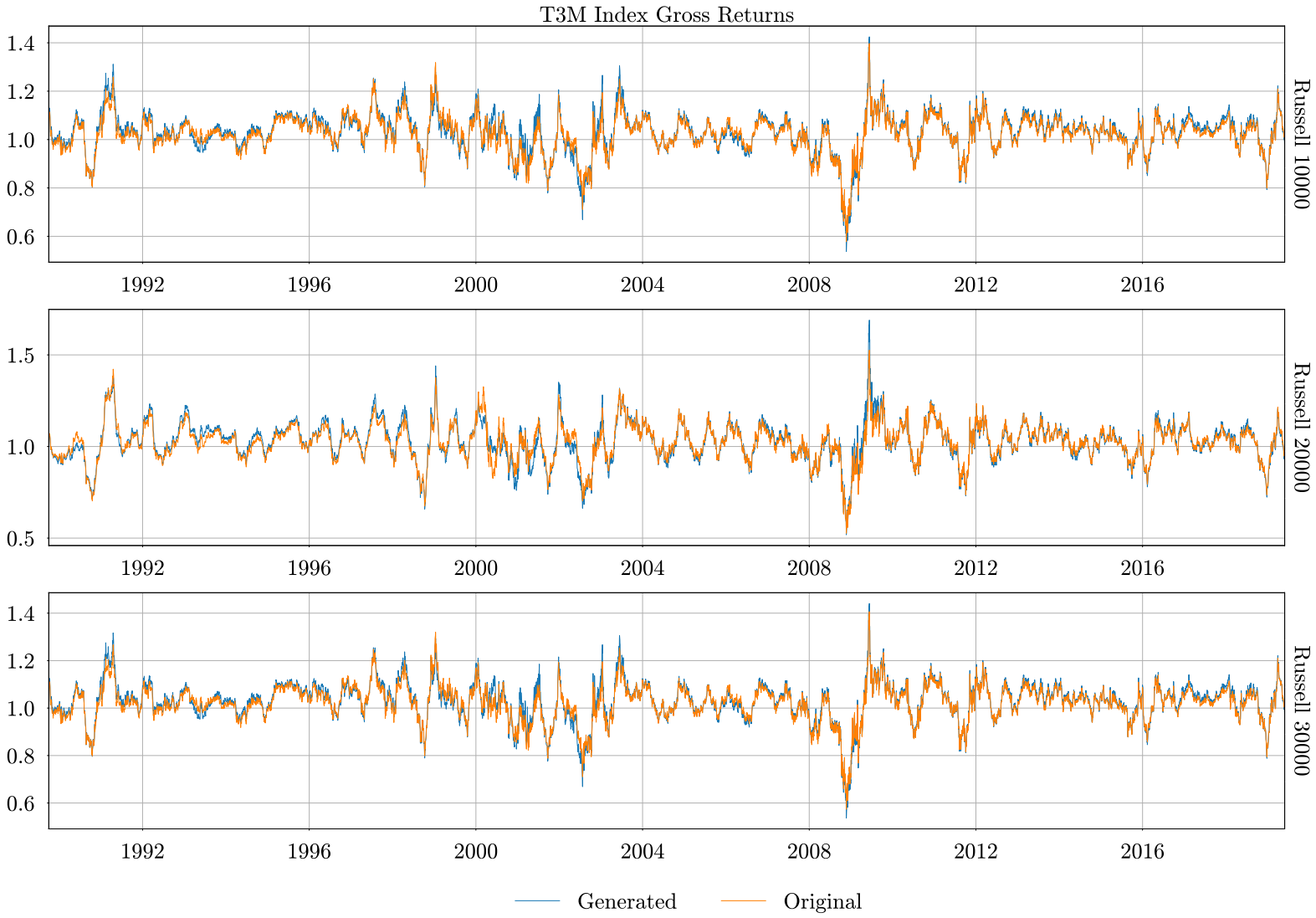

Figure 4.3: We compare the T3M gross returns for the time period June 1989 to June 2019 belonging Russell 1000, 2000 and 3000 generated with our reconstruction methodology (in blue) versus the original Russell US indexes (in orange).

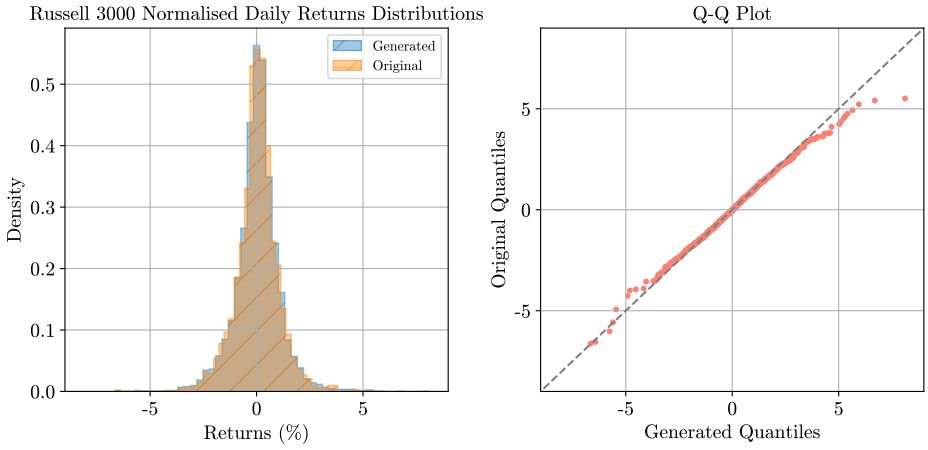

Figure 4.4: On the left panel we compare between the normalised daily returns histogram of the Russell 3000 replicated index (orange area) and the original index (blue area), from June 1989 to June 2004. On the right panel the corresponding Q-Q plot between the two distributions is presented.

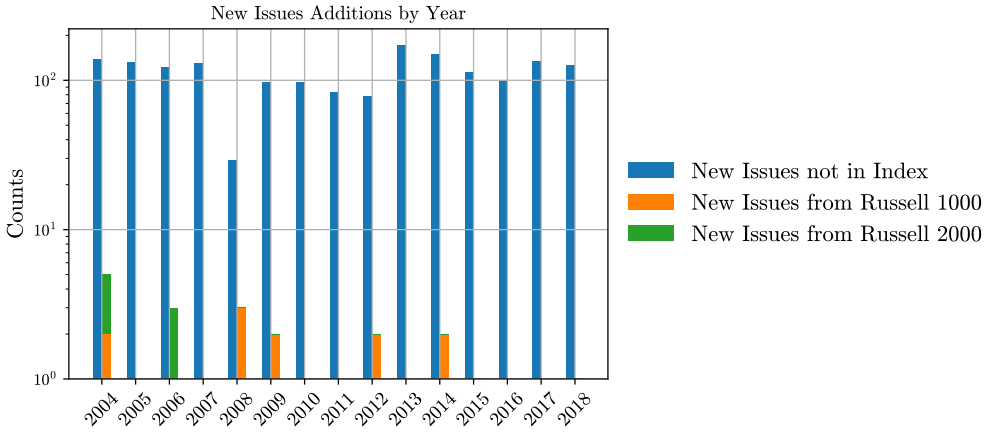

Figure 4.5: Comparison of the number of new IPOs in each year in the following groups: *"New Issues not in Index"* for securities which are not in the Russell 3000 index, *"New Issues from Russell 1000"* and *"New Issues from Russell 2000"* ,between 2004-2018.

4.5 Price Impact on Index Additions and Crowding

In this section we measure the temporary and permanent price impact for the annual additions and deletions in the Russell 3000 index. Moreover, we conduct a careful analysis on temporary and permanent price impact for new IPO's which are added to the the Russell 3000 index, estimating such quantities near the dates of

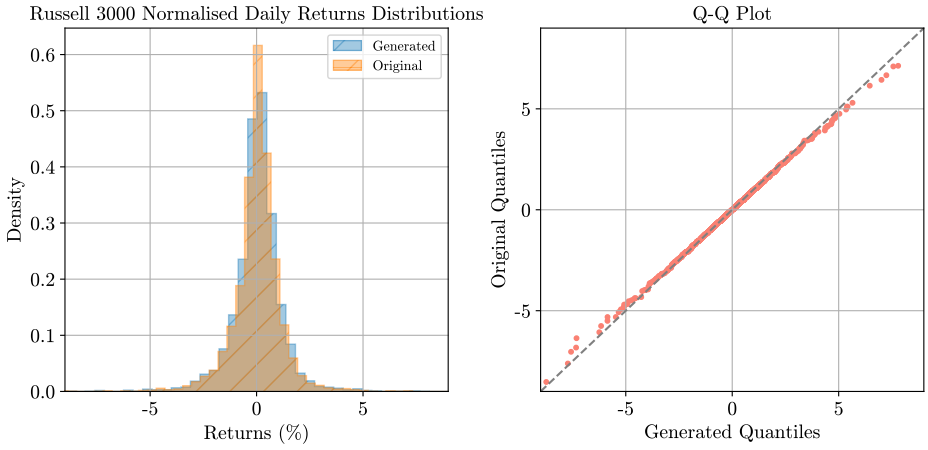

Figure 4.6: On the left panel we compare between the normalised daily returns histogram of the Russell 3000 replicated index (orange area) and the original index (blue area), from June 2004 to June 2019. On the right panel the corresponding Q-Q plot between the two distributions is presented.

quarterly and annual rebalances. Studying the aforementioned price impact allows us to test whether the majority of market participants follow the index rebalance annually or quarterly. Specifically, for each year from 2004 to 2018 we test the following hypotheses:

- whether the most recent Q3, Q4 and Q1 quarterly additions remaining in the Russell 3000 index at annual rebalance, present a significantly different price impact compared to all the other additions in the index, near the date of the annual rebalance.

- whether near each of the Q3, Q4 and Q1 rebalances, the quarterly additions have a price impact significantly different from other Russell 3000 index members, which have not changed their index membership in the most recent annual rebalance.

As a result we shed light on crowded and less crowded trades on new stock additions to the Russell 3000 index, in proximity of the annual and quarterly rebalance dates.

Madhavan, in his seminal work Madhavan (2003), measured the mean perma-

nent and temporary price impacts generated by the annual addition and deletions of securities to the Russell U.S. indexes. Specifically, Madhavan focused on the 1996-2001 period, that is, before the index reconstitution methodology was updated to include the quarterly IPO additions as discussed in Section 4.2. He computed the permanent and temporary price impact in terms of the log-returns produced by the securities within the following time intervals: for permanent impact, from the end of May until two months thereafter and for temporary impact from June 30 until one month thereafter. We recall that the end of May coincides with the annual rank day and June 30 can be considered the date of the reconstitution, as it can be inferred by Table 4.2. It was found that for index additions over the period 1996-2001, the mean temporary impact and the mean permanent impact for the Russell 3000 index were 5.4% and 3.3%, respectively. For index deletions in the Russell 2000 index, the results were more modest with a mean temporary impact of 0.7% and a mean permanent impact of –1.6% (see Table 1 and 2 therein).

Quantifying temporary and permanent market impact is especially of interest to the market microstructure literature as well as to financial institutions since they are often found to be two of the main sources of transaction costs.

Analogously to Madhavan (2003), we determine the permanent and temporary price impacts associated to the annual reconstitution of the index both for index additions and deletions. We adopt the methodology from Section 5.2 of Madhavan (2003) and quantify the temporary market impact as,

$$R_{temp} = \ln(p_1) - \ln(p_2) \tag{4.5.1}$$

and the permanent market impact as,

$$R_{perm} = \ln(p_2) - \ln(p_0), \tag{4.5.2}$$

where p_0, p_1 and p_2 are the stock prices at the annual rank day, one month thereafter and two months thereafter, respectively. Table 4.6 reports the measurement for the permanent and temporary market impact for annual additions and deletions.

The columns $\bar{R}_{temp}$ and $\bar{R}_{perm}$ contain the mean temporary and permanent market impact, respectively, expressed in terms of percentages with the corresponding standard errors in parenthesis. The column № contains the size of the sample considered. Note that we included in this analysis also the new IPOs which were added to the index on the annual rebalance, but not the ones that were added in the quarterly rebalancing of Q3, Q4 and Q1 of the same year.

We remark that after 2008, the temporary market impact often presents a negative sign, presumably amenable to the 2010s bull market which signed a positive trend in the equity stock market, as also it has been documented by financial news e.g. WSJ Staff (2019); Davies (2019); Randewich (2019). Nonetheless, in many years deletions still present a combination of positive temporary price impact and negative market impact regardless of the positive trend aforementioned. Moreover, we also measure a more moderate price impact for deleted securities, analogously to what has been observed by Madhavan (2003) for the time period 1996-2001. A regression model can be applied in order to fully test the effect of market trends on R_{perm} and R_{temp}. Since both the reference market index S&P 500 and individual stock monthly returns present significant autocorrelations across different lags Jegadeesh (1990), this type of analysis is quite involved and is left to a future work.

As discussed in Section 4.2, from the 2004 annual reconstitution the Russell U.S. indexes has started receiving quarterly additions with newly issued securities in order to provide a version of the indexes which better resemble the equity market. We therefore investigate if such quarterly updates are really implemented by market participants via quarterly reconstitutions of the index portfolios.

We recall that the price impact measured on the index additions arises from the transactions generated by traders portfolio rebalances. In fact, close to the annual reconstitution period, market participants review their equity portfolios tracking the indexes: buy and sell orders are based on their beliefs on what constituents will be added and deleted from their current portfolio composition. It follows that the securities which are already present in the equity portfolio aforementioned at the time of the annual review and are believed to remain in the new roster of

Price Impact in Russell 3000 Index										
	Annual Additions					Annual Deletions				
Year	$\bar{R}_{temp}$		$\bar{R}_{perm}$		№	$\bar{R}_{temp}$		$\bar{R}_{perm}$		№
2005	-5.1	(0.6)	9.7	(1.1)	344	-4.9	(1.1)	5.2	(1.8)	242
2006	4.6	(0.7)	-10.7	(1.0)	348	2.0	(0.8)	-7.1	(1.1)	232
2007	6.4	(0.8)	-8.6	(1.0)	328	3.3	(0.7)	-3.2	(1.1)	198
2008	2.1	(0.9)	-9.0	(1.0)	373	5.9	(2.1)	-18.6	(2.7)	200
2009	-1.6	(0.9)	8.8	(1.3)	302	-5.2	(1.6)	-0.6	(2.6)	190
2010	5.6	(0.8)	-9.3	(1.3)	296	2.0	(1.3)	-10.8	(1.9)	200
2011	-0.7	(0.7)	-5.1	(1.0)	273	-1.0	(1.3)	-5.1	(1.4)	161
2012	1.5	(0.8)	-1.5	(1.1)	265	-1.1	(1.9)	-6.6	(2.4)	148
2013	-4.7	(0.8)	6.1	(1.1)	236	-3.2	(1.6)	-4.5	(2.9)	121
2014	7.2	(0.7)	-0.3	(0.9)	289	3.0	(1.2)	0.2	(1.4)	178
2015	4.5	(1.2)	-4.2	(1.6)	254	12.8	(1.9)	-16.5	(2.4)	162
2016	-5.4	(0.6)	1.0	(1.2)	283	0.2	(1.6)	-0.9	(2.2)	163
2017	-0.8	(0.8)	1.8	(1.2)	285	1.8	(1.1)	1.0	(1.8)	156
2018	-0.2	(1.0)	1.5	(1.6)	270	2.6	(1.7)	-5.8	(2.2)	155

Table 4.6: A comparison of the mean permanent and temporary price impact for additions and deletions during the annual rebalance of the Russell 3000 index. The mean impacts are expressed in terms of percentages. In parenthesis the standard error of the mean.

securities, will not see an excess of transactions comparable to those of the new additions and deletions. Indeed, this is the reason why the index effect literature focuses exclusively on annual index additions and deletions.

In the hypothesis of a portfolio manager tracking the index at each quarter rebalance, at the time of the annual reconstitution she would mainly have to buy shares of the securities which she believes will be added to the index, and which were not added in any of the most recent Q3, Q4 and Q1 quarterly rebalances. Contrarily, a portfolio manager tracking the index annually would need to buy the securities which she thinks are going to be added based on the previous annual index rebalance. Therefore, the latter portfolio manager may also buy securities that were added at the most recent Q3, Q4 and Q1 quarterly rebalances, which are believed to remain in the index during the upcoming annual reconstitution.

If the majority of market participants were to update their index portfolios

at each quarter, we would not expect to see significant market impact in those securities which were added at the most recent Q3, Q4 and Q1 rebalances, and are believed to stay in the index in the upcoming annual reconstitution. On the other hand, one may consider the case where the majority of market participants update their index portfolios only at annual rebalances. In this case we would expect that the securities which were added at the most recent Q3, Q4 and Q1 rebalances to behave in a very similar fashion to any other security added to the index in the same year. In this section we are going to check which of these cases applies in the market.

Figure 4.7 compares the distribution of the permanent and temporary price impact for each annual reconstitution from 2005 to 2018, near the annual reconstitution dates. The top panel shows the distributions of the permanent price impact computed via (4.5.2), while the bottom panel shows the distributions of the temporary market impact as defined in (4.5.1). For each year, the *"Quarterly Additions"* group, which appears in orange, are the securities which were added at the most recent Q3, Q4 and Q1 rebalances and which remained in the index in the upcoming annual reconstitution. The group *"New Additions"*, in blue, represents any other security added to the index in the same year. We observe a very good agreement for the distributions at each year, supporting the hypothesis that securities in the *"Quarterly Additions"* group and those in the *"New Additions"* group are traded by market participants in a very similar fashion within the time frame of up to two months after the annual reconstitution date.

We further investigate the observed similarity between the *"Quarterly Additions"* group and the *"New Additions"* group near the annual reconstitution date, under minimal assumptions. We conduct a two-sample t-test assuming unequal variances and unequal sample sizes under the null hypothesis that the two groups are sampled from the same distribution. The t-statistic, which we denote by t_{obs}, is defined in (C.2.1). Here, y refers to the log-returns of the *"New Additions"* group and z stands for the returns of the *"Quarterly Additions"* group according to (4.5.1) and (4.5.2). We apply a bootstrap algorithm with 10,000 repetitions for each year.

We refer to Algorithm C.2.1 in Appendix C.2 for the procedure used to calculate the p-values. In order to account for multiple hypothesis tests at each year from 2005 to 2018, we need to modify the p-values which are given by Algorithm C.2.1 by using the Benjamini-Hochberg procedure (see Section 3 of Benjamini and Hochberg (1995)). In Appendix C.3 we describe the transformation that needs to be applied on the p-values (see (C.3.2) and Algorithm C.3.1 therein). When adjusting for multiple testing, the p-values for the hypothesis for the permanent price impact tests and those for the hypothesis temporary price impact tests are adjusted separately.

Table 4.7 reports the two-tailed adjusted p-values of our test statistic for each year from 2005 to 2018. Only in one year out of fourteen, namely 2006, the mean permanent price impacts of the two groups were found to be significantly different at 0.05 significance level. As for the temporary market impact the two groups were found to be significantly different only on three years out of fourteen, namely 2006, 2011 and 2016. Nonetheless, such discrepancy could have already been deduced from Figure 4.7, where the blue and orange temporary price impact distributions present visibly different features.

The reconstitution methodology introduced in Section 4.4 allows us to keep track of the quarterly index additions in the Russell 1000, 2000 and 3000 indexes at each quarter. This allows us to test the complementary hypothesis of whether the new quarterly additions receive any abnormal price impact soon after the corresponding quarterly rank day. In fact, in the case in which most of market participants were to rebalance their index portfolio annually, the new quarterly additions would not see any significant excess of price impact compared, for example, to the securities which are already present in the index.

As already discussed in this section, the new annual additions present an excess of price impact measurable up to the end of July of the corresponding year, i.e. two months after the annual rank day. Moreover, as shown in Table 4.3, the Q3 rank day usually falls approximately in the middle of August. Hence, it might be the case that some new annual additions could continue to present a measurable excess of price impact in the proximity of Q3 rank day.

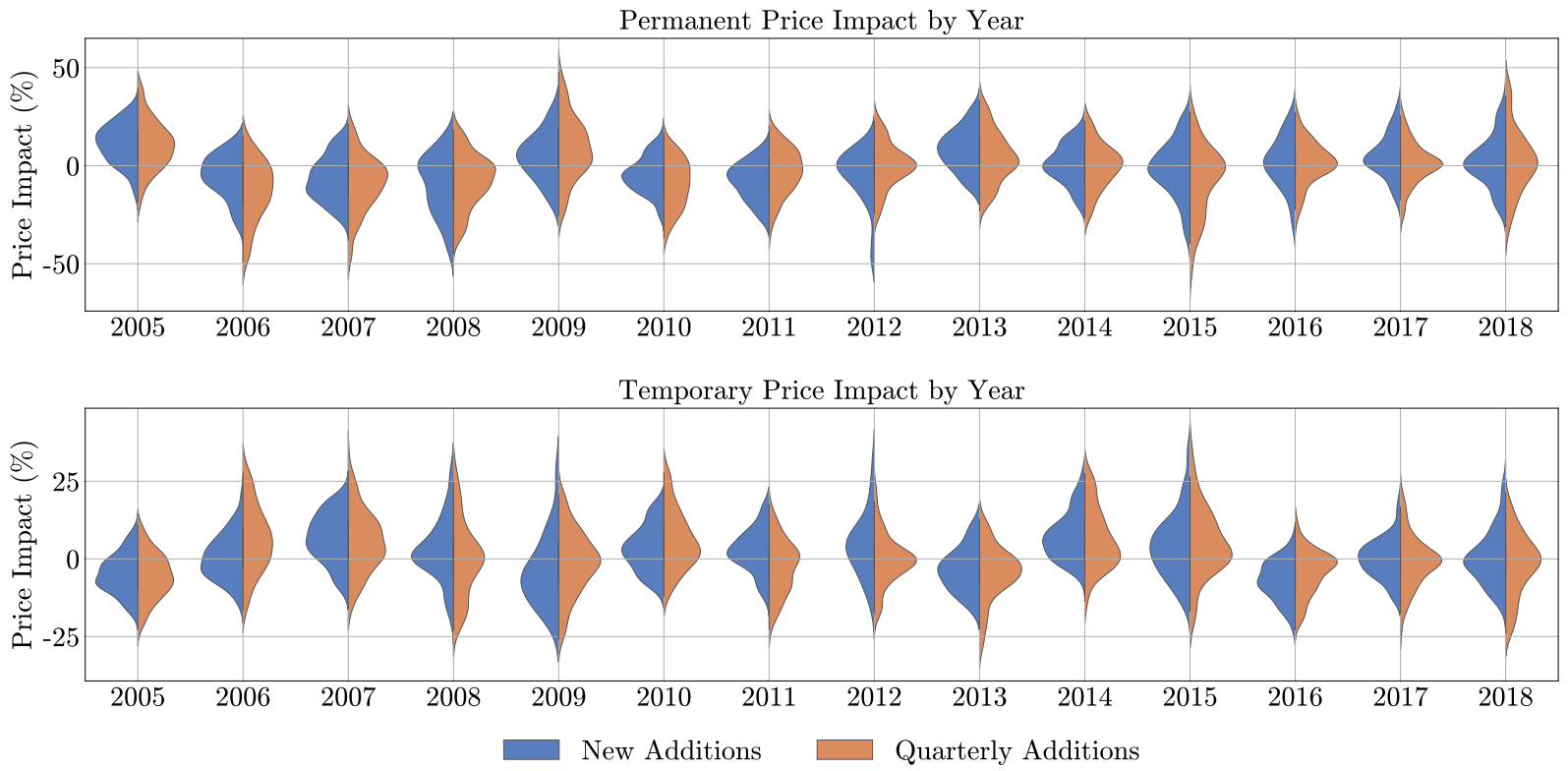

Figure 4.7: A comparison of the permanent and temporary impact distributions by year for the *"Quarterly Additions"* group and the *"New Additions"* group, for the Russell 3000 index. The *"Quarterly Additions"* group are the securities which were added at the most recent Q3, Q4 and Q1 rebalances and which remained in the index in the upcoming annual reconstitution. The *"New Additions"* represent any other security added to the index in the same year.

	Permanent Impact		**Temporary Impact**	
Years	t_{obs}	p	t_{obs}	p
2005	-0.455	0.755	-1.261	0.322
2006	-3.782	0.001	3.798	0.002
2007	-1.246	0.340	-0.326	0.870
2008	1.186	0.340	-1.605	0.255
2009	1.278	0.340	0.180	0.932
2010	-2.745	0.055	1.843	0.209
2011	2.302	0.077	-3.195	0.013
2012	2.549	0.055	-2.431	0.055
2013	-1.490	0.327	-1.382	0.322
2014	-0.373	0.755	-1.273	0.322
2015	-1.339	0.340	0.011	0.988
2016	0.032	0.972	2.812	0.026
2017	-1.546	0.322	-0.778	0.553
2018	0.644	0.653	-0.834	0.553

Table 4.7: Observed test statistic and the corresponding two-tailed p-values at 0.05 level of significance, for each year from 2005 to 2018 under the null hypothesis that the *"Quarterly Additions"* group and the *"New Additions"* are sampled from the same distribution.

The only securities in the index which can be safely considered devoid of the aforementioned excess of price impact are those who have not changed their index membership in the most recent annual rebalance. In fact, even securities who remained in the Russell 3000 index during the most recent annual rebalance, but have moved from the Russell 2000 index to the Russell 1000 index, might still present an excess of price impact. This effect is generated by the buy orders of those market participants following the Russell 1000 index. Therefore, we investigate if the price impact measured on the new quarterly additions and those securities that have not changed their index membership in the most recent annual rebalance present measurable differences.

For each quarter we conduct, similarly to what we did for the annual rebalance, a two-samples t-test assuming unequal variances and unequal sample sizes. Our t-test is done under the null hypothesis that the new quarterly additions and the securities that have not changed their index membership in the two most recent annual rebalances are sampled from the same distribution. Again, we take the

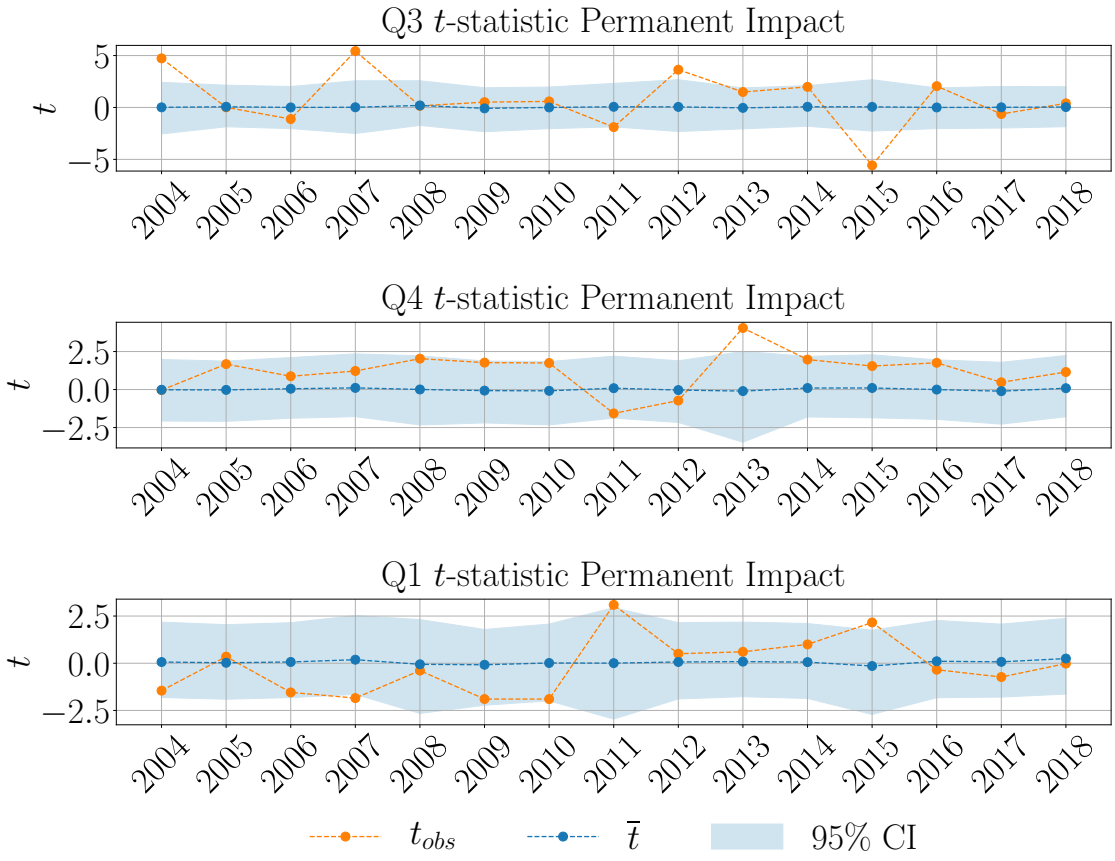

Figure 4.8: Permanent price impact case. The mean test statistic $\bar{t}$ is plotted in the blue line for the new quarterly additions versus those securities that have not changed their index membership in the most recent annual rebalance. The light blue bands are the 95% confidence intervals for t-test statistic. Observed test statistic t_{obs} is presented in the orange line.

10,000 repetitions for the bootstrap resampling as in Algorithm C.2.1.

We define the mean test statistics $\bar{t}$ to be the mean of the bootstrap t-distribution created in Algorithm C.2.1, for the two-samples t-test, measuring permanent price impact. Here y and z refer to the two months log-returns starting on the quarter rank day, for stocks which are already in the index and for quarterly additions, respectively.

The 95% confidence interval is also derived by using a bootstrap percentile method, as defined in (C.2.2). The 95% confidence interval needs to be further adjusted for multiple testing, as introduced by Benjamini and Yekutieli (2005) and further discussed in Section "False Coverage Statement Rate-Adjusted CIs" of

Groppe (2017). This is done analogously to the p-value corrections of Table 4.7, see Algorithm C.3.2 in Appendix C.3 for the exact procedure. When adjusting for multiple testing, the 95% confidence interval for the hypothesis for the Q3, Q4 and Q1 permanent price impact are adjusted separately. Figure 4.8 presents the mean test statistics $\bar{t}$ for the two-samples t-test for permanent price impact (in the blue line), along with the 95% confidence interval (the light blue region). In the orange line we show the observed test statistics t_{obs} from (C.2.1)

Finding t_{obs} outside the 95% confidence interval would mean that we must reject the null hypothesis that the two samples come from the same distribution, and accept the alternative hypothesis that the distributions generating the two samples are different. We remark that only three years out of fifteen present two or more significant observed test statistics t_{obs}, namely 2007 and 2015.

Similarly, in Figure 4.9 we present in the blue line the mean test statistic $\bar{t}$ from Algorithm C.2.1, for temporary price impact. Here y and z refer to the one months log-returns starting on the quarter rank day, of stocks which are already in the index and of quarterly additions, respectively. In the light-blue region we plot the 95% confidence interval, which is derived along the same lines as in Figure 4.8. In the orange line we show the observed test statistic t_{obs} from (C.2.1), for temporary price impact. We observe that only four years out of fifteen present two or more significant observed test statistics t_{obs}, namely 2011, 2013, 2015 and 2017. Nonetheless, the majority of the significant t_{obs} are only marginally significant. It is reasonable to believe that the results in the years 2007 and 2009 might have been biased by the unfolding of the 2007-2008 financial crisis.

Ultimately, no compelling evidences were found to conclude that the majority of market participants follow the quarterly index rebalances, as shown by Figures 4.8 and 4.9. Moreover, the similarities between the price impact distributions observed in Figure 4.7 are in favour of the hypothesis that most market participants focus on the annual index rebalance, disregarding the quarterly index additions until the entire index portfolio has to be reviewed to take into account the changes brought by the annual index reconstitution.

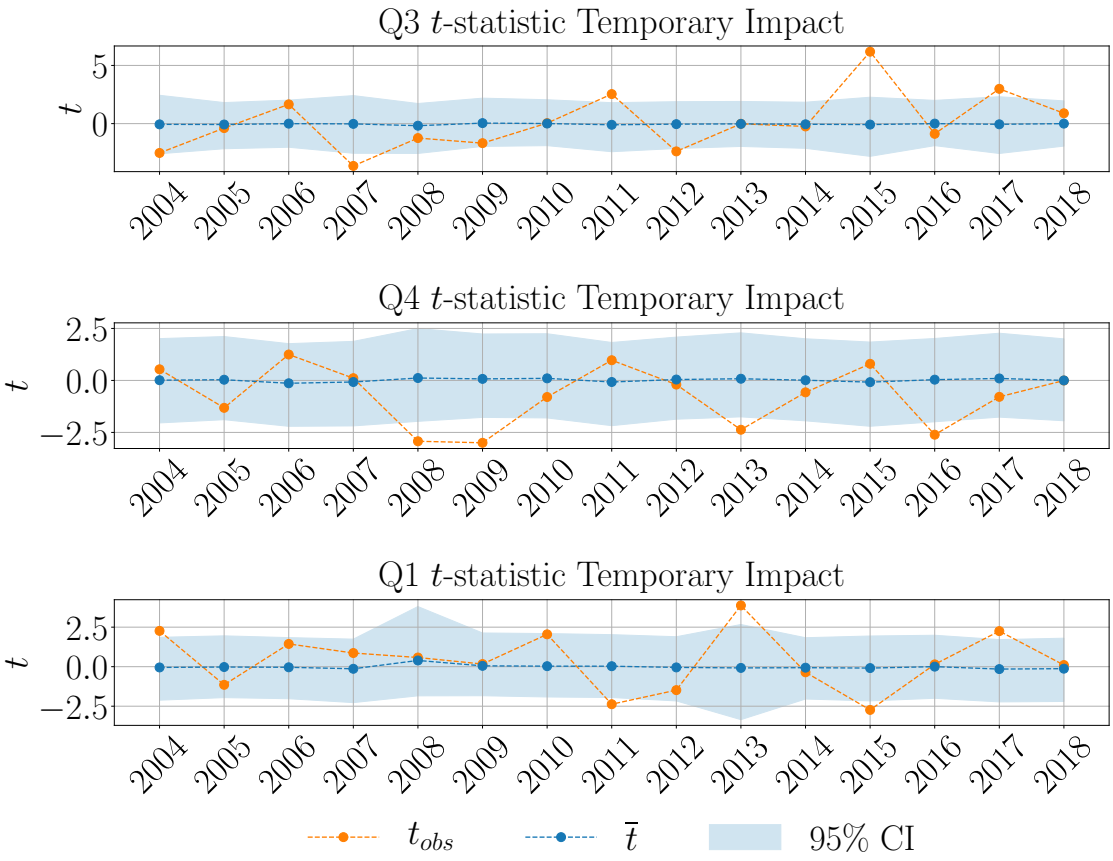

Figure 4.9: Temporary price impact case. The mean test statistic $\bar{t}$ is plotted in the blue line for the new quarterly additions versus those securities that have not changed their index membership in the most recent annual rebalance. The light blue bands are the 95% confidence intervals for t-test statistic. Observed test statistic t_{obs} is presented in the orange line.

The non-crowding phenomenon around quarterly rebalance dates, points out a possibility for profitable trading strategies on IPOs additions. A trader who wishes to track the new index additions could purchase new IPOs additions around quarterly rebalance dates, with relatively low transaction costs. These IPOs could be sold later by the trader near the annual rebalance date, where the stock price will experience a significant increase due to price impact.

4.6 Conclusions

This chapter was built out of two parts. On the first part we dealt with reconstruction of Russell US indexes. We reviewed the main features of the Russell US index reconstitution methodology, starting from the index eligibility criteria to the quarterly IPOs addition procedure. Our analysis focused on the years 1989-2019 . We split our analysis into two time windows: the first is 1989-2004, and the second is 2004-2019, with 2004 being the year in which the quarterly IPOs addition were introduced. By a careful choice of approximations to the aforementioned methodology we reproduced the Russell 1000, 2000 and 3000 indexes to a very high degree of accuracy, using only CRSP US Stock database for our index reconstruction. We remark that the CRSP database, which is part of the Wharton Research Data Services (WRDS) database, is frequently used by researchers in the field and is available in many academic institutions.

The index constituents and their corresponding weights are released via a python package called *pyndex* (see Micheli (2020)), in the purpose to make this an accessible and standard platform for researches in the field, as the Russell indexes historical data is often unavailable for academic studies.

In the second part of the chapter, we studied crowding phenomenon on strategies that tracking the Russell 3000 index. We measured the temporary and permanent price impact for the annual index additions and deletions from 2005 to 2018. We compared the permanent and temporary price impact affecting the securities added in the Q3, Q4 and Q1 quarterly rebalances and remaining in the

index versus the new index additions that didn't belong to the Russell 3000 index at any time in the previous rebalance year. Such measurements suggested a larger presence (or crowding) of trading strategies that are tracking the index additions annually compared to those who rebalance quarterly. This phenomenon implies that indexing strategies can experience reduced transaction costs by buying new IPOs additions closely quarterly rebalance dates.

It was shown in Volpati et al. (2020) that common strategies, which are based only on momentum signals, are crowded and therefore would give a rather poor profitability. Our finding add additional information on crowding phenomena, as we show that indexing strategies are indeed crowded on the one year scale but much less crowded on the 3 months scale near quarterly rebalances.

4.7 Data availability statement

Wharton Research Data Services (WRDS) was used in preparing the paper Micheli and Neuman (2019). This service and the data available thereon constitute valuable intellectual property and trade secrets of WRDS and/or its third-party suppliers.

5

Outlook

In this thesis, we have investigated multi-agent market equilibria through mathematical models and empirical analyses. In Chapter 2 we developed a new mathematical model for a game of fast and slow optimal trading and determined the corresponding Stackelberg equilibrium via a novel approach based on the theory of Fredholm integral equation. Chapter 3 was dedicated to the first known comparison of a closed-loop equilibrium of a market impact game with the corresponding open-loop equilibrium and central planner solution. Finally, Chapter 4 developed a novel approach to reconstruct the Russell indexes and studied the presence of crowding on the Russell 3000 index constituents.

However, our results raise new questions and point us to interesting directions for future research. The work of Chapter 2 could be extended to consider a Stackelberg game where the high frequency trader plays the role of the leader while the institutional investor plays the role of the follower. If a solution to such equilibrium exists, it could be compared with the results of Chapter 2 and lead us to identify the main differences between these Stackelberg equilibria. Further research could include quantifying the approximation error of the numerical method introduced in Chapter 2 as well as considering increasingly realistic scenarios such as a model where the initial inventory of each trader is random and known only to the agent that owns it.

The comparison of Chapter 3 is interesting and new but limited only to the trading features of our model. Further extensions to our work could consider investigating how systemic risk changes across the different types of equilibria, analogously to what has already been studied by Carmona et al. (2013) for the case of a mean-field game.

In conclusion, the work presented in this thesis provides a strong foundation for further research into field of multi-agent market equilibria and we hope that our work will inspire future researchers to explore the questions and directions we have identified.

A

Appendix for Chapter 2

A.1 An Example of Spectral Decomposition of G

In this section we give an example of the spectral decomposition of G in Lemma 2.8.3 for the case where $\phi^1 = 0$. We continue to assume that Assumption 2.3.1 holds.

Lemma A.1.1. *Let $\psi \in C([0,T])$ and recall that K_1 be defined as in (2.7.3). Then, K_1 satisfies for $0 \le t \le T$,*

$$\frac{d}{dt}(\mathsf{K}_1^*\psi)(t) = -r_t^1(\mathsf{K}_1^*\psi)(t) - \psi(t), \quad (\mathsf{K}_1^*\psi)(T) = 0.$$

In particular, $(\mathsf{K}_1^*\psi)(t)$ is continuously differentiable on $[0,T]$.

Proof. The proof follows the same lines of Proposition 2.9.4 hence we just just give the outlines. We now take a derivative of $\mathsf{K}_1^*\psi$ with respect to time using (2.7.4), (2.3.3) and (2.3.4) to get

$$\begin{aligned}\frac{d}{dt}(\mathsf{K}_1^*\psi)(t) &= \frac{d}{dt}\left(\xi_t^- \int_t^T \xi_s^+ \psi(s) ds\right) \\ &= -r_t^1(\mathsf{K}_1^*\psi)(t) - \psi(t), \quad \text{for all } 0 \le t \le T.\end{aligned}$$

Note that from (2.7.4) it follows that

$$(\mathsf{K}_1^*\psi)(T) = 0.$$

□

Proposition A.1.2. *Let* G *be defined as in* (2.3.11) *and assume that* $\phi^1 \equiv 0$. *Let* $(z_n)_{n=1}^{\infty}$ *be the increasing sequence of real positive roots of the following equation,*

$$\cot(z) = -\frac{(2\alpha - \kappa_1)}{\lambda_1}\frac{T}{z}. \tag{A.1.1}$$

Then the eigenvalues $(\zeta_n)_{n=1}^{\infty}$ *and the eigenfunctions* $(\psi_n)_{n=1}^{\infty}$ *of* G *are given by*

$$\psi_n(t) = \frac{2}{\sqrt{\zeta_n}}\frac{\sin\left(\frac{t}{\sqrt{\zeta_n}}\right)}{\sqrt{\frac{2T}{\sqrt{\zeta_n}} - \sin\left(\frac{2T}{\sqrt{\zeta_n}}\right)}}, \qquad \zeta_n = \frac{T^2}{z_n^2}. \tag{A.1.2}$$

Proof. We first show that the eigenvalues $(\zeta_n)_{n=1}^{\infty}$ and eigenfunctions $(\psi_n)_{n=1}^{\infty}$ are arising from solutions to an ODE. Then we show that the solutions of the ODE can be determined in terms of the roots to (A.1.1).

Let ζ be an eigenvalue of G and ψ the corresponding eigenfunction, i.e. ζ and ψ satisfy

$$(\mathsf{G}\psi)(t) = \zeta\psi(t), \quad 0 \le t \le T. \tag{A.1.3}$$

From Lemma 2.8.3 it follows that $\zeta > 0$ and $\psi \in L^2([0,T])$. Proposition 2.9.4 shows that $(\mathsf{G}\psi)(t)$ is continuously differentiable over $[0,T]$, therefore, it follows from (A.1.3) that $\psi(t)$ is continuously differentiable over $[0,T]$. We take a derivative on both sides of (A.1.3) to obtain that (ζ,ψ) must satisfy

$$\frac{d}{dt}(\mathsf{G}\psi)(t) = \zeta\psi'(t), \quad \text{for all } 0 \le t \le T. \tag{A.1.4}$$

Proposition 2.9.4 shows that $(\mathsf{G}\psi)$ is the solution to (2.9.5), therefore we can sub-

stitute (2.9.5) in (A.1.4) to get that ψ must satisfy

$$r_t^1(\mathsf{G}\psi)(t) + (\mathsf{K}_1^*\psi)(t) = \zeta\psi'(t), \quad \text{for all } 0 \le t \le T. \tag{A.1.5}$$

Proposition 2.6.7 proves that r^1 is the solution to (2.6.27). When $\phi^1 \equiv 0$ it can be computed explicitly as follows,

$$r_t^1 = \frac{2\alpha - \kappa_1}{(t-T)(2\alpha-\kappa_1) - 2\lambda_1}, \quad t \in [0,T].$$

Note that under Assumption 2.3.1, r^1 is continuously differentiable on $[0,T]$.

Since we have proved that $\psi(t)$ is continuous, it follows from Proposition A.1.1 that $(\mathsf{K}_1^*\psi)(t)$ is continuously differentiable on $[0,T]$. We take a derivative on both sides of (A.1.5) to get

$$\frac{dr_t^1}{dt}(\mathsf{G}\psi)(t) + r_t^1\frac{d}{dt}(\mathsf{G}\psi)(t) + \frac{d}{dt}(\mathsf{K}_1^*\psi)(t) = \zeta\psi''(t),$$

and then use (2.9.5) to get that ψ satisfies

$$\frac{dr_t^1}{dt}(\mathsf{G}\psi)(t) + (r_t^1)^2(\mathsf{G}\psi)(t) + r_t^1(\mathsf{K}_1^*\psi)(t) + \frac{d}{dt}(\mathsf{K}_1^*\psi)(t) = \zeta\psi''(t), \quad 0 \le t \le T. \tag{A.1.6}$$

By applying (2.6.27), (A.1.5) and (A.1.1) to (A.1.6) we get that ψ must satisfy

$$-\psi(t) = \zeta\psi''(t), \quad 0 \le t \le T. \tag{A.1.7}$$

Recall that $\zeta > 0$, hence it follows from (A.1.3) and Proposition 2.9.4 that ψ satisfies the initial condition $\psi(0) = 0$. The terminal condition $\psi'(T) = -\left(\frac{2\alpha-\kappa_1}{\lambda_1}\right)\psi(T)$ follows by combining (A.1.5) with (2.6.27), (A.1.3) and $(\mathsf{K}_1^*\psi)(T) = 0$ (see Proposition A.1.1). It follows that (ζ, ψ) satisfy

$$\psi''(t) = -\frac{1}{\zeta}\psi(t), \quad 0 < t < T, \quad \psi(0) = 0, \quad \psi'(T) = -\left(\frac{2\alpha-\kappa_1}{\lambda_1}\right)\psi(T). \tag{A.1.8}$$

We show that (A.1.1) has an infinite number of positive roots. To see this, note

that since $2\alpha - \kappa_1 \geq 0$ by Assumption 2.3.1, then for any $n \geq 1$,

$$\lim_{z \to (n-1)\pi^+} \cot(z) + \frac{2\alpha - \kappa_1}{\lambda_1} \frac{T}{z} = +\infty,$$
$$\lim_{z \to n\pi^-} \cot(z) + \frac{2\alpha - \kappa_1}{\lambda_1} \frac{T}{z} = -\infty.$$

Since $\cot(z) + \frac{2\alpha - \kappa_1}{\lambda_1} \frac{T}{z}$ is continuous over the intervals $((n-1)\pi, n\pi)$ for any $n \geq 1$, then it follows by the intermediate value theorem that (A.1.1) has a root in the interval $((n-1)\pi, n\pi)$ for any $n \geq 1$.

Next we identify ζ_n as in (A.1.2). Let z_n be the n^{th} positive root of (A.1.1) and let ζ_n, ψ_n be defined as in (A.1.2). First, note that since $z_n > 0$, then

$$2z_n - \sin(2z_n) > 0. \tag{A.1.9}$$

From (A.1.2) and (A.1.9) it follows that

$$\frac{2T}{\sqrt{\zeta_n}} - \sin\left(\frac{2T}{\sqrt{\zeta_n}}\right) > 0,$$

therefore, the function $\psi_n(t)$ is well-defined for all $t \in [0, T]$ and $||\psi_n||_{L^2} = 1$. Using the following identity which arises from (A.1.8),

$$\cos(z_n) = -\frac{(2\alpha - \kappa_1)}{\lambda_1} \frac{T}{z_n} \sin(z_n),$$

it is easy to verify that ψ_n in (A.1.2) solves (A.1.8) with $\zeta = \zeta_n$ for any $n \geq 1$. This completes the proof. □

B

Appendix for Chapter 3

B.1 Proof of Proposition 3.3.3 and Lemma 3.6.10

Before proving Lemma 3.6.10, we will introduce two intermediate results which will help us to disentangle the dependence of the parameter e on λ. We remark that to prove our result we will use certain identities for e and f (see (B.2.1) and (B.2.2)) which we have postponed to Appendix B.2 for better readability. In particular, we will exploit the identity $e(\lambda) = 1/h_4(\lambda)$ stated in (B.2.1).

Lemma B.1.1. *For all λ sufficiently small we have,*

$$h_4 = \sqrt{\frac{\gamma}{\lambda}} h_4^0 + \mathcal{O}(1), \tag{B.1.1}$$

where

$$\begin{aligned} h_4^0 = & \frac{\overline{D}(\delta_N^*) + \delta_N^*}{N} \\ & - \frac{(N+1)(\delta_N^* - \overline{D}(\delta_N^*)(N-1))^2}{8N^2\left(\bar{D}(\delta_N^*)(N-1)^2 + (N^2-N-1)\,\delta_N^*\right)^2} \\ & \times \left(\overline{D}(\delta_N^*)(N-1)\left(N^2+2N-3\right) + \left(3N^2-4N-3\right)\delta_N^*\right). \end{aligned} \tag{B.1.2}$$

Proof. Recall that h_4 was defined in (B.2.2). From the expansions of a and d in

(3.6.35) and (3.6.34) we get,

$$h_{4,1} = \frac{(N-1)d + 2aN}{\lambda(N+1)^2} = \left(\frac{\overline{D}(\delta_N^*) + \delta_N^*}{N}\right)\sqrt{\frac{\gamma}{\lambda}} + \mathcal{O}(1). \tag{B.1.3}$$

Define

$$h_{4,2} = \frac{2(2d-(N-1)a)^2\left(-a\left(N^2+2N-3\right)+4d-\lambda\left(N^2-1\right)\rho\right)}{h_2\lambda(N+1)^2\left(2h_2-\lambda(N^2-1)(2\beta+\rho)\right)}. \tag{B.1.4}$$

We expand $h_{4,2}$ by using the power series of a and d and the definition of h_2 in (B.2.2) to obtain

$$\begin{aligned} h_{4,2} = &-\sqrt{\frac{\gamma}{\lambda}}\frac{(N+1)(\delta_N^* - \overline{D}(\delta_N^*)(N-1))^2}{8N^2\left(\overline{D}(\delta_N^*)(N-1)(N+1)+\left(N^2-N-1\right)\delta_N^*\right)^2} \\ &\times\left(\overline{D}(\delta_N^*)(N+1)\left(N^2+2N-3\right)+\left(3N^2-4N-3\right)\delta_N^*\right)+\mathcal{O}\left(1\right). \end{aligned} \tag{B.1.5}$$

Plugging (B.1.3) and (B.1.5) into (B.2.2) then indeed yields

$$h_4 = h_{4,1} + h_{4,1} + \beta + \rho = \sqrt{\frac{\gamma}{\lambda}}h_4^0 + \mathcal{O}(1), \tag{B.1.6}$$

with h_4^0 defined in (B.1.2). □

From Lemma B.1.1 we observe that in order to prove Lemma 3.6.10, we need to derive the sign of h_4^0, which in turn will give us the sign of $e = 1/h_4$. We define the following function,

$$\begin{aligned} &\chi_N(y) \\ &= \frac{\overline{D}(y)+y}{N} \\ &\quad - \frac{(N+1)\left(\left(N^3+3N^2-N-3\right)\overline{D}(y)+\left(3N^2-4N-3\right)y\right)\left(y-(N-1)\overline{D}(y)\right)^2}{8N^2\left(\left(N^2-1\right)\overline{D}(y)+\left(N^2-N-1\right)y\right)^2} \\ &\quad - \frac{2N^2}{(N+1)\left((N+1)\overline{D}(y)+(2N+1)y\right)}. \end{aligned} \tag{B.1.7}$$

In the following lemma we argue that

$$h_4^0 - \frac{1}{(N+1)\Delta(N)} = \chi_N(\delta_N^*),$$

and we also show that $\chi_N(\cdot)$ vanishes once we plug-in δ_N^*. This is a key ingredient in the proof of the sign of h_4 as suggested by (B.1.1).

Lemma B.1.2. *For h_4^0 as in (B.1.2) and Δ given by (3.5.22), we have*

$$h_4^0 = \frac{1}{(N+1)\Delta(N)}.$$

Proof. By substituting the expressions for h_4^0 from (B.1.2) and Δ from (3.5.22), we obtain

$$h_4^0 - \frac{1}{(N+1)\Delta(N)} = \chi_N(\delta_N^*).$$

We will show that for any $N \geq 2$, δ_N^* satisfies

$$\chi_N(\delta_N^*) = 0, \tag{B.1.8}$$

which will prove the result.

First, we aggregate all the terms appearing on the right hand side of (B.1.7) in one fraction, that is

$$\chi_N(\delta_N^*) = \frac{\mathcal{S}_1(\delta_N^*)}{\mathcal{S}_2(\delta_N^*)},$$

where,

$$
\begin{aligned}
\mathcal{S}_1(y) &= \mathcal{R}_1 + \mathcal{R}_2,\\
\mathcal{R}_1(y) &= -4N^9y^2 + 4N^8y^4 + 47N^8y^2 - 6N^7y^4 - 52N^7y^2 - 66N^6y^4 - 90N^6y^2 + 34N^5y^4\\
&\quad + 108N^5y^2 + 144N^4y^4 + 39N^4y^2 + 12N^3y^4 - 36N^3y^2 - 82N^2y^4 - 12N^2y^2 - 9N^9\\
&\quad + 33N^8 - 42N^7 + 18N^6 + 3N^5 - 3N^4 - 42Ny^4 - 6y^4,\\
\mathcal{R}_2(y) &= 14(N+1)N^7y^3\overline{D} - 22(N+1)N^6y^3\overline{D} - 58(N+1)N^5y^3\overline{D} + 56(N+1)N^4y^3\overline{D}\\
&\quad + 68(N+1)N^3y^3\overline{D} - 22(N+1)N^2y^3\overline{D} - 9(N+1)N^8y\overline{D} + 44(N+1)N^7y\overline{D}\\
&\quad - 54(N+1)N^6y\overline{D} - 6(N+1)N^5y\overline{D} + 37(N+1)N^4y\overline{D} - 6(N+1)N^3y\overline{D},\\
&\quad - 6(N+1)N^2y\overline{D} - 30(N+1)Ny^3\overline{D} - 6(N+1)y^3\overline{D},\\
\mathcal{S}_2(y) &= 2(N-1)N^2(N+1)(\overline{D}(N+1) + 2Ny + y)\left(\overline{D}\left(N^2-1\right) + \left(N^2-N-1\right)y\right)^2.
\end{aligned}
$$

and we abbreviate $\overline{D}(y)$ to $\overline{D}$. Hence, in order to prove (B.1.8) we need to show that

$$\frac{\mathcal{S}_1(\delta_N^*)}{\mathcal{S}_2(\delta_N^*)} = 0,$$

which is implied by $\mathcal{S}_1(\delta_N^*) = 0$ and $\mathcal{S}_2(\delta_N^*) \neq 0$. This is proved by a direct substitution and by Lemma 3.6.9(i) which identifies δ_N^*. □

Now we are ready to prove Lemma 3.6.10.

Proof of Lemma 3.6.10. From Lemmas B.1.1 and B.1.2 it follows that for all sufficiently small λ,

$$h_4 = \sqrt{\frac{\gamma}{\lambda}}h_4^0 + \mathcal{O}(1) = \sqrt{\frac{\gamma}{\lambda}}\frac{1}{(N+1)\Delta(N)} + \mathcal{O}(1). \tag{B.1.9}$$

From (3.5.22) we have that $\Delta(N) > 0$. Recall that from (B.2.1) we have that $e = \frac{1}{h_4}$ and this completes the proof. □

The following intermediate result is an important step in proving Proposition 3.3.3.

Lemma B.1.3. *For λ sufficiently small we have*

$$M_{rate} = \sqrt{\frac{\gamma}{\lambda}}\Delta(N) + \mathcal{O}(1), \quad M_{aim} = 1 + \mathcal{O}(\sqrt{\lambda}). \tag{B.1.10}$$

for the nonnegative function $\Delta(N)$ defined in (3.5.22).

Proof. The representation of M_{rate} in (3.6.18) and (3.6.39) yield

$$M_{rate} = \sqrt{\frac{\gamma}{\lambda}}\Delta(N) + \mathcal{O}(1), \tag{B.1.11}$$

where $\Delta(N)$ is given by (3.5.22) and does not depend on λ. From (3.6.18), (3.5.12) and (B.2.1) we have

$$M_{aim} = \gamma\frac{\bar{a}}{M_{rate}} = \gamma\frac{e}{\lambda(N+1)M_{rate}} = \frac{\gamma}{\lambda(N+1)h_4 M_{rate}}. \tag{B.1.12}$$

Using (B.1.11) and (B.1.9) we obtain that, for λ small enough,

$$M_{aim} = \frac{\gamma}{\lambda(N+1)}\frac{1}{\left(\sqrt{\frac{\gamma}{\lambda}}h_4^0 + \mathcal{O}(1)\right)}\frac{1}{\left(\sqrt{\frac{\gamma}{\lambda}}\Delta(N) + \mathcal{O}(1)\right)} = \frac{1}{(N+1)h_4^0\Delta(N)} + \mathcal{O}(\sqrt{\lambda}). \tag{B.1.13}$$

Finally, plugging in the result of Lemma B.1.2 for h_4^0, we get

$$M_{aim} = 1 + \mathcal{O}(\sqrt{\lambda}) \tag{B.1.14}$$

as asserted. □

Proof of Proposition 3.3.3. The asymptotic expansions for M_{rate} and M_{aim} were already proved in Lemma B.1.3.

In view of this result, it now remains to derive the asymptotics of the value function. For J^n as in (3.3.2) we define

$$J^n(\dot{\varphi}^n, \dot{\varphi}^{-n}) = \bar{w}_1(\lambda) - \bar{w}_2(\lambda) - \bar{w}_3(\lambda), \tag{B.1.15}$$

where

$$\bar{w}_1(\lambda) = \left(1 + 2\lambda N (M_{rate})^2 \frac{M_{aim}}{\gamma}\right)\left(\frac{M_{rate}M_{aim}}{\gamma}\right)\frac{\sigma^2}{\rho(2\beta+\rho)(\beta+\rho+M_{rate})},$$
$$\bar{w}_2(\lambda) = \lambda N \left(\frac{M_{rate}M_{aim}}{\gamma}\right)^2 \frac{\sigma^2}{2\beta\rho+\rho^2},$$
$$\bar{w}_3(\lambda) = \left(\frac{\gamma}{2} + \lambda N (M_{rate})^2\right)\left(\frac{M_{rate}M_{aim}}{\gamma}\right)^2 \frac{2\sigma^2}{\rho(2\beta+\rho)(\rho+2M_{rate})(\beta+\rho+M_{rate})}.$$

Using (3.3.3) we can write

$$M_{rate} = \sqrt{\frac{\gamma}{\lambda}}\Delta(N) + r_1(N) + \mathcal{O}\left(\sqrt{\lambda}\right), \quad M_{aim} = 1 + a_1(N)\sqrt{\lambda} + \mathcal{O}(\lambda),$$

for some explicit functions r_1, a_1 of N, where the explicit dependence in N is omitted in what follows to ease notation. Using Taylor expansion, we can in turn derive power-series expansions of $\bar{w}_1$, $\bar{w}_2$ and $\bar{w}_3$ around $\lambda = 0$,

$$\begin{aligned}
\bar{w}_1(\lambda) &= \frac{(1+2\Delta^2 N)\sigma^2}{\gamma\rho(2\beta+\rho)} + \frac{\sigma^2}{\Delta\gamma^2\rho(2\beta+\rho)}\big(a_1\Delta\gamma + 4a_1\Delta^3\gamma N + 4\Delta^2\sqrt{\gamma}Nr_1 \\
&\quad - \sqrt{\gamma}\beta - 2\Delta^2\sqrt{\gamma}N\beta - \sqrt{\gamma}\rho - 2\Delta^2\sqrt{\gamma}N\rho\big)\sqrt{\lambda} + O(\lambda), \\
\bar{w}_2(\lambda) &= \frac{\Delta^2 N\sigma^2}{\gamma\rho(2\beta+\rho)} + \frac{2N\sigma^2(a_1\Delta^2\gamma + \Delta\sqrt{\gamma}r_1)}{\gamma^2\rho(2\beta+\rho)}\sqrt{\lambda} + O(\lambda), \\
\bar{w}_3(\lambda) &= \frac{(1+2\Delta^2 N)\sigma^2}{2\gamma\rho(2\beta+\rho)} + \frac{\sigma^2}{4\Delta\gamma^{3/2}\rho(2\beta+\rho)}\big(4a_1\Delta\sqrt{\gamma}(1+2\Delta^2 N) - 2\beta \\
&\quad + 2\Delta^2 N(4r_1 - 2\beta - 3\rho) - 3\rho\big)\sqrt{\lambda} + O(\lambda).
\end{aligned}$$

After inserting these expansions into (B.1.15), we obtain the asserted leading-order asymptotics (3.3.4) of the optimal value. More details on these calculations can be found in the Mathematica companion of this chapter. □

B.2 Identities for the Proofs of Lemmas 3.6.1 and 3.6.10

In this section we provide some identities for the coefficients of the system (3.5.5)–(3.5.11), which were used in Section 3.5 and in the proof of Lemma 3.6.1.

First, the coefficients e, f and c are given by,

$$
\begin{aligned}
e &= \frac{1}{h_4}, \\
f &= \frac{1}{\lambda(N+1)h_4(h_3-(\rho+\beta))} \\
&\quad \times \left(d + h_3\lambda(N-1) - \frac{2h_1^2(N-1)}{(N+1)\left(4a(N-1)+2d(N-3)+\lambda\left(N^2-1\right)\rho\right)} \right), \\
c &= \frac{2\left(-\frac{\left(\frac{1}{h_4}-\frac{N-1}{h_4(N+1)}\right)(d+h_3\lambda(N-1))}{2\lambda} - \frac{2h_1^2(N-1)}{h_4\lambda(N+1)^2\left(4a(N-1)+2d(N-3)+\lambda\left(N^2-1\right)\rho\right)} - \frac{\left(\frac{1}{h_4}-\frac{N-1}{h_4(N+1)}\right)^2}{4\lambda} \right)}{h_4\lambda(N+1)(-\beta+h_3-\rho)} \\
&\quad -2\beta-\rho
\end{aligned}
\tag{B.2.1}
$$

where

$$
\begin{aligned}
h_1 &= 2d-(N-1)a, \\
h_2 &= 2a(N-1)+d(N-3)+\lambda\left(N^2-1\right)(\beta+\rho), \\
h_3 &= -\frac{2a(N-1)+(N-3)d}{\lambda(N-1)(N+1)}, \\
h_4 &= \frac{2(2d-(N-1)a)^2\left(-a\left(N^2+2N-3\right)+4d-\lambda\left(N^2-1\right)\rho\right)}{h_2\lambda(N+1)^2\left(2h_2-\lambda(N^2-1)(2\beta+\rho)\right)} + \frac{(N-1)d+2aN}{\lambda(N+1)^2} \\
&\quad +\beta+\rho.
\end{aligned}
\tag{B.2.2}
$$

C

Appendix for Chapter 4

C.1 CRSP US Financial Data

The analysis in Chapter 4 is extensively based on the financial data available in the CRSP dataset. We summarise some of the main features of the databases considered.

The financial information regarding the securities used for this study was retrieved from the `CRSPQ:DSF` dataset, which consists of the quarterly updated CRSP daily stock data. The `CRSPQ:DSF` dataset contains all the major daily financial indicators for the securities traded in the U.S. stock market, including stock closing prices, daily returns and outstanding shares. On the other hand, the `CRSPQ:DSFHDR` dataset contains the metadata related to each security in the `CRSPQ:DSF`. The information stored in the `CRSPQ:DSFHDR` file includes for example the initial day of trading for each security, the name of company to which the security belongs to as well as its Standard Industrial Classification.

Two labels are required in order to identify a company and its underlying securities. The identifier `permco` uniquely identifies a company in CRSP; it is neither reused once a company cease to exist, nor changed in case the company's name is subject to modification. Each company in CRSP may be traded on one or more securities therefore it is necessary to uniquely identify them in order, for example, to

compute the company's market capitalisation. CRSP provides a unique five-digit permanent identifier for each security, under the name of `permno`, which neither changes during an issue's trading history, nor is reassigned after an issue ceases trading. For each security, the daily returns, assuming dividend reinvestment, are given by the column `ret` in the `CRSPQ:DSF` file.

As discussed in Section "Calculations" of Wharton Research Data Services (2020), the market capitalisation of a given company in CRSP can be found by computing,

$$\sum_i p_t^i \cdot v_t^i,$$

where p_t^i is the unadjusted close price of day t of security i and v_t^i is the corresponding unadjusted number of its shares outstanding. The sum is taken over all the securities belonging to the given company. Here, p_t^i and v_t^i corresponds to the columns `prc` and `shrout` of the `CRSPQ:DSF` dataset, respectively.

The selection of the securities with prices greater than 1$ discussed in Section 4.2 is performed over the adjusted stock prices. Following Section "Adjusting for Stock Splits and Other Corporate Actions" of Wharton Research Data Services (2020) the adjusted stock price of securities i is given by

$$\frac{p_t^i}{\beta_t^i},$$

where p_t^i is the unadjusted close price of security i at day t and β_t^i is the corresponding price adjustment factor. Here β_t^i is stored in column `cfacpr` of `CRSPQ:DSF` dataset. The share types in CRSP are identified through a two-digit code, named as `hshrcd`, describing the type of shares traded. The file `CRSPQ:DSFHDR` stores the `hshrcd` for all the financial securities belonging to the `CRSPQ:DSF` dataset. Following Appendix A.2 in Chapter 3 of Fong (2005), common stocks are represented by a `hshrcd` equal to 10 or 11.

In order to establish which IPOs will be included in which quarterly addition, one has to consider the corresponding IPO date. In CRSP, the first day of trading corresponding to an IPO is stored in the `begdat` variable from `CRSPQ:DSFHDR`

dataset. The most widely used database in IPO research is SDC Platinum from Thomson Financial, which is currently not available in WRDS or CRSP. As reported in Wharton Research Data Services (2020), a comparison between SDC and `CRSPQ:DSFHDR` indicates that the first trading days agree in 76% of cases. This confirms that the IPO dates in the `CRSPQ:DSFHDR` dataset can be reliably used for the index reconstruction.

C.2 Bootstrap Two-Samples t-test

In this section we summarise some useful results on bootstrap two samples t-test, which are taken from Chapter 16.2 of Efron and Tibshirani (1994).

We consider two samples $\boldsymbol{z}$ and $\boldsymbol{y}$ of sizes n and m, respectively, from possibly different probability distributions F and G. We would like to test the null hypothesis $H_0 : F = G$. Let $\boldsymbol{x}$ be the collection of all the observations in $\boldsymbol{y}$ and $\boldsymbol{z}$. We test H_0 with the following two-samples unequal variance and unequal size statistic $t(\cdot)$,

$$t_{obs} \equiv t(\boldsymbol{x}) = \frac{\bar{z} - \bar{y}}{\sqrt{\bar{\sigma}_1^2/n + \bar{\sigma}_2^2/m}}, \tag{C.2.1}$$

with

$$\bar{\sigma}_1^2 = \frac{1}{n-1}\sum_{i=1}^{n}(z_i - \bar{z})^2, \quad \bar{\sigma}_2^2 = \frac{1}{m-1}\sum_{i=1}^{m}(y_i - \bar{y})^2,$$

where $\bar{z}$ and $\bar{y}$ are the means of samples z and y, respectively. Algorithm C.2.1 computes the bootstrap test statistic and the corresponding two-tailed p-values. In our analysis we take the number of bootstrap repetitions N to be 10000.

Moreover, as discussed in Chapter 13.3 of Efron and Tibshirani (1994), given a level of significance α, the corresponding confidence interval for the bootstrapped distribution of the test statistic t can be found using the *bootstrap percentile method*. Let $\hat{\Phi}$ be the empirical cumulative distribution function of the bootstrap test statistic t. The $(1-\alpha)$ confidence interval are given by,

$$(\hat{\Phi}^{-1}(\alpha/2), \hat{\Phi}^{-1}(1-\alpha/2)), \tag{C.2.2}$$

Algorithm C.2.1 Bootstrap test statistic for testing $F = G$

1. Draw N samples of size $n + m$ with replacement from $\boldsymbol{x}$. Call the first n observations $\boldsymbol{z}^*$ and the remaining m observations $\boldsymbol{y}^*$.

2. Evaluate $t(\cdot)$ on each sample,

$$t(\boldsymbol{x}^{*,k}) = \frac{\bar{z}^* - \bar{y}^*}{\sqrt{(\bar{\sigma}_1^*)^2/n + (\bar{\sigma}_2^*)^2/m}}, \quad k = 1, 2, \dots N$$

   where $\bar{\sigma}_1^*$ and $\bar{\sigma}_2^*$ are defined on $\boldsymbol{z}^*$ and $\boldsymbol{y}^*$ accordingly.

3. Approximate two-tailed p-values by

$$\hat{p}_{boot} = 1 - \frac{\sum_{j=1}^{N} \mathbb{1}_{\{-t_{obs} \leq t(\boldsymbol{x}^{*,j}) \leq t_{obs}\}}}{N}.$$

where $\hat{\Phi}^{-1}(\alpha/2)$ and $\hat{\Phi}^{-1}(1-\alpha/2)$ by definition correspond to the $\alpha/2$ and $1-\alpha/2$ percentiles, respectively.

C.3 Multiple Testing

In this section we summarise some of the results regarding the Benjamini-Hochberg (BH) correction for independent multiple testing.

As discussed in Section 2.b of Y. Benjamini and Yekutieli (2009), the p-values can be adjusted for multiple testing according to the BH procedure via Algorithm C.3.1. Section 3 of Benjamini and Hochberg (1995) clarifies that in the BH procedure the test statistics are assumed to be independent. Let $H_{0,i}$ with $i = 1, \dots, m$, be the null hypotheses, and p_i be the corresponding p-values. One can alternatively compute the BH-adjusted p-values as follows

$$P_{(i)}^{BH} = \min\left(\left(\min_{j \geq i} mp_j/j\right), 1\right). \tag{C.3.2}$$

Then, $P_{(i)}^{BH} \leq \alpha$ if and only if $H_{(i)}$ is among the discoveries when using the BH procedure at significance level α.

Algorithm C.3.1 Multiple testing at significance level α

Let $H_{0,i}$ with $i = 1, \ldots, m$ be the null hypotheses, and p_i be the corresponding p-values.

1. Sort the p-values as $p_{(1)} \leq p_{(1)} \leq \ldots \leq p_{(m)}$ and let $p_{(k)}$ be the largest value such that
$$p_{(k)} \leq \frac{k\alpha}{m} \tag{C.3.1}$$
2. If no such k exists, select no discovery. Otherwise, reject the k hypotheses corresponding to $p_{(1)}, \ldots, p_{(k)}$, declaring these findings to be discoveries.

As further discussed in Section "False Coverage Statement Rate-Adjusted CIs" of Groppe (2017), the Benjamini-Hochberg procedure can be applied to confidence intervals for multiple comparisons as shown in the following algorithm.

Algorithm C.3.2 Adjusted Confidence Intervals for Multiple-Testing

1. Apply the BH procedure to the p values from the family of m tests, where m is the total number of hypothesis tests.
2. For any p value that is significant after the BH procedure, construct a confidence interval for the corresponding test with coverage $1 - \alpha'$, where α' is:
$$\alpha' = \left(\frac{k}{m}\right)\alpha,$$
with k is defined as in (C.3.1).

In Chapter 4 we take α to be 0.05. Therefore, in order to compute the bootstrap confidence interval, adjusted to the Benjamini-Hochberg framework, we use α' in place of α in (C.2.2).

Bibliography

R. Almgren and N. Chriss. Optimal execution of portfolio transactions. *Journal of Risk*, 3(2):5–39, 2000.

K. E. Atkinson. *The Numerical Solution of Integral Equations of the Second Kind*. Cambridge Monographs on Applied and Computational Mathematics. Cambridge University Press, 1997.

N. Barberis. Investing for the long run when returns are predictable. *Journal of Finance*, 1(55):225–264, 2000.

P. Barroso, R. M. Edelen, and P. Karehnke. Crowding and Tail Risk in Momentum Returns. Available at SSRN: https://ssrn.com/abstract=3045019, 2017.

C. Belak, J. Muhle-Karbe, and K. Ou. Liquidation in target zone models. *Market Microstructure and Liquidity*, 2019.

Y. Benjamini and Y. Hochberg. Controlling the false discovery rate: A practical and powerful approach to multiple testing. *Journal of the Royal Statistical Society: Series B (Methodological)*, 57(1):289–300, 1995.

Y. Benjamini and D. Yekutieli. False discovery rate–adjusted multiple confidence intervals for selected parameters. *Journal of the American Statistical Association*, 100(469):71–81, 2005.

E. N. Biktimirov, A. R. Cowan, and B. D. Jordan. Do demand curves for small stocks slope down? *Journal of Financial Research*, 27(2):161–178, 2004.

A. L. Boone and J. T. White. The effect of institutional ownership on firm transparency and information production. *Journal of Financial Economics*, 117(3): 508–533, 2015.

G. Bormetti, L. M. Calcagnile, M. Treccani, F. Corsi, S. Marmi, and F. Lillo. Modelling systemic price cojumps with Hawkes factor models. *Quantitative Finance*, 15(7):1137–1156, 2015.

B. Bouchard, M. Fukasawa, M. Herdegen, and J. Muhle-Karbe. Equilibrium returns with transaction costs. *Finance and Stochastics*, 22(3):569–601, 2018.

M. K. Brunnermeier and L. H. Pedersen. Predatory trading. *Journal of Finance*, 60(4):1825–1863, August 2005.

F. Bucci, M. Benzaquen, F. Lillo, and J. P. Bouchaud. Slow decay of impact in equity markets: insights from the ANcerno database. Preprint, available online at https://arxiv.org/abs/1901.05332, 2019.

F. Bucci, F. Lillo, J. P. Bouchaud, and M. Benzaquen. Are trading invariants really invariant? Trading costs matter. *Quantitative Finance*, pages 1–10, 2020a.

F. Bucci, I. Mastromatteo, Z. Eisler, F. Lillo, J. P. Bouchaud, and C. A. Lehalle. Co-impact: crowding effects in institutional trading activity. *Quantitative Finance*, 20(2):193–205, 2020b.

BusinessWire Press Release. Russell Indexes to add IPOs on a quarterly basis change in methodology enhances market representation of index. *BusinessWire*, 2004.

F. Caccioli, M. Shrestha, C. Moore, and J. D. Farmer. Stability analysis of financial contagion due to overlapping portfolios. *Journal of Banking & Finance*, 46:233–245, 2014.

F. Caccioli, J. D. Farmer, N. Foti, and D. Rockmore. Overlapping portfolios, contagion, and financial stability. *Journal of Economic Dynamics and Control*, 51:50–63, 2015.

J. Cai and T. Houge. Long-term impact of Russell 2000 index rebalancing. *Financial Analysts Journal*, 64(4):76–91, 2008.

L. M. Calcagnile, G. Bormetti, M. Treccani, S. Marmi, and F. Lillo. Collective synchronization and high frequency systemic instabilities in financial markets. *Quantitative Finance*, 18(2):237–247, 2018.

F. Capponi and R. Cont. Trade duration, volatility and market impact. Available at SSRN: https://ssrn.com/abstract=3351736, 2019.

P. Cardaliaguet and C.-A. Lehalle. Mean field game of controls and an application to trade crowding. *Mathematics and Financial Economics*, 12(3):335–363, 2018.

B. I. Carlin, M. S. Lobo, and S. Viswanathan. Episodic liquidity crises: cooperative and predatory trading. *Journal of Finance*, 65:2235–2274, 2007.

R. Carmona. *Lectures on BSDEs, Stochastic Control, and Stochastic Differential Games with Financial Applications*. Financial Mathematics. Society for Industrial and Applied Mathematics, 2016.

R. Carmona, J.-P. Fouque, and L.-H. Sun. Mean field games and systemic risk. Preprint, available online at https://arxiv.org/abs/1308.2172, 2013.

R. A. Carmona and Z. A. Yang. Predatory trading: a game on volatility and liquidity. Preprint, available online at https://carmona.princeton.edu/download/fe/PredatoryTradingGameQF.pdf, 2008.

Á. Cartea and S. Jaimungal. Incorporating order-flow into optimal execution. *Math. Fin. Econ.*, 10(3):339–364, 2016.

A. Cartea, S. Jaimungal, and J. Penalva. *Algorithmic and High-Frequency Trading*. Cambridge University Press, 2015.

P. Casgrain and S. Jaimungal. Mean field games with partial information for algorithmic trading. Preprint, available online at https://arxiv.org/abs/1803.04094, 2019.

P. Casgrain and S. Jaimungal. Mean-field games with differing beliefs for algorithmic trading. *Mathematical Finance*, 30(3):995–1034, 2020.

S. Champonnois and J. Sefton. Managing transaction costs in dynamic trading. Available at SSRN: https://ssrn.com/abstract=2480311, 2021.

Y. C. Chang, H. Hong, and I. Liskovich. Regression discontinuity and the price effects of stock market indexing. *The Review of Financial Studies*, 28(1):212–246, 2014.

H. Chen, G. Noronha, and V. Singal. Index changes and unexpected losses to investors in S&P 500 and Russell 2000 index funds. Available at SSRN: https://ssrn.com/abstract=651950, 2005.

H. L. Chen. On Russell index reconstitution. *Review of Quantitative Finance and Accounting*, 26(4):409–430, 2006.

X. Chen, J. H. Choi, K. Larsen, and D. J. Seppi. Learning about latent dynamic trading demand. Preprint, available online at https://arxiv.org/abs/2105.13401, 2021a.

X. Chen, J. H. Choi, K. Larsen, and D. J. Seppi. Asset Pricing Puzzles and Price-Impact. Available at SSRN: https://ssrn.com/abstract=3465159, 2021b.

P. Collin-Dufresne, K. Daniel, and M. Saglam. Liquidity regimes and optimal dynamic asset allocation. *Journal of Financial Economics*, 136(2):379–406, 2020.

R. Cont. Statistical modeling of high-frequency financial data. *IEEE Signal Processing*, 28(5):16–25, 2011.

R. Cont and J. P. Bouchaud. Herd behavior and aggregate fluctuations in financial markets. *Macroeconomic Dynamics*, 4(2):170–196, 2000.

R. Cont and A. de Larrard. Price dynamics in a markovian limit order market. *SIAM Journal on Financial Mathematics*, 4(1):1–25, 2013.

R. Cont, A. Kukanov, and S. Stoikov. The price impact of order book events. *Journal of Financial Econometrics*, 12(1):47–88, 2014.

M. Cremers, A. Pareek, and Z. Sautner. Short-Term Investors, Long-Term Investments, and Firm Value: Evidence from Russell 2000 Index Inclusions. *Management Science*, 2020.

G. Davies. The great bull market reaches its 10th birthday. *Financial Times*, 2019. Available online at: https://www.ft.com/content/4f941406-5157-11e9-b401-8d9ef1626294.

J. De Lataillade, C. Deremble, M. Potters, and J.-P. Bouchaud. Optimal trading with linear costs. *Journal of Investment Strategies*, 1(3):91–115, 2012.

R. T. Dean and W. T. M. Dunsmuir. Dangers and uses of cross-correlation in analyzing time series in perception, performance, movement, and neuroscience: The importance of constructing transfer function autoregressive models. *Behavior Research Methods*, 48(2):783–802, 2016.

M. F. Djete. Large population games with interactions through controls and common noise: convergence results and equivalence between open–loop and closed–loop controls. Preprint, available online at https://arxiv.org/abs/2108.02992, 2021.

S. Drapeau, P. Luo, A. Schied, and D. Xiong. An FBSDE approach to market impact games with stochastic parameters. Preprint, available online at https://arxiv.org/abs/2001.00622, 2019.

B. Efron and R. Tibshirani. *An Introduction to the Bootstrap*. Chapman & Hall/CRC Monographs on Statistics & Applied Probability. Taylor & Francis, 1994.

I. Ekeland and R. Témam. *Convex Analysis and Variational Problems*. Society for Industrial and Applied Mathematics, 1999.

D. Evangelista and Y. Thamsten. On finite population games of optimal trading. Preprint, available online at https://arxiv.org/abs/2004.00790v3, 2020.

H. G. Fong. *The World of Risk Management*. World Scientific, 2005.

G. Freiling. A survey of nonsymmetric Riccati equations. *Linear Algebra and its Applications*, 351-352:243–270, 2002.

G. Fu, P. Graewe, U. Horst, and A. Popier. A mean field game of optimal portfolio liquidation. *Mathematics of Operations Research*, 2021.

N. Gârleanu and L. H. Pedersen. Dynamic trading with predictable returns and transaction costs. *Journal of Finance*, 68(6):2309–2340, 2013.

N. Gârleanu and L. H. Pedersen. Dynamic portfolio choice with frictions. *Journal of Economic Theory*, 165:487 – 516, 2016.

J. Garnier, G. Papanicolaou, and T.-W. Yang. A risk analysis for a system stabilized by a central agent, 2015. Preprint, available online at https://arxiv.org/abs/1507.08333.

D. M. Groppe. Combating the scientific decline effect with confidence (intervals). *Psychophysiology*, 54(1):139–145, 2017.

T. Hendershott, C. M. Jones, and A. J. Menkveld. Does algorithmic trading improve liquidity? *The Journal of Finance*, 66(1):1–33, 2011.

G. Ip and J. Perry. Central Banks Grapple With Rate Decisions As Markets Tumble. *Wall Street Journal*, 2007. Available online at: https://www.wsj.com/articles/SB118666332147492919.

N. Jegadeesh. Evidence of predictable behavior of security returns. *The Journal of Finance*, 45(3):881–898, 1990.

A. Khandani and A. W. Lo. What happened to the quants in august 2007?: Evidence from factors and transactions data. Available at SSRN: https://ssrn.com/abstract=1288988, 2008.

A. Kirilenko, A. S. Kyle, M. Samadi, and T. Tuzun. The flash crash: The impact of high frequency trading on an electronic market. *Journal of Finance*, 72(3): 967–998, June 2017.

D. Lacker. On the convergence of closed-loop nash equilibria to the mean field game limit. *Annals of Applied Probability*, 30(4):1693–1761, 2020.

D. Lacker and L. Le Flem. Closed-loop convergence for mean field games with common noise. Preprint, available online at https://arxiv.org/abs/2107.03273, 2021.

D. Lacker and A. Soret. Many-player games of optimal consumption and investment under relative performance criteria. *Mathematics and Financial Economics*, 14 (2):263–281, 2020.

D. Lacker and T. Zariphopoulou. Mean field and n-agent games for optimal investment under relative performance criteria. *Mathematical Finance*, 29(4):1003–1038, 2019.

M. Laurière and L. Tangpi. Convergence of large population games to mean field games with interaction through the controls. Preprint, available online at https://arxiv.org/abs/2004.08351, 2020.

C.-A. Lehalle and E. Neuman. Incorporating signals into optimal trading. *Finance and Stochastics*, 23(2):275–311, 2019.

A. Lipton, U. Pesavento, and M. G. Sotiropoulos. Trade arrival dynamics and quote imbalance in a limit order book. Preprint, available online at http://arxiv.org/abs/1312.0514, 2013.

A. Madhavan. The Russell reconstitution effect. *Financial Analysts Journal*, 59 (4):51–64, 2003.

H. Markowitz. Portfolio selection. *The Journal of Finance*, 7(1):77, 1952.

R. Martin. Optimal trading under proportional transaction costs. *RISK*, 8(27): 54–59, 2014.

A. Micheli and E. Neuman. Evidence of Crowding on Russell 3000 Reconstitution Events. Preprint, available online at https://arxiv.org/abs/2006.07456. *To appear in Market Microstructure and Liquidity*, 2019.

A. Micheli and E. Neuman. Fast and slow optimal trading with exogenous information. Preprint, available online at https://arxiv.org/abs/2210.01901, 2022.

A. Micheli, J. Muhle-Karbe, and E. Neuman. Closed-loop nash competition for liquidity. Preprint, available online at https://arxiv.org/abs/2112.02961, 2021.

L. Moreau, J. Muhle-Karbe, and H. Soner. Trading with small price impact. *Mathematical Finance*, 27(2):350–400, 2017.

E. Neuman and A. Schied. Protecting pegged currency markets from speculative investors. *Mathematical Finance*, 32(1):405–420, 2022.

E. Neuman and M. Voß. Trading with the crowd. Preprint, available online at https://arxiv.org/abs/2106.09267, 2021.

E. Neuman and M. Voß. Optimal signal-adaptive trading with temporary and transient price impact. *SIAM Journal on Financial Mathematics*, 13(2):551–575, 2022.

A. A. Obizhaeva and J. Wang. Optimal trading strategy and supply/demand dynamics. *Journal of Financial Markets*, 16(1):1 – 32, 2013.

A. A. Obizhaeva and Y. Wang. Trading in crowded markets. Available at SSRN: https://ssrn.com/abstract=3152743, 2019.

M. O'Hara. High-frequency trading and its impact on markets. *Financial Analysts Journal*, 70(3):18–27, 2014.

Z. M. Onayev and V. M. Zdorovtsov. Predatory Trading Around Russell Reconstitution. Available at SSRN: https://ssrn.com/abstract=3021022, 2008.

J. L. Ossinger. Stocks fall on liquidity concerns. *Wall Street Journal*, 2007. Available online at: https://www.wsj.com/articles/SB118666160663092899.

A. F. Perold. The implementation shortfall. *The Journal of Portfolio Management*, 14(3):4–9, 1988.

A. Petajisto. The index premium and its hidden cost for index funds. *Journal of Empirical Finance*, 18(2):271–288, 2011.

D. Porter and D. S. G. Stirling. *Integral equations: A Practical Treatment, from Spectral Theory to Applications*. Cambridge University Press, 1990.

N. Randewich. Wall Street's oldest-ever bull market turns 10 years old. *Reuters*, 2019. Available online at: https://uk.reuters.com/article/usa-stocks-bull/rpt-wall-streets-oldest-ever-bull-market-turns-10-years-old-idUKL1N20V1RJ.

I. Roşu. Fast and slow informed trading. *Journal of Financial Markets*, 43:1–30, 2019.

Y. Sannikov and A. Skrzypacz. Dynamic trading: price inertia and front-running. Preprint, available online at https://www.gsb.stanford.edu/faculty-research/working-papers/, 2016.

A. Schied and T. Schöneborn. Liquidation in the face of adversity: stealth vs. sunshine trading. EFA 2008 Athens Meetings Paper, Available at SSRN: https://ssrn.com/abstract=1007014, 2009.

V. Volpati, M. Benzaquen, Z. Eisler, I. Mastromatteo, B. Toth, and J. P. Bouchaud. Zooming in on equity factor crowding. Preprint, available online at https://arxiv.org/abs/2001.04185, 2020.

M. Voß. A two-player price impact game. Preprint, available online at https://arxiv.org/abs/1911.05122, 2019.

R. Wigglesworth. Goldman Sachs' lessons from the 'quant quake'. *Financial Times*, 2017. Available online at: https://www.ft.com/content/fdfd5e78-0283-11e7-aa5b-6bb07f5c8e12.

W. M. Wonham. On a matrix Riccati equation of stochastic control. *SIAM Journal on Control*, 6(4):681–697, 1968.

WSJ Staff. Inside a Decadelong Bull Run, 2019. Available online at: https://www.wsj.com/articles/inside-a-decade-long-bull-run-11552041001.

R. H. Y. Benjamini and D. Yekutieli. Selective inference in complex research. *Philosophical Transactions of the Royal Society A: Mathematical, Physical and Engineering Sciences*, 367(1906):4255–4271, 2009.

E. Zarinelli, M. Treccani, J. D. Farmer, and F. Lillo. Beyond thesquare root: Evidence for logarithmic dependence of market impact on sizeand participation rate. *Market Microstructure and Liquidity*, 01(02):1550004, 2015.

G. Zuckermann, J. R. Hagerty, and D. Gauthier-Villars. Impact of Mortgage Crisis Spreads. *Wall Street Journal*, 2007. Available online at: https://www.wsj.com/articles/SB118664884606092848.

Sitography

European Commission. Investment services and regulated markets - Markets in financial instruments directive (MiFID), 2018. Available online at: https://finance.ec.europa.eu/capital-markets-union-and-financial-markets/financial-markets/securities-markets/investment-services-and-regulated-markets-markets-financial-instruments-directive-mifid_en.

FTSE Russell. Russell U.S. Indexes – Annual Reconstitution, 2017. Available online at: https://www.ftserussell.com/press/ftse-russell-announces-schedule-annual-russell-us-index-reconstitution.

FTSE Russell. Russell U.S. Indexes Review Timetable - March 2020 and Annual Reconstitution Timetable - June 2020, 2020a. Available online at: https://research.ftserussell.com/products/index-notices/home/getnotice/?id=2595207&_ga=2.179740323.629831544.1587596713-1989757251.1586952995.

FTSE Russell. Our story, 2020b. Available online at: https://www.ftserussell.com/about-us/our-story.

FTSE Russell. Russell U.S. equity indexes v4.5 – Construction and Methodology, 2020c. Available online at: https://research.ftserussell.com/products/downloads/Russell-US-indexes.pdf.

A. Micheli. pyndex - Russell index reconstruction package, 2020. Available online at: https://github.com/alemicheli/pyndex.

U.S. Securities and Exchange Commission. Equity market structure literature review part II: high frequency trading, 2014. Available online at: https://www.sec.gov/marketstructure/research/hft_lit_review_march_2014.pdf.

Wharton Research Data Services. Overview of CRSP U.S. stock data, 2020. Available online at: https://wrds-www.wharton.upenn.edu/login/?next=/pages/support/data-overview/wrds-overview-crsp-us-stock-database/.